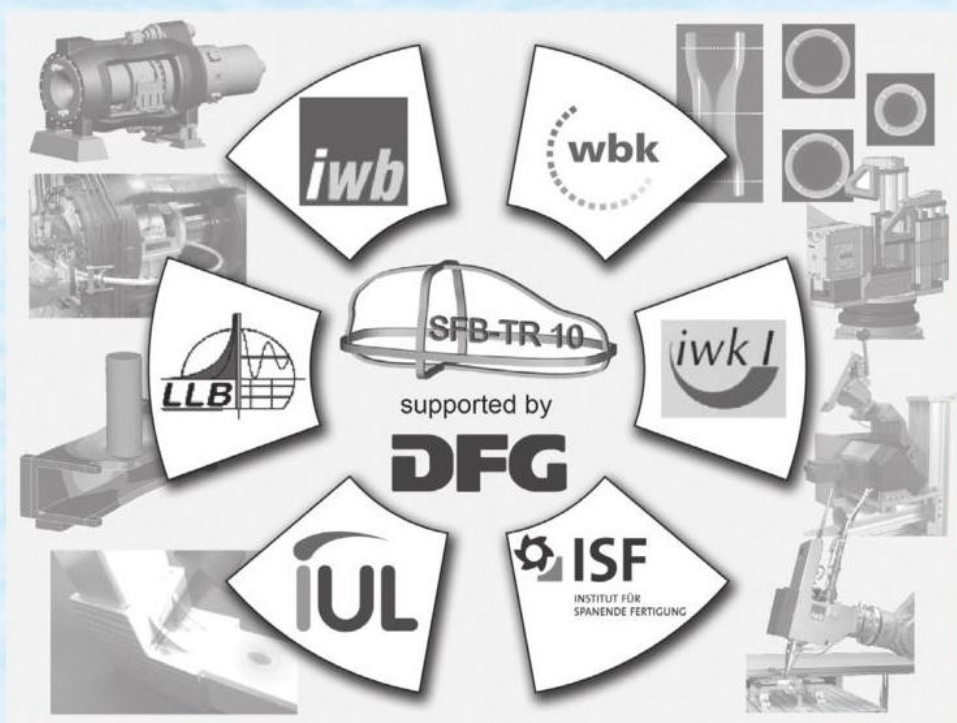# Flexible Manufacture of Lightweight Frame Structures

Phase II: Integration

Edited by
Klaus Weinert, Jürgen Fleischer,
A. Erman Tekkaya, Michael Zäh,
and Marco Schikorra

ttp TRANS TECH PUBLICATIONS

Flexible Manufacture of Lightweight Frame Structures

Flexible Manufacture of Lightweight Frame Structures

Phase II: Integration

Edited by

Klaus Weinert, Jürgen Fleischer, A. Erman Tekkaya, Michael Zäh, and Marco Schikorra

Preface

The market's increasing demands on lightweight construction for a reduction of fuel consumption in transportation systems as well as reduced material resources is becoming of increasing importance. This aspect is even more underlined by the current discussion of reducing the green house gas emissions caused by production processes. In this context, considerate use of energy intensive materials such as aluminum plays a major role.

The Transregional Collaborative Research Center / TR10 "Integration of forming, cutting, and joining for the flexible production of lightweight space frame structures", set up by the German Research Foundation (DFG) at the Universities of Dortmund, Karlsruhe, and Munich, specially aims at research on small batch production systems for lightweight space frame structures. This research team focuses on the ambitions aim of creating a scientific basis for the development of innovative manufacturing processes and design methods for a flexible, integrated process chains. This chain should comprise production techniques like

- three-dimensional rounding during extrusion,
- extrusion of continuously reinforced profiles,
- cutting on the fly,
- five-axis machining,
- hybrid laser welding and friction stir welding, and
- joining by electromagnetic high speed forming or high pressure tube forming.

This work is accomplished in a coupled simulative and experimental way so that there is a complete virtual process chain parallel to the real one comprising the extrusion process, handling robots, and cutting and joining machines. Following the first funding period 2003-2006, the current funding period lasting until 2010, has already increased by 4 more projects covering the additional joining technique friction stir welding, an enhanced process chain simulation, numerical analysis of composite profiles, and the transfer from basic composite extrusion technology to the production of aircraft stringer profiles in industrial surroundings.

This content of technology development, simulation of production processes, and integrated consideration will be found in the organization of the following peer reviewed articles. It outlines certain aspects of theoretical and experimental projects while setting up the process chain.

Dortmund   *Klaus Weinert*

January 2008   *Marco Schikorra*

Table of Contents

Manufacture of 3D Curved Profiles for Structure Components

D. Becker[1,a], M. Schikorra[1,b] and A. E. Tekkaya[1,c]

[1]Institute of Forming Technology and Lightweight Construction,

Technische Universität Dortmund, Baroper Str. 301, 44227 Dortmund, Germany

[a]dirk.becker@iul.uni-dortmund.de, [b]marco.schikorra@iul.uni-dortmund.de,
[c]erman.tekkaya@iul.uni-dortmund.de

Abstract. Curved Profile Extrusion (CPE) is an extension of the common extrusion process and offers the possibility to manufacture three-dimensionally curved profiles. Due to the flexibility of the process different curvatures can be produced with the same setup, which makes this technique efficient especially for low volume production. The process is characterized by a controlled lateral deflection of the strand which influences the material flow in the die and causes the profile curvature. In this paper, a direct comparison of the power rating between warm bending and CPE is presented. Furthermore, the investigations concerning the choice of support strategy of the surmounting profile by a robot to increase the curvature accuracy are continued. Finally, some extensions of the equipment are explained to increase the level of process integration.

Introduction

Modern transportation engineering applies multiple types of lightweight construction, concerning e.g. the materials science, design, and manufacturing. In the automotive industry the use of aluminum in structure components is shown by Audi in the A8 and, furthermore, in the sports car R8 to reduce the weight by up to 40%. The application of extruded profiles in these space frames offers different designs of cross sections so that an optimization by topology can be accomplished. Due to the wide choice of cross sections an integration of functions can be obtained, which supports the reduction of weight [1,2]. Thinking further in this direction, the large number of joints could be reduced using more curved profiles. In general, curved profiles are obtained by a bending process which influences unfavorable the profile geometry by elastic springback, cross section deformation, and the reduced formability. In contrast to this, the innovative process Curved Profile Extrusion (CPE), which was developed by the Institute of Forming Technology and Lightweight Construction, avoids these negative properties in workpieces like structure components.

Curved profile extrusion is an alternative production method to the conventional process chain to manufacture curved profiles. This production type is based on the conventional bar extrusion process in which the exiting strand is deflected by a numerically controlled guiding tool so that the curvature is based on a kinematic shape generation. On the one hand, the deflection of the profile causes compression stress at the inner bearing and amplifies the friction. On the other hand, tensile stress is superposed at the outer bearing which increases the material velocity. Due to the already plasticized material in the die the superposed moment produces no springback, and no residual stress in the curved profile. Additionally, the material of the manufactured profile offers nearly the full formability so that a following forming process, e.g. hydroforming, is still possible to add further details in design [3, 4, 5].

Process Comparison

A more detailed analysis of CPE helpful to separate this warm forming process from a conventional warm bending process especially regarding the sensitivity against external influences is obtained by the comparison of the loads which are required to achieve the curvature. Both process experiments are applied directly at the extrusion press with the same profile geometry of a round rod of 36.5 mm diameter to establish comparable initial conditions. The extrusion speed is set to 2 mm/s for the ram corresponding to 32 mm/s for the profile speed. This leads to an exiting temperature of the profile between 430°C and 450°C, using a preheated billet at 550°C and a container temperature of 450°C. The linear axis system which is installed for curved profile extrusion is also used for the warm bending process. In order to record the force of the deflection, a load cell is integrated in the guiding tool system, displayed in fig 1.
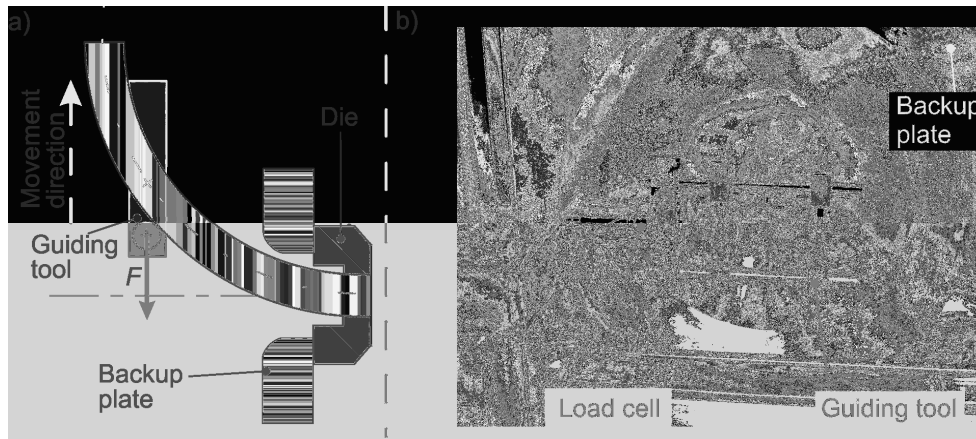
Fig. 1: a) Sketch of the force measurement direction; b) Real setup at the press

In general, the guiding tool for CPE has two rotary degrees of freedom so that it orientates automatically in tangential direction to the profile. But for the force measurement this rotatory movements should be prevented to detect the force for deflection. The deflection movement of the guiding tool was generated as described in the chapter *Flexible Profile Support* below and is driven by a PLC control. The CPE experiment is applied by a synchronous movement of the guiding tool to the profile speed to produce a constantly plane curved profile with a radius of 1,500 mm. In contrast to this, the warm bending test is not operated parallel to the extrusion process. First, the extrusion process is started and run until the steady state is reached, which is the case when the target speed is attained and the press force slowly decreases. Then, the press stops and the same deflection of the guiding tool starts to introduce the bending process. The results of both force measurements are shown in fig. 2.
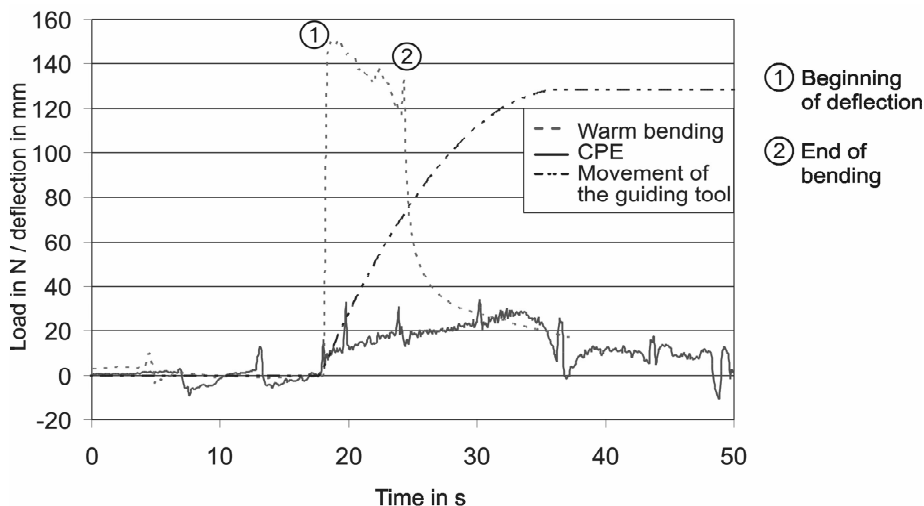
Fig. 2: Load results of warm bending and CPE

The diagrams indicate that CPE requires only minimal forces of maximal 34 N to deflect the strand for the curvature generation. In comparison to CPE, the warm bending process needs initial forces which are nearly five times higher (up to 150 N) to deflect the profile. This circumstance makes the definite difference between CPE and warm bending obvious, but also makes it necessary to move the guiding tool on the correct path without any external influencing forces which over-determine the manufacturing process. Some of the influencing factors are discussed in the following.

Compensation by Profile Support

Factors of Influence. The accuracy of the curvature depends on several influencing factors. The detailed analysis of the geometrical condition of the manufacturing cell has to be completed to assure correct deflections corresponding to the desired profile line. As it was investigated by Klaus [4], the geometrical parameters, the distance between guiding tool and die, the distance of the deflection and the angle between the press axis and the linear axis are determined by a practical calibration of the system assisted by a non-linear optimization. Due to the warm forming process the thermal conditions in the die as well as in the profile have to be taken into account. The profile line can also be influenced by quenching after the exit of the profile so that some sections distort more than others which largely depends on the cross section design. Because of the consideration of three-dimensionally curved profiles the use of a table for the profile support in the run out of the extrusion press is not possible. Therefore, bending and torsion effects occur due to the influence of gravity [6].

Flexible Profile Support. Introduced in [6], the profile support is realized and investigated for plane curved profiles by a six-axis robot type Kuka KR150-2 with a second guiding tool attached to the robot´s arm. The results of support strategies applied with a constant distance between the first and the second guiding tool for constantly curved profiles have to be transferred to the manufacture of three-dimensionally curved profiles by CPE. Due to the complex geometries of three-dimensionally curved profiles the movement for the profile support behind the guiding tool has to be very flexible. The calculation of the movement data for the constantly plane curved profiles is easy, but considering the additional dimension in the curvature requires a movement path similar to a 3D-spline. Now, the support strategy is expanded from the constant distance between the first and the second guiding tool to an attendant support of the profile. By the help of a CAD/CAM chain the movement data for the complex profile shape can be generated. The process chain begins with the CAD model of the desired structure profile from which the neutral line has to be extracted. This line is imported into a CAM system applicable for kinematics simulation. There are two CAM systems used in the Collaborative Research Center which are CATIA V5 with the module DMU kinematics or MOSES, which is an added application to AutoCAD [7,8]. Both CAM systems offer the possibility to simulate the manufacturing process in which the profile is guided tangentially through the die. Additionally, the movements of the guiding tool and the robot can be checked regarding the working range of the kinematics and the collision with the components of the manufacturing cell before the real process takes place. During the simulation the generation of the movement data for the guiding tool and the tool center point of the robot are recorded. The program code is exported to the robot system where the real tests of the movements are made before the production begins. The described experiments are carried out with the help of the CAM system MOSES. A surface in the virtual production cell defines the support position of the second guiding tool. In this case, the surface is a hemisphere with the center point at the position of the bearing. In the beginning of the extrusion process the second guiding tool starts at a position directly behind the first guiding tool and follows the profile synchronously to the profile velocity. If the tool center point of the second guiding tool reaches the hemisphere, it only moves along the surface, but will not leave it for the rest of the process (fig. 3).
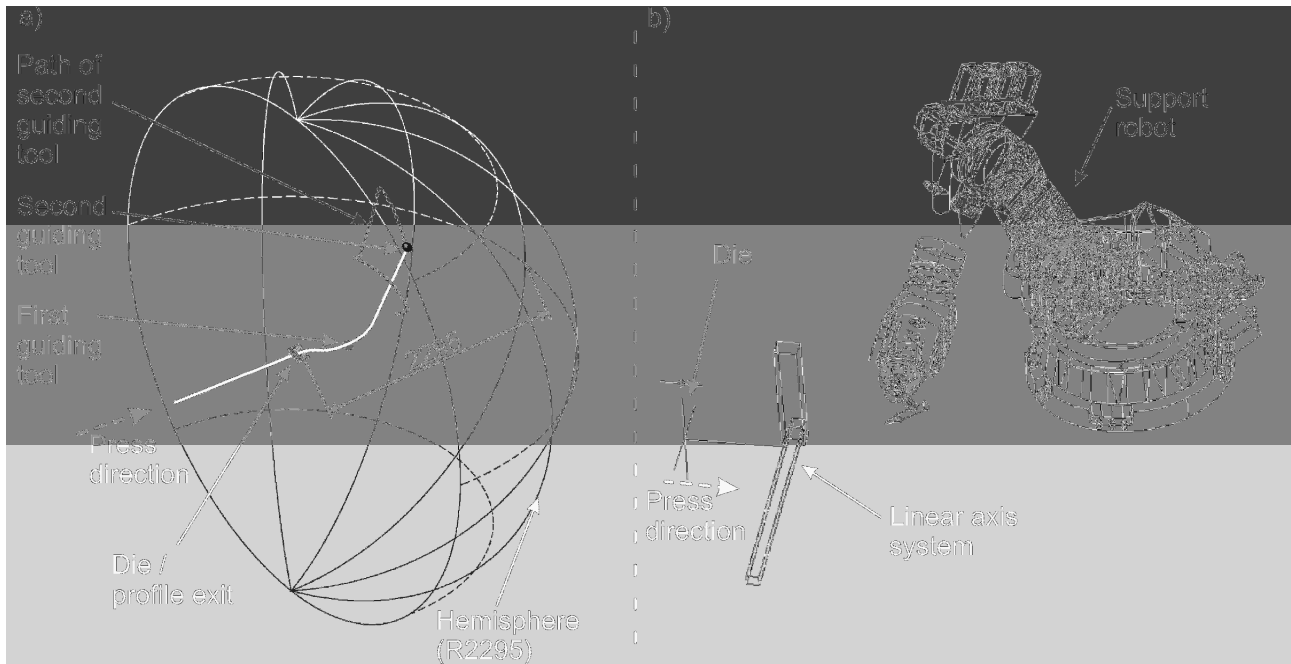
Fig. 3: Data generation cell (a) and virtual robot cell (b)

The chosen hemisphere as support surface has to be adjusted by the parameters radius and distance from the die concerning the accuracy of the manufactured profile. With regard to the bending and torsional stresses in the profile calculated by means of mechanical equations two radii of the hemisphere, 2085 mm and 2295 mm, both with their center at the position of the die, were applied for one part of the demonstrator profile frame, the motorcycle BMW C1 (fig. 4).
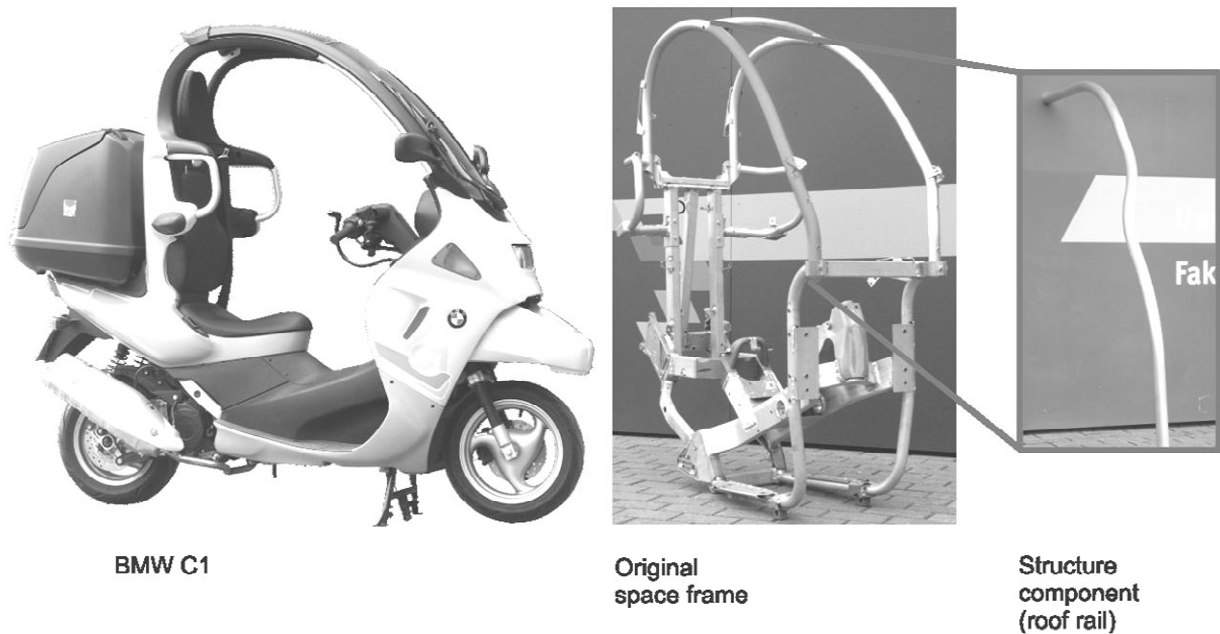
Fig. 4: Demonstrator vehicle and structure

The results of the experimental investigations are shown by a shape comparison between the target model and the manufactured structure component with the help of a 3D optical digitizer (GOM: ATOS I+Tritop) displayed in fig. 5. Considering the entire profile for the best-fit analysis, the deviations in some very few positions on the profile reach up to +/- 7 mm. In large parts the profile obtains the target contour with a deviation of +/- 3 mm.

Profile segments

Arc length:
a - 100 mm
b - 489 mm
c - 577 mm
d - 50 mm

Complete profile

Surface deviation
in mm
7.0
3.0
0
-3.0
-7.0

Segments a + b

Surface deviation
in mm
0.5
0.2
0
-0.2
-0.5

8.5°

Segment c

Surface deviation
in mm
1.0
0.5
0
-0.5
-1.0
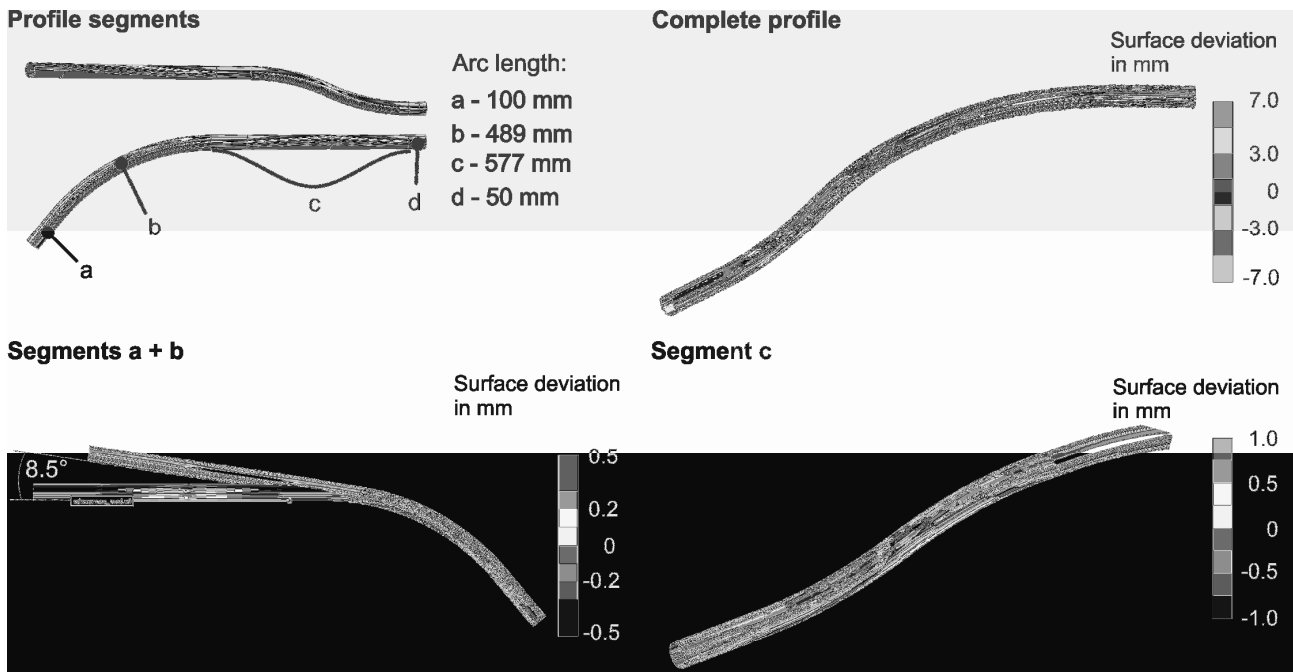
Fig. 5: Curvature accuracy of different profile segments

The profile accuracy can be examined regarding the segments of the profile, which are distinguished by the movement of the guiding tool during the manufacturing process. In fig. 5, the four segments a, b, c, and d with the following characteristics are displayed.

a　- straight profile at the beginning

b　- constantly plane curved part

c　- vertical s-shaped part

d　- straight profile at the end

The correct initial configuration of the manufacturing cell will be shown by the accuracy of the straightness in the segment a. All following parts depend on the accuracy of the previous parts. This is the reason why the failure will increase more and more towards the end of the profile. With respect to the front part, in particular segment a and b, the deviations are determined predominantly in the arc length. The difference between the manufactured and target angle is measured with 8.5°. Contrary to this, the surface deviation amount to a maximum of +/- 0.5 mm towards the end of the arc of the manufactured profile. One reason of this deviation can be found in the performance of the synchronization between the profile speed and the deflection movement of the guiding tool. The synchronization of the presented experiments is applied by the ram speed and the press ratio, which differs due to the elongation of the press frame and the unsteady temperature conditions. The s-shaped segment most likely achieves the desired accuracy of +/- 1 mm. Although the surmounting profile behind the second guiding tool is very long, approximately more than 1,000 mm, the straightness of the last part is identified with +/- 0.5 mm.

Manufacturing Cell for CPE

Extension of the Movement Range. In the Collaborative Research Center TR10 the complete process chain of forming, cutting, and joining is investigated. Therefore, one aim in this wide research work is the cooperation between the individual subprojects, which leads to many interfaces in communication and also in the real process chain. In particular, the forming process by CPE is followed by the flying cutting described in the paper "accuracy of a flying cutting device" of this

issue, displayed [fig. 6a]. Both subprojects use a 6-axis robot which has to be synchronized and very flexible according to the curvature of the desired profile. Thus, the flexibility in positioning the robot for its profile supporting task also during the process is increased by setting it on a linear axis (Kuka KL1500). Additionally, the spectrum of support strategies and curvatures can be enhanced by the functions of the larger working range. Fig. 6a shows the fixed positioning of the cutting and supporting robot at the state of the knowledge of the first funding period in 2006. The current setup of the linear axis is parallel to the press axis to enlarge the range in one direction (see fig. 6b). In the future, the design of the short process chain between CPE and the flying cutting is planned according to the sketch in fig. 6c so that the collision between the robots is prevented and it is still possible to deliver the profile by the support robot to the subsequent machining or joining cell.
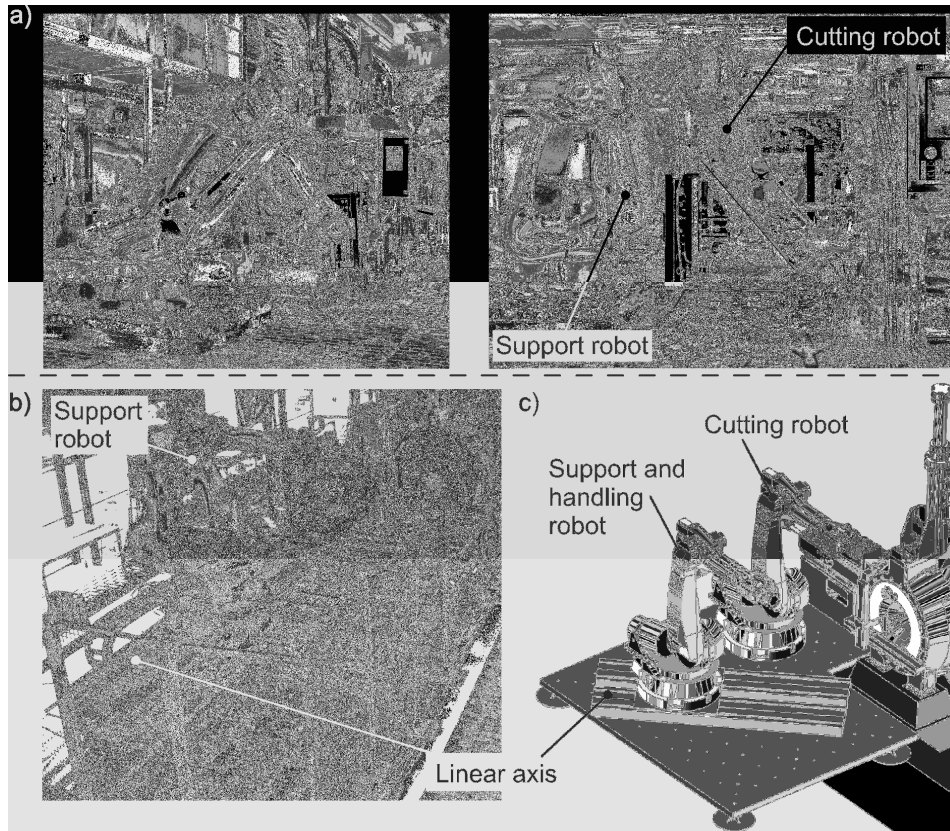
Fig. 6: Manufacturing cell: a) First setup expertise in 2006; b) Current setup;
c) Future setup with two robots

In-line Quenching. The standard aluminum alloy 6060 has to be cooled down directly after the extrusion process to preserve a fine distribution of the alloying elements. This precipitation hardening is used to achieve the required mechanical properties [9]. Due to the flexible setup of the manufacturing cell and the sideward movement of the profiles of CPE the conventional straight cooling section is not applicable. Therefore, the quenching process begins already in front of the kinematics, directly behind the die, by a simple perforated ring fed with air pressure to blow parallel towards the press direction. A second ring was installed at the guiding tool to support a fast cooling, displayed in fig. 7a. In order to minimize the sensitivity against contact with the handling kinematics later on in the process chain and to follow the objective of using high strength aluminum alloys, the cooling rate has to be increased. On this account, a spray mist quenching was developed which limits the cooling to a small area to minimize the contamination of the kinematics. In fig. 7b, the equipment of the spray mist cooling is displayed with four spray guns to quench the profile equally, which prevents distortion. The diagram shows the quenching effect on the profile surface cooling down from the solution temperature to below 200°C in a very short time so that cooling rates of 20°C/s are possible. The low mark in the temperature curve represents the end of quenching

by mist spray with a subsequent heat flux of the neighboring areas up to a temperature of 150°C. The first tests show very good results, but the integration into the process chain has to be proved in the future.
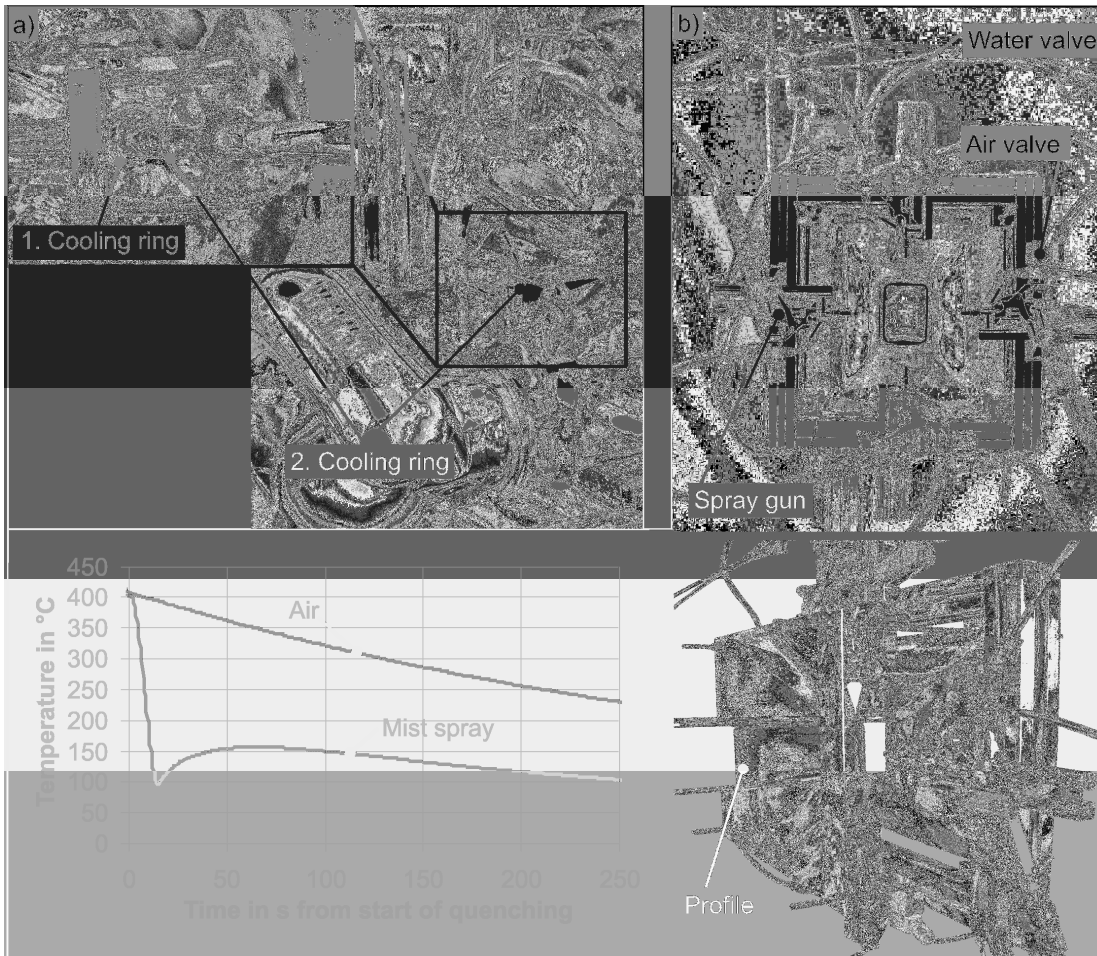
Fig. 7: a) Cooling by air pressure; b) Cooling by mist spray

Summary

The investigations show that CPE, in comparison to a conventional warm bending process, requires considerably less forming capacity so that this method is energy-efficient in addition to the better mechanical properties. Furthermore, the further development of the manufacture of three-dimensionally curved profiles provides the application of complex shaped structure components. Regarding the accuracy of the profiles, the influence of gravity makes it difficult to accomplish high standards as demanded by customers like the transportation industry. The application of a robot for profile support against the effects of gravity offers a possibility to set the contour deviations to a level below +7/-3 mm and even below +/-0.5 mm in some profile segments. Due to the flexibility of CPE and the integration in the process chain the manufacturing cell needs to be adapted in the same way. Therefore, the robot is mounted on a big linear axis to expand the working range for profile support and handling. Additionally, the quenching process is considered to implement it directly in the process chain by a fast mist spray cooling device with cooling rates of up to 20°C/s.

Acknowledgment

References

[1] H. H. Braess, U. Seiffert: Space-Frame. Chapter 6.1.2, In: Vieweg Handbuch Kraftfahrzeugtechnik, Vieweg Verlag (2007).

[2] Chr. A. Sawyer: Body Beautiful. In: Automotive Design & Production, Gardner Publications Inc, Vol. August 2007 (http://www.autofieldguide.com/articles/080704.html).

[3] M. Kleiner: Patent EP 0 706 843 B1: Verfahren und Vorrichtung zur Herstellung von gekrümmten Werkstücken (1999).

[4] D. Arendes: Direkte Fertigung gerundeter Aluminiumprofile beim Strangpressen. Dr.-Ing. Dissertation (PhD-Thesis), Universität Dortmund, Shaker Verlag, Aachen 1999. ISBN 3826564421

[5] A. Klaus: Verbesserung der Fertigungsgenauigkeit und der Prozesssicherheit des Rundens beim Strangpressen. Dr.-Ing. Dissertation (PhD-Thesis), Universität Dortmund, Shaker Verlag Aachen 2002, ISBN 3-8322-0208-0.

[6] A. Klaus, D. Becker, M. Kleiner: Three-Dimensional Curved Profile Extrusion – First Results on the Influence of Gravity. In: Advanced Materials Research: Flexible Manufacture of Lightweight Frame Structures, Vol. 10 (2006), pp. 5-12, ISBN 0-87849-403-0.

[7] J. Fleischer, C. Munzinger, G. Stengel: Flying Cutting of Spatially Curved Extrusion Profiles. In: Advanced Materials Research: Flexible Manufacture of Lightweight Frame Structures, Vol. 10 (2006), pp. 5-12, ISBN 0-87849-403-0.

[8] J. Bickendorf: Automatic controller source code generation for Rounding during Extrusion. In: VDI-Berichte No. 1892 (2005) pp. 1061-1072, ISBN 3-18-091892-6.

[9] F. Ostermann: Anwendungstechnologie Aluminium. Springer Verlag 1998. ISBN 3-540-62706-5

Embedding of Alumina Reinforcing Elements in the Composite Extrusion Process

Daniel Pietzka[1,a], Marco Schikorra[1,b], and A. Erman Tekkaya[1,c]

[1]Institute of Forming Technology and Lightweight Construction,

University of Dortmund, Baroper Str. 301, 44221 Dortmund, Germany

[a]daniel.pietzka@iul.uni-dortmund.de, [b]marco.schikorra@iul.uni-dortmund.de, [c]erman.tekkaya@iul.uni-dortmund.de

Abstract. Extruded aluminum profiles are essential for lightweight constructions in contemporary transport and automotive applications. The reinforcement of such aluminum-based profiles with high-strength materials offers a high potential for weight reduction and an improvement of functional and mechanical properties.

In comparison to conventional composite extrusion using fiber or particle reinforced billets, the alternatively developed process for the embedding of endless reinforcing elements provides enormous advantages regarding extrusion forces, load-adapted reinforcement, and tool abrasion. In this extrusion process with conventional billets, modified tools with portholes are used to position reinforcing elements from outside the pressing tool and to embed them into the material flow during the pressing operation.

This composite extrusion process is part of the research work started in 2003 and carried out within the scope of the Collaborative Research Center SFB/TR10. To increase the potential of composite extrusion with endless reinforcing elements, the manufacture of composite extrusion profiles with high-strength non-metallic alumina wires is planned. Due to the wires' specific properties, e.g. high stiffness, their deflection behavior must be analyzed to guarantee a stable feeding-in process. In this paper the specific behavior of alumina reinforcing elements regarding the feeding-in process is analyzed by experimental investigations. The main influencing factors are determined and a process window is deduced.

Introduction

The production of composite extrusion profiles with continuous reinforcing elements, which are embedded in an aluminum matrix, is an innovative process for manufacturing structural components in automotive and aerospace engineering. A high-strength reinforcing material is inserted into the welding chamber in the form of metallic wires and the wires are bonded with the material flow during the extrusion process [1].

To increase the reinforcing effect and to reduce the weight still further, it is judicious to use non-metallic reinforcing elements which have a higher specific strength and stiffness than metallic components (Table 1). One possibility of combining the lightweight material aluminum with endless non-metallic components is provided by alumina fibers. However, on the one hand alumina fibers have a high tensile strength, but on the other hand the fibers are brittle and rough considering bending forces. During the composite extrusion process, the reinforcements are redirected before they reach the welding chamber. Because of the wire's material properties with the non-distinct plastic material behavior and the applied bending stresses, which arise during the feeding-in of alumina elements, experimental investigations are necessary to guarantee a stable infeed without tearing of the reinforcement.

Material	R_m [MPa]	E [GPa]	ρ [g /cm^3]	E/ρ [GPa· cm^3 /g]
Spring steel 1.4310 ($\varnothing$ 1mm)	> 1950	185	7.8	23.7
Nickel-based alloy ($\varnothing$ 1mm)	1300-1600	205	8.1	25.3
Alumina fibres	until 3100	until 400	4.0	until 100

Table 1: Mechanical properties of reinforcing elements [2]

Process Principle of Composite Extrusion

In the composite extrusion process, a homogenous billet is used as base material and the hybrid is formed inside a special tool by feeding a second material into the metal flow during the extrusion. The billet material splits in front of the sealing plate into upper and lower strands, which join again in the welding chamber (Fig. 1 left). The reinforcing elements are fed from the sides into the tool where they are deflected towards the press direction within a cartridge provided with channels, still separated from the billet material. The elements get in contact with the base material in the welding chamber where the two different materials bond under high pressure and temperature [3, 4].
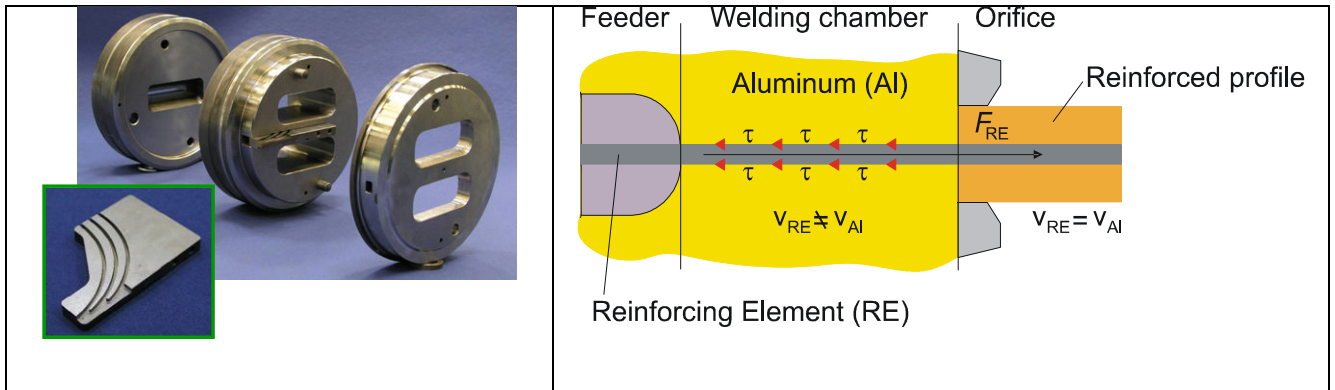
Fig. 1: Tool design and conditions in the welding chamber [5]

The reinforcing element is introduced at a 90° angle into the die (Fig. 1 left). Holes in the die direct the round reinforcement to integrate into the metal flow. During the extrusion process, no external force is needed to feed in reinforcing wires, because the metal flow leads to a tension stress in press direction on the wire surface [5] (Fig. 1 right).

To assure a stable manufacturing process of profiles with continuous reinforcing elements, it is important that the reinforcing wires are fed without tearing. In consequence of the redirection during the feeding, a bending moment appears on the wire. The occurring stresses for linear elastic loading depend on the radius of the cartridge channels, the diameter, and the Young's modulus of the used wires. The maximum bending stress σ_{max} of a wire with a circular cross section of the diameter d and the Young's modulus E, which is controlled via a cylinder with the radius r, can be calculated with the following equation [6]:

$$\sigma_{max} = \frac{E \cdot d}{2 \cdot r + d} \qquad (1)$$

If the bending moment exceeds the yield stress, a plastic deformation of the reinforcing element will occur. Especially the feeding-in of ceramic wires involves special demands due to the fact that they are less flexible than metallic wires which are used for composite extrusion. Moreover, a small bending radius can lead to the fracture of the element.

Behavior of Alumina Reinforcing Elements

Ceramic fibers can generally not withstand the occurring shear and tensile stresses during the extrusion process without prior preparation due to the lack of internal load transfer inside the fiber bundle. An advantageous arrangement for using non-metallic wires in composite extrusion is represented by fiber-reinforced metal matrix composite wires. Composite wires could serve as a reinforcing element providing internal load transfers and helping to overcome the disadvantages regarding the extrusion process of fiber bundles. The reinforcing ceramic fibers are embedded in a light metal matrix by a continuous pressure infiltration process before extrusion. In addition, using the same matrix material for the composite wire and the extrusion process should prevent problems at the interface between the surrounding base material and the composite wire [7].

The non-metallic wire for the experimental investigations was provided by the IWK1 (Institute of Materials Science and Engineering 1, University of Karlsruhe). The composite wire has matrixes of almost pure aluminum and was reinforced by infiltration with approximately 40 vol. % ceramic alumina fibers (Al_2O_3). The wire has a diameter of 1 mm and oval Nextel440 fibers were infiltrated.

To guarantee a stable feeding of the composite wire into the composite extrusion process, the deflection has to be determined. In experimental investigations, the force which is needed to pull the wire out of the cartridge was measured to evaluate the deflection ability of the reinforced wire. Because during the extrusion process, the metal flow leads to a tension stress in press direction on the wire which pulls the wires into the welding chamber. For the experiments, a special cartridge with different channels with milled radii from 20 mm up to 100 mm in steps of 10 mm was manufactured so that the behavior can be determined for a variety of channels. The resulting tensile force was quantified with a piezoelectric sensor (Fig. 2).
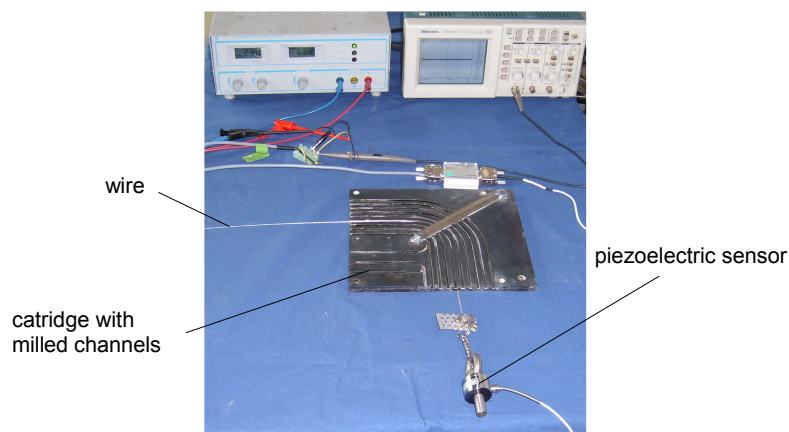
Fig. 2: Experimental set-up

The tests were done between room temperature and the maximal temperature of 500°C, which is equal to the maximally reached temperature inside the extrusion tool during the composite extrusion process. Because of the low dimension and the ambient aluminum matrix, the composite wire cools down to room temperature very fast so that the temperature-depending experiments were done inside a furnace. Fig. 3 shows the cooling behavior of the double composite wire.
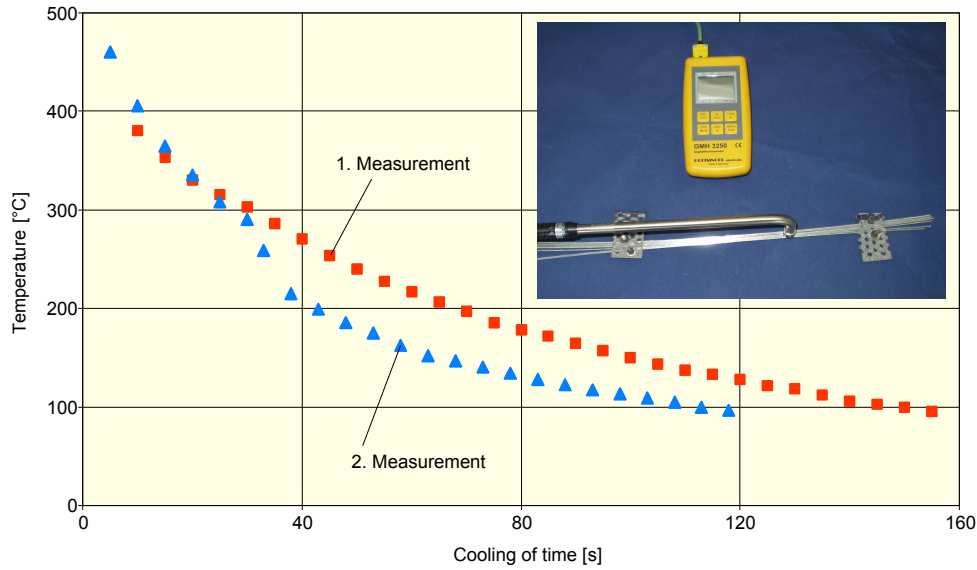
Fig. 3: Cooling behaviour

Fig. 4 shows the results of the measured forces which were needed to pull wires through the cartridge channels at room temperature. For comparison purposes, the experiments were also accomplished with spring steel (1.4310), which was already successfully used for the production of composite profiles with endless reinforcing elements. Per used wire and radius five tests were executed.
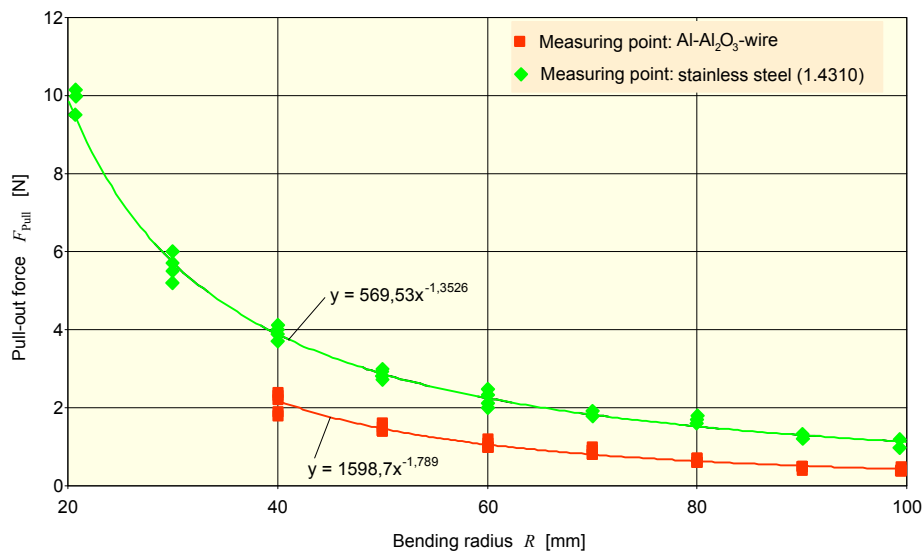
Fig.4: Pulling force at room temperature

The Al-Al$_2$O$_3$-wire breaks at cartridge radii less than 40 mm, as shown in Fig. 4. The spring steel was deflected without tearing for all tested radii and the needed forces were higher. Generally, the detected forces increased when reducing the radius of the supply channels. Analogue equation (1) the maximum stress raises with decreasing bending radius. The strength must be absolutely larger than the maximally reached bending stresses and the resulting friction forces so that the reinforcement wire will not break and can be supplied without failure. For aluminum-alumina composite wires with a fiber percentage by volume of 50 %, a tensile strength of approximately 1300 MPa can be expected [8]. Even at a temperature of 775°C, when the matrix is partially melted, strengths still ranging between 500 and 700 MPa are reached [9]. An accurate prediction of the wires' strength cannot be done because the amount of the ceramic fibers in the wires is not exactly known. The material properties in fiber direction strongly depend on the fiber quantity in relation to the total volume, the type of the fibers, and the characteristics of the fiber matrix connection and

vary accordingly in larger extent [9]. It is possible that small pores remained during the infiltration of the fiber bundle where the liquid matrix material was not able to penetrate and this phenomenon has a negative effect on the material properties of the wire [10]. Fig. 5 shows a polished micrograph section of the used Al-Al$_2$O$_3$-wire.
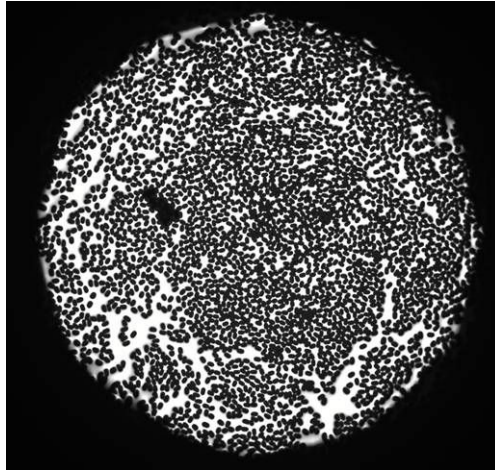
Fig. 5**:** Polished micrograph section (IWK1)

During the successive increase of the temperature, the aluminum base should weaken and permit small movements of the fibers, thus allowing a lower stress and pull-out force, which involves a better redirection ability. It cannot be assumed that the ceramic fiber bundles become more flexible at temperatures of up to 500°C because the melting point of alumina lies approximately above 2050°C [11]. Fig. 6 shows the results of the measurement up to a temperature of 200°C for a bending radius of 50 mm. The pull-out forces of the spring steel decrease continuously, which is a consequence of the falling Young's modulus. The Young's modulus of solid materials decreases usually with increasing temperature due to the decreasing atomic binding forces [12]. However, the composite exhibits another behavior, at first the pull-out forces became less, but in the further run of the curve the forces rise strongly. The minimum is probably due to the sinking Young's modulus, but the rise is justified by other effects, for example friction.
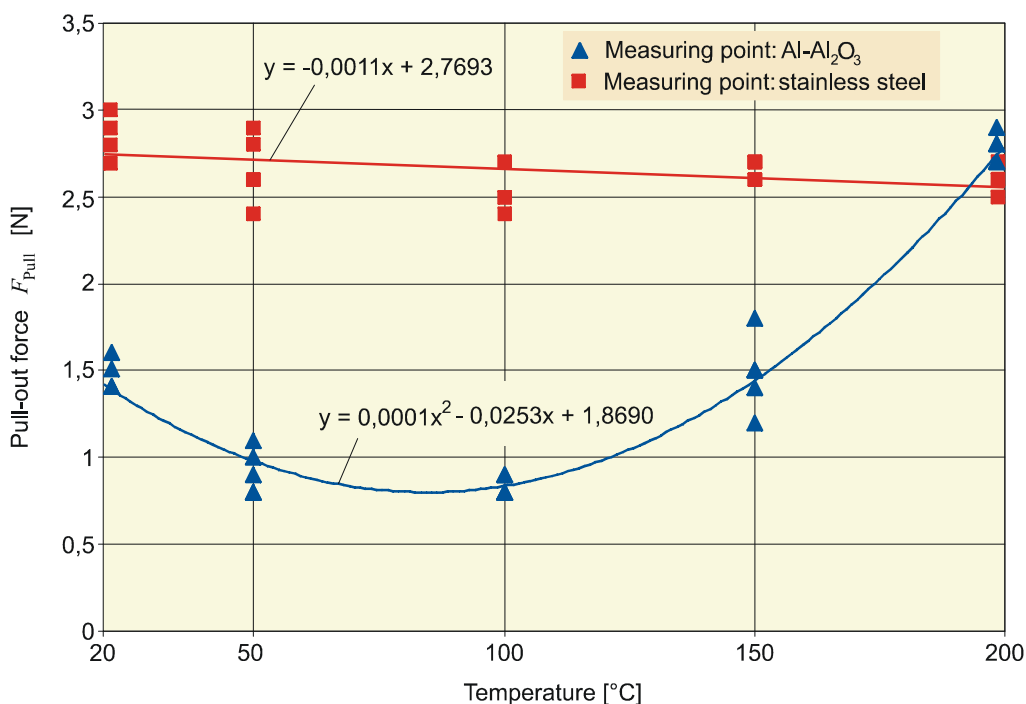
Fig. 6: Temperature-dependent deflection behavior up to 200°C

According to the friction model of *Coulomb,* the frictional force depends linearly on the regular force which affects the contact surface orthogonally. The regular force towards the supply channel bottom will not be considered by reason of the low death load of the composite wires. But the regular force in wall direction has an important influence on the friction due to the stresses. To analyze the influence of friction on the feeding-in process, tests with the lubricant boron nitride ($\alpha-$BN) to reduce the friction and without lubricants were made. Fig. 7 shows the results.

The use of the lubricant boron nitride reduced the pull-out force significantly. During the test, it was not possible to guarantee a continuous lubricant film. That is the reason why the composites broke above a temperature of 450°C. Moreover, the oxide skin of the aluminum matrix has a strong influence on the frictional forces [13]. A rise in temperature leads to the oxide skin getting larger, which results in an increase of the surface roughness and finally to higher friction forces.
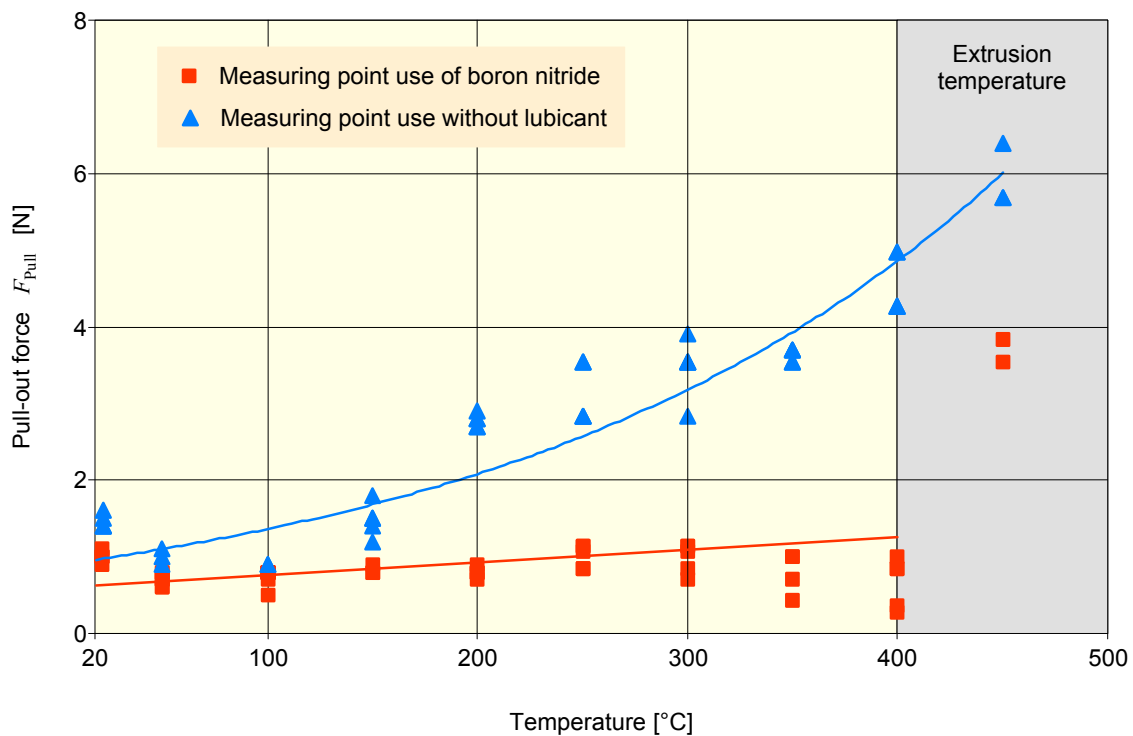
Fig. 7: Temperature-depending deflection behavior up to 500°C

Deduction and Analysis of a Process Frame

Influencing Factors. In the experimental investigations, only the break of composite wires appeared as observed disturbance. The reason for the break of the wires is stress above the maximum tensile and shear strength. The arising tensions depend directly on the bending radius of the cartridge, the tribological system, and the wire characteristics (Fig. 8). The friction, for example, can be reduced by a surface coating of the cartridge channels.
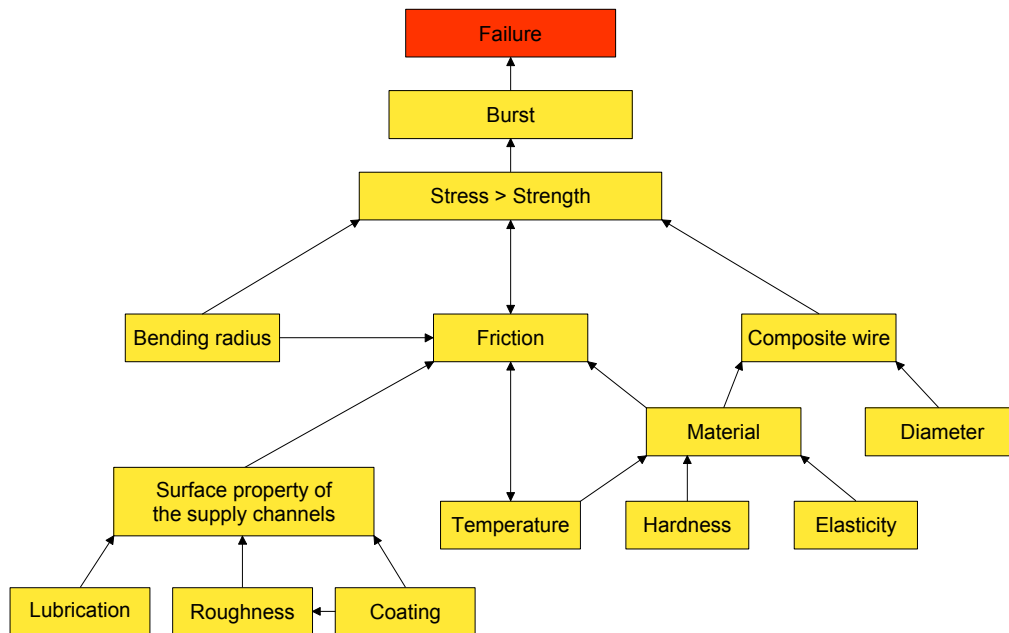
Fig. 8: Process-related influences

Process Window. Based on the pull-out test, a process window for the feeding-in of ceramic reinforced wires can be deduced. Fig. 9 shows a process window for a stable feeding-in process. For the composite extrusion process, only the range at temperatures between 400° and 500°C is relevant. The degradation of deflection characteristics during the rise in temperature is due to the increasing friction. To guarantee a high process stability, a minimum radius of 60 mm is needed. By the application of a suitable coating, the feeding-in up to a radius of 30 mm could be possible. But, on the other hand, a coating could be negative for the interface between reinforcing element and aluminum base, if the coating reached the welding chamber bounded to the wires.
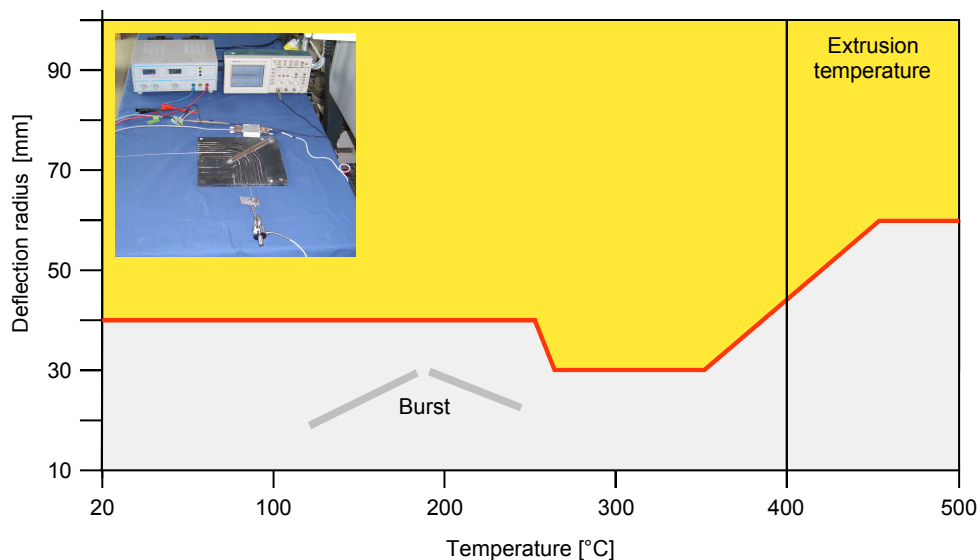
Fig. 9: Process window

Conclusion and Outlook

The production of continuously reinforced profiles by use of an aluminum matrix and reinforcing elements made of steel or ceramic wires offers a great potential for modern lightweight constructions. In addition, ceramic fibers feature a high specific strength and stiffness compared

with heavy metallic components. The feeding-in process of ceramic reinforcements demands specific requirements because of the high stiffness and brittleness. In the scope of the present paper, the deflection behavior of the composite wires was analyzed on the basis of the needed pull-out force. In general, the pulling force decreases with increasing radius. The deflection behavior also depends on the temperature, whereas friction has a great influence, too. Accordingly, a process window for a stable embedding could be deduced. At first, the rising temperature leads to decreasing process limits, but at temperatures above 350°C, the influence of the cumulative oxide skin dominates. To enhance the process limits, an adequate coating of the supply channels should be used to reduce negative tribological effects.

Acknowledgement

References

[1] Schomäcker, M.; Schikorra, M. Kleiner, M.:*4 Years of Research on Composite Extrusion for Continuous Reinforcement of Aluminum Profliles.* Conference: Aluminum Two Thousand, Florence, 2007

[2] Weidemann, K.: *Werkstoffsysteme für verbundstranggepresste Aluminiummatrixverbunde.* Shaker Publishing, Aachen 2007

[3] Klaus, A.; Schomäcker, M.; Kleiner, M.: *First Advances in the Manufacture of Composite Extrusions for Lightweight Constructions.* Light Metal Age Vol. 62 (2004), No. 8 pp. 12-21

[4] Aluminium Walzwerke Singen: *Verfahren zur Herstellung von Verbundprofilen sowie Vorrichtungen zu dessen Durchführung.* German Patent Application Publication DT 2414178

[5] Schomäcker, M.: *Verbundstrangpressen von Aluminiumprofilen mit endlosen metallischen Verstärkungselementen.* Shaker Publishing, Aachen, 2007

[6] Timoshenko, S. P.; Gere, J. M.: *Mechanics of Materials.* PWS Publishing, Boston, 1997

[7] Weidenmann, K. A.; Schomäcker, M.; Kerscher, E.; Löhe, D.: Kleiner, M.: *Composite Extrusion of Aluminum Matrix Specimens Reinforced with Continuous Ceramic Fibers.* Light Metal Age Vol. 63, (2005), No. 5 pp. 6-10

[8] Weber, L.; Canalis-Nieto, P.; Rossoll, A.; Mortensen, A.: *Fracture, Strength of Alumina Fibre Reinforced Aluminium Wire with and without a Torsional Prestrain.* In: Acta Mater., 2000

[9] Kientzl, Imre; Dobránsky, J.: *Production and Examination of Double Composites.* Material Science Forum Vols. 537-538 (2007), pp. 191-197

[10] Moser, B.; Rossoll, A.; Weber, L.; Beffort, O.; Mortensen, A.: *Damage evolution of Nextel 610 alumina fibre reinforced aluminium.* In: Acta Mater., 2004

[11] Kern, F.; Wenzelburger, M.; von Niessen, K.; Gadow, R.: *Stofflicher Leichtbau mit Sinterkohlenstoff und Verbundwerkstoffen.* Themenheft Forschung: Leichbau, University of Stuttgart, 2007

[12] Schatt, W.; Worch, H.: *Werkstoffwissenschaft.* 9. Edition, Wiley-Vch Publishing, 2002

[13] Lorenz, H.; Köhler, M.: *Experimentelle Untersuchungen der haftungsbestimmenden Mechanismen zwischen metallischen Körpern.* Vortragstexte des DGM-Symposiums: Reibung und Verschleiß, Editor: Fischer, A.; Wiley-Vch Publishing, 2000

Documentation of the Corrosion of Composite-Extruded Aluminium Matrix Extrusions using the Push-Out Test

M. Merzkirch[1, a], K. A. Weidenmann[1, b], E. Kerscher[1, c] and D. Löhe[1]

[1]Institut für Werkstoffkunde I, Universität Karlsruhe (TH), Kaiserstr. 12, 76131 Karlsruhe, Germany

[a]matthias.merzkirch@kit.edu, [b]kay.weidenmann@kit.edu, [c]eberhard.kerscher@kit.edu, [c]detlef.loehe@kit.edu

Abstract. A possibility to increase both stiffness and strength of aluminium-based structures for the application in lightweight profiles for vehicle space frames is the use of composite extrusions in which high-strength metallic reinforcements are incorporated. Within the scope of the present investigations, composite-extruded profiles with wire-reinforcements made of austenitic spring steel 1.4310 (X10CrNi18-8), in an aluminium matrix AA6060 (AlMgSi0.5), which were exposed to different corrosive media for different times, were characterised in terms of the debonding shear strength using the push-out-technique. The formation of a galvanic couple could be conceived mathematically in regard of terms describing the formation of a shear-impeding layer and the corrosive attack. Thereby the parameters for the different media could be determined.

Introduction

Aluminium and its alloys are highly qualified candidate materials for lightweight automotive constructions due to their low density in addition to the outstanding formability. If the designed space is limited, reinforced aluminium-matrix-based profiles present an attractive solution to increase both specific stiffness and specific strength. The bar extrusion technology represents a promising alternative to conventional casting techniques and is a solid state manufacturing route for composites. This can be realized in two different ways: first, the regular extrusion of discontinuously reinforced composite billets or, secondly, the composite extrusion of regular billets using modified extrusion dies which allow an in situ continuous reinforcement during the extrusion process. In the welding chamber of the extrusion press, the reinforcing elements, e.g. wires or ropes, are embedded into the matrix under high pressure at high temperature with controlled position inside the profile to optimize the load capacity [1].

Wire-reinforced composite-extruded aluminium matrix composites are appreciated as an efficient material concept. However, corrosive attack between the relatively basic matrix alloy and the electrochemically more noble reinforcing elements as a result of the electrically conductive contact could be a problem. Due to the formation of a galvanic couple, the interface between the composite components which is responsible for the internal load transfer between matrix and reinforcing component and finally important for the mechanical capability of the composite material is susceptible to enhanced corrosive attack.

In addition to the qualitative evaluation of the interface and the damage due to the corrosive load by means of classical metallographic analysis, the push-out test, first proposed by Marshall [2], offers a possibility to measure quantitatively the shear strength of the composite interface and its change as a function of time. By means of an indenter, one single reinforcement is loaded axially until damage of the interface occurs. Ideally the interface only experiences shear loads. Actually, due to the lateral expansion by the compression load, a certain normal stress occurs [3]. Neglecting this, the maximal debonding shear strength is calculated through the load maximum of the load-displacement curve (Fig. 1),

$$\sigma_{deb} = \frac{F_{max}}{\pi \cdot d \cdot h} \tag{1}$$

in the case of thin samples and by knowledge of the diameter of the reinforcing element and the thickness of the sample [3,4].
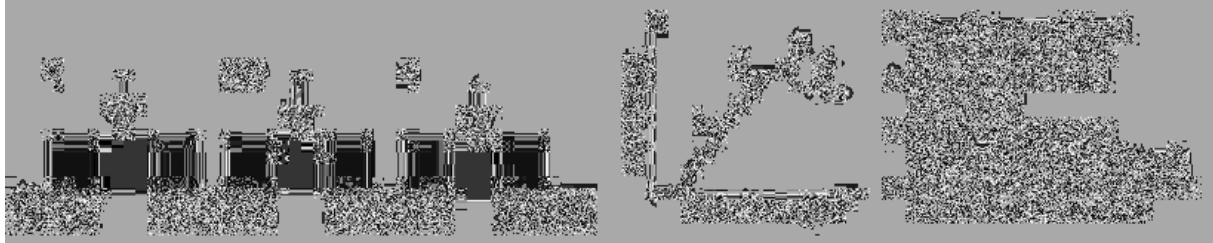
Figure 1: Functional principle and schematic load-displacement graph of
a fibre push-out-test   [4]

According to [5] the degree of corrosive damage can be quantified by the weight loss per time or the rate of surface attack. This is also valid for the change of tensile and fracture strength or yield strength with time. Within this work the time-dependent change of the debonding shear strength serves as a measure for damage evolution.

Based on a constant rate of corrosion with a simultaneous consideration of an eventual increase in the debonding shear strength by the formation of an oxide layer, which impedes the shearing, the following mathematical approach for the description of the change of the debonding shear strength is proposed:

$$\sigma_{deb}(t) = \sigma_{deb}^0 + A \cdot t^n - B \cdot t \tag{2}$$

Here, σ_{deb}^0 is the debonding shear strength at the beginning (without a corrosive load). The term $A \cdot t^n$ describes the potential formation of a shear-impeding layer; the term $B \cdot t$ describes a linear corrosion.

Experimental

Sample Materials. The analysed composite profiles with a rectangular cross section of 56x5 mm² were produced on a 10 MN bar extrusion press modified for composite extrusion. The profile was tempered in air directly after the bar extrusion thereby age hardening the aluminium matrix AA6060 (AlMgSi0.5) (naturally aged state T4). The reinforcing wires, made from stainless austenitic spring steel, 1.4310 (X10CrNi 18-8) had a diameter of 1 mm. The wires were cleaned with acetone prior to the bar extrusion. The ram speed of the plunger of the bar extrusion machine was 1 mm/s at a press ratio of 1:60. The samples for the push-out test, which were cut on a precision cut-off machine, had a thickness of 1 mm.

Experimental setup. The corrosion tests were realised in special multi compartment cases. Fig. 2 shows the experimental setup. The outer case was filled with the corrosive medium in which compressed air was blown through a frit to assure an adequate bath movement. A smaller inner case, having many holes to assure the circulation of the medium and in which the push-out samples were situated, hung in the large outer case.

Figure 2: Multiple chamber case for corrosion tests: overview (left), detailed exposure of the periphery of the sample

Four corrosive media were used: commercial deionised water (H_2O), a 2 % common salt solution (NaCl), a 2 % caustic soda solution (NaOH) and a street dirt suspension after DIN ISO 9462 (street) [6]. The last one also contained 0.6 % common salt and served for the simulation of a contamination, as it appears for the application of composite materials in road traffic. The caustic soda was chosen to attack the aluminium. The common salt should mainly act on the spring steel, which is, due to its composition, not saltwater-proof. The deionised water served as a neutral reference solution. The air stream through the chamber was regulated with an analogue flow measuring device to constant 3 l/min. Altogether 36 samples were exposed to each medium. 12 samples each were taken out after 10 h, 100 h and 1000 h, and the debonding shear strength was characterised with the push-out-test. For determining σ^0_{deb}, the debonding shear strength of samples without any corrosive load was measured. The push-out tests were carried out on a universal testing machine because of the relatively large diameter of the wire requiring high loads. The universal testing machine had a registration hardness probe with a cone shaped indenter and a calotte point [7]. From the measured force maximum the debonding shear strength was determined with Eq. 1. Directly after reaching the decrease of the force (see Fig. 1) the test was interrupted to avoid failure of the interface region by penetration of the cone shaped indenter. The damaged push-out samples were investigated metallographically.

Results

Change of the debonding shear strength. The change of the debonding shear strength depending on the exposure time to the medium is shown in Fig. 3. It is noticeable that for every medium the debonding shear strength values after 10 h of exposure time in relation to the reference debonding shear strength σ^0_{deb} increase slightly. After 100 h only the debonding shear strength values of in NaOH exposed samples decrease in relation to the value of 10 h. After 1000h the samples which were exposed to deionised water show only slight changes while the reduction of the debonding shear strength of the other samples is significant. The debonding shear strength of those samples which were exposed to NaOH could not be determined because the aluminium matrix was completely severed.
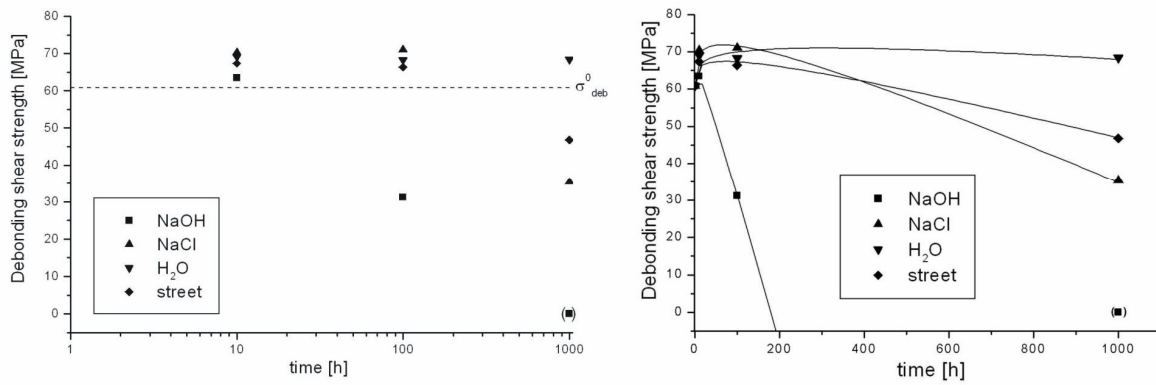
Figure 3: Averages of the debonding shear strength of the spring steel reinforced profiles after being exposed to different media (logarithmic scale, left side) and interpolated curve
(linear scale, right side).

The evolution of the debonding shear strength was described mathematically with a parabolic growth of the oxide layer (n=0.5), at first. However, Table 1 shows that the corrosion rate B is influenced by the growth of the oxide layer, see Eq. 2.

Table 1: Parameters for the description of the debonding shear strength

Medium	n = 0.5		n = 0.25	
	A	B	A	B
H_2O	1.24	0.03	3.24	0.01
NaOH	2.26	0.52	3.83	0.42
NaCl	2.07	0.02	5.16	0.06
street	1.19	0.05	3.05	0.03

Indeed the medium NaOH has the highest B-value (the strongest decrease), which is approved by Fig. 3. In comparison to the B-value of the distilled water and the street dirt suspension the value of the medium NaCl seems to be too small. The presumed linear corrosion process is better described when a parabolic growth of order 4 (n=0.25) is assumed. There, the corrosion rate B increases in the range H_2O – street – NaCl – NaOH, as observed for the debonding strength in the push-out tests. The linearly applied data is shown in Fig. 3 and interpolated with the help of the parameters in Table 1 (n=0.25). For the calculation of the above mentioned parameters the value of the medium NaOH for 1000 h is disregarded, because no debonding shear strength was measured.

A good accordance between the measured data and the interpolated curves is given with Eq. 2 using n=0.25.

Metallographic investigations. Comparing the surfaces of the samples which were exposed for 10 h, every sample type shows the same. Compared to an unexposed sample the surfaces of all exposed samples are tarnished. Fig. 4 shows this with an example of 2 samples, which were exposed for 10 h to a common salt solution and a street dirt suspension, respectively.
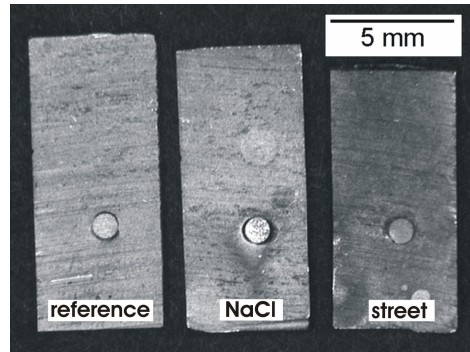
Figure 4:Macroscopic images of the surfaces of the samples after 0 h exposure time (left) and after 10 h exposure time to NaCl (middle) und street dirt suspension (right).

The development of the damage is shown in transverse sections prepared after the push-out tests. As expected, the damage is concentrated on the interface between wire and matrix [8,9]. The wire itself does not show any corrosion traces in any medium. Far from the interface the matrix is only slightly corroded, with the exception of samples exposed to NaOH. There, a global etch attack comes up on the aluminium, which finally leads to a dissolution. Fig. 5 shows exemplarily the development of the damage on samples exposed to NaCl.
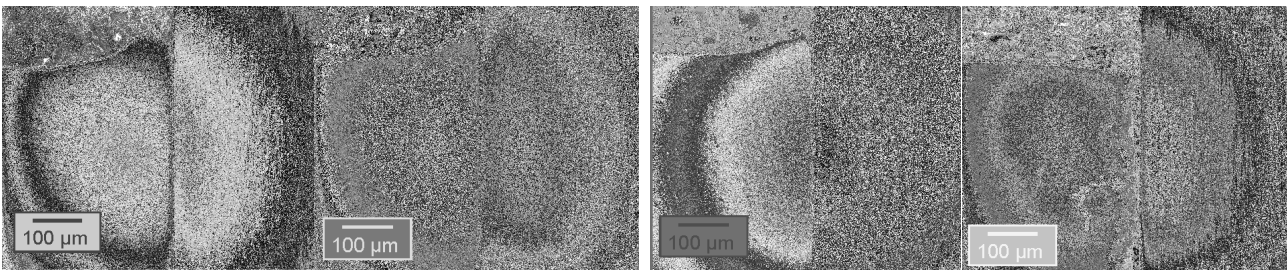
Figure 5: Transverse sections of pushed out samples after 0 h exposure time and after 10 h, 100 h and 1000 h exposure time to NaCl (f.l.t.r.).

Additionally, the comparison of a sample exposed 100 h to deionised water with a sample exposed to NaOH for the same time shows the degree of damage, Fig. 6.
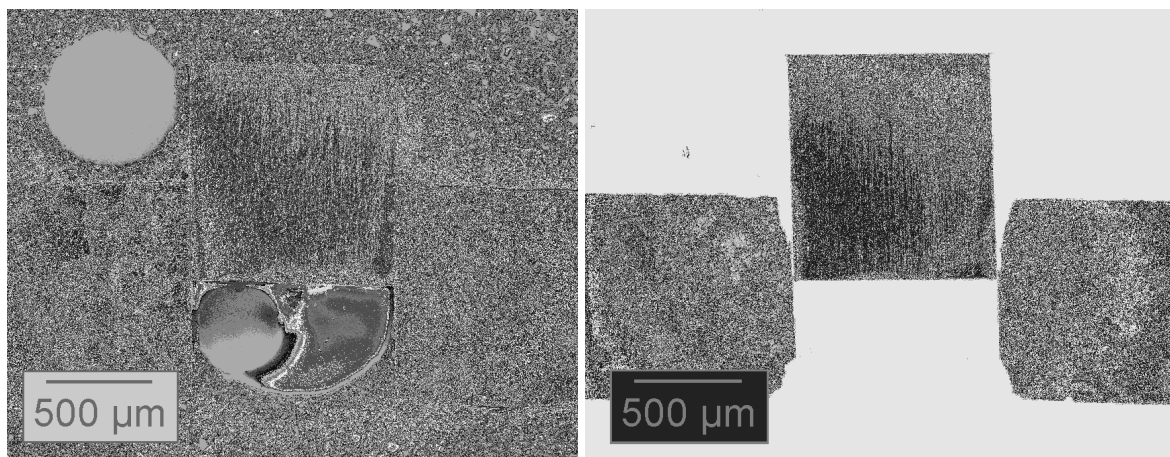
Figure 6: Transverse sections of pushed out samples after 100 h exposure time to H_2O (left) and to NaOH (right).

Summary

The investigations showed that corrosion damage appears in the investigated compounds by forming a galvanic couple between the matrix (AA6060) and the wires (1.4310) during the exposure to different media according to [8,9]. This can be quantified with the push-out test. Thereby the damage or the corrosion rate respectively is dependent on the used medium and increases in the range H_2O – street – NaCl – NaOH. The change of the debonding shear strength with the exposure time could be quantitatively expressed by

$$\sigma_{deb}(t) = \sigma_{deb}^0 + A \cdot t^{0,25} - B \cdot t \tag{3}$$

For every medium the debonding shear strength increases at first. This may be ascribed to the influence of the forming tarnishing layer, which is very thin and hardly to recognize under the light microscope. By comparison of the medium street dirt suspension and NaCl with respect to the corrosion rate B, a ratio of 1:2 exists, whereupon the ratio between the NaCl concentrations is 1:3.33. The damage must be led back to other mechanisms in the case of the street dirt suspension. All in all, only long exposure times or a very strong corrosion impact of the medium (NaOH) lead to a clear reduction of the debonding shear strength. The decrease can be traced back to the removal of the matrix material. In the case of the sample which was exposed 100 h to NaOH, the supporting interface had only half of its initial length – consistently the debonding shear strength should be reduced to about 50 %, as was approved by the measurements.

Overall, it can be summarized that the damage starts from the front surface - and therefore on a real lightweight structure of composite profiles from the exposed side. Therefore the critical damage of the bearing structure through corrosion is excluded or avoidable by protective coatings.

References

[1] M. Kleiner, M. Schomäcker, M. Schikorra, A. Klaus, Mat.-wiss. u. Werkst. Vol. 35/7 (2004), p. 431-439.

[2] D. B. Marshall, J. Am. Ceram. Soc. Vol. 67 (1984), C259-260.

[3] T. W. Clyne, P. J. Withers, *An Introduction to Metal Matrix Composites*, Cambridge University Press, Cambridge, Great Britain, (1993)

[4] J. Janczak, R. Stackpole, G. Bürki, L. Rohr, 17th Int. SAMPE. Basel, Schweiz, (1996)

[5] E. Mattsson, *Basic Corrosion Technology for Scientists and Engineers*, IOM Communications, London, Great Britain, (2001)

[6] DIN ISO 9462, *Skibindungen für den alpinen Skilauf – Sicherheitstechnische Anforderungen und Prüfungen*, Beuth-Verlag, Berlin, (2004)

[7] K. A. Weidenmann, C. Fleck, V. Schulze, D. Löhe, in: M. Schlimmer, *Verbundwerkstoffe und Werkstoffverbunde*, DGM-Matinfo-Verlag, 45-50, (2005)

[8] J. J. Theler, A. Wagner, A. Ames, *Herstellung von Aluminium/Stahl-Verbundstromschienen mit metallurgischer Bindung,* Metallwissenschaft. und Technik 3, 223-227, (1976)

[9] A. Wagner, U. Hodel, *Aluminium-/Stahl-Verbundprofil mit metallischer Bindung zwischen Stahl und Aluminium,* Metallwisschenschaft und Technik [2] 147-151, (1979)75

Accuracy of a Flying Cutting Device

Christian Munzinger[1,a], Juergen Fleischer[1,b], Gregor Stengel[1,c],
Markus Schneider[1,d]

[1]wbk Institute of Production Science, Universität Karlsruhe (TH),
Kaiserstr. 12, D-76131 Karlsruhe, Germany

[a]munzinger@wbk.uka.de, [b]fleischer@wbk.uka.de, [c]stengel@wbk.uka.de, [d]schneider@wbk.uka.de

Abstract. The prototype for the flying cutting of spatially curved extrusion profiles developed as part of the Collaborative Research Center Transregio 10 (SFB/TR 10) was tested as an integrated part of the overall system in first test runs. The profiles resulting from this process give proof of the potential involved in both, the novel curved profile extrusion (CPE) and the automatic supporting and cutting device. For subsequent automated processing to become possible, however, the reliably achievable accuracy of extruded profiles needs to be further improved. By the example of the extruded profiles produced so far, this article discusses potential factors that may impair profile accuracy and presents approaches and methods for the improvement of accuracy.

Introduction

The previous grant period of the Collaborative Research Center Transregio 10 (SFB/TR 10) was dedicated to a study of the theoretical basics and the elaboration of concepts for a process chain for the flexible production of three-dimensionally curved aluminium profiles.

During the first phase of the Collaborative Research Center Transregio 10, subproject A4 conceived and implemented a prototype for a cutting and guiding device required for the novel "multi-axis CPE" [1]. The prototype of the system includes a so-called flying saw and a transfer tool, which are used as tools for a standard industrial robot (Figure 1). The prototype of the flying cutting device allows for the guiding and cutting of three-dimensionally curved profiles [2]. The production of spatially curved profiles requires the relevant forces of gravity and acceleration to be absorbed by the flying cutting device in order to prevent undesired deformation that might otherwise be caused by these forces. Neither may there be any influences resulting from the cutting process that affect the profile during manufacturing. Besides, accelerations and velocities higher than in mere robot applications can be achieved through the use of highly dynamic additional axes in the tool of the flying saw und the transfer tool. The transfer tool allows the semi-automatic transfer of the cut profiles to other machining points [3].
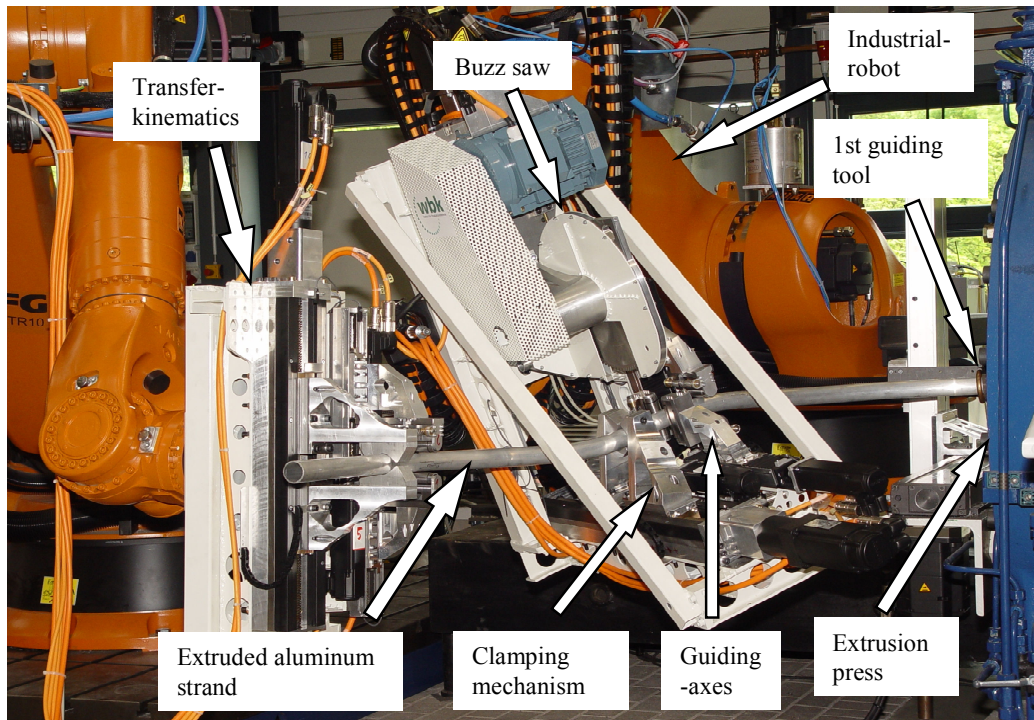
Figure 1: Prototype of the flying cutting device (wbk, iul) [2]

All kinematic mechanisms involved in the production process need to be operated synchronously in terms of their movements in order to guarantee the reactionless support of the profile during the actual production process. In case of the prototypically implemented system presented here, this is ensured through a primary NC control. The NC control takes care of the synchronous activation of all kinematic mechanisms involved in the process on the basis of its design as an electronic transmission. During this process, the NC control transfers the reference paths identified in an offline programming environment to the respective axes in real time [4].

In the summer of 2006, the overall system comprising both the extrusion press and the guiding tool belonging to subproject A1, "multi-axis CPE", which is located in Dortmund, and the flying cutting device and kinematic transfer mechanism from subproject A4, located in Karlsruhe, was set up in a process chain for the first time. In first tests, the functionability of this concept regarding the production of aluminium extruded profiles was proved.

Motivation and Objective

The initial focus during the first grant period was the verification of the feasibility of the fly-cutting process. Towards the end of the first grant period, first trials with the overall system produced extruded profiles which were measured in order to determine the profile contour accuracy achieved so far. The measurements were performed with a coordinate measurement arm. The identified actual profile contour data was then compared with the reference contour from the CAD. The deviation of the measured profiles as compared to the reference geometry was measured at 14 measuring points for the purpose of evaluation. Figure 2 – top shows an example of a measured profile in comparison with the reference contour. A summary of the other results can be seen from Figure 2 – bottom.
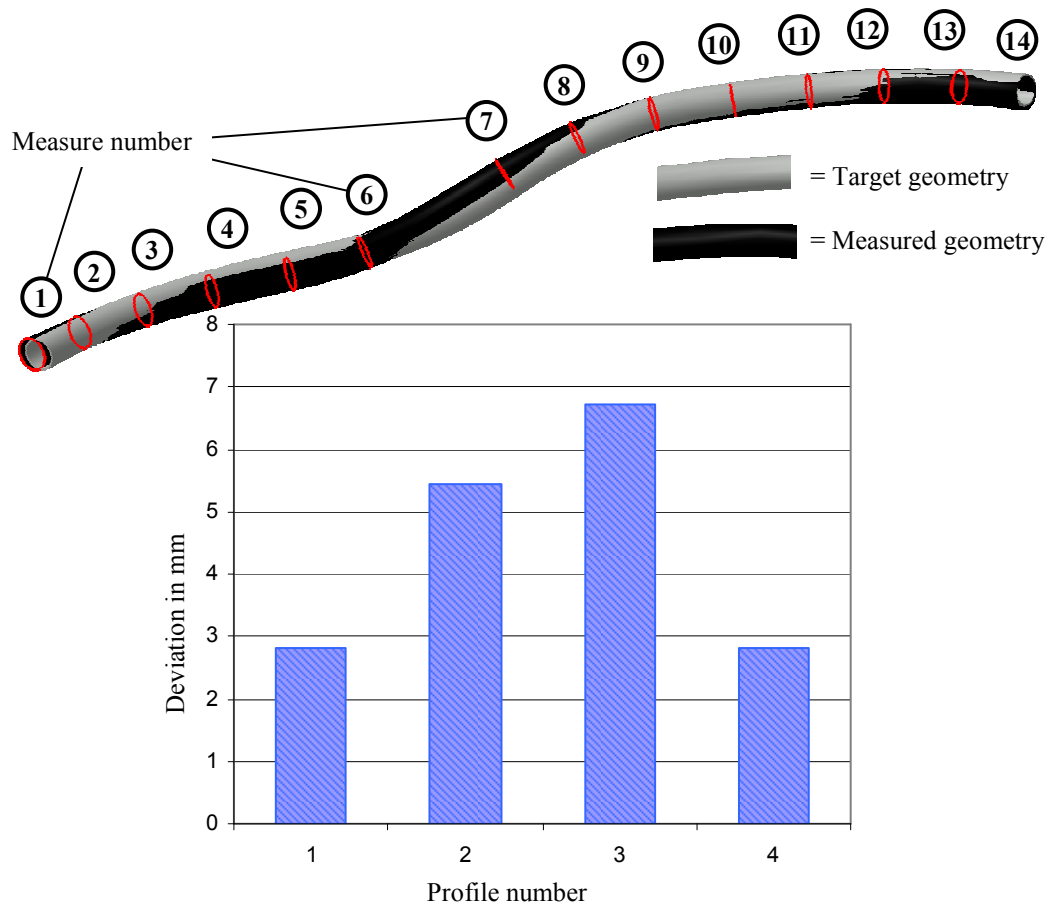
Figure 2: Measured profile contour (above, wbk), summary of measurements (below, wbk)

The deviations shown by the extruded profiles resulting from the process chain of the subprojects A1 and A4 combined are similar to the contour deviations of the extruded profiles that have so far been produced by subproject A1 with manual support of the profiles [5]. The medium error in terms of contour deviation across all measured profiles amounted to a deviation of 4.5 mm for a profile length of approx. 1400 mm and a radius of 560 mm.

The current funding period is aimed at increasing the accuracy of the profile contour, because the accuracies achieved with the flying cutting device so far are insufficient for subsequent automated machining processes. For this goal to be achieved, the first step to be taken is a detailed analysis of the entire process. To that end, preliminary investigations are required to identify the boundary conditions during the operation of the flying cutting device and to determine the main influencing factors affecting the accuracy of the profile contour. Based on the results of the analysis, concepts for the calibration of the flying cutting device and the kinematic transfer mechanism are then conceived and implemented.

Influencing factors

Studies of the overall system facilitate the identification of a high number of factors impairing accuracy that result from various system components. Some of these factors regarding CPE have already been presented in [6] and [7]. The effects of gravity and profile cantilever length on profile contour deviation were studied. Besides, a first estimation regarding the possible effects of tilting the first guiding tool was carried out. There are additional influencing factors for the overall process and the flying cutting device that can be seen from the following fault/effects diagram (see Figure 3).
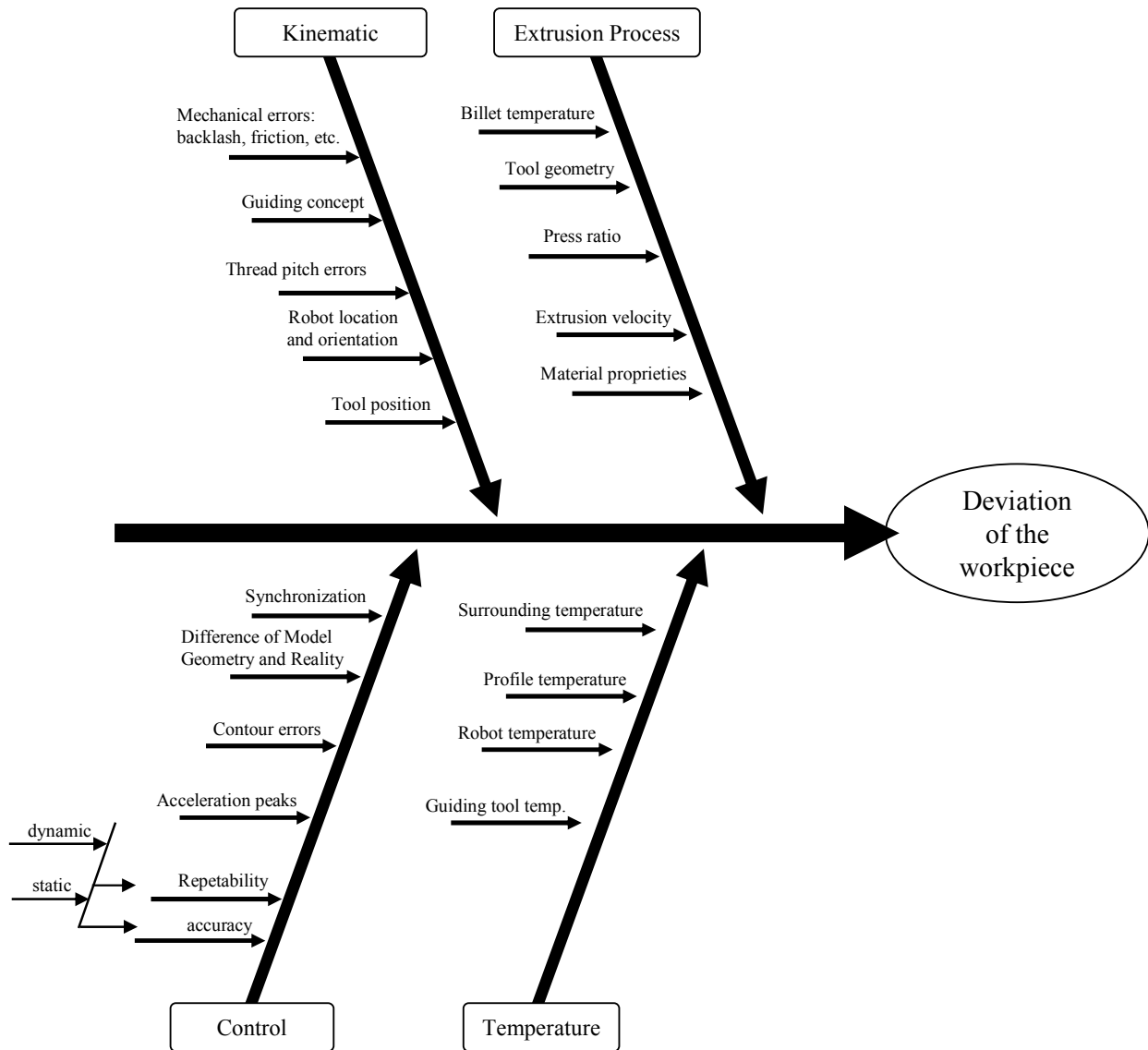
Figure 3: Fault/Effects diagram (wbk, following [6], [7], [8])

The factors affecting contour accuracy can be grouped in four error categories: kinematic mechanism, extrusion process, control and temperature. The enumeration of these influencing factors does not imply a rating in terms of either significance or quantitative effect of the contour deviation in case of occurrence of the respective error. The next working steps, therefore, consist in the identification and evaluation of the individual influencing factors. Subsequently, suitable methods for error compensation are to be elaborated and implemented.

Influences resulting from the kinematic mechanism such as an inclination of the robots or the guiding tool can be identified by adequate measuring methods. These usually repeated errors can then be minimized by an exact positioning of the components or by adjusting the control model.

The trials and operations presented in this article relate to the identification of the statistic and temperature-induced deviations of the employed kinematic mechanisms. Following projects shall deal with other influencing factors such as control and thermal workpiece deformation.

Static deviations of the kinematic mechanism

For the identification of deviations at the TCP (Tool Center Point) of the flying cutting device, a laser tracker was used to record a point grid with a spacing of 100 mm between each point and a measuring envelope of LxWxH = 1000 mm x 1000 mm x 800 mm in front of the extrusion press. For the calibration of the measuring envelope, the zero level and the corresponding Cartesian coordinate system were determined on the basis of three calibrated points. Subsequent measurements were carried out in the envelope that had thus been calibrated. The deviations identified for the measuring envelope can be seen in Figure 4.
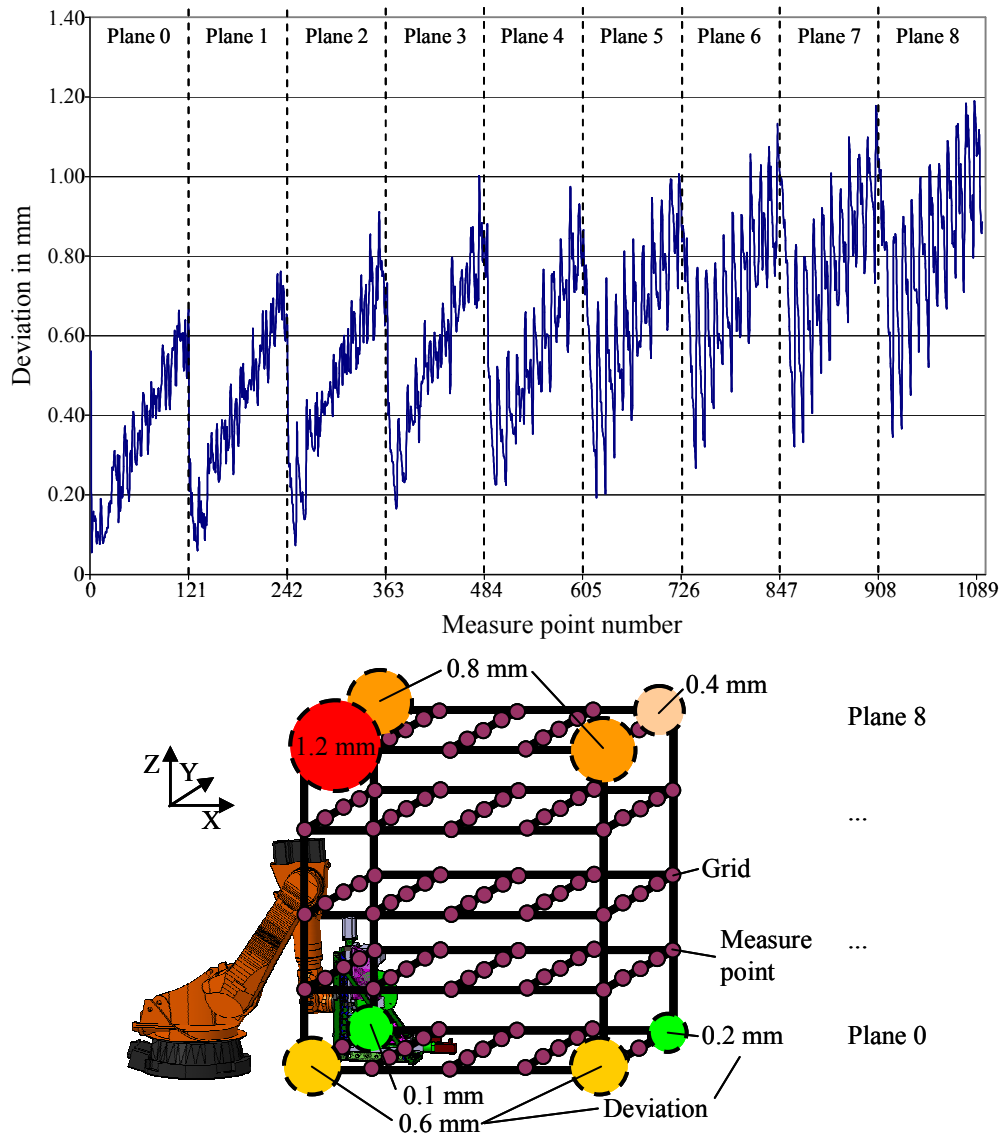
Figure 4: Identified absolute deviations in a measuring envelope of 1000mm x 1000mm x 800mm (wbk)

The distribution of individual errors shows growing position deviations with increasing distance in x, y and z directions. The absolute deviations from the actual positions amount to 1.2 mm in the upper section of the measured space (see marking Figure 4, bottom) and to up to approx. 0.6 mm in the lower section. The absolute deviation is calculated on the basis of the respective reference and actual components of the measurement values according to the following formula:

$$Error\_Absolute = \sqrt{(x_{nom} - x_{act})^2 + (y_{nom} - y_{act})^2 + (z_{nom} - z_{act})^2}$$ **Formula 1: Absolute error**

The measurements substantiated a significant deviation of the actual position of the TCP of the flying cutting device regarding the absolute position. A compensation of these errors is indispensable if high accuracies of the profile contour should be achieved.

An approach to the compensation of static deviations

[9] and [10] present different methods for the achievement of industrial robot accuracy increases through calibration. Basically, these methods can be subdivided into numerical or data-based calibration and model-based static and dynamic calibration. A model-based static calibration is already performed by the robot manufacturer. One approach to a further increase of profile accuracy is, therefore, data-based or numerical calibration of the control and the overall system on the basis of correction values for path generation. Improving the system's accuracy by this method, the three-dimensional working envelope is first subdivided into a grid structure. Afterwards, the respective position offset between reference and actual position can be determined for each grid position. By interpolating between the grid points the intermediate errors can be described, too. This method is mainly used for the calibration of machine tools because of the cartesian arrangement of axes which impedes any alteration of main axis orientation. With regard to the flying cutting device, the working envelope in front of the extrusion press can be assumed to be very limited because of the restrictions resulting from the CPE. The possible axis positions of the industrial robots are also limited by CPE, which allows good results through numerical calibration according to [11], too.

The identified measurement values may now be used as a database for the creation of an error model. This error model can then be used for a numerical calibration of the motion paths of the flying cutting device. To that end, for the correction of the paths generated offline in accordance with the deviations identified with the error model, an additional process can be added after the path generation for the fly-cutting. The updated reference lists are then used by the primary NC control for control of the system.

Influences resulting from a temperature increase caused by the extrusion press

Temperature influences on the industrial robots and the guiding tools represent another cause of contour deviations on the profile accuracy. The extrusion process is based on an aluminum forming process at high temperatures of 450 °C. Due to their position right in front of the extrusion press, the industrial robots and guiding tools used operate in an inhomogeneous temperature field and are heated from one side. Besides the intrinsic heating of the industrial robot in operation, the resulting deformation represents another source of errors regarding path deviations. One specific particularity of the CPE is significant when it comes to analyzing the thermal deviation behavior. Although the required robot path depends on the intended workpiece geometry, the probability of the robot being in front of the extrusion press is very high. In this section, any position deviations of the industrial robot have got a particularly high impact on the contour accuracy of the profiles because of the leverage effect in that area.

In order to reduce deviations in this working envelope, a robot position suitable with regard to thermal aspects was chosen in a first step. It is important to keep the distance between the flying saw and the robot base as small as possible. Furthermore, the height of the cutting device is supposed to match the height of the robot base as much as possible to allow the thermal expansions of both oscillations in z direction to compensate each other to the largest possible extent.

In order to examine the influences of this process-induced heating on the industrial robots in a second step, the robot cell for fly-cutting was additionally equipped with a heating zone used to simulate the temperature generated by an extrusion process in the industrial environment. The heat-

ing zone consists of several ceramic heating elements connected in series which are continuously adjustable to temperatures from 20 °C to 750 °C. The heated section of the heating zone is approx. 1100 mm x 900 mm large, and, thus, corresponds to the area used for the extrusion press of the Collaborative Research Center.

The pilot testing performed as part of subproject A1 identified the following temperatures at the actual extrusion press during operation:

Measuring Position	Temperature
Surface Temperature of Press	80 °C
First Guiding Tool	45,3 °C
500 mm behind First Guiding Tool (Air Temp.)	30,7 °C
1000 mm behind First Guiding Tool (Air Temp.)	28,3 °C
1500 mm behind First Guiding Tool (Air Temp.)	26,6 °C
Room Temperature	24,4 °C

Figure 5: Temperatures in the periphery of the extrusion press (iul/wbk)

According to these results, the air temperature in the periphery of the robot, which is situated about 800 mm away from the extrusion press, exceeds the regular room temperature by approximately 10 K. In order to simulate the heat generated by the extrusion press, the heating zone was set to 100 °C surface temperature. At a distance of 450 mm from the heating zone, the temperature increase amounted to approx. 7 K at a level of 400 mm above the floor, whereas 1350 mm above the floor it was 13 K. 1500 mm away from the heating zone, the temperature increase was still approx. 2 K at a level of 400 mm above the floor.

The industrial robot and the flying cutting device were then equipped with 45 temperature sensors to measure the surface temperature of the components. A 60-channel temperature measurement module designed for relative measurements was used for temperature sensing, allowing a 6-second cycle of measuring-data acquisition with a resolution of 1/10 °C.

In order to measure TCP displacement and an alteration of the absolute and repetitive accuracies during operation of the flying cutting device with partial temperature impact, a point grid with a spacing of 400 mm between measuring points was approached periodically with the industrial robot in continuous operation within a working envelope of LxWxH = 800 mm x 800 mm x 800 mm in front of the heating zone. The x, y and z position of the TCP were identified by means of a laser tracker by the Faro company. The positions approached with the robot correspond to a working envelope in front of the extrusion press that is particularly important for compensation. Simultaneously, the temperature changes at the measuring points were recorded. **Figure 6** shows the setup of the test rig.
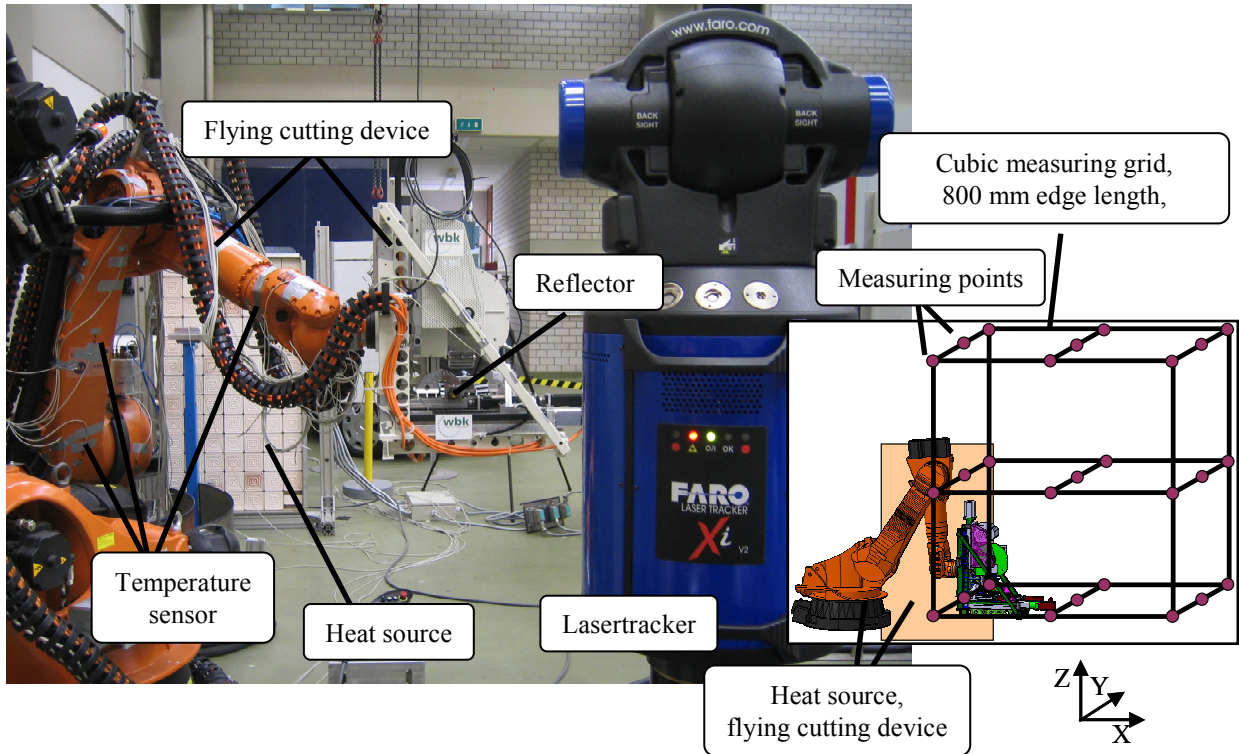
Figure 6: Test rig for the simulation of the temperature impact (wbk, left),
schematic illustration of the measured points (wbk, right)

The measurements were discontinued once stable temperature conditions had been achieved, i.e. after approx. 6 hours. The results showed a maximum temperature increase of approx. 9 K at the robot and the flying cutting device in the upper section of the tool. Temperatures were generally higher in the front section of the system, which can be explained by the affected parts being exposed to direct radiation emanating from the heating zone. **Figure 7** provides a summary of the results of the temperature increase at the side facing the heat source (front side).
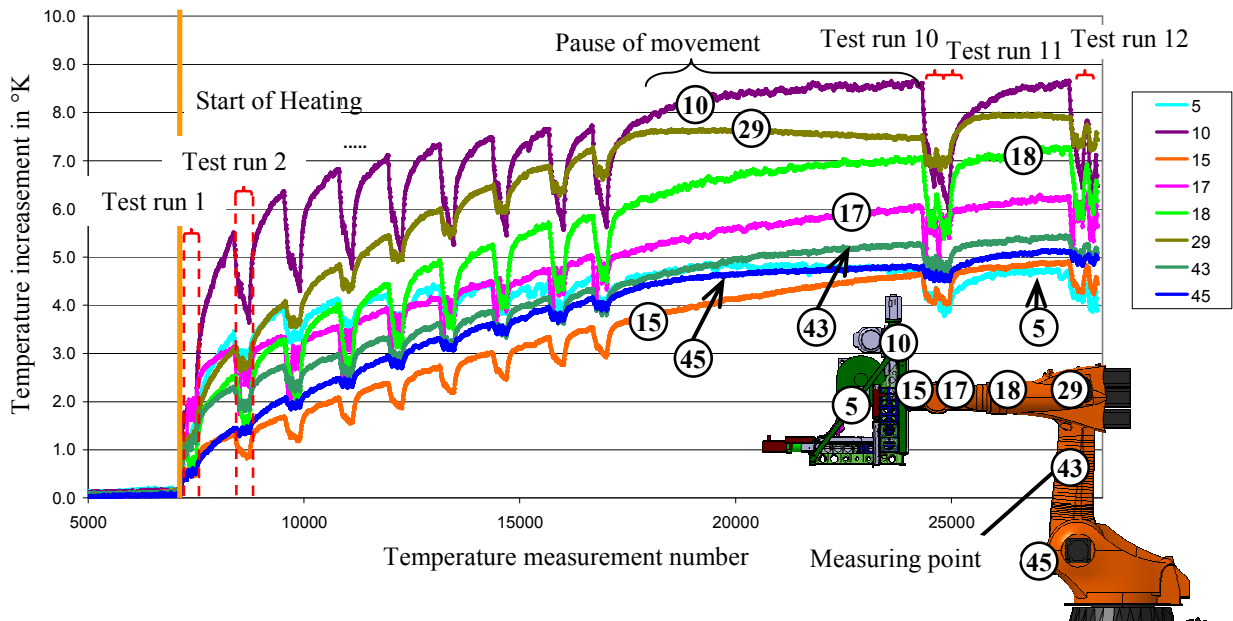
Figure 7: Temperature measurements, partial heating, front side (wbk)

The sawtooth-shaped temperature changes displayed in Figure 7 result from the measurement motion of the robot when recording the grid points. During the 5-minute long measurement motions, temperatures decrease by a maximum of 2 K each, whereas the temperature continues to in-

crease during the 15 minute break between measurements while the robot is positioned in the starting spot in front of the heat source. Between measurements 9 and 10 there was a 45 minute break, and there was another 30 minute break between measurements 11 and 12.

The temperature development along the upper robot arm includes measuring points 15, 17, 18 and 29, the maximum temperature increase being 8 K. Along the lower arm including measuring points 43 and 45, temperatures exceed the initial value by up to 5.2 K. The temperature at the saw frame amounts to approx. 8.8 K at measuring point 10 and approx. 4.5 K at measuring point 5 in the steady-state condition. **Figure 8** shows the temperatures on the back side facing away from the heating zone by way of comparison.
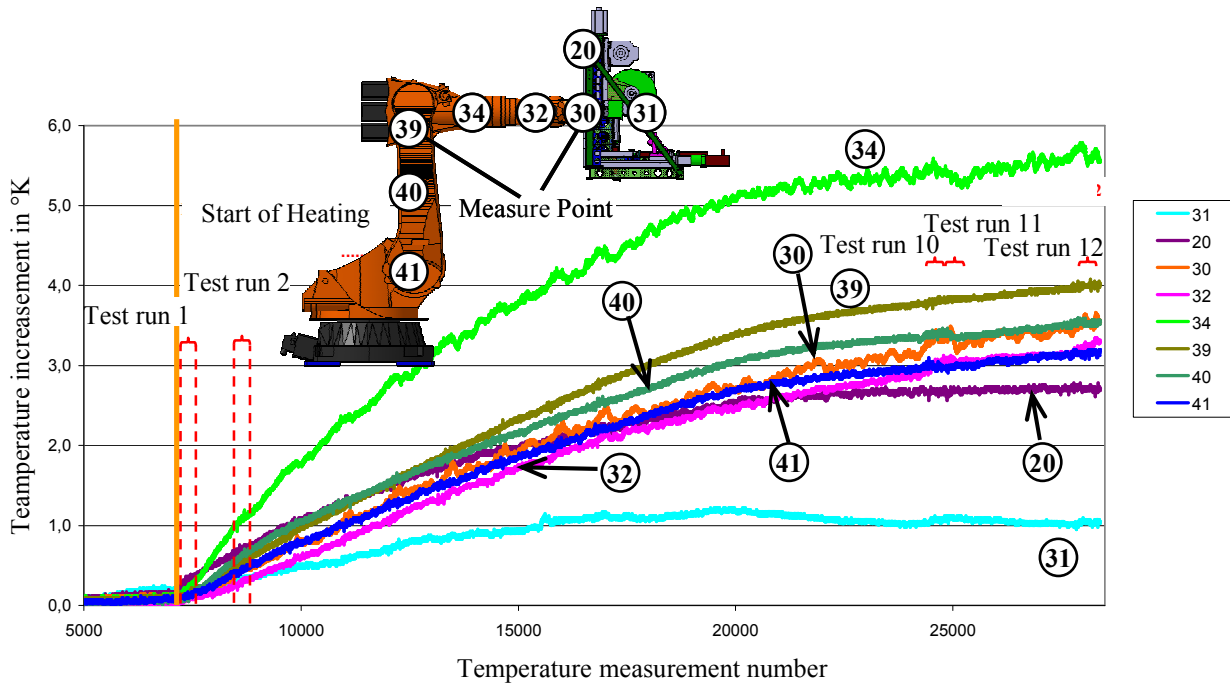
Figure 8: Temperature measurements, partial heating, back side (wbk)

The component surface temperature was generally lower on the back side than on the front side. There was no drop of temperatures during measurement motions like the decrease identified on the front side. Temperature distribution along the upper robot arm, beginning at the flange, exceeded the initial temperature by up to 5.8 K at the end of the measurements. Along the lower robot arm, the temperature increase amounted to a maximum of 4.0 K as compared to the initial temperature. The temperature at the saw frame had increased by approx. 2.8 K at measuring point 20 and by approx. 1 K at measuring point 31 at the end of the measuring process.

The measured temperature difference between front and back side of the robot amounted up to 4 K between measuring points 29 and 39. The maximum difference between front and back side at the fifth axis of the robot was approx. 2.9 K right at the upper robot arm. The difference at the remaining measuring points was between 1.3 K and 1.8 K. The temperature difference between measuring point 5 on the front side and measuring point 31 on the back side was approx. 4 K at the longitudinal struts of the saw frame.

The heating caused by the simulated extrusion press led to non-uniform temperature increases across all robot axes. The temperature differences on the front and back side of the kinematic structure cause a change in length and a deformation of the individual axes through thermal deflection. This leads to a change of the robot pose and the robot paths during operation, which is detrimental to accuracy. The overall impact of the heat on the robot structure was recorded by measuring the position of the TCP during measurement motions of the flying cutting device. Both the relative TCP

displacement in x, y and z direction and the relative total error as compared to the initial measurement are shown in Figure 9 on the basis of measurements at two different measuring points.
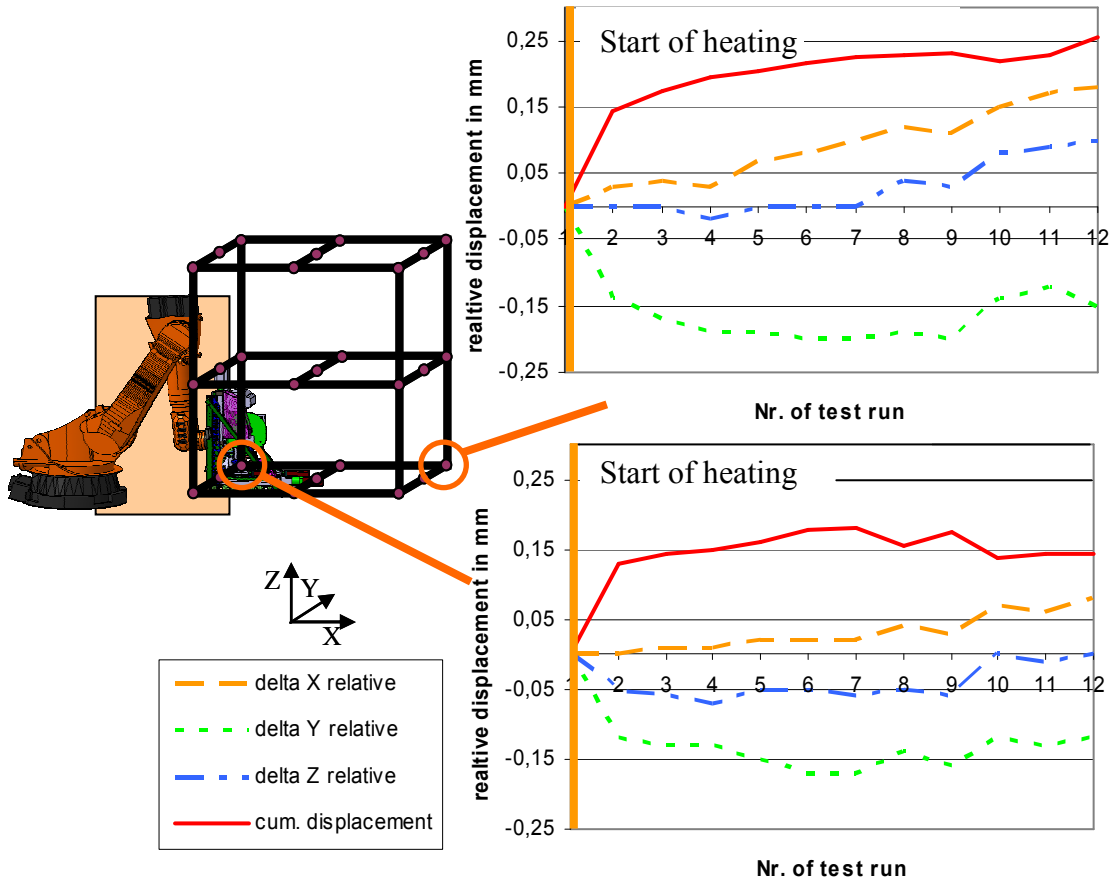
Figure 9: TCP displacement, partial heating (wbk)

Figure 9 shows an increase in TCP deviation during the first two measurements. As displayed in Figures 7 and 8, this is caused by the stronger temperature increase of the robot structure during the heat-up phase. Afterwards, the temperature increase decelerates and the TCP deviation rises to a smaller extent. The total additional displacement of the TCP at the examined measuring points caused by the temperature-induced deformation affecting the robot amounts up to 0.25 mm.

The TCP displacement in y direction is more pronounced than in x and z. The development of TCP displacement in x and z direction is mainly caused by the change in length of both the lower and the upper robot arm. In **Figure 10**, this development has been tested and proved by setting up a model. The robot structure was adjusted according to the first measuring point by means of a simplified model consisting of two thermally variable bars corresponding to the robot arms in terms of length. The elongation of the bars caused by an averaged temperature increase from the measured values at the front and back side of the robot were used to calculate the respective displacement of the TCP.
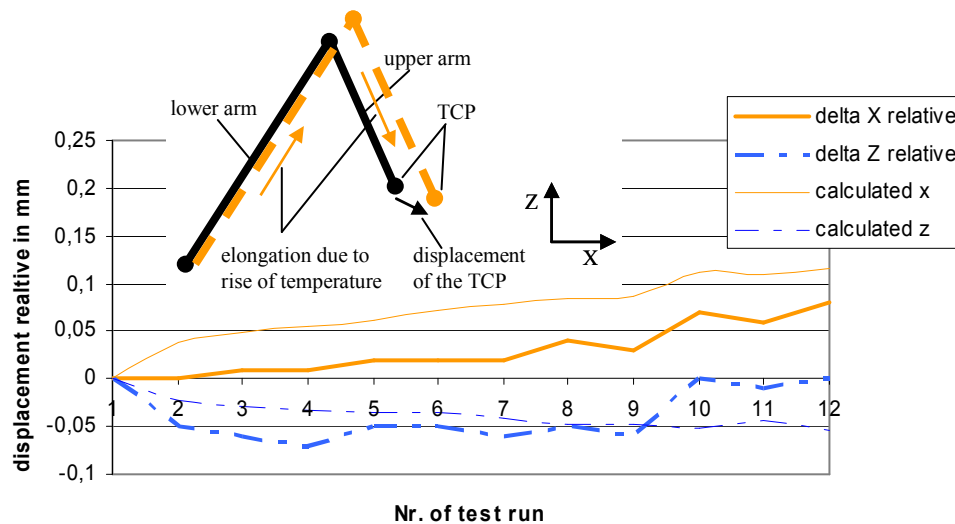
Figure 10: Comparison of calculated and measured TCP displacement in y and z direction (wbk)

The calculation from the simplified model in Figure 10 shows a good agreement between measured and calculated values in x and y direction. The discrepancy with the measured values can be explained by the model with some simplification, as not all the components of the flying cutting device were taken into consideration. **Figure 9** shows that TCP displacement is mainly caused, though, by the large displacement of the y position in the negative direction. The deviations in this direction may amount up to 0.2 mm. This displacement cannot be calculated by means of the simplified model, because the temperature difference between front and back side leads to the thermal deflection of the heated components.

When evaluating the measurement results, it should be considered that the intrinsic heating of the robot drives needs to be added to the identified thermal deformations during real operation. Besides, prior to measurements, the position of the robot was chosen to allow the thermal changes in length of the oscillations to compensate each other to the largest possible extend due to their spatial orientation. This effect can be seen in Figure 10.

Previous measurements show that the heating of the robot axes causes an additional displacement of the TCP in the robot poses. The deformations of the robot axes caused by heating affect the path of the flying cutting device during movement. As mentioned above, however, the final contour of the profile is directly dependent on the path taken by the flying cutting device during CPE regarding the production of extrusded profiles. The mere numerical calibration of the motion paths of the flying cutting device and, thus, error compensation based on the absolute accuracy of the robot would not be sufficient to minimize errors during the production of extruded profiles and increase their accuracy. The measurements carried out up to date show further potential through an additional compensation of the errors caused by temperature increases, whereas it needs to be taken into account that a good positioning of the robot may already reduce the thermal deformations considerably. Following work will try to achieve the mathematical description of the overall structure in order to calculate the influences of heating resulting from both process and drives on thermal deflection. One approach to the accuracy increase of robot paths and extruded profiles will then consist in the use of the conceived mathematical model for path generation through the consideration of temperature increases at the flying cutting device and the robot.

An integrated calibration approach for the improvement of the accuracy allows for the temperature-related influences to be additionally accounted for by means of a supplementary learning in-line calibration during the production process. Previously developed and established methods for the in-line calibration of robot applications cannot be applied to the flying cutting device used for the extrusion process. These methods are mostly based on a calibration system working with a reference object that is both temperature stable and distortion-free. During working mode of the robot cell, additional sensors fitted to the robot measure the robot-pose which is to be calibrated via previously

determined poses in relation to the reference object. Subsequently, the sensors identify a possible deviation of the actual pose from the reference pose. The robot model stored in the control is corrected to match the measured sensor values on the basis of a suitable algorithm. In the case of extrusion, the flying cutting device is required to continuously support the manufactured profile, which impedes any movement towards a reference object during operation. A calibration strategy like this cannot be used for this application.

One approach to a learning in-line calibration of the flying cutting device would consist in the use of measurement data from the downstream quality assurance of the extruded profiles. Deviations of the extruded profile would be recorded right after cutting and transfer and then stored in an error model on the basis of a suitable method linking the error to the movement and position of the robot at a specific time. As mentioned above, accuracy requirements are not equally high in different locations of the working envelope. In accordance with the law of the lever, the accuracy needs to be higher close to the guiding tool of the extrusion press than at a greater distance from it. Statistically, calibration accuracy is rising close to the guiding tool and falling when moving away from it because of the higher probability of the robot acting in the front section of the working envelope close to the extrusion press. An iterative method allows for a gradual increase of the absolute accuracy with every extruded and measured profile and for the continuous compensation of thermal modifications in particular.

Summary and outlook

This article presents the possibility of manufacturing curved aluminum extruded profiles by using a flying cutting device and a kinematic transfer mechanism. Contour deviations shown by the profiles that have been manufactured so far facilitated the determination and examination of factors affecting contour accuracy. The accuracies and errors in position deviations achieved up to date were determined by means of the direct impact of a position deviation of the flying cutting device on the target profile contour and measurements. The necessity of calibration was identified and explained on the basis of these measurements regarding the statistical accuracies of the robots operating in the working envelope in front of the extrusion press and of examinations of the effects of partial heating resulting from the extrusion press that affects robot accuracy. On the basis of these measurement results, approaches to static calibration and to a learning in-line calibration were presented.

Future work will be dedicated to investigations how the measurement results can be used for the calibration of robot paths with the aim to increase profile accuracy in a first step through improving the accuracy in the reference paths of the flying cutting device. Besides this, the details of the approach to a learning in-line calibration and to a mathematical description of the flying cutting device are to be worked out in order to be eventually able to compensate temperature-related influences on kinematic structures during operation.

Furthermore, already initiated tests on dynamic deviations during profile manufacturing have to be extended by the synchronous recording of robot paths during the manufacturing of extruded profiles. Subsequently, the results create the basis for accuracy improvements of the overall system by extending existing models.

Acknowledgement

References

[1] Kleiner, M; Klaus, A.; Becker, D.: Innovative Fertigung von 3D-gekrümmten Strangpress-profilen. ZWF 98 (2003) H. 10, S. 476ff.

[2] Fleischer, J.; Munzinger, C.; Schneider, M.; Stengel, G.: Fliegendes Abtrennen, In: Fort-schrittsberichte VDI Reihe 2 Nr. 661, VDI-Verlag Düsseldorf, 2007, ISBN 9783183661022

[3] Fleischer, J.; Schmidt-Ewig, J. P.: Innovative Machine Kinematics for Combined Handling and Machining of Three-Dimensional Curved Lightweight Extrusion Structures, Annals of the CIRP 54 (2005), pp. 317-320

[4] Fleischer, J.; Munzinger, C.; Stengel, G.: Flying Cutting of Spatially Curved Extrusion Pro-files, In: Advanced Materials Research: Flexible Manufacture of Lightweight Frame Struc-tures, Band 10 (2006), pp. 35-42

[5] Klaus. A.; Becker, D.; Kleiner, M.: Three-Dimensional Curved Profile Extrusion – First Re-sults on the Influence of Gravity In: Advanced Materials Research: Flexible Manufacture of Lightweight Frame Structures, Band 10 (2006), pp. 5-12

[6] BMBF-Projekt 02PP2410: „Gerundete Strangpressprofile aus Al- und Mg-Legierungen für ultraleichte Tragwerke, BMBF Abschlussbericht, 2005

[7] Becker, D.; Kleiner, M.; Schikorra, M.: Mehrachsiges Runden beim Strangpressen In: Fort-schrittsberichte VDI Reihe 2 Nr. 661, VDI-Verlag Düsseldorf, 2007, ISBN 9783183661022

[8] DIN EN ISO 9283: Industrieroboter – Leistungskenngrößen und zugehörige Prüfmethoden, 1998

[9] Wiest, U.: Kinematische Kalibrierung von Industrierobotern, Dissertation, Shaker-Verlag Aachen, 2001. ISBN 3826586093

[10] Bongardt, T.: Methode zur Kompensation betriebsabhängiger Einflüsse auf die Absolutge-nauigkeit von Industrierobotern, Dissertation, Herbert Utz Verlag, 2003, ISBN 3831603324

[11] Dauster, Katja :Prozessangepasste, lernende Roboterregelung für Montageprozesse, In: Fort-schrittsberichte VDI Nr. 925, VDI-Verlag Düsseldorf, 2002, ISBN 3183925087

Machining of Lightweight Frame Components

D. Biermann[1,a], K. Weinert[1,b], A. Zabel[1,c], T. Engbert[1,d] and J. Rautenberg[1,e]

[1]Institute of Machining Technology, Technische Universität Dortmund,

Baroper Str. 301, 44227 Dortmund, Germany

[a]biermann@isf.de, [b]weinert@isf.de, [c]zabel@isf.de, [d]engbert@isf.de, [e]rautenberg@isf.de

Abstract. Lightweight frame components made of aluminum and load optimized connecting elements allow the reduction of weight and energy consumption as well as the increase of payload. Complex frame structures which nowadays can be designed and optimized with the help of modern simulation technologies require the use of adapted manufacturing technologies. Especially the flexible machining of single or limited products on the basis of common machining strategies is still inefficient and economically unacceptable. This article describes the development of adequate strategies for a high quality machining using simultaneous five-axis milling. Consequently, the machining of composite extruded aluminum profiles with continuously embedded steel-wire elements and the preparation of joining areas on nodes and commonly extruded profiles for innovative joining by forming processes have been analyzed.

Introduction

Modern lightweight frame components are the basis for many constructions in automotive engineering and aerospace industry. These load-optimized and highly customized products need to fulfill the particularly complex requirements of certain applications, so the costs of manufacturing can increase easily due to a great variety.

The investigations described in this article are part of a project within the "Collaborative Research Center (SFB/TR10)" which is supported by the German Research Foundation (DFG). It deals with the development of handling, machining and joining of single lightweight structures in a flexible process chain [1]. Fig. 1 shows the main aspects of the project A6.
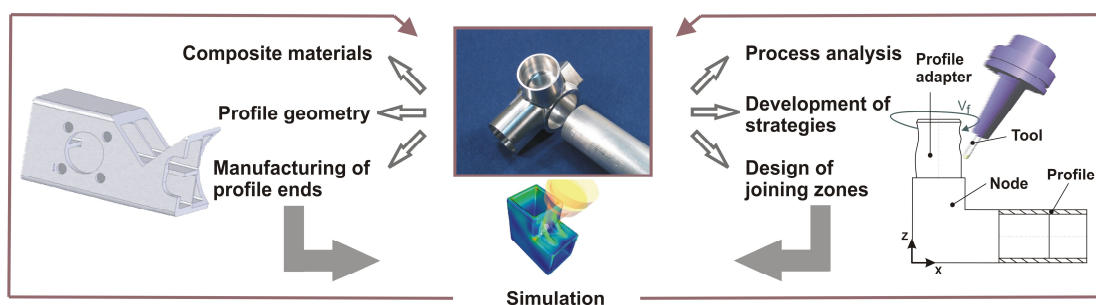
Fig. 1: Requirements for machining modern lightweight components

The machining of modern steel-wire reinforced aluminum profiles with various profile geometries is still regarded as critical in consideration of tool wear [2]. The manifold requirements of machining composites depend on the materials used and their configuration, the chosen tools and strategies on the one hand and on the specifications of the connecting elements and the joining zones on the other hand. Simulations help to support, control, evaluate and optimize the processes [3]. This article focuses on the evaluation of milling strategies for machining continuously

reinforced materials, the effects of the strategies on tool wear, and the quality of the machined surfaces and the milling preparation of areas that are necessary to increase the efficiency of hydro-bulged joints.

Milling Strategies for Continuously Reinforced Materials

Milling operations always offer a number of options. After a detailed process analysis, apparently similar looking options often show large differences that affect tool wear and machining quality without changing process duration. Milling strategies must be adapted to workpiece and material, which is especially difficult, when two different materials are combined in a composite material. Continuously reinforced extruded profiles are an attempt to create new lightweight and highly resilient structures, but the combination of a light metal matrix material with endless wire-like reinforcing elements, offers new challenges for the machining technology. Referring to the machining of boreholes, circular milling has generally proved to be an adequate alternative to the conventional drilling process [4]. In addition to the right choice of tool shape, substrate and coating as well as adapted cutting parameters for macroscopic inhomogeneous composites a modulation of the milling strategy can be relevant for tool life. Measurements have shown that the mechanical load on the tool is significantly higher while cutting the reinforcing element than during the machining of aluminum matrix material [5]. Depending on the milling strategy, part of the minor cutting edge and part of the major cutting edge of a single edge milling tool, are stressed differently. The effects become clear when taking a closer look at a case differentiation.

A view from the spindle of a three-axis machining center in direction of the workpiece allows an easy explanation of two different strategies. To specify the position of the tool when machining the workpiece in 2D-drawings, depth levels are defined along the borehole axis. The gap between tool and workpiece prior to the machining operation is defined as a positive z value. When just touching the surface of the workpiece the z value is zero, going further the z value becomes negative. The whole workpiece has a thickness of $t = 5$ mm, the reinforcing fiber has a diameter of $d = 1$ mm in this example and is located in the middle of the profile. Therefore, the reinforced area lies nominal between $z = -2$ mm and $z = -3$ mm if the machining starts at $z = 0$ mm and the tool reaches the bottom of the profile at $z = -5$ mm. With an axial infeed of $a_p = 3$ mm per helix, the tool moves along an arc of $\varphi = 120°$ of its circular path projected onto the xy-plane, which is perpendicular to the borehole axis while the tool moves one millimeter further in z-direction. If the reinforcement fiber lies eccentric in a borehole, the infeed motion in the range of $z = -2$ mm to $z = -3$ mm can either be done in the area of the reinforcement or in the matrix material so that it is possible to position the load, acting on the tool, caused by the reinforcing fiber, exactly on selected parts of the major and minor cutting edges. Two different strategies have been object of experimental investigations:

Strategy 1: The cutting of the fiber is done by both, the major cutting edge and the minor cutting edge. The exclusive machining of the reinforcing element by the minor cutting edge is not possible, but to make a difference between the two strategies, the machining of the fiber by the minor cutting edge is increased to a maximum while the stress on the major cutting edge is reduced to a minimum. Therefore, the infeed motion in the range from $z = -2$ mm to $z = -3$ mm, is done in the area of the reinforcement, causing high stresses on the corner of the tool.

Strategy 2: The cutting of the fiber is exclusively done by the major cutting edge of the tool. In the range from $z = -2$ mm to $z = -3$ mm, where the reinforcement element is located, the infeed motion is done aside from the fiber in matrix material so the minor cutting edge and the corner are not getting in contact with it. Therefore, wear on the minor cutting edge and the corner must refer to the machining of aluminum only.
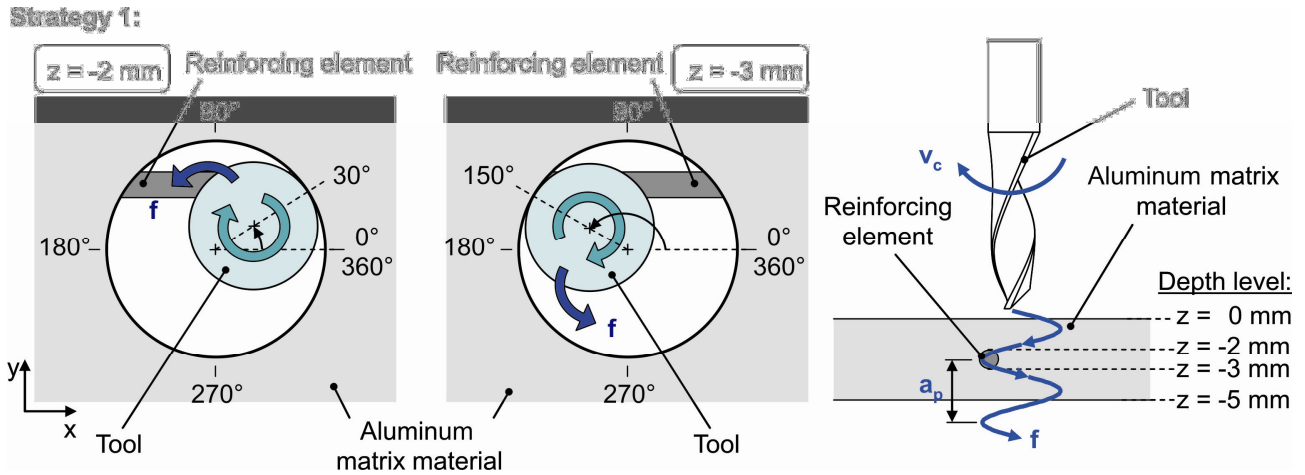
Fig. 2: Cutting the reinforcing element with major and minor cutting edge
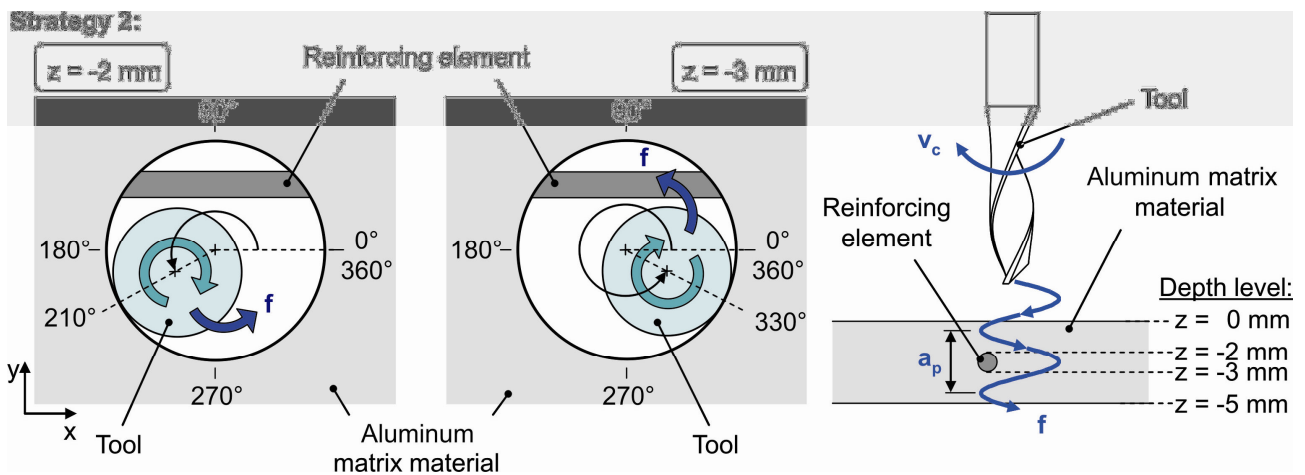
Fig. 3: Cutting the reinforcing element with major cutting edge only

The two strategies are realized by a slight variation in the starting point. The milling process is started while the tool is in front of the workpiece and the starting point describes the positive space between tool and surface. After being placed concentric above the subsequent borehole the milling cutter moves radial in the positive direction of the x-axis. The starting position is marked in Fig. 2 and Fig. 3 by the angle of $\varphi = 0°$. Afterwards the tool begins to move along the helical path until reaching the programmed depth. Therefore, the starting point determines the angle in the xy-plane that is reached when the tool starts to cut the fiber (z = -2 mm).

When using strategy 1, the depth level of z = -2 mm has to be reached at an angle of $\varphi = 30°$ so at a depth of z = -3 mm the angle is $\varphi = 150°$ (cp. Fig. 2). When using strategy 2, the tool has to reach the depth level of z = -2 mm at an angle of $\varphi = 210°$ (cp. Fig. 3). With an infeed of $a_p = 3$ mm the angle at a depth of z = -3 mm is $\varphi = 330°$ and the deepest point of the reinforcing fiber is undercut. The minor cutting edge is not involved in cutting the fiber. The experimental research was done with uncoated tools with a diameter of d = 5 mm to generate tool wear rapidly. The diameter of the boreholes produced was D = 8.5 mm. To analyze wear progression qualitatively referring to the influence of the machining strategy, major and minor cutting edge were analyzed under a light-optical microscope in regular intervals. Selected pictures are displayed in an overview in Fig. 4.

In general, the wear progress turned out differently. While the contour of the minor cutting edge and the corner including the chamfered area remained in quite a good condition during the tests when using strategy 2, the minor cutting edge showed chipping after producing a few boreholes when using strategy 1. These chippings concentrated at the corner of the tool and due to the rough surface of the damaged regions, aluminum adhesion occurred. After producing 70 boreholes the differences were obvious. Strategy 1 caused massive chipping at the corner as well as on the minor cutting edge while the corner and the minor cutting edge were less significantly damaged using strategy 2.

	New tool	Strategy 1: Tool wear after 70 boreholes	Strategy 2: Tool wear after 70 boreholes
Minor cutting edge			
Major cutting edge			
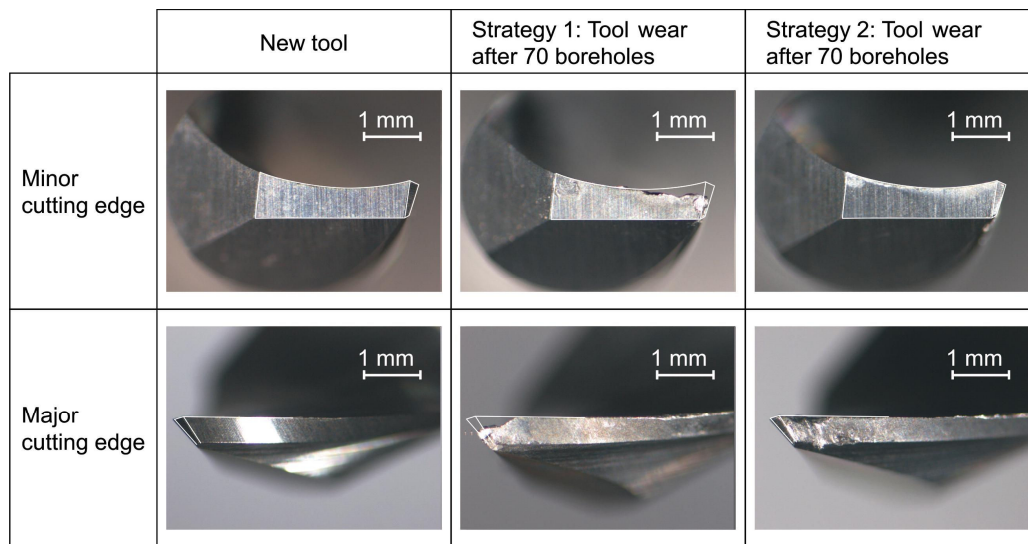
Fig. 4: Photographic images of the tool wear when using different milling strategies

Strategy 1 is an attempt to reduce the stress on the major cutting edge, but it is impossible to avoid contact with the fiber. The feed motion in the range of z = -2 mm and z = -3 mm occurs in the area of reinforcement. During the progress of feed motion, not the entire fiber material is removed, so the major cutting edge completes the cutting on the following rotation on the helical track which causes wear along the major cutting edge due to surface disruptions. Hence, not only the massive chipping at the corner of the tool but also the damage along the major cutting edge has to be considered when rating the strategy.

After producing a few boreholes with strategy 2, a damaged region was observed on the major cutting edge close to the corner. The rough surface was covered with aluminum due to adhesion. Further cutting operations led to an increased number of small bursts on the major cutting edge which took up the biggest part in machining the reinforcing element. In general, the contour of the major cutting edge remained quite well. Again, two regions were affected by wear. In addition, to the part of the edge close to the corner, which became rounded due to the small chippings mentioned above, there was a region in far distance to the corner that showed similar wear characteristics as seen in strategy 1.

The high flank wear on the minor cutting edge as well as the burst of the corner were often reasons for early tool failure during past circular milling investigations [5]. The major cutting edge of the used tools has got a bigger wedge angle and therefore, a better stability of the edge so wear resistance is better according to chippings. The investigations concerning the use of different circular milling strategies when cutting continuously reinforced aluminum profiles indicate a close connection between tool wear and milling strategy. Besides the known influencing parameters of machining like cutting velocity or feed rate, there is an additional parameter to set when machining reinforced profiles. If the implementation of different strategies is possible, the variation of strategy may influence tool wear without changing process duration. In this case, strategy 2 would be far

more suitable for the machining operation described above than strategy 1 considering the wear characteristics of the tool. The mechanical impact during the machining of the reinforcing element is the main reason for the initiation of tool wear. The milling strategy needs to be adapted in a way that parts of the tool with low wear resistance, like the corner, are less involved in machining the reinforcing element and more rigid parts, like the major cutting edge, remove most of the hard material. The adaptation of the milling strategy will improve the quality of the borehole as well as the endurance of the tool.

Milling of reinforced profile ends. To connect single profiles to an entire frame, it is necessary to finish the ends of the profile after cutting them to the right length. Again, the milling strategy is of major importance when cutting continuously reinforced material. To take advantage of the flexibility of the milling process, the same tools can be used in this peripheral milling application. Thus, non-productive time is reduced when different cutting operations have to be done to complete a workpiece. Due to the different mechanical loads generated in machining aluminum matrix material and steel, surface imperfections occur at the workpiece. The analysis of the surface by use of a confocal whitelight microscope reveals the topography as shown in Fig. 5. The produced surface is uneven.
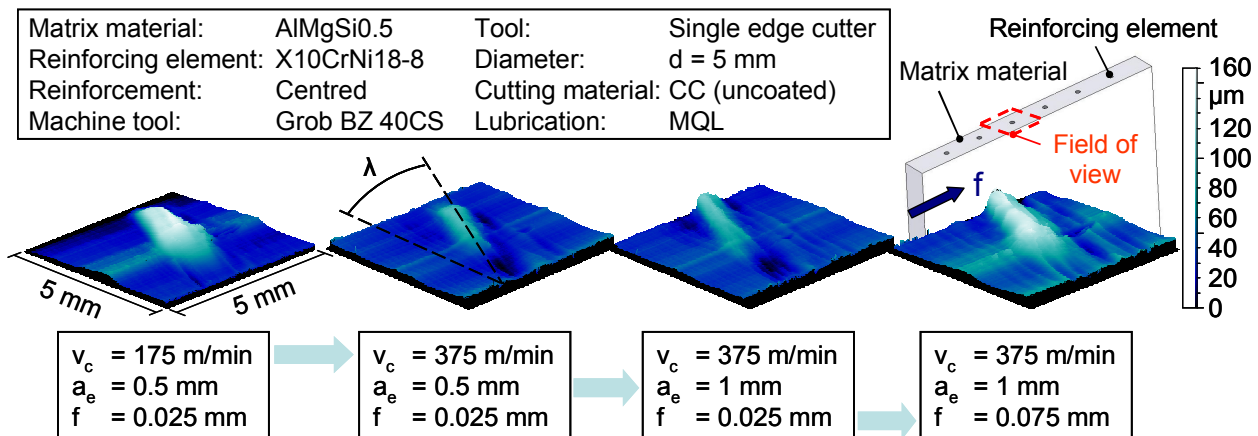
Fig. 5: Surface unevenness when milling reinforced profile ends

Single edge milling cutters with small diameter lack in bending stiffness due to their capacious chip flute. The tool is deflected radially when the reinforcement fiber is cut. A material wall builds up corresponding to the twist angle and the bending line of the tool. The height of the material wall is dependent on the cutting parameters. So if the bending stiffness of the tool used is low, surface imperfections can be reduced by choosing a combination of high cutting speed and small depth of cut as well as low feed rate.

Preparation of Joining Areas by Milling

The milling of lightweight aluminum connecting elements (nodes) and the preparation of areas for following joining methods is the second focus within this project. The difficulties in simultaneous five-axis milling and the combination with a simulation system that allows to noticeably reduce oscillations of long tools, to adapt the recent engagement conditions between cutting tool and workpiece, to harmonize the tool movement, and to provide a process-safe collision detection and avoidance, which have been described in [2].

One aspect in machining nodes is the preparation of areas that help to increase the tensile and torsional strength between the node and a joined tube. Functional surfaces with specific surface roughnesses are relevant in several mechanical parts which are moving against another part (e.g.

bearings and axis, cylinders and pistons, gears) or fixed (e.g. sealing surfaces or force-fit and form-fit connections). According to the strength of a joint, the surface quality of connected lightweight elements plays an important role for the resistance against tension, or torsion.

Aluminum tubes and nodes can be joined using additional material (e.g. welding, soldering, bonding) or without (hydroforming, EMU, rolling in, Friction Stir Welding (FSW) to obtain a force-fit, form-fit or adhesively joined connection. The main focus in this article is the preparation for surfaces that can be used for joining by dieless hydroforming.

Exemplarily, Fig. 6 shows an aluminum node with adapters for joining three different tubes. Two tubes can be joined by welding; a third profile can be joined by hydroforming. There are two different basic ways of structuring a surface of a joining zone. The macro-structure allows the profile to fit into the structured areas of the node to increase the strength of the joint. The micro-structure/surface roughness is important for a grouting between the inner and the outer part. Although the transition between both influencing factors is fluent, a measurable surface roughness (e.g. smaller than 50 μm) and a structure, which can have the form of a groove or a pocket and has a visible depth (e.g. greater than 0.1 mm), can be distinguished. Both factors have a particular influence on the strength of a hydroformed connection. Whereas the micostructure, according to the influence on the friction and the tangential stress between both joining partners, leads to a more force-fit based connection, macrostructured elements offer a high potential to increase the form-fit. To reduce the complexity of the workpieces for basic research, the necessary part of the node is substituted by a ring element (Fig. 6, right side).
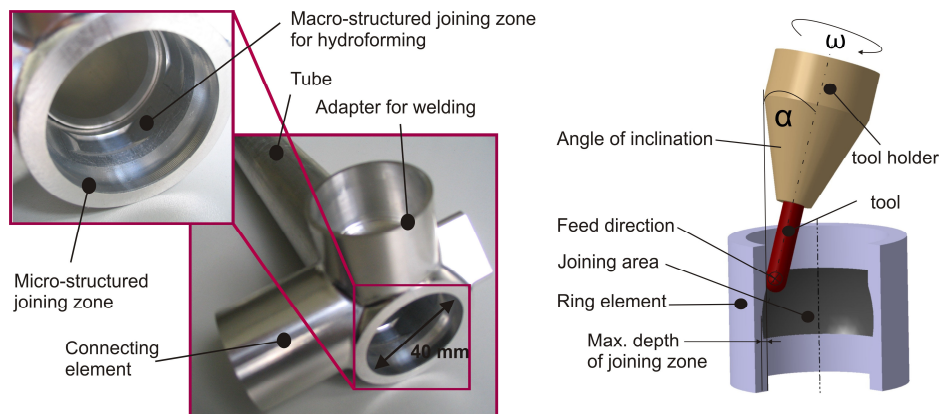
Fig. 6: Joining areas at an aluminum node (left) and substituted ring element (right)

Joining by dieless hydroforming

Joining by dieless hydroforming or hydro-bulging is one of the hydroforming processes and is a feasible process for manufacturing of tubular joints in lightweight frame structures [6]. The detailed description of the process principle for joining by dieless hydroforming (as indicated in Fig. 7), as well as more detailed experimental investigations on force-fit joints are explainend in [7] and briefly in the article "New Aspects of Joining by Forming of Tubular Workpieces" inside of this issue. This information could be summarized as follows: In a special fixture, the inner tube is inserted into the outer ring element. The hydro-probe is fed into the tube and the hydro-medium is set under pressure and directed into the gap between the hydro-probe and the inner surface of the tube. O-ring seals limit the length of the joint area and close the chamber in which the forming process takes place. After releasing the pressure, the tube-ring element recovers elastically but maintains the plastic deformation of the tube that has been produced during the bulging operation.
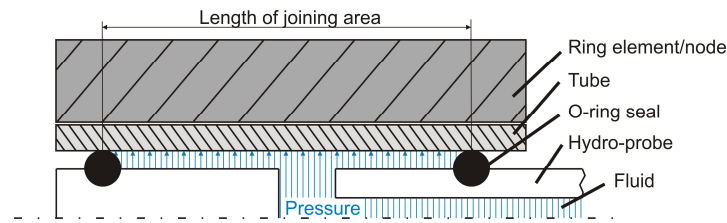
Fig. 7: Principle of hydrobulging

Manufacturing of Lightweight Connecting Elements. The manufacturing of the pockets (not described in this article) and the specific layout of the surfaces on the ring elements has been produced by five-axis CNC machining on a Deckel-Maho milling machine (DMU 50 Evolution) at the Department of Machining Technology, University of Dortmund. This multi-axis machining concept has been chosen to provide a flexible possibility for an efficient process of these lightweight components and to fulfill the requirements of geometric accuracy and surface quality. The main focus was put on a finishing process with a reproducible roughness. The NC-data was generated by a common CAM-system as used for the manufacturing of dies and moulds. High process forces as they appear in machining of hard and hardened materials [8] were not expected for the surface finishing process of the outer ring so that a deformation of the thin-walled specimen could be excluded.

To fulfill the restrictions of flexibility and efficiency, the use of standard tools is inevitable. Ball end mills with a diameter of 6 mm with a coating that reduces the adhesive behavior of the ductile aluminum alloy have been used to provide a high flexibility in covering a wide range of micro- and macro-structures with process-safe strategies. Ball end mills also allow producing small radii at the bottom of macro-structured pockets. If the radii of the tools are too small, machining time would increase and a process-safe manufacturing can not be guaranteed due to small flutes that limit the handling and transportation of the chips. The main difficulties in machining the inner areas of a ring segment are similar to the machining of cavities in die and mould industry [9, 10]. Collisions between the tool or the tool holder need to be avoided and the range of angles of inclinations, which also depend on the length of the tool and the tool holder, and the depth of the undercut of the joining area is limited (s. Fig. 6, right side).

Micro-Structured Surfaces. Several variations of milling parameters (s. Fig. 9) have been carried out in order to find process-safe, repeatable strategies that allow manufacturing selective surfaces with a ball end mill with a diameter of 6 mm. To hold up the required flexibility, a wide range of parameters has been covered (Fig. 9). The average surface roughness Rz, as it is an internationally used and standardized value, has been used as criterion to describe the surface. All experiments were used without lubrication in order to evaluate economic, process-safe manufacturing parameters, contrary to the common use of a full floating coolant. The strategy that was chosen is a helix-based finishing process. The CAM-system generates the NC-data in a way that the ball end of the tool is milling the structure of the joining zone in a continuous, helical movement. This guarantees a constant quality of the surface and avoids time-consuming, idle movements of the tool.

In a first step, visible damages of the surface were identified. Visible damages can be either blurrings (Fig. 9, right side) or tear-offs and lead to a significant detraction in categorizing the surfaces. An aggregation of blurrings can be identified as matt-shining spots in the manufactured surfaces. Measuring the average surface roughness Rz does not give a repeatable value to describe the quality surface in a reproducible way and it can be assumed that a blurred surface has an influence on the interlocking of the outer ring and the tube after the joining process that can not be clearly identified. The exposure that was made with a confocal whitelight microscope (type:

NanoFocus µsurf) demonstrates the irregular appearance of the damages which can result from temporary built-up edges [11] and chips that have not been directly forwarded through the flutes of the tool due to their adhesive behavior, which is supported by the dry milling process. A tool wear related change of the appearance of damages could not be detected during the experiments.

Material: EN AW-6060 / ISO AlMgSi0,5
Tool: Ball end mill, D = 6 mm
Strategy: Simultaneous five-axis milling finishing
Cutting speed: v_c = 200 m/min
Feed rate: f_z = 0.1 mm
Angle of inclination: β = 15°
Axial depth of cut: a_p =0.3 mm
Radial depth of cut: a_e =0.5 mm

Ring segment

Exposure of a confocal whitelight microscope

Surface damage

Material: EN AW-6060 / ISO AlMgSi0,5
Tool: Ball end mill, D = 6 mm
Strategy: Simultaneous five-axis milling finishing
Cutting speed: v_c = 200 m/min
Feed rate: f_z = 0.05 mm
Angle of inclination: β = 15°

Range of varied parameters

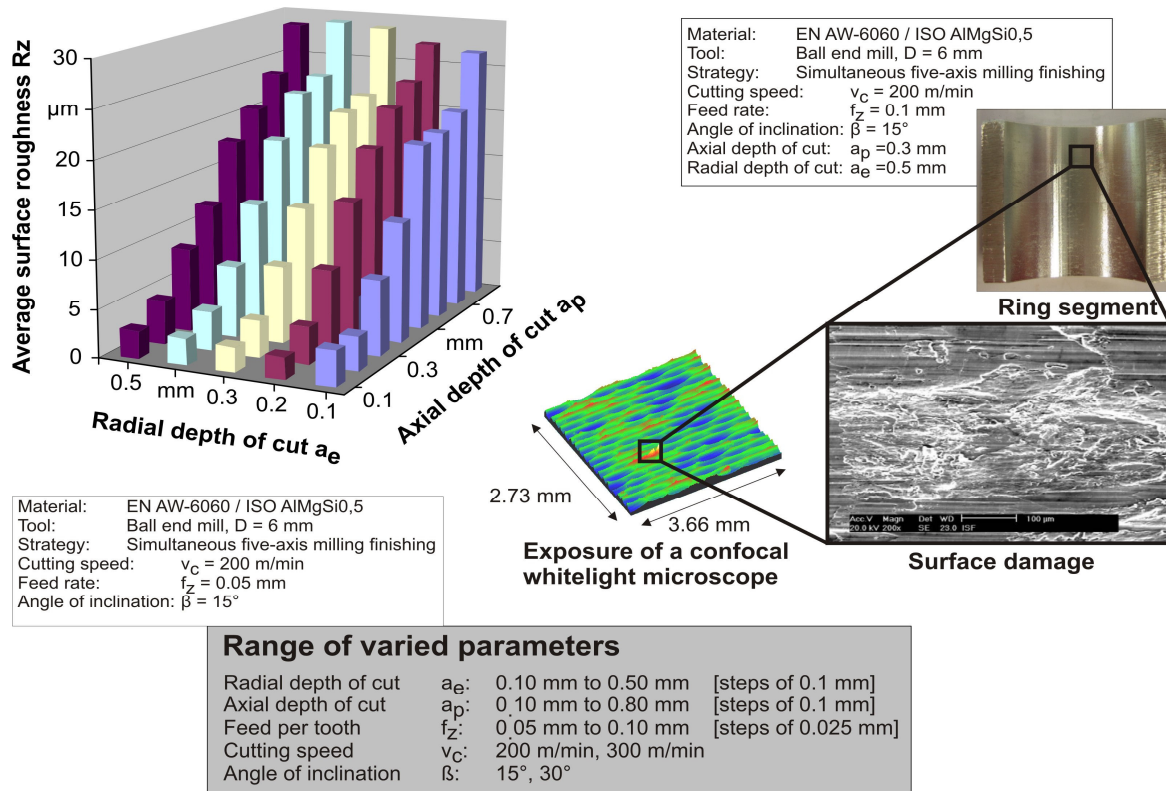|			
Radial depth of cut	a_e:	0.10 mm to 0.50 mm	[steps of 0.1 mm]
Axial depth of cut	a_p:	0.10 mm to 0.80 mm	[steps of 0.1 mm]
Feed per tooth	f_z:	0.05 mm to 0.10 mm	[steps of 0.025 mm]
Cutting speed	v_c:	200 m/min, 300 m/min	
Angle of inclination	ß:	15°, 30°	

Fig. 9: Surface roughnesses on milled ring elements

It is known that aluminum alloys require high cutting speeds to achieve an adequate surface quality [12]. The specimens that were manufactured with the higher cutting speed of v_c = 300 m/min showed a surface quality without visible damages and were selected as a basis for further investigations. When using a ball end mill, the variation of the angle between the tool and the surface also allows varying the effective cutting speed of the cutting edge that is in contact with the material. While the effective cutting speed at the tip of the tool is zero, it reaches its maximum when the maximum diameter of the ball end is in use. Therefore, a lowering of the angle of inclination increases this effective cutting speed and supports the needs for a reproducible process.

The axial depth of cut (exemplarily shown in one set of parameters in Fig. 9, left side) is identified as the main influencing factor, whereas the radial depth of cut shows no significant influence. This corresponds with cognitions about the theoretical roughness from literature [13]. The measured values are similar to the calculated values. The real values are always a bit higher than the estimated values, but they approximate with increasing axial depth of cut. Smaller depths of cut (a_p < 0.5 mm) lead to an increase of the difference up to 6 µm so that, for the demands of a precise description of higher surface qualities, a control by measuring is inevitable.

In a next step the manufacturing of the inner surface of the ring elements was transferred to an exemplary preparation of tubes on the outer surface for three different surface structures. The ring elements were left unmanufactured and after the hydro-bulging process the tensile strength was tested on a ZWICK tensile testing machine (type 1475) to verify the quality of the joint. The results of the tests can be seen in Fig. 10.
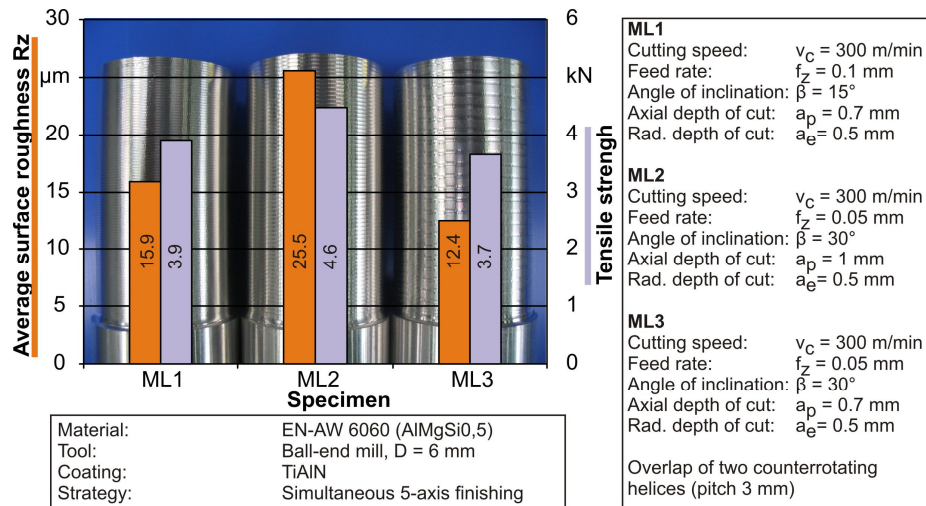
Fig. 10: Tensile strength of surface-structured tubes

It is obvious that the roughness of the surface has an influence on the tensile strength of a hydro-bulged connection between a surface structured tube and a non-structured ring element. The higher the manufactured roughness gets, the stronger becomes the joint. This results in the assumption that a rougher surface is helpful for an increase of the grouting between inner and outer part and therefore supports the resistance against a tensile load. While a non-structured cylindrical joint prepared by drilling with an average surface roughness below Rz = 5 μm has a disrupting force of 2.45 kN (not included in Fig. 10). The use of a tube that has a roughness of Rz = 15.9 μm leads to an increase in strength of 60 %. A tube with a surface roughness of Rz = 25.5 μm needs a disrupting force of 4.6 kN to destroy the joint, which equals with an increase of 100 %. For further optimization of the strength of tubular joints it will be necessary to find out the maximum in the average surface roughness that still allows a grouting. If the depths between the milled lines become too intense, the ratio of contact area to total area would change and only the peaks of the surface would carry the load and would therefore reduce the strength of a connection. But up to a surface roughness of Rz = 25.5 μm, an enhancement of the strength of a joint is verifiable.

Summary

Tool wear and surface quality are affected by the milling strategy used in machining composites. It is possible to determine which part of the tool is stressed by cutting the reinforcing element and in some cases the load can be shifted to the most rigid part of a tool to increase endurance. Surface imperfections occur during peripheral milling operations due to a radial deflection of the tool. Stiffer tools and an adapted setting of the cutting parameters can improve the result. Simultaneous five-axis milling strategies allow a reproducible structuring of the surface of lightweight connecting elements in order to control and increase the tensile strength of joints manufactured by hydrobulging. Further investigations for the preparation of joining areas will be carried out to achieve a dedicate overlay between micro-structures and free-formed macrostructures and to characterize the influence of the tool geometry. The adequate use of tools and strategies for milling lightweight frame components reduces tool costs and to increases economic efficiency of the process as well as the quality of the products.

References

[1] M. Kleiner, M. Schomäcker, A. Klaus: *Verbundstrangpressen.* In: Aluminium, International Journal for Industry, Research and Application, Volume 80 (2004) 12, pp. 1370-1374

[2] K. Weinert; N. Hammer; J. Rautenberg: *Analysis and Simulation of Cutting Technologies for Lightweight Frame Components.* In: Flexible Manufacture of Lightweight Frame Structures, Kleiner, M. et al. (eds.), TTP Trans Tech Publications Ltd, Switzerland, Vol. 10 of Advanced Materials Research, ISBN 0-87849-403-0, pp. 53-64, 2006

[3] J. Mehnen, J. Rautenberg, M. Hagedorn, J. Schaefer: *Fertigung von Leichtbaustrukturen.* In: Spanende Fertigung, 4. Ausgabe, Hrsg. K. Weinert, Vulkan Verlag, Essen, 2005, ISBN 3-8027-2935-8, pp. 403-410.

[4] K. Weinert, T. Engbert, S. Grünert, and N. Hammer, *Bearbeitungs- und Simulationskonzepte für die Zerspanung dünnwandiger und langfaserverstärkter Leichtmetallrahmenstrukturen.* In: Tagungsband Symposium Strangpressen, 26.- 27. Oktober in Weimar, WILEY-VCH Verlag, 2006, S. 183-196; ISBN 978-3-527-31844-5

[5] K. Weinert, T. Engbert, S. Grünert and N. Hammer: *Machining of Thin-Walled Structures and Continuously Reinforced Light-Metal-Matrix Composites.* Sixth International Conference on High Speed Machining, 21. – 22. March 2007, San Sebastian, Spain, digitally published on CD, 7 pages

[6] W. Przybylski; J. Wojciechowski; M. Marré; M. Kleiner: *Influence of Design Characteristics and Manufacturing Process Parameters on the Strength of Tubular Aluminium Joints Produced by Hydroforming.* In: Archives of Mechanical Technology and Automation, Vol.27 Nr. 1, Polish Academy of Science, 2007, ISSN 1233-9709

[7] M. Marré; W. Homberg; A. Brosius; M. Kleiner: *Umformtechnisches Fügen.* In: Fortschr. Ber. VDI Reihe 2 Nr. 661, VDI-Verlag Düsseldorf, 2007, ISBN 9783183661022

[8] C. E. Becze; P. Clayton; L. Chen; T.I. El-Wardany; M. A. Elbestawi: *High-speed five-axis milling of hardened tool steel.* International Journal of Machine Tools and Manufacture, Vol. 40, Issue 6, May 2000, pp. 869-885

[9] K. Weinert, K.; J. Rautenberg; T. Surmann; J. Mehnen: *Simulation of the Milling Process for Lightweight Aluminum Connectors.* Production Engineering – Research and Development, Annals of the German Academic Society for Production Engineering, XII (2005) 1, ISBN 3-9807670-6-x, pp. 125-128

[10] A. Zabel, M. Stautner: *Einsatzfelder der mehrachsigen Frässimulation.* wt Werkstattstechnik online, 95 (2005) 1-2, pp. 56-61

[11] P. Albrecht: *New Developments in the Theory of the Metal-Cutting Process, Part I, The Ploughing Process in Metal Cutting.* Trans. ASME 82, 1960, pp. 348-358

[12] W. König; F. Klocke: *Fertigungsverfahren 1 - Drehen, Fräsen, Bohren.* VDI Verlag Düsseldorf, 1997

[13] S. Hock: *Hochgeschwindigkeitsfräsen im Werkzeug- und Großformenbau.* Shaker Verlag, Aachen, 1996

Influence of Process Parameters on Structure and Mechanical Properties of Joints produced by Electromagnetic Forming and Friction Stir Welding

P. Barreiro[1, a], V. Schulze[1,b] and D. Löhe[1,c]

[1]Institute of Materials Science and Engineering I, University of Karlsruhe,

Kaiserstr. 12, Karlsruhe 76131, Germany

[a]pablo.barreiro@iwk1.uni-karlsruhe.de, [b]volker.schulze@iwk1.uni-karlsruhe.de,

[c]detlef.loehe @iwk1.uni-karlsruhe.de

Keywords: Electromagnetic forming, friction stir welding, joining.

Abstract. Electromagnetic compression of tubular profiles with high electrical conductivity is an innovative joining process for lightweight structures. The components are joint using pulsed magnetic fields which apply radial pressures of up to 200 MPa to tubular work pieces causing a symmetric reduction of the diameter with typical strain rates of about 10^4 sec^{-1}. Since there is no contact between the components to be joined and the joining machine, any damage of component's surface can be avoided. Friction stir welding (FSW) is a relatively new solid state joining technique and has been extensively developed for aluminum, magnesium, copper and titanium alloys as well as steels. The primal advantages of the process in comparison to conventional fusion welding are better mechanical properties, low residual stresses and distortion, and reduced occurrence of defects. In the present article, the influence of process and material parameters on the joint's characteristics, material's microstructure and the mechanical properties of electromagnetic compressed joints and friction stir welds using reinforced aluminum profiles is analyzed. The strength of the joint is determined by tensile tests. Finally, possible improvements of both techniques are outlined.

Introduction

The reduction of weight of motor vehicle body components is commonly reached by using lightweight materials and manufacturing processes which allow for thin-walled structures. However an indispensable requirement is the availability of suited joining technologies which provide high strength joints for the main structure of vehicles. A vast experience is available for conventional joining processes like welding, screwing, clinching, riveting and gluing, but they require a complex preparation of the joint before the joining process is performed. Furthermore reinforced aluminum profiles cannot be joined by conventional fusion joining processes. Joining by forming processes like electromagnetic forming and the solid state joining technique friction stir welding offer possible resorts since they have the potential to fulfill the requirement of strength while allowing for the employment of reinforced aluminum profiles. Especially for structural components made of reinforced aluminum profiles both processes are suitable and of increasing industrial interest. Besides this, composite materials or two non-weldable alloys may be joined. However, the influence of process parameters on the performance of the joints is hardly investigated and deeper knowledge about this relationship is necessary to establish electromagnetic forming in industrial production [1-7]. Therefore, experimental investigations were made to evaluate both feasibility and capability of joining by both processes while varying the process parameters.

Process principle

Electromagnetic forming. Electromagnetic forming is a high speed process using a pulsed magnetic field to form metals with high electrical conductivity such as aluminum. The energy density of a pulsed magnetic field is used for the contactless forming of a workpiece. Fig. 1 shows a schematic representation of the related joining process which concerns an electromagnetic tube compression. A tubular workpiece is placed coaxially inside a forming coil L. The coil is connected with a capacitor C and a switch, forming a RLC circuit.
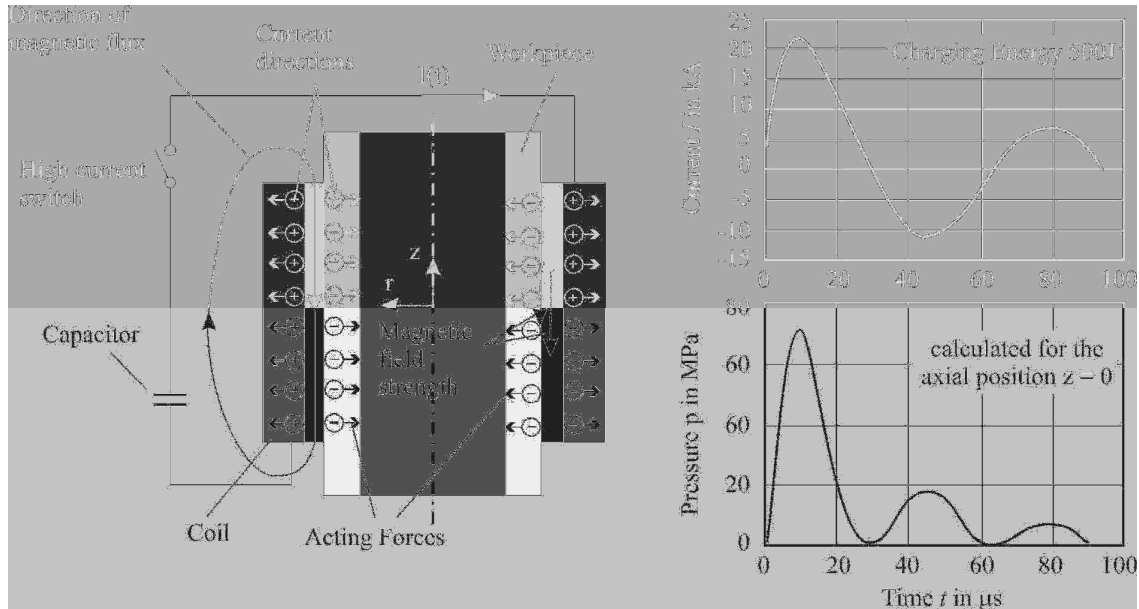

Fig. 1: Schematic representation of the process [1, 2].

After the capacitor bank has been charged with a desired energy it is suddenly discharged by closing a high current switch. The capacitor discharges a sinusoidal current which generates an alternating magnetic field in the coil. According to Lenz's law, an eddy current is induced in the workpiece flowing in the opposite direction to its cause. The current as well as the magnetic field penetrate the workpiece wall but are inhomogeneously distributed due to the skin effect. The resulting magnetic pressure p(t,r,z) is determined by the energy density of the magnetic field outside H_o and inside H_i of the workpiece and can be calculated on the basis of the measured coil current by [8]:

$$p(r,t,z) = \frac{1}{2} \cdot \mu_0 \cdot \left(H_o^2(r,t,z) - H_i^2(r,t,z) \right) \quad (1)$$

The resulting pressure pulse acts in the radial direction on tube and tool coil (see Fig. 1). If the yield strength of the tube is exceeded, radial necking occurs. A joint produced by electromagnetic forming can be realized by compressing a tubular component on a mandrel. The force which takes effect on the mandrel's surface by the impact of the compressed tube leads to an elastic or elastic-plastic deformation of the mandrel. After this, the corresponding elastic recovery of mandrel and tube proceeds. If a full relaxation of the mandrel is prevented by the tube, a permanent pressure in radial direction is established. The load, which the joints can transmit, strongly depends on the process parameters. Of these, the charging energy and initial gap between components are the most important ones as they yield to different impact velocities of the components to be joint [8-12].

Friction stir welding. Friction Stir Welding is a solid state joining process, in which a cylindrical shouldered tool with a counterclockwise threaded pin is rotated at a constant speed (*n*) and inserted with a force (*F*) into the adjacent material of the two pieces of material. The pin's length is slightly

less than the weld depth required and the tool shoulder should be in intimate contact with the work surface. Frictional heat is created between the wear resistant pin and the two work pieces, which are butted together and clamped onto a backing bar. The materials to be joined soften due to the generated heat, without reaching the melting point, and allow the pin to traverse along the joint with a certain feed (v). As the tool moves between the plates, the material is plasticized by the frictional heat at the front of the rotating pin and transported to the back. The joining of both plates is facilitated by severe plastic deformation in the solid state involving dynamic recrystallization of the base material [13-16]. Fig. 1 shows a schematic representation of the welding process.
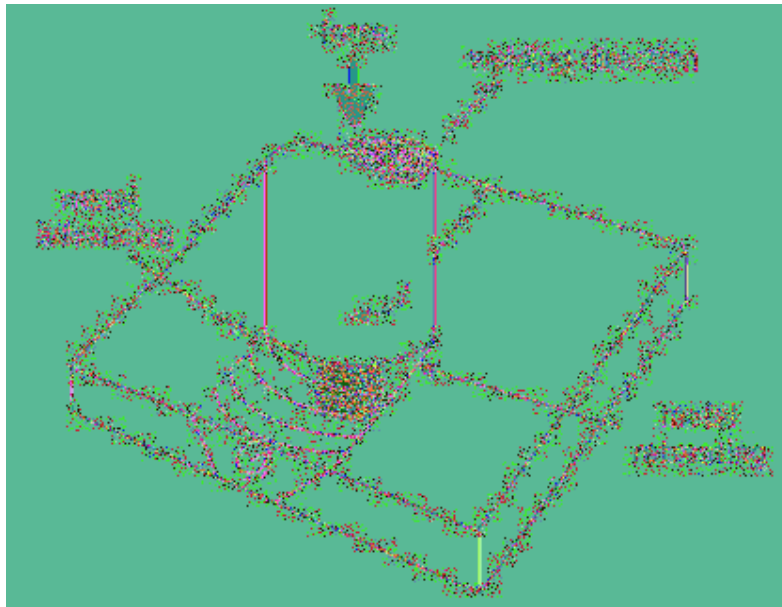

Fig. 2: Schematic representation of the friction stir welding process [17].

Several load components act on the welding tool during the joining process. An axial force is necessary to keep the correct vertical position of the tool relative to the materials surface. The lateral movement of the tool is accomplished by a force acting in the welding direction. Finally a clockwise torque is required to rotate the tool [13-16].

One of the most important advantages of FSW is the absence of the typical welding defects like porosity, solidification and liquation cracks. In general, FSW was found to produce a low concentration of defects and is very tolerant to parameter's and material's variations [13-16].

Materials and testing method

Force fit joints. For the present experimental investigations aluminum tubes were electromagnetically compressed on mandrels at the Institute of Forming Technology and Lightweight Construction, University of Dortmund (Germany). The material of both joint components was AA6060. The outer diameter of the tube was 20 mm with a wall thickness of 1 mm. In addition the gap between tube and mandrel was 1.2 mm. Fig. 3 shows a scheme of a test tube deformed by electromagnetic compression. The joining process was made with charging energies of 1.1 kJ and 1.5 kJ.
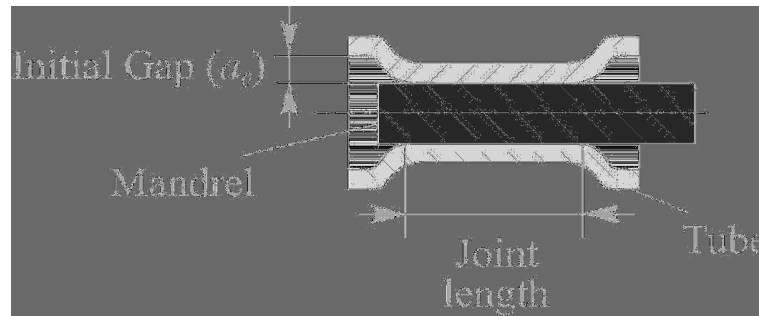
Fig. 3: Schematic representation of a test tube.

In order to analyze the influence of the mandrel's surface on the mechanical properties of the joint, the surface topography was altered by shot peening. As shot media Al_2O_3 with a mean diameter of 20 - 30 µm (EKR320) and glass beads with a mean diameter of 20 - 30 µm (MJ550B) were used. In addition, the shot pressure was varied from 0.5 up to 1.5 bar. After that, the surface topography and the residual stresses after shot peening were determined in order to evaluate the effect of peening.

The strength of the joints was determined by tensile tests using a universal testing machine Zwick 1478 with a maximum force of 200 kN. The crosshead velocity was 2 mm/min. The quantities measured were the force and the relative displacement of the tubular component.

In order to analyze the influence of the friction welding between the components to be joint during cyclic loading, several joints were cyclically preloaded and then tested by monotonously increasing loading. The cyclic preloads at swelling loads ($R = \sigma_{min}/\sigma_{max} = 0$) were carried out in a 63 kN Instron (Fast-Track 8800) servo-hydraulic machine. The test frequency was 2 Hz. The maximum load was varied from 2 kN to 6 kN. The quantities measured were the force, the relative displacement of the tubular component, and the complete displacement of the test tube. The relative displacement of the tubular component was measured with a capacitive sensor (small measuring range with high resolution) and the complete displacement of the test tube was measured with an inductive sensor (large measuring range with low resolution). The experiments were stopped after 10, 100 and 1000 cycles.

FSW welds. For the present work aluminum butt welds in with austenitic spring steel 1.4310 (with a diameter of 1 mm) reinforced sheets of the alloy AA6060 were produced at the Institute for Machine Tools and Industrial Management of Technical University of Munich (Germany). The reinforced sheets had a thickness of 5 mm and a width of 55 mm. Both sheets exhibited 5 steel reinforcing elements. During the welding process the feed (*v*) was maintained constant by 150 mm/min, but the rotational speed (*n*) was varied in 4 steps from 750 up to 1500 rpm. The welding process was carried out using two different pins with a length of 4.7 mm, one with a diameter of 4 mm and the other with a diameter of 5 mm. A piece of each sample was extracted in order to determine the welding seam's geometry and microstructure and the presence of welding defects (using micrographs).

In order to analyze the deformation behavior in tensile tests, two specimens were taken out of each welded sample. Each sample for tensile tests had two reinforcing elements. The weld seam was located in each case in the middle of the sample and was perpendicular to the test direction. The tensile tests were carried out in a 100 kN Zwick machine with a crosshead velocity of 2 mm/min. Force and strain were measured.

Experimental results

Force fit joints. Fig. 4 left shows the correlation between peeing induced residual stresses in the mandrel and shot pressure for both shot media. The compressive residual stresses at the mandrel's surface are strongly increased by shot peening. This increase is stronger in case of glass beads

compared to Al_2O_3 particles. The different impulses of the shot media at the same shot pressure are responsible for the higher plastic deformation of the mandrel's surface in case of glass beads. Fig. 4 right shows the correlation between roughness and shot pressure for both shot media. The roughness of the mandrel's surface is strongly increased by peening at small shot pressure. A further increase of the shot pressure results in decreasing surface roughness. The findings are almost identical for both shot media.
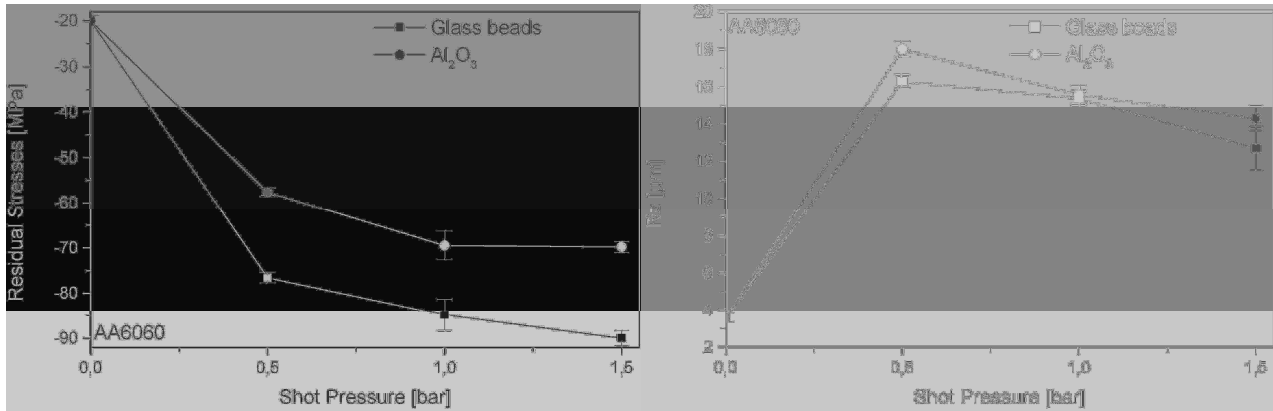

Fig. 4: Left: residual stresses at mandrel's surface after shot peening. Right: roughness of the mandrel after shot peening.

Inspite of the fact that the mandrel's roughness after shot peening by different shot pressures are similar, the surface's morphology shows substantial differences.

Fig. 5 shows scanning electron surface micrographs of two mandrels, which were shot peened with glass beads (left) and Al_2O_3 (right) at a shot pressure of 0.5 bar. The difference between highest and lowest point is similar in both cases. However the resulting surface is clearly smoother after shot peening with glass beads than with A_2O_3 particles.
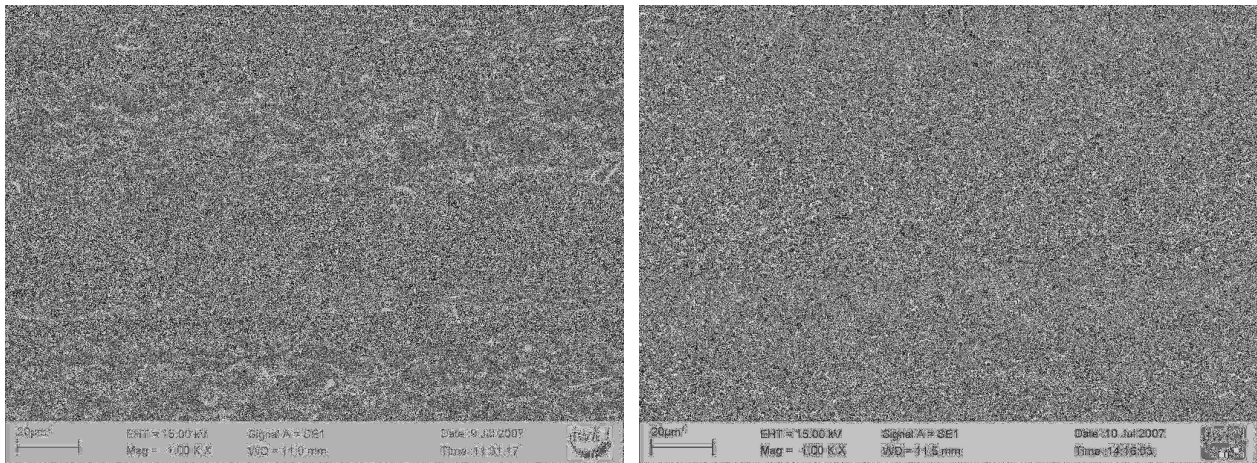
Fig. 5: Surface of shot peened mandrels (air pressure 0.5 bar). Left: glass beads, 20 - 30 μm. Right: Al_2O_3, 20 - 30 μm.

As shown by Fig. 6, the pull-out force increases with increasing shot pressure for both shot media. However this increase is rather weak in case of joints whose mandrels were shot peened with glass beads. On the other hand, the reachable pull-out forces of joints, whose mandrels were shot peened with Al_2O_3 particles at pressures of 1 bar or more, are more than twice as high as of joints with unpeened mandrels [12].

Fig. 6: Development of the pull-out force of joints with shot peened mandrels.

Joints whose mandrels were shot peened with Al_2O_3 particles partially exhibit form fit in the contact area between tube and mandrel due to the shot peening induced surface morphology and therefore show higher pull-out forces than joints with unpeened mandr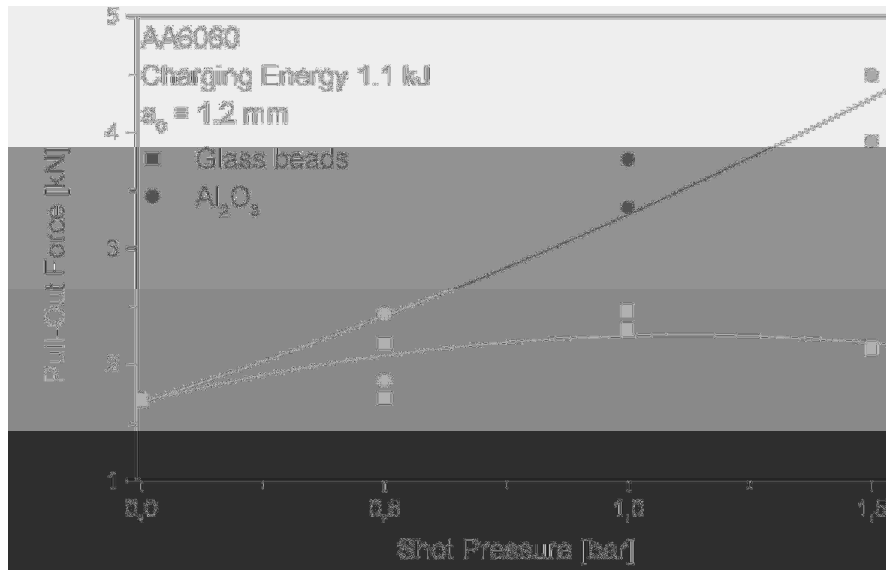els. This effect leads to pull-out-forces which would have needed a charging energy of 1.5 kJ in case of unpeened mandrels [12].

Fig. 7 shows as an example the force elongation curves of samples, which were cyclically preloaded with a maximum force of 4 kN in comparison with an as joint sample. An increase of the achievable pull-out loads after the cyclic preload can be observed.
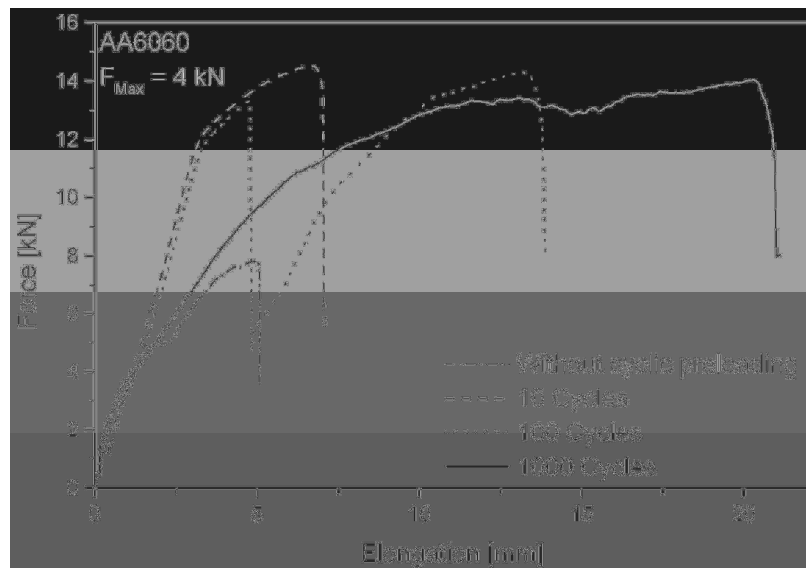
Fig. 7: Force elongation diagrams of cyclically preloaded joints.

A distinct pull-out force cannot be recognized in case of the joint which was preloaded for 10 cycles. The joint can transfer a maximal force of 15.2 kN, which corresponds to the tensile strength of the AA6060 tube. In case of a joint which was cyclically preloaded for 100 cycles, a pull-out force of 13.3 kN can be determined. At this point, the force decays drastically because both parts (mandrel and tube) start to glide on each other. After this a "seizing effect" occurs leading to slip between the two components, increasing ploughing effects and therefore to a maximum transferable load of 14.3 kN. Finally, the load drops down when both components are completely pulled off. The joint which was cyclically preloaded during 1000 cycles shows a pull-out load of 3.77 kN. Subsequently, the seizing effect occurs until the tube is completely pulled out of the mandrel.

Fig. 8 summarizes the development of the pull-out forces as a function of the maximum force and the number of cycles of preloading.

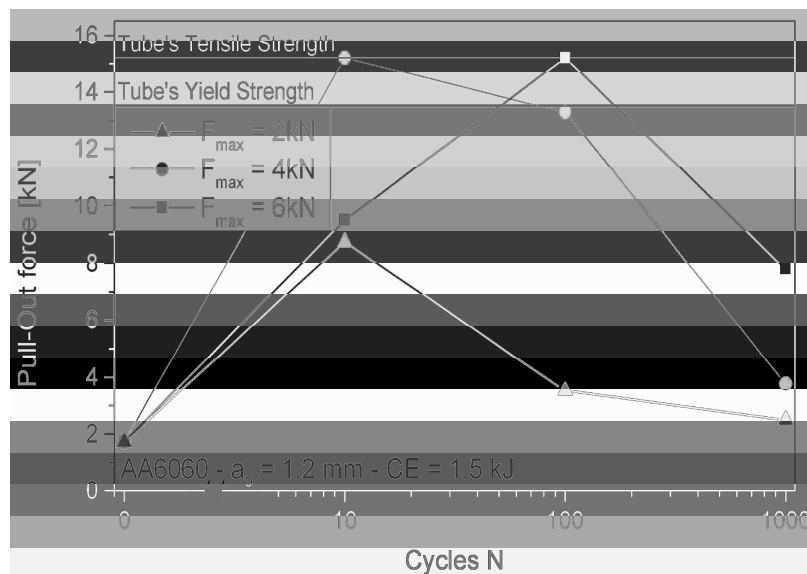Fig. 8: Dependence of the pull-out load on the maximum force and the number of cycles after preload tests.

At all preload forces investigated, a severe increase of the pull-out force can be achieved. This is most pronounced at 4 or 6 kN, where the tube´s tensile strength was reached after 10 or 100 cycles, resp. At 2 kN the force seems to be too low in order to achieve a sufficiently high friction welding effect. At all preloading conditions the pull-out force is steeply decreasing at high numbers of cycles of preloading. This may be due to initiaton of fatigue damage. Therefore only a small gap between the positive effect of friction welding and the detrimental effect of damaging during preloading remains.

FSW welds. Fig 9 shows micrographs acquired along the weld seam of specimens welded with rotational speeds of 750, 1000, 1200 and 1500 rpm, respectively and using a pin with a diameter of 5 mm. All micrographs show cuts through the weld with viewing direction parallel to the pin axis. The weld seam is placed in the middle of the image and the welding direction is from right to left. With respect to the investigated welding parameters, the shape and morphology of the weld zone is parameter dependent. The reinforcement elements can only be observed on the right side of the weld seam (upper part of the images). This means that the reinforcement elements were pushed up on the right side and pulled down on the left side of the weld seam due to the thread contour of the welding pin. Furthermore the reinforcement elements were bended in the welding direction. In addition, steel splitters from the reinforcement elements and holes in the weld seam can be observed. The probability for welding defects decreases by increasing the rotational speed. Holes are hardly observable for a rotation speed of 1500 rpm. However the welding zone still shows steel splitters.
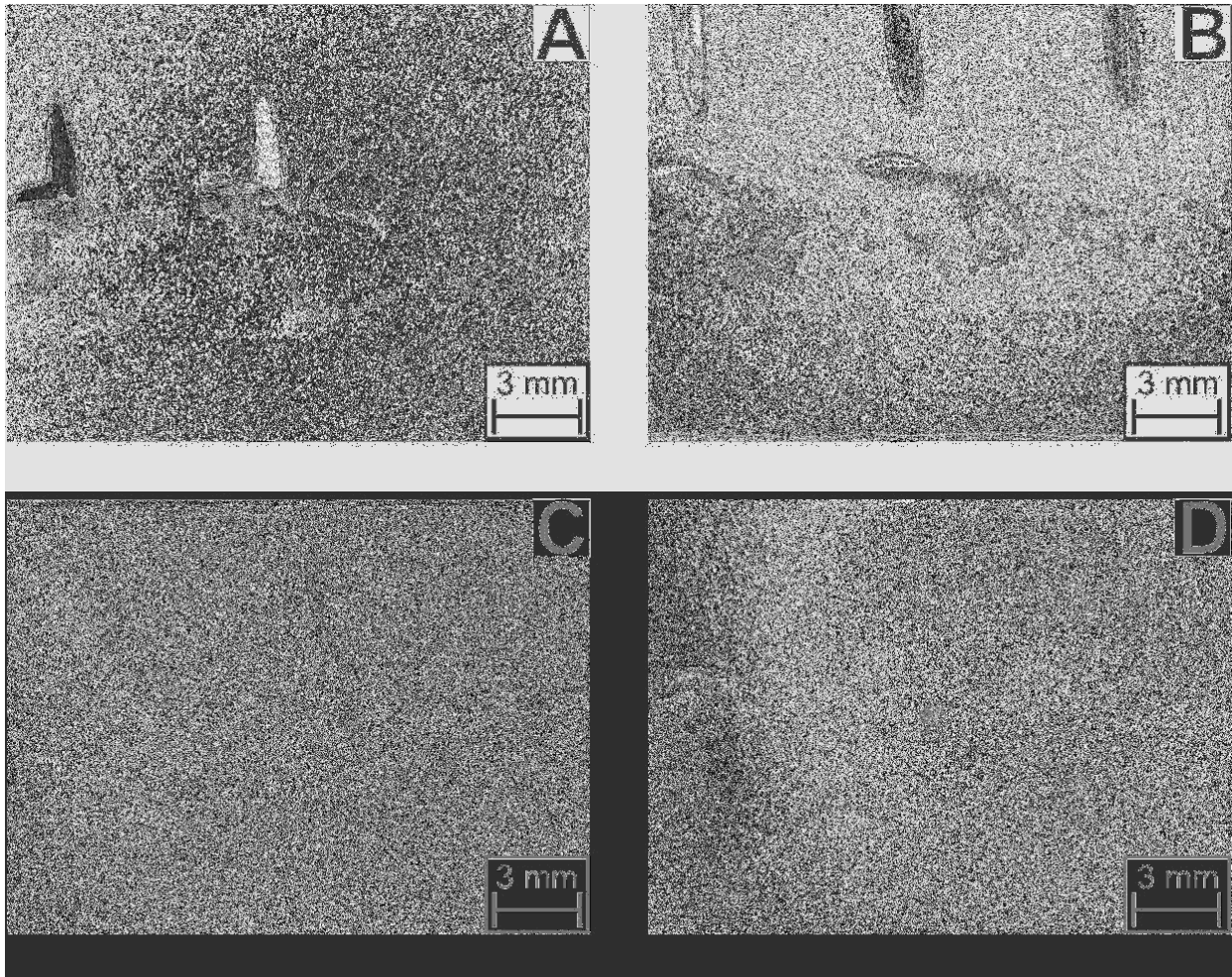
Fig. 9: Microstructure of weld seam welded with different rotational speeds and a 5 mm long pin.
A: 750 rpm. B: 1000 rpm. C: 1250 rpm. D: 1500 rpm.

Tensile tests were carried out on several samples welded with all four different rotational speeds. Fig. 10 shows the dependence of the ultimate tensile strength R_m on the circumferential speed determined from the rotational speed and the pin diameter for the both pin diameters. The achievable R_m increases with increasing speed. There is a slight increase of the strength at the pin diameter of 5 mm compared to 4 mm at low circumferential speeds which vanishes at about 320 mm/s. Compared to the ultimate tensile strength of the matrix material in the initial T4 state, which was 160 MPa [18] a maximum of 140 MPa is reached. Therefore at high speeds overaging effects may be responsible for the reduced strength. At lower speeds the additional effects of the pores and the splitters of the wire lead to a more severe reduction of the strength. As the larger pin diameter leads to a better circulation of the matrix material at even lower rotational speeds it yields to a slightly higher strength.

Fig. 10: Dependence of the R_m on the circumferential speed and the pin diameter.

Conclusions
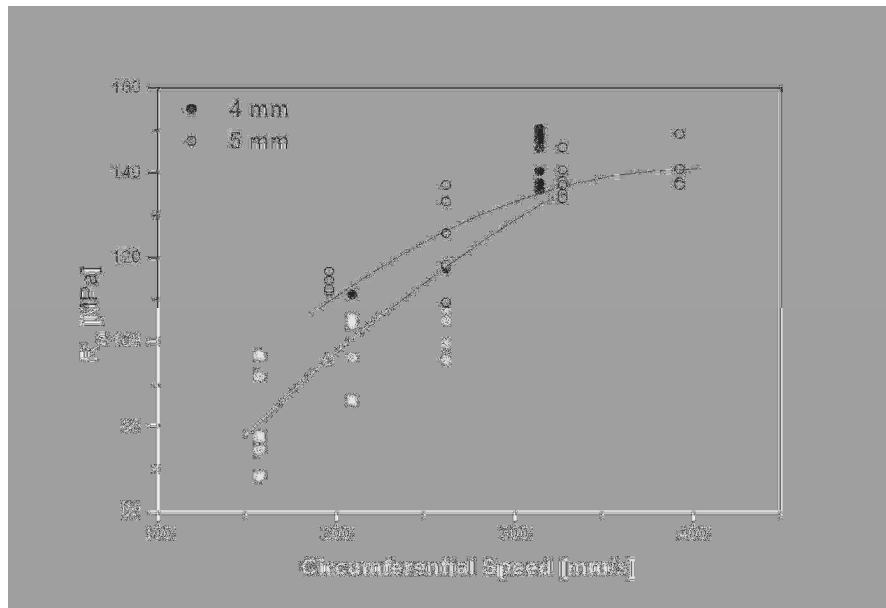
Electromagnetic forming. The mechanical properties of joints produced by EMF can be improved with mechanical pre or post welding treatments. The mandrel component can be shot peened in order to improve the achievable pull-out forces. During the shot peening treatment of the mandrel the shot pressure should be as high as possible. The shot media should be square-cut, in order to achieve form fit elements in the contact area between join partners. Joints can also be cyclically preloaded in order to improve the achievable pull-out loads. For this tube and mandrel must be of the same material.

Friction stir welding. In the present work it was shown that friction stir welding gives the possibility to weld reinforced aluminum sheets. Since the microstructure, the presence of defects in the weld seam as well as the strength of welds results improved, welding with high circumferential and speeds seems to be favourable. However, welding imperfections like steel splitters from the reinforcement elements and holes in the weld seam were still found. Further research is needed in this area in order to improve the quality of welded components.

Acknowledgements

References

[1] D. Mamalis, A. Manolakos, A. Kladas, A. Koumoutsos: *Electromagnetic forming and powder processing: Trends and developments*. Applied Mechanics Reviews (2004) 57, pp. 299-324.

[2] M. Kleiner, C. Beerwald, W. Homberg: *Analysis of Process Parameters and Forming Mechanisms within the Electromagnetic Forming Process*. CIRP Annals 2005, Vol.1

[3] W. Homberg, M. Marré, M. Kleiner: *Umformtechnisches Fügen leichter Tragwerkstrukturen*. Aluminium Vol.80 (2004) 12, pp1396-1400.

[4] F. Bach, M. Rodman, A. Rossberg, J. Weber, L. Walden: *Verhalten von Aluminiumwerkstoffen bei der elektromagnetischen Blechumformung.* Proc. 2. Kolloq. Elektromagnetische Umformung, 28. Mai 2003, Dortmund, pp. 11–18.

[5] M. Zaeh, D. Eireiner, L. Papadakis: *Friction Stir Welding with Modern Milling Machines / Requirements, Approach and Application.* Proceedings of the 5th International Friction Stir Welding Symposium, Metz (France), 2004

[6] D. Eireiner: *Rührreibschweißen mit Bearbeitungszentrum*, in: Maschine + Werkzeug 104, Heft 9 (2005), pp. 56-58

[7] D. Eireiner: *Friction stir welding using NC milling machines*, in: Welding and Cutting 3 (2004) 4, pp. 220-223

[8] C. Beerwald: Grundlagen der Prozessauslegung und -gestaltung bei der elektromagnetischen Umformung. Universität Dortmund - IUL, Dr.-Ing. Diss., Reihe Umformtechnik, Shaker Verlag, Aachen 2005, ISBN 3-8322-4421-2.

[9] P. Barreiro, V. Schulze, D. Löhe: *Development and Effects of Residual Stresses in Joints Produced by Electromagnetic Compression and its implication on the Mechanical Properties*, in: Reimers, W. (ed.), Proc. Europ. Conf. On Residual Stresses 7, Sept. 2006, pp. 485-490

[10] P. Barreiro, V. Schulze, D. Löhe, M. Marré, Ch. Beerwald, W. Homberg, M. Kleiner: *Strength of tubular joints made by electromagnetic compression at quasi-static and cyclic loading*, in: Kleiner, M. (ed.), Proc. Int. Conf. High Speed Forming, März 2006, pp. 107-116

[11] V. Schulze, P. Barreiro, D. Löhe: *Investigation of the Influence of Process Parameters on the Structure and the Mechanical Properties of Joints Produced by Electromagnetic Compression*, in: Advanced Materials Research: Flexible Manufacture of Lightweight Frame Structures, Band 10 (2006) pp. 79-88

[12] M. Kleiner, D. Löhe, M. Marré, Ch. Beerwald, P. Barreiro, V. Schulze, W. Homberg: *Investigation of force-fit joints produced by electromagnetic tube compression*, in: Annals of the German Academic Society for Production Engineering, WGP, Vol. XIII/1 (2006), pp. 227-230

[13] U. Henneböhle, J. Silvanus: FSW-basic-principles and recent trends. In: DVS-Berichte, Band 237 (2005) pp. 498-501

[14] A. Meyer, C. Schilling, A. von Strombeck: Development and series production of multi-dimensional FSW on industrial components, in: DVS-Berichte * Band 237 (2005) pp. 505-508

[15] S. Kallee, J. Kell, W. Thomas, C. Wiesner: Development and implementation of innovative joining processes in the automotive industry, in: DVS-Berichte * Band 237 (2005) pp. 509-515

[16] L. Cederqvist: A weld that lasts for 100000 years - friction stir welding of copper canisters for spent nuclear fuel, in: DVS-Berichte * Band 237 (2005) pp. 502-504

[17] Information on http://www.msm.cam.ac.uk/phase-trans/2003/FSW/aaa.html

[18] K. A. Weidenmann: *Werkstoffsysteme für verbundstranggepresste Aluminiummatrixverbunde*, Dissertation an der Universität Karlsruhe (2006), Shaker Verlag Aachen

Joining by Compression and Expansion of (None-) Reinforced Profiles

Marré, M.[1, a], Brosius, A.[1, b] and Tekkaya, A.E.[1, c]

[1]Institute of Forming Technology and Lightweight Construction,

Technische Universität Dortmund, Baroper Str. 301, 44221 Dortmund, Germany

[a]michael.marre@iul.uni-dortmund.de, [b]alexander.brosius@iul.uni-dortmund.de,
[c]erman.tekkaya@iul.uni-dortmund.de

Abstract. One major objective of the Collaborative Research Center SFB/TR10 is the flexible and competitive production of frame structures which meet the requirements of lightweight design. The development of composite extrusion by embedding continuous reinforcing elements, like e.g. steel wires, in profiles during the extrusion process illustrates one approach to fulfill these conditions. To assemble such composite profiles, joining processes and strategies have to be developed taking into account the special composite material characteristics. In addition, the flexible production of lightweight frame structures in small quantities generates more requirements on the joining technology. The feasibility of joining by forming has been carried out investigating experimentally both conventionally extruded and reinforced profiles. Therefore, joining profiles to lightweight frame structures by both expansion and compression has been examined. The necessary forming pressure for the joining by forming processes was applied to tubular workpieces by a medium (hydroforming) and by a magnetic field (electromagnetic compression). Joints have been manufactured by these two processes to transmit axial loads either by force- or form-fit.

Introduction

Traditionally, industrial joining processes, which are largely thermal, can produce high quality joints in sufficient quantities. Within the SFB/TR10 new composite materials are produced by composite extrusion and are supposed to be joint to a frame structure [1]. In conventional extrusion processes for the manufacturing of reinforced extruded profiles composite billets are used. A promising alternative is the composite extrusion of conventional billets. Here, continuous reinforcing elements like wires are embedded in the aluminum matrix during the extrusion process by use of modified porthole dies. In porthole dies, which are used for the manufacturing of hollow sections, the mandrel, which forms the inner contour of the profile, is fixed by bridges. The billet material spreads in front of the bridges and flows through the material inlets. Behind the bridges it rejoins in the welding chamber. In the described composite extrusion process the bridges are used to supply the reinforcing elements. The tools are divided into three parts: the die, the supply element, and the sealing element, see also Fig 1. The reinforcing elements are fed from the outside and are deflected inside the tool towards the extrusion direction. In the welding chamber the reinforcing elements join the aluminum alloy. In the scope of research of the SFB/TR10 different types of metallic reinforcing elements were embedded and analysed concerning the resulting properties. The experiments focused on high strength steel wires with a tensile strength of approx. 2000 MPa. In current investigations the process will be enhanced in terms of the embedding of composite wires, like Al_2O_3 fibres which are infiltrated in an aluminum matrix [2]. Nevertheless, if composite workpieces, like composite extruded aluminum profiles with embedded steel fibres, are supposed to be joined, welding processes are likely to be insufficient. Indeed, the melting temperatures of the embedding matrix (e.g. AA6060) and the reinforcing element (e.g. 1.4310) can differ significantly, making the manufacture of homogeneous joints using welding methods alone impossible. Joining by forming offers an attractive al-

ternative solution to thermal joining because of its high potential to maintain the joint between embedding matrix and reinforcing element. In addition, special requirements on the joint design must be fulfilled to achieve the aim of the SFB/TR10, which is the low volume production of lightweight, highly stressable and stiff frame structures made of tubes or profiles.
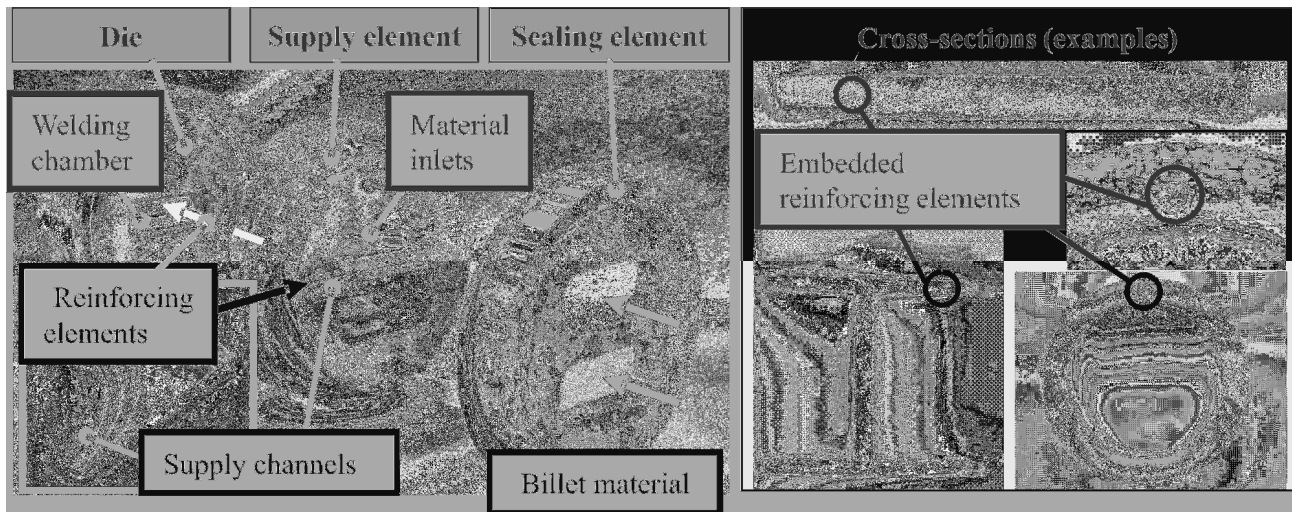

Fig. 1: Tool for composite extrusion with continuous reinforcing elements and examples of manufactured cross-sections

Therefore, a joint design must be carried out under comprehensive aspects to exclude suboptimal solutions. Furthermore, there are interacting partially conflicting requirements in the field of material characteristics, design and production engineering which have to be considered as well [3]. To achieve feasible joint designs taking pre- and post-manufacturing processes, manufacturing time, and its cost into account as well, an intense and collaborative cooperation between the projects of the SFB/TR10 is mandatory.

Generally, joints which are merely produced by forming processes are able to transmit e.g. axial loads by means of dominating force- (alternatively named as interference) or form-fit. In addition, a transmission of load could be proceeded by a combination of both mechanisms. If a very high energy is supplied, a so called magnetic pulse welded connection is producible as well by a high speed forming process [4]. This process will be neglected in the further description, as the article focuses on dominant force and form-fits. As dominating form-fit joints transmit a load partly by force-fit, the experimental investigations predominantly focussed on producing force-fit joints. Joining by compression has been done by electromagnetic forming; joining by expansion has been performed by a dieless hydroforming process.

Joining by Electromagnetic Compression

Electromagnetic forming (EMF) is a high speed process using a pulsed magnetic field to form metals with high electrical conductivity such as aluminium. Joining is the most common industrial application of the EMF-process. Due to the contact free forming process the joining of coated fuel pipes is an example of a feasible application. Furthermore, the joining of composite material as well as structural components is of an increasing interest. Especially for structural components made of aluminium alloys (with good electrical conductivity) the EMF-process is suitable and of increasing industrial interest.

Process-Principle of EMF. As the energy density of a pulsed magnetic field is used for the contactless forming of a workpiece, the resulting deformation is closely related to the electromagnetic properties. The process model (Fig. 2) can be described as an oscillating circuit which includes the capacitor C, the resistance R, and the inductance L of the pulse generator as well as the consumer load consisting of tool coil and workpiece, here a solenoid and a tube. After the capacitor bank has

been charged it is suddenly discharged by the closing of a high current switch. As a result, a damped oscillating current flows through the coil, generating a corresponding magnetic field. According to Lenz's law, a current in the workpiece will be induced flowing in the opposite direction to its cause. Due to the skin effect the current is induced on the tube's surface first. The magnetic field penetrates the workpiece wall in the course of the process' progression. The resulting pressure pulse acts orthogonally on both the field strength and the induced current, i.e. in a radial direction on tube and tool coil, as Fig. 2 shows [8].

In contrast to quasi-static forming processes, the pressure pulse in EMF causes high strain rate effects in the formed material [9]. The resulting magnetic pressure $p(t,r,z)$ is determined by the energy density of the magnetic field outside H_a and inside H_i of the workpiece and can be calculated on the basis of the measured coil current, displayed in Eq. 1 and described in detail in [10].

$$p(t,r,z) = \frac{1}{2} \cdot \mu_0 \cdot \left(H_a^2(t,r,z) - H_i^2(t,r,z) \right) \tag{1}$$

The calculated pressure distribution about time for the axial mid-position inside the coil is shown in Fig. 2. If the yield strength of the tube is exceeded, a permanent reduction of diameter occurs. Furthermore, a common and useful tool for forming operations by electromagnetic compression is a field concentrator or fieldshaper [9], which is placed into the gap between the tool coil and tube.
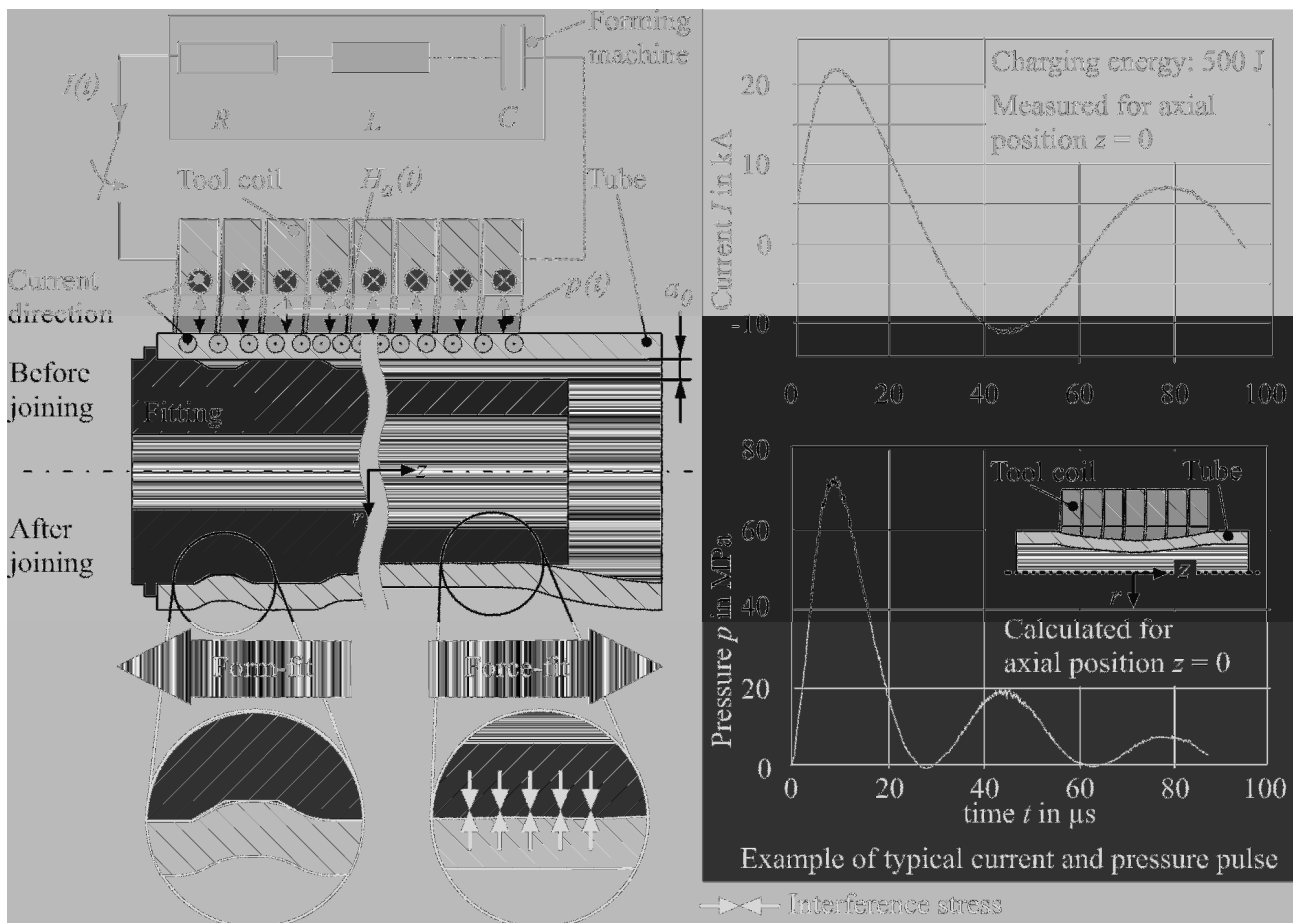
Fig. 2: Process principle of joining by electromagnetic compression with a tool coil

The purpose is, on the one hand, based on handling operations before and after forming and, on the other hand, to influence and concentrate the magnetic field's dilation respectively. In case of a setup with a fieldshaper the above described process principle is modified as follows:

Process-Principle of EMF Using a Fieldshaper. As known from the setup with a direct acting tool coil, a sudden discharge of the capacitance causes a damped sinusoidal current in the tool coil,

which correlates to a strong magnetic field. This magnetic field induces a current in the fieldshaper. Due to the skineffect this current circulates in opposite direction to the coil current at the outer surface of the fieldshaper and in the same direction as the coil current at the inner surface of the fieldshaper (the so called concentrating area (compare Fig. 3)).

Fig. 3: Arrangement and operating mode of a fieldshaper in a toolcoil [11]
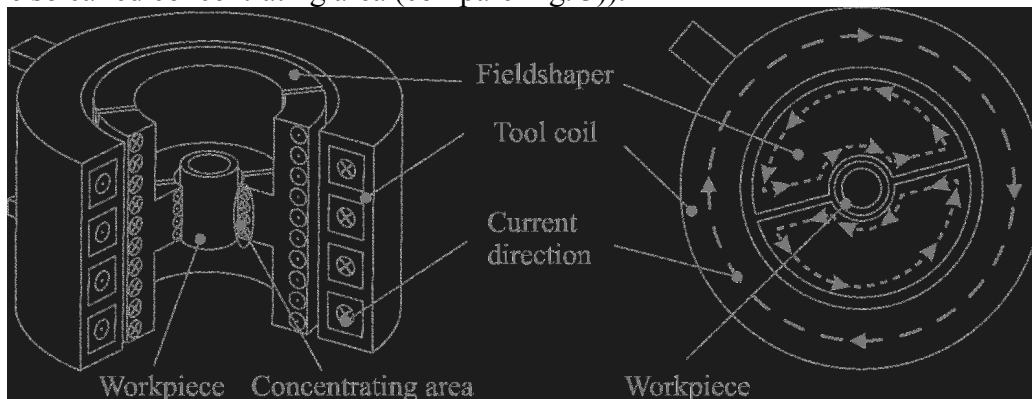
In most cases this inner surface is significantly smaller than the outer surface; therefore, the current density in this case is much higher than at the outer surface. According to the magnetic field in the gap between the fieldshaper and tube, a current is induced in the workpiece in the region of the concentrating area. If this current is closed, it shields the magnetic field. As known from the setup with a direct acting tool coil, the energy density in the gap between workpiece and tool coil is much higher than the energy density within the tube. In comparison to the setup with a direct acting tool coil, the efficiency coefficient of the process declines if a fieldshaper is used. This is evident because the extra gap volume between tube and fieldshaper has to be filled additionally with a magnetic field. Furthermore, the calculation of the course and the distribution of the magnetic field, and therefore also of the magnetic pressure, is much more complex and should therefore be performed using a simulation tool. However, the energy density again equates a magnetic pressure perpendicular to the magnetic field which causes the workpiece deformation [8].

Joints Made by EMF. In general, joints produced by electromagnetic tube compression can transmit forces by dominating force-fit or dominating form-fit. The strength of interference-fits manufactured so far is strongly depending on the area of the contact zone, the friction coefficient, and the remaining interference stress in the contact zone. While the first two aspects directly influence the strength of the joint, the last one effects the strength via material parameters like yield point and Young's modulus as well as on the geometrical stiffness of the parts to be joined [13].The constriction velocity of a tube being compressed (measured by a light shadowing method) as well as its mass determines the kinetic energy at the moment of impact and, therefore, the force which takes effect on the mandrel. Assuming a massive mandrel first, during this deformation process the tube is deformed plastically and the mandrel's deformation remains purely elastic [12]. After a decrease of the forces a corresponding elastic recovery of mandrel and tube occurs. If a full relaxation of the mandrel is prevented by the tube, a permanent pressure in the joining area (in the radial direction) is established. This pressure is a balanced condition of the mandrel's stress relief, on the one hand, and the resulting stress (caused by the elastic recovery of the mandrel) in the tube, on the other hand.

In Fig. 4, the influence of the compression velocity (determined by the charging energy) and the ratio of inner and outer mandrel's diameter on the strength of the joints are presented.
Using hollow mandrels with variable inner diameter at a constant outer diameter, the ratio of inner and outer diameter of the mandrel $Q=D_i/D_a$ has been defined as a representative value. The influence of Q on the push-out force has been experimentally examined by Bühler / v. Finckenstein [14]. They identified three characteristic areas for joining a copper tube onto a steel mandrel by EMF, as displayed in Fig. 4. Recent investigations proved the transferability of these results to aluminum alloys as well [13].
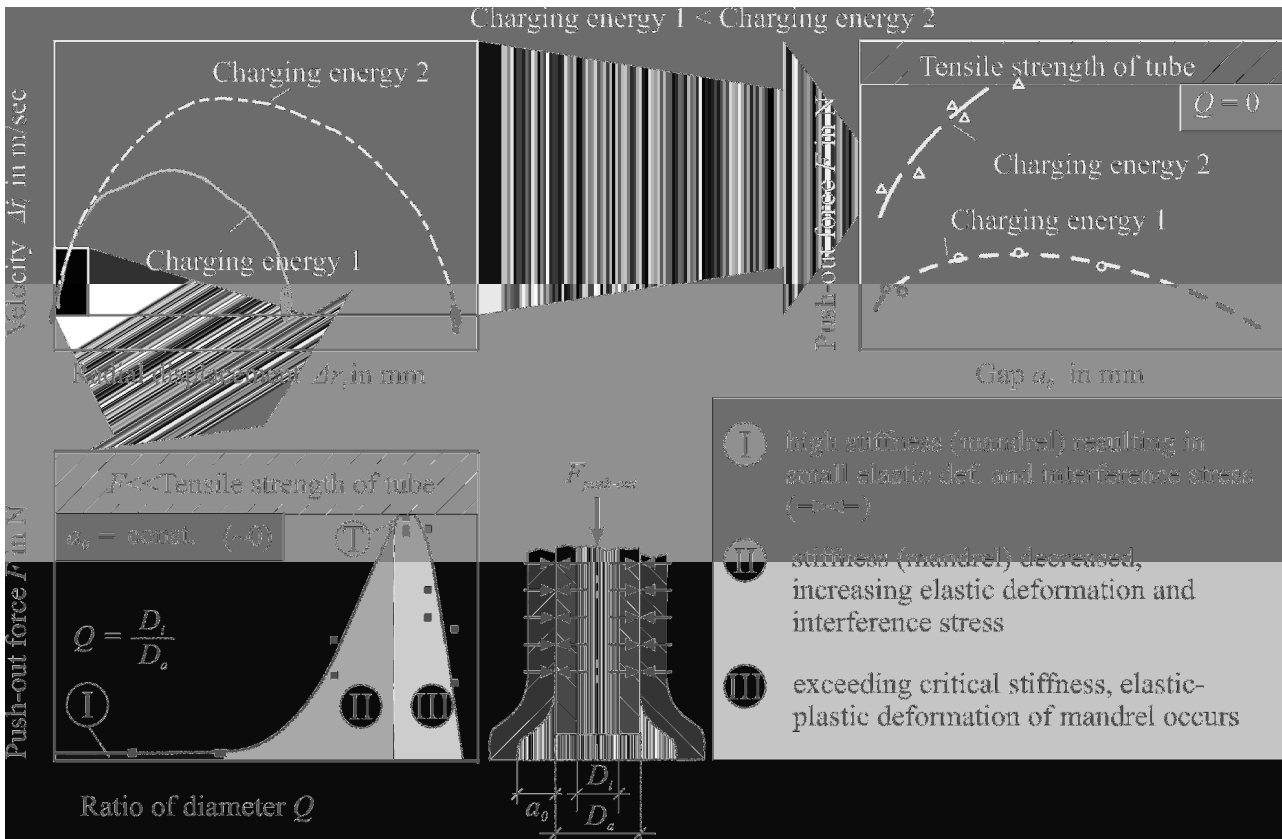
Fig. 4: Influence of the compression velocity and the ratio of inner and outer diameter on the push-out force in principle

Joining of Composite Extruded Profiles. The compression velocity (depending on the pressure pulse and the gap a_0, see Fig.4) plays a decisive role in the joining process. Selecting a suitable gap a_0 between mandrel and tube depends e.g. on an allowable diameter reduction of the tube. To determine the reduction limit of the composite extruded tubes, several composite extruded tubes of the same batch have been electromagnetically compressed. Taking the forming behaviour of composite extrudes tubes into account; an experimental setup was used consisting of a forming machine, a tool coil, fieldshaper and a composite extruded tube. This setup was used for both compressing the tube without a mandrel and for the joining process.

The charging energy, and therefore the resulting pressure pulse, was increased stepwise from sample to sample. By increasing the acting pressure pulse the resulting radial displacement was increased as well. The axial contour after forming was determined with a Zeiss coordinate measuring machine (Prismo VAST 5 HTG). As expected, an increase of the charging energy, and therefore of the pressure acting on the tube's surface, leads to a higher deformation degree of the tube. In addition, there is a slight increment of the deformed zone's length so that a clearly recognizable elongation of the tube occurs. The axial elongation of the tube causes at first a detachment of matrix and reinforcing element. Along with a continuing reduction of the diameter, necking of the reinforcing element occurs.

Fig. 5 displays micrographs made from a sectional cut in longitudinal direction of the tube's axis as well as in cross direction. Detachments as well as necking of the reinforcing element are clearly recognizable in the micrographs. Furthermore, the weld seam, which is determined by the extrusion process, is damaged by the forming process so that crack propagation is initialized.
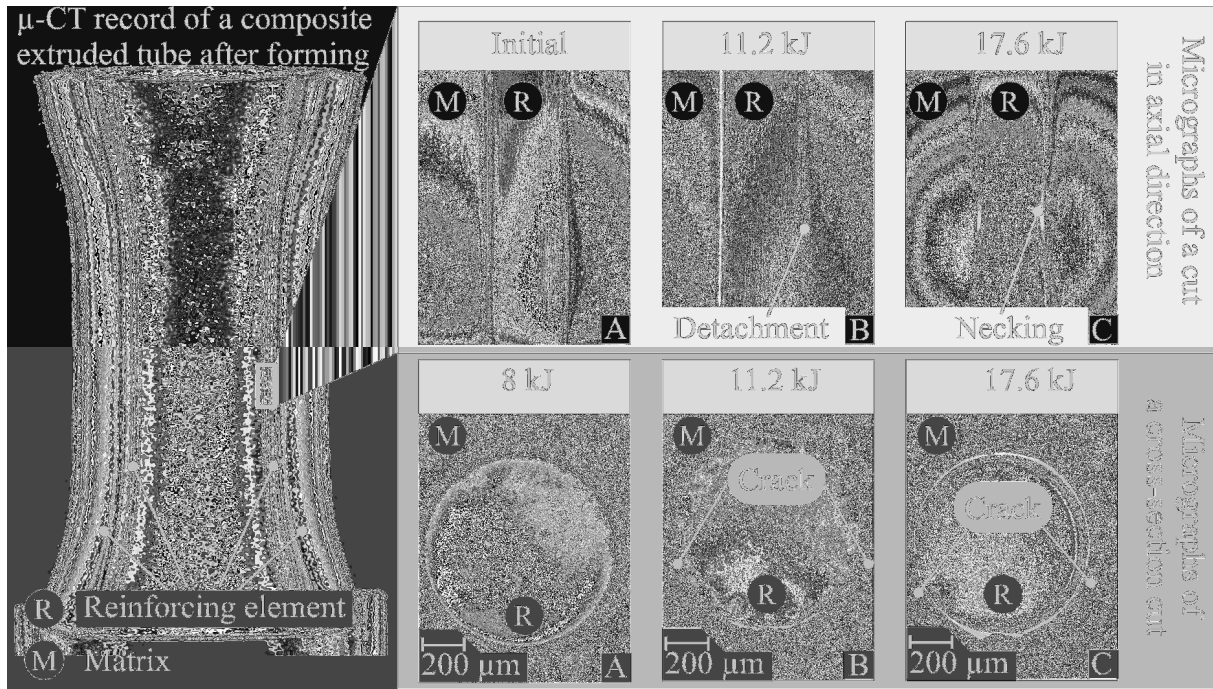
Fig. 5: Interface characteristics of matrix and tube after forming

Force-Fit Joining of Composite Extruded Tubes. Taking the above mentioned results into account, a suitable process window for joining composite extruded tubes by EMF can be deduced. Targeting a faultless interface between matrix and reinforcing element, a diameter reduction of 2 mm (7.4 %) seems suitable for joining. Finally, manufacturing of common dominating form-fit joints, where the tube is formed into distinct large grooves, has to be excluded as well because of high local strain of the tubes material.

Manufacturing sufficient joints remains still possible, but an adaptation of the joining partner design is binding. Considering a feasible strength a diameter ratio of $Q = 0.7$ (see Fig. 4) was manufactured ($D_i = 24$ mm; $D_a = 34$ mm). The parameters of the joining process were chosen guaranteeing that the inner joining partner was compressed merely elastically, which is indicated in Fig. 6.
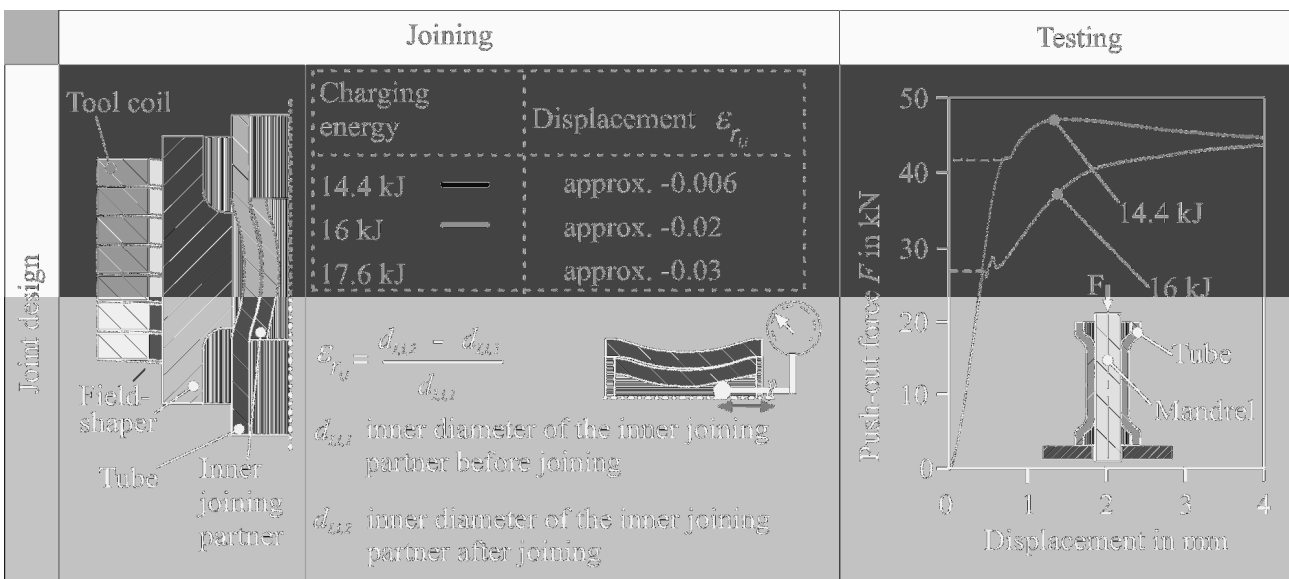

Fig. 6: Experimental results of joining and testing of an exemplarily force-fit joint with composite extruded tubes

The joint's strength was determined on a Zwick tensile test machine by pushing out the mandrel. A maximum transferable load of 40 kN was evaluated.

Form-Fit Joining of Composite Extruded Tubes. As discussed before, the implementation of a dominant form-fit joint by forming composite extruded tubes onto a grooved mandrel is possible, if the groove depth is adapted to the forming behaviour because of the limited allowable deformation of the composite extruded tube. Therefore, the inner joining partner was machined by cut knurling so that a rough surface with many grooves or corrugated surface respectively was manufactured. The maximal depth of the grooves was limited to 500 μm so that a maximal reduction of 1.1 % could occur. After that, composite extruded tubes were joined with such mandrels and tested by pushing out the mandrel. A maximum transferable load of at least 70 kN was determined, as displayed in Fig. 7. In spite of the fact that the tube's forming velocity is very low because of the small initial gap a_0, the achievable push-out forces can be significantly improved by employing mandrels with a cut knurled surface.
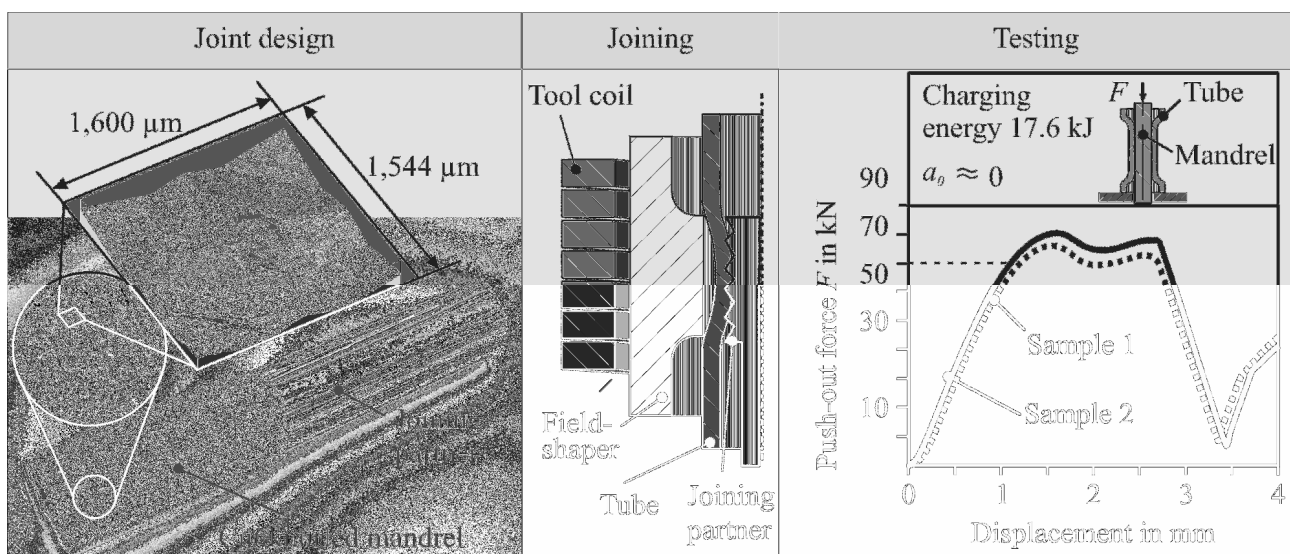

Fig. 7: Experimental results of joining and testing of cut knurled mandrels

Joining by Dieless Hydroforming

Investigations which are describing the joining by dieless hydroforming in this chapter have been done using conventional extruded tubes (without reinforcing elements) made of aluminium AA6060. Taking the process of dieless hydroforming into account, the pressure acts locally underneath a certain joining area instead of pressurizing a complete semi-finished part, as used in conventional hydroforming processes of tubes and sheet metal. The joining area is pressurized by a special joining tool, introducing it as hydro-probe. The hydro-probe is inserted into the tube, after that the working medium, which is set under pressure filles the gap between the probe and the inner surface of the tube. A sealing is limiting the joining area in circumference as well as in longitudinal direction.

Process-Principle of Joining by Hydroforming. The process of joining by dieless hydroforming can be classified into three characteristic phases, which are indicated in Fig. 8. In the first phase the tube will be expanded within the clearance's (gap's) limit, after that both parts (tube-ring) are expanding together until a maximal radial displacement is reached, which is determined by a related joining pressure (Fig. 8 a-b). The pressure ideally determines an elastic-plastic deformation of the tube, but a straight elastic deformation of the ring. Consequently, Kollmann [6] suggests for the manufacturing of shrinkage fits a maximum plastic deformation of approximately 30% concerning the total cross section of the joining partner. After releasing the pressure both tube and ring are recovering elastically. Subsequently, the elastic recovery of the ring is prevented by the expanded

tube, as the plastic deformation remains (Fig. 8 c). Furthermore, the prevented elastic recovery of the ring results in interference fit between the joining partners (tube and ring). As known from the manufacturing of camshafts, the joining partners should be arranged with increasing yield points from the inner to the outer joining partner, if both joint partners possess the same Young's-modulus [5]. Joining of aluminum and magnesium as well as the influence of maximum expansion under pressure, ring's wall thickness, and initial gap on the joint's strength have been briefly presented in [3] and more detailed discussed taking tools and repeatability into account in [15]. From an engineering point of view the working parameters of the fluid pressure p_f presents an important value for estimating the resulting joint's strength. According to research work performed by Garzke [5], the values of interference pressures p, which is the stress in the contact area of tube and ring, can be approximately computed.
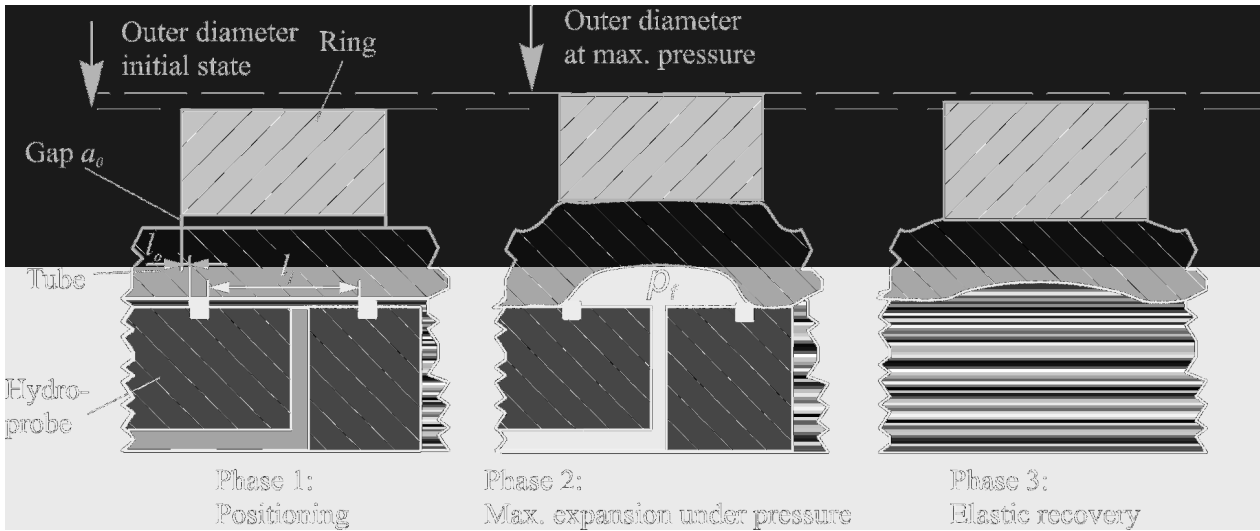

Fig. 8: Process principle of joining by dieless hydroforming
l_o – overlapping length from O-ring to ring's front end; l_j – length of joining area

The corresponding formula, which takes the influence of the mentioned working fluid pressure p_f along with the joining partner design and material properties into account, is described in Eq. 2 as follows:

$$p = \frac{\left[p_f - R_{ei} \cdot \ln\left(\frac{1}{Q_i}\right)\right] \cdot \frac{1}{E_o} \cdot \left[\frac{1+Q_o^2}{1-Q_o^2} + v_o\right] + \frac{2 \cdot Q_i^2}{E_i\left(1-Q_i^2\right)} \cdot R_{ei} \cdot \ln(Q_i)}{\frac{1}{E_o} \cdot \left[\frac{1+Q_o^2}{1-Q_o^2} + v_o\right] + \frac{1}{E_i} \cdot \left[\frac{1+Q_i^2}{1-Q_i^2} - v_i\right]} \cdot \tag{2}$$

p – interference pressure in N/mm^2,
p_f – working fluid pressure in N/mm^2,
R_{ei} – elastic limit of the tube material in N/mm^2,
E_i – modulus of elasticity of the tube material in N/mm^2,
E_o – modulus of elasticity of the ring material in N/mm^2,

v_i – Poisson´s ratio of the tube material,
v_o – Poisson´s ratio of the ring material,
Q_i – diameter coefficient of the tube $Q_i = d_i/d_o$,
Q_o – diameter coefficient of the ring $Q_o = D_i/D_o$.

The calculated interference pressure p is a regularly distributed, tangential mean value, which has been derivated assuming plane stress, maximum shear stress criterion, and ideal plastic material.

Force-Fit Joining of Extruded Tubes. Therefore, the real distribution of the tangential strain in the joint after the joining process could not be indicated. Furthermore, buckling of the rings occurs so that a barrel-like shape of the ring results. Experimental investigations have been carried out to detect the developing shape during the joining process and the causal tangential stress as well as its

distribution in axial direction on the ring's surface after the joining process. Tests have been done using ARAMIS by gom, which is a non-contact optical 3D deformation measuring system. Starting with the first recorded image, which represents the initial, undeformed state of the ring ARAMIS compares following digital images and stepwise calculates the displacement and deformation of the ring. As the system operates with two independent cameras, it is particularly suitable for three-dimensional deformation measurements under static and dynamic load in order to analyze deformations and strain during the joining process. Fig. 9 displays the major strain and its axial distribution after the joining process on the ring's surface.

As a result of the overlapping lenght l_o, the ring's front end, whose position is indicated as area *I* in Fig. 9, applies a pressure radially against the tube's wall, introducing it as rim stress. Consequently, a major strain in this area is determined as negative, whereas another major strain between the O-ring sealings, indicated as area *II*, remains positive. Subsequently, this determines some requirements for both process guiding and process design. Taking the process design into account, the length of the ring and joining length l_j should be designed equally at best in length to avoid buckling and an unregular axial distribution of major strain as well as causal rim stress. Therefore, the overlapping length l_o should be designed as small as possible. Consequently, process guiding has to be designed so that an accurate positioning of the hydro-probe (and therefore of the sealing) is guaranteed.
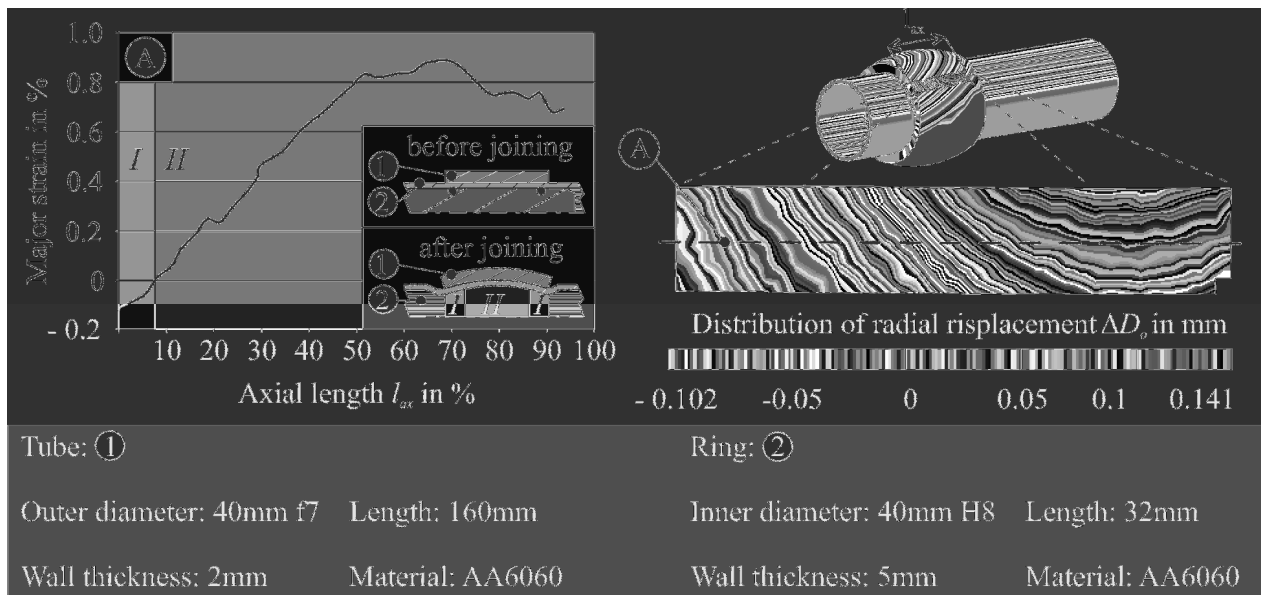

Fig. 9: Optically measured distribution of major strain on the ring's surface after joining

Form-Fit Joining of Extruded Tubes. Furthermore, joining could be done by forming the tube into a grooved ring. Designing feasible grooves offers a wide range of appropriate groove shapes. Basic experimental investigations have been done to carry out the influence of the groove's shape on the joint's strength. As indicated in Fig. 10, groove shapes have been manufactured according to basic geometrical layouts, which are in detail round (R), trapezoid (T), rectangular (RE), and triangle or v-shaped (V). To evaluate comparable results in terms of the joining quality, groove length, groove width, and radii of the groove's edge were machined in the same way. Moreover, process parameters like the ring's expansion during the joining process as well as the material of tube and ring were identically used for the experimental investigations.

The maximal transferable load was determined by tensile tests on a Zwick Z250. To identify the quality of the form-fit joints, the acceptable load of a cylindrical (C) force-fit joint was chosen as a reference. Consequently, the final shape of the tube section, which was formed into the groove, was investigated as well. After joining was finished, cutouts were machined to evaluate the quality of the manufactured shape of the tube's section. Both axial load and final shape are indicated in Fig. 10 in

comparison to the groove's shape. As expected, according to the publication of Dudziak [16], small radii were not produceable by the applied pressure, which was increased during the joining process until elastic deformation of the ring occurs.

Taking the applied pressure into account, the elastic deformation of the outer ring determines a process limit for manufacturing both force- and form-fit joints. Furthermore, a pre-damaging of the tube by the manufacturing of a form-fit joint, e.g. caused by a cut of the grooves edge, was not detactable. Subsequently, taking rectangular grooves (RE) into account, resistance against axial load is dominantly caused by the form-fit. Evidently, this is due to the very small area of contact between tube and ring, as indicated by the micrograph in Fig. 10. If an axial load is applied to the joint, failure proceeds by bending or pushing of the tube's wall backwards to its initial geometry. The bending momentum is applied at the groove's edge. If the groove edge is rounded (R) or chamfered (T), the contact situation changes from point or line contact to an area contact situation. Consequently, slipping of the tube's wall about the grooves edge and shoulder occurs more evident, which leads to less resistance against axial load. Taking v-shaped grooves into account, a stabilization of the joint could be generated by the opposing groove's shoulder, which then leads to a higher resistance against deformation.
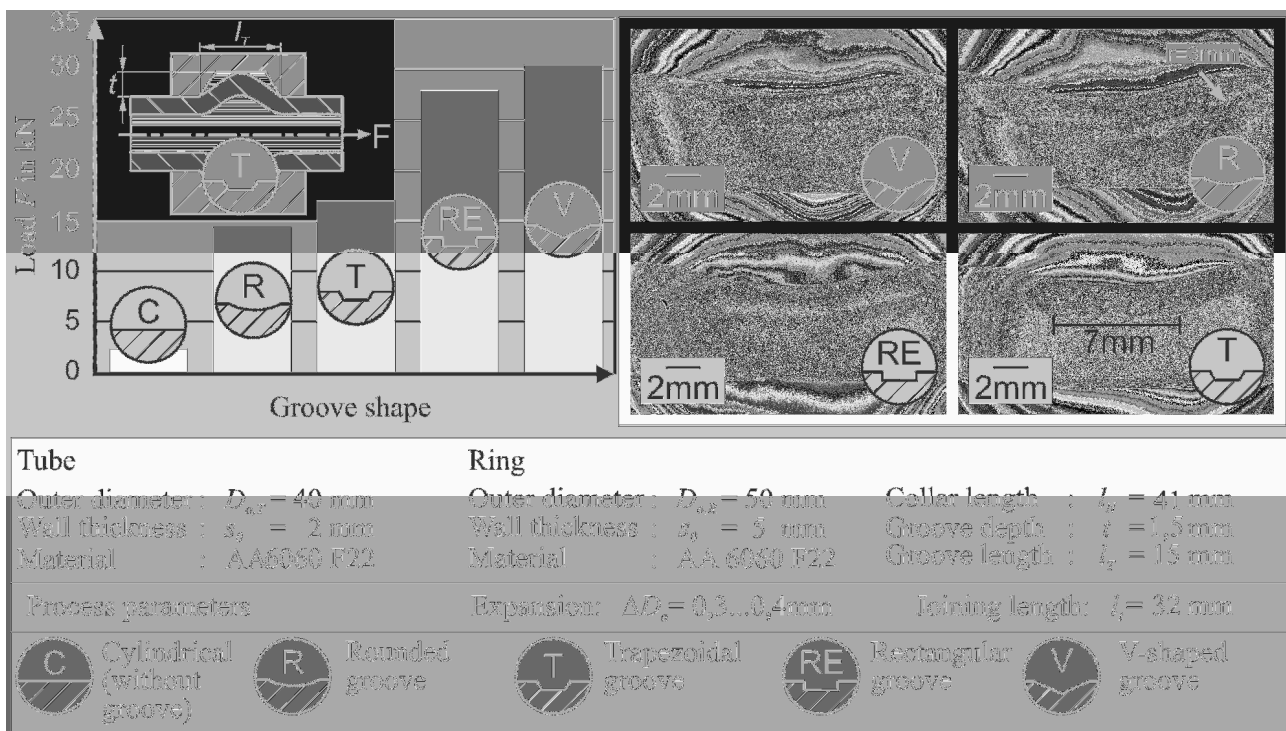
Fig. 10: Quality of form-fit joints taking different groove shapes into account

Form-fit joints are able to resist higher axial loads compared to force-fit joints. Besides the grooves geometry its shape is a major influencing factor on the joint as well. The shape determines the maximum load as well as possible points at risk from corrosion, if tube's material is not properly formed into the groove.

Taking corrosion into account tube's material is formed into rounded grooves (R) at best, which leads to minor risk of corrosion. In addition, tube's material was not properly formed into the other investigated groove shapes. This leads to higher risk of corrosion due to gaps between the tube and the ring in which fluid e.g. water could remain after joining. As a result, corrosion proceeds in these cases from the inside to the outside. Because corrosion starts from inside the joint both appearance and development is hardly to detect.

Summary and Outlook

In this paper, the processes of joining by compression - using an electromagnetic pulsed pressure - and by expansion - using a quasistatic high water pressure - of aluminium profiles have been described.

At first, the forming behavior of composite extruded tubes, compressed by electromagnetic forming has been analyzed, taking material characteristics e.g. the forming behaviour into account. The allowable forming limit of the composite extruded tube which is important for selecting feasible the joining parameters was finally limited by crack initiations in the profile. Furthermore, dominating force-fit and form-fit joints have been exemplarily manufactured considering the low acceptable deformation of the composite extruded tube. As a result, the pull-out forces could be increased from 40 kN in force-fit joints to 70 kN in form-fit joints in a first step.

Future investigations have to be conducted in the extrusion process as well as in the joining process. The composite extrusion process will be further improved in order to produce composite extruded profiles with an increased number of reinforcing elements along with a smaller wall-thickness. In addition, the forming limit of composite extruded tubes has to be increased as well. Investigations on the joint design have to proceed as well. For instance, if cut knurling is used, effects on the joint under cyclic load focusing on crack initiation need to be investigated. As cut-knurling is one surface for increasing the joint's strength

Thereafter, joining of tubular workpieces by dieless hydroforming seems to be feasible as well. Joints produced by this process are able to transmit high axial loads. Positioning of the tool remains a major objective for introducing this joining process into manufacturing, targeting a homogenous expansion of tube and ring. Unsuitable positioning determines inhomogeneous expansion of the ring, which leads to an irregular development of the interference stress in the contact zone between tube and ring. Furthermore, the geometric shape of the expanded ring occurs barrel-like, which has to be considered in future investigation, if parts of more geometric complexity like nodes are joined. As a major process characteristic is the very small necessary degree of deformation for producing force-fit joints, the process seems suitable for further investigations, taking the joining of composite extruded profiles into account. At present, joining of profiles without a round cross-section remains difficult due to sealing and leaking challenges related to the tool design so that further development is needed here.

Furthermore, joining of profiles with a small forming limit like the composite extruded tubes determines more investigations targeting higher resisting loads. Consequently, effects of structuring the surface in micro- as well as in macro-scale on the joints quality need to be investigated.

Acknowledgements

References

[1] A. Klaus, M. Kleiner: Research for a Flexible Production of Lightweight Space Frame Structures, In: Advanced Materials Research: Flexible Manufacture of Lightweight Frame Structures, Band 10 (2006), pp. 89-100

[2] M. Kleiner, M. Schomäcker, A. Klaus: Influencing Factors on the Manufacture of Composite Extrusions, In: Annals of the German Academic Society for Production Engineering, WGP, Vol XIII/1 (2006)

[3] W. Homberg, M. Marré, C. Beerwald, M. Kleiner: Joining by forming of lightweight frame structures, In: Advanced Materials Research: Flexible Manufacture of Lightweight Frame Structures, Band 10 (2006), pp. 89-100

[4] M. Kojima, K. Tamaki: Factors affecting the result of electromagnetic welding of aluminum tube. Transactions of the Japan Welding Society, 1953–59, 1988.

[5] M. Garzke: Auslegung innenhochdruckgefügter Pressverbindungen unter Drehmomentbelastung. Diss. TU Clausthal, VDI Verlag Düsseldorf, 2001

[6] F. Kollmann: Welle-Nabe-Verbindungen, Gestaltung, Auslegung, Auswahl, Springer Verlag Berlin (1984)

[7] M. Marré, W. Homberg, A. Brosius, M. Kleiner: Umformtechnisches Fügen In: Fortschr. Ber. VDI Reihe 2 Nr. 661, VDI-Verlag Düsseldorf, 2007, pp. 215-245

[8] F. Wilson: High Velocity Forming of Metals, A.S.T.M.E, Englewood Cliffs, USA, 1964

[9] P. Zhang, G. Daehn: Analysis of the electromagnetic impulse joining process with a field concentrator. In: Ghosh S, Jose M, Castro JM, Lee JK, editors. In: Proceedings of the eighth international conference on numerical methods in industrial forming processes, Columbus, OH, 2004. pp. 1253–58.

[10] C. Beerwald: Grundlagen der Prozessauslegung und -gestaltung bei der elektromagnetischen Umformung. Universität Dortmund - IUL, Dr.-Ing. Diss., Reihe Umformtechnik, Shaker Verlag, Aachen 2005, ISBN 3-8322-4421-2.

[11] Schnelle Magnetische Umformung. Firmenschrift der Puls-Plasmatechnik GmbH, Dortmund, 1990

[12] P. Barreiro, V. Schulze, D. Löhe, M. Marré, C. Beerwald, W. Homberg, M. Kleiner: Strength of tubular joints made by electromagnetic compression at quasi-static and cyclic loading, In: 2nd International Conference on High Speed Forming, 20.3.-21.3.2006, Dortmund, Germany, Proceedings, pp.107 -166, ISBN 3-00-018432-5

[13] M. Kleiner, M. Marré, C. Beerwald, W. Homberg, D. Löhe, P. Barreiro, V. Schulze: Investigation of force-fit joints produced by electromagnetic tube compression, In: Annals of the German Academic Society for Production Engineering, WGP, Vol. XIII/1 (2006), pp. 227-230

[14] H. Bühler, E. von Finckenstein: Fügen durch Magnetumformung, Werkstatt und Betrieb, 101. Jahrg., Heft 9 (1968) pp. 209-215

[15] W. Przybylski, J. Wojciechowski, M. Marré, M. Kleiner: Archives of Mechanical Technology and Automation, Vol.27 Nr. 1, Polish Academy of Science, 2007, S. 152-167 ISSN 1233-9709

[16] K.-U. Dudziak: Prozessmodell zum Innenhochdruckumformen von hohlwellenförmigen Werkstücken, Fortschrittsberichte VDI, Reihe 2, Nr.368 VDI Verlag GmbH, Dissertation Universität Paderborn (1996)

Bifocal Hybrid Laser Beam Welding and Friction Stir Welding of Aluminium Extrusion Components

Michael F. Zaeh[1,a], Paul Gebhard[1,b], Sonja Huber[1,c], Markus Ruhstorfer[1,d]

[1]Institute for Machine Tools and Industrial Management *iwb*, Technische Universität München, Boltzmannstr. 15, 85748 Garching, Germany

[a]michael.zaeh@iwb.tum.de, [b]paul.gebhard@iwb.tum.de, [c]sonja.huber@iwb.tum.de, [d]markus.ruhstorfer@iwb.tum.de

Abstract

On a global market, new products are subject to rising requirements regarding strength and quality. Simultaneously, the conservation of the environment and natural resources has become a key priority. One approach to these demands is the weight reduction of mechanical components by lightweight construction. The Transregional Collaborative Research Center (TR 10), funded by the German Research Foundation (DFG), is therefore working on the "Integration of forming, cutting and joining for the flexible production of lightweight space structures". The use of light metals, like aluminium and composite materials is a main part in the TR10 process chain. This paper deals with the challenges of welding of light weight components made out of EN AW-6060. It shows the use and potentials of two innovative joining processes, particularly suited for welding aluminium. Especially developed for the fusion welding of aluminium components, BHLW (Bifocal Hybrid Laser Beam Welding), combines a Nd:YAG and a high power diode laser. The paper will give insight into the findings of the achieved results so far and line out the further proceedings with regard to critical parameters and their effect on the overall laser welding process. For the welding of aluminium composite materials, which play a big role in the TR10 process chain, Friction Stir Welding (FSW) is evaluated. As a solid state joining process, it can be used for the welding of materials that are hardly weldable with fusion welding techniques. In this paper, results of basic experiment for the joining of reinforced aluminium and the resulting process forces are presented.

Introduction

The continuing worldwide trend towards light weight construction has led to an increasing application of light metals like aluminium. This applies not only to the use of component parts. Aluminium is also more and more utilised in light metal welded structures. Particularly in the automotive and aeronautical industry, components and welded constructions made out of aluminium and its alloys are in high demand. This development has already led to a row of innovations in joining processes trying to overcome limitations regarding the weld ability of aluminium. Yet, many of these difficulties remain still unsolved and often complicate the use of aluminium structures in industrial applications. The Transregional Collaborative Research Center (TR 10), combining the research activities of the University of Dortmund, the Universität Karlsruhe and the Technische Universität München, works on the "Integration of forming, cutting and joining for the flexible production of lightweight space frame structures". In this project, the focus of the *iwb* lies on joining technologies for the welding of aluminium extrusion components made of EN-AW 6060 by BHLW (Bifocal Hybrid Laser Beam Welding) and FSW (Friction Stir Welding).

BHLW is investigated and developed at the *iwb*. Emphasising on investigating the inner procedures of the BHLW process and to improve the systems engineering, the first phase of the project, funded by the DFG was concluded successfully [1]. Future work packages will see to refine the welding process using novel laser sources and to integrate an online process monitoring system.

Including a process monitoring system will allow for gaining more process knowledge and securing the weld seam quality during welding of light weight aluminium structures.

Friction Stir Welding (FSW) was developed in 1991 at The Welding Institute (TWI) in Cambridge [2] and is a solid state joining process. In this project, it is used for welding aluminium extrusion components which are reinforced by steel wires and are hardly weldable with traditional fusion welding techniques.

Bifocal Hybrid Laser Beam Welding of Aluminium

The experimental setup for the Bifocal Hybrid Laser Welding incorporates a 3 kW Nd:YAG laser and a 3 kW high power diode laser (HPDL), both integrated by one optical head and acting in the same process zone. During the first funded research period the diode laser was integrated in the optical head and the Nd:YAG laser was linked via a fibre optic cable. This resulted in a bulky optical setup with an inherent 25 % loss of power from the diode laser beam by attaching it via an optical fibre cable. Transferring both lasers via fibre cable would entail that the welding process could not work because of the lack of HPDL power. The specifications of the whole welding system are defined by the lasers and the optical system. Because of the HPDL transmitted directly with a beam parameter product (BPP) of 85 x 200 mm*mrad a rectangular focus (f = 150 mm) of 0.9 x 3.7 mm can be generated. Unlike the diode laser the utilised Nd:YAG laser has a BPP of 25 mm*mrad transformed by a focussing lens (f = 150 mm) into a circular focus with a diameter of d = 0.45 mm. By adjusting the optical system the positioning of both foci is possible and offers beneficial welding effects [3]. In Fig. 1 a measurement of their power density distribution and the relative positioning of both laser foci are displayed.
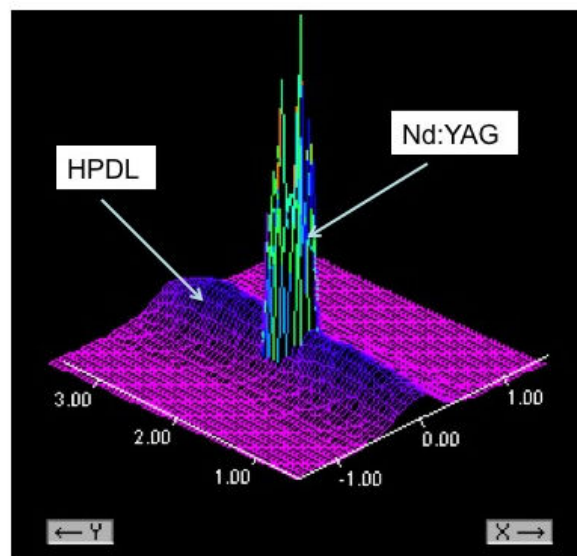

Fig. 1: The measurement of the intensity distribution of the HPDL superimposed by the Nd:YAG laser illustrates the relative lateral positions of the foci during BHLW

Fusion Welding Characteristics of the Aluminium Alloy EN AW-6060

The considered aluminium alloy in terms of extruded profiles of the EN AW-6060 (AlMgSi0.5) temper T66 demands the admixture of filler wire AL4046 A (SG-AlSi12) for welding to prevent hot cracks. During fusion welding some aluminium alloys tend to be susceptible to hot cracks generation [4]. Hot cracks weaken the welded joint by decreasing the tensile strength. As it could be seen in [4] the applicability of fusion welding to aluminium alloys depends a lot on the alloy's individual composition. An alloy with a concentration of 0.5 % Si and 0.3 % Mg is most uneligible

for fusion welding [5]. Considering the composition of the used alloy EN AW-6060 the laser welding technique presented in this paper was mainly designed for laser welding of aluminium alloys tending to have hot cracks after fusion welding. Especially this certain aluminium alloy is deemed to be hardly weldable.

BHLW joins the deep penetration effect of an Nd:YAG laser with the conduction mode welding of a HPDL. The beams of the lasers are superimposed in the process zone thereby inducing several synergetic effects. By virtue of the superposition the welding process differs in energy transfer efficiency compared to the individual welding processes. However it is not yet possible to explain this synergy by consideration of data already known. Welded joints of the aluminium alloy EN AW-6060 by BHLW show a significant reduction of porosity independent of the used gas in comparison to the individual Nd:YAG laser welding. Process pores emerge in aluminium because of a repeated closure of the keyhole [6]. During BHLW processing it can be assumed that the rectangular HPDL spot assists the Nd:YAG laser process. Besides the reduction of pores inside the seam, the HPDL affects the quality of the weld seam surface. The positive effects of the HPDL welding concerning surface quality of weld seams demonstrate an advantage during BHLW [3].

In the course of the first phase of TR 10 a new optical head was developed. This optical head offers a more accurate lateral and vertical positioning of the laser foci relative to each other in contrast to the optical head used during the experiments conducted in phase 1. However, the execution of the experiments was constricted by the imprecise and limited adjustment of the foci positioning of both lasers. Consequently it is hardly possible to examine the effects of varying the relative position of the foci. An additional optical component enables the option for creating and varying the rectangular focal spot layout (Fig. 2a) of the HPDL which is essential to remove the oxide layer. In order to continue the research on the BHLW technique in terms of welding of aluminium structures the new possibilities for adjustments and more laser power will help to refine the investigations of the BHLW process. With the objective to substantiate the already existing results, experiments will be done by variation of the relative foci position of the foci in lateral and vertical direction (Fig. 2b, 2c) of two differently shaped laser spots.

The influence of focal variations should provide an indication of the interaction with geometrical, material and process parameters. Varying joint geometries, e.g. butt and lap joints, will be analysed with regard to the following seam parameters:

Joint geometry:
- welding depth
- welding width
- cross sectional area

Joint quality:
- quality of the weld seam surface
- imperfections
- disposition of the filler wire
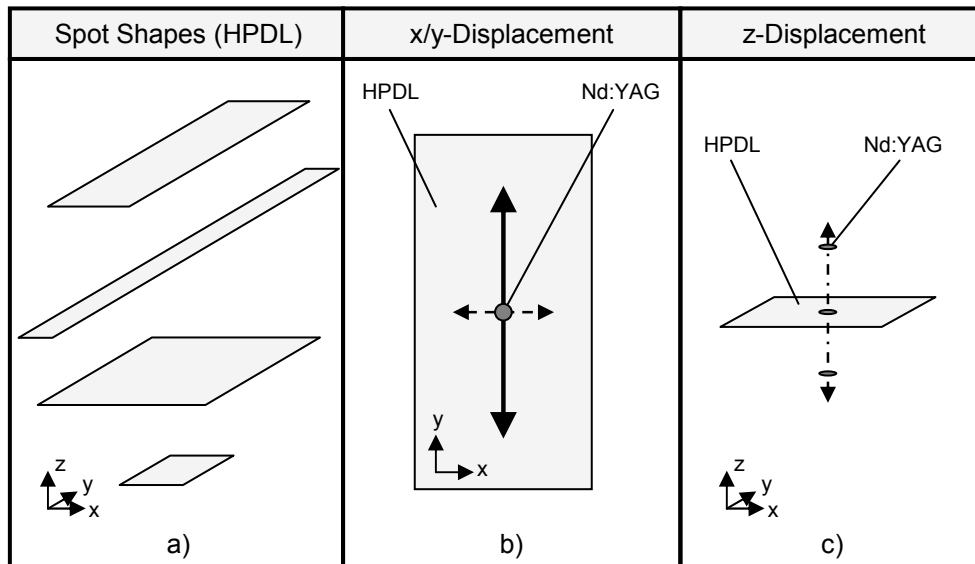- sensitivity to hot cracks generation

Fig. 2a, b, c: a) Various possible shapes of the HPDL focal spot. By varying the focal spot shape the welding process can be affected. b) relative displacement of HPDL and Nd:YAG focal spot in lateral direction. c) relative displacement of HPDL and Nd:YAG focal spot in vertical direction

Since welding results depend not only on parameters of adjustment, but also on the specific parameters of the laser beam, experiments will be made with two different combinations of laser sources. The combination of a 3 kW Nd:YAG laser with a 6 kW HPDL or an 8 kW fibre laser with a 6 kW HPDL are imaginable. The deployment of the 6 kW HPDL will clarify the influence of the HPDL on the BHLW process. Thereby the influence on frontal oxide layer removal, magnification of the melt pool, welding depth, reduction of porosity and the homogenous disposition of filler wire can be continuously examined. Supplying two individual lasers via fibre optic cable to an enhanced optical head allows for a considerable weight reduction and reduced dimensions.
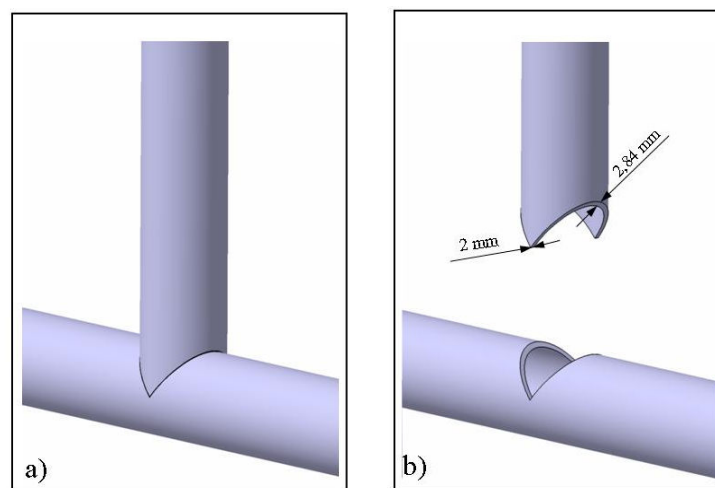
Fig. 3: T-joint of round aluminium profiles (Ø 40 mm), a) joint geometry of the T-joint, b) modification of the thickness along the faying surfaces for welding

This step will enable an application of the BHLW to weld aluminium structures. Working with spatial structures poses the general problem of reduced accessibility in beam welding resulting in a reduced angle of incidence of the beam. Due to the substitution of the Nd:YAG laser by an 8 kW fibre laser investigations regarding the work piece thicknesses will be possible. This is a step towards examining the welding of structural parts. Fig. 3 shows a T-joint of round profiles with a

diameter of 40 mm and faying surfaces prepared for laser welding. Alongside the cross section an increase of the welded thickness occurs.

Process monitoring during BHLW

Despite the exhibited raise in the quality of the weld seams, experiments showed that online surveillance of the process and as such assuring quality is still an issue at hand. Up to now the welding process of aluminium lacks the stability and continuity to allow for a straightforward use of online optical methods for melt pool observation and quality assurance. As the screen sequence in Fig. 4 a) demonstrates, the welding of aluminium with an Nd:YAG laser shows unstable characteristics. The images demonstrate the staggering lighting conditions during Nd:YAG laser welding. During BHLW of aluminium the lighting conditions of the welding process are in contrast quite homogeneous, as observed with a high-speed camera (Fig. 4 b)).
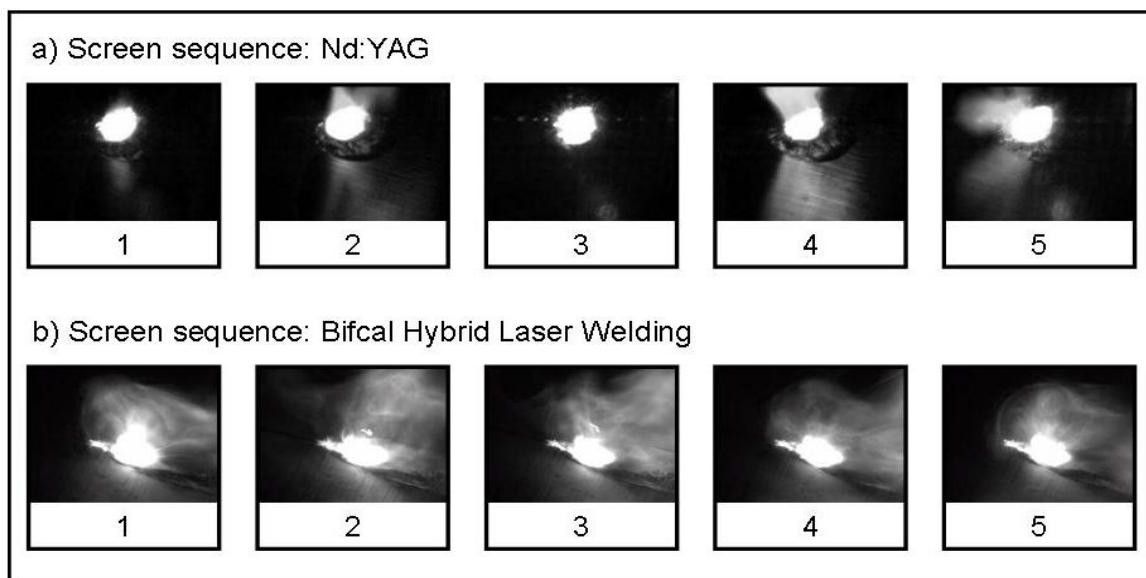

Fig. 4: Screen sequences of a high speed camera show: a) Nd:YAG welding: luminosity of the process radiation shows fluctuation b) BHLW: luminosity of the process radiation is stable

Since optical methods locate failures inside the weld seam by detecting process irregularities deviating from the process radiation during welding [7], an unstable welding process will complicate the analysis. In literature different optical methods using this principle for process monitoring can be found [7, 8, 9]. As the BHLW process shows homogeneous lighting conditions, a proper process monitoring should provide the potential to observe the process zone surface. In order to gain more information about the BHLW process, spectroscopic measurements will be done. Dimensioning for the process monitoring will be possible by analysing the spectroscopic measurements. The spectroscope measures the process radiation including the thermal radiation of the melt pool, the emissive element lines and the metal oxide molecule bands. When focussing a high power laser like an Nd:YAG laser or a fibre laser beam onto a work piece, the irradiance leads to a fast local heating and an intense evaporation of material. The evaporated material absorbs the laser radiation and generates the so called laser-induced breakdown, which means the plasma generation [10].

Spectroscopic measurements were done for the individual Nd:YAG welding of aluminium alloy EN AW-6060. Therefore a spectrometer sensitive for the wavelengths 380 nm to 880 nm was utilised. Fig. 5 demonstrates the experimental set-up for the spectroscopic measurements.
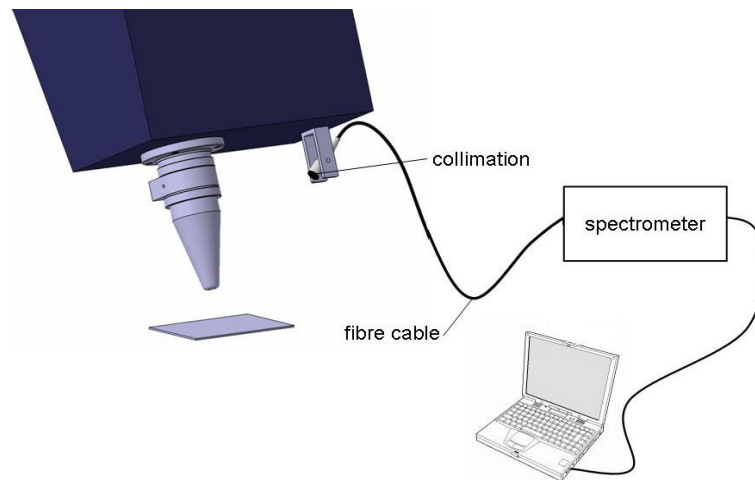

Fig. 5: Experimental set-up to measure the spectral intensity distribution during Nd:YAG welding with a spectrometer ($\lambda = 380$ nm – 880 nm)

The collimating lens of the fibre coupled spectrometer was clamped to the bottom of the optical head and oriented towards the focal spot of the Nd:YAG laser. An additional high speed camera was implemented for documentation.
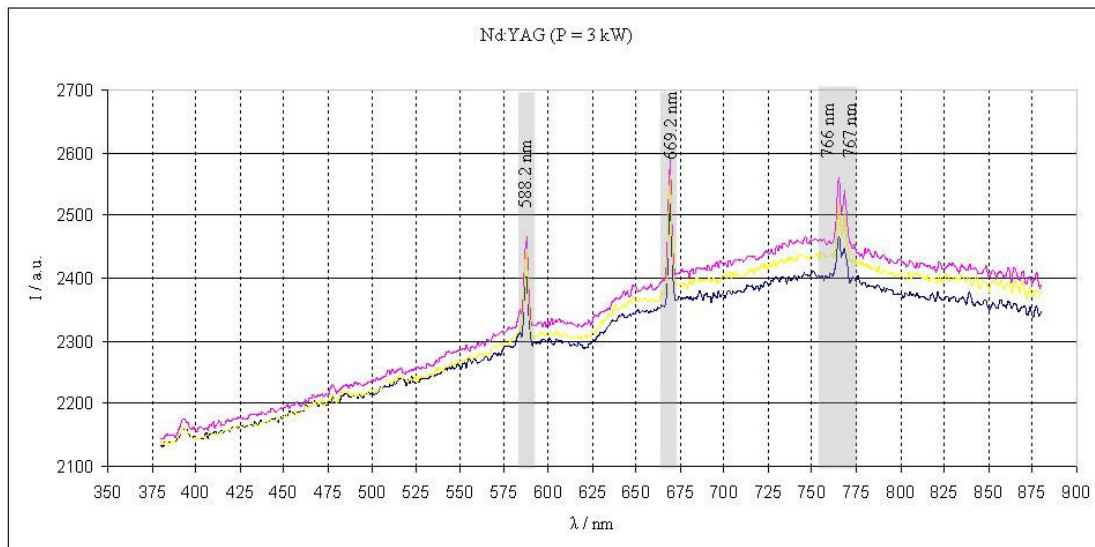
Fig. 6: Spectrum during 3 kW Nd:YAG welding of EN AW-6060. A few of the elemental lines are indicated.

The result is displayed in Fig. 6 showing the spectrum of the radiation of the melt pool and plasma plume during Nd:YAG welding. For the observation of the process zone the emissive element lines and the metal oxide molecule bands will interfere, because they are caused by the transitions inside the plasma. For dimensioning the monitoring system a wavelength band area should be chosen, where no emissive element lines are, otherwise the plasma plume will be considered. To create a suitable monitoring system it is necessary to carry out spectroscopic measurements and analysis for the 6 kW HPDL welding as well as for the Bifocal Hybrid Laser Welding.

Friction Stir Welding of non-reinforced and reinforced aluminium alloys

As mentioned before, BHLS is a suitable joining process for the production of high quality seams in aluminium structures. Yet, it is only applicable for the welding of homogeneous aluminium alloys. Modern materials science often develops composite materials which are supposed to be superior to their respective base materials. In the TR10, such a composite material was created. It was developed and manufactured at the Institute of Forming Technology and Lightweight Construction (IUL) of the University of Dortmund. The base material is an aluminium alloy EN AW-6060 T4 which is reinforced with six steel wires with a diameter of 1 mm (see Fig. 7). These wires are made out of a stainless, austenitic steel 1.4310 (X10CrNi18-8), which for example is used for pens or sheets in car production [11].
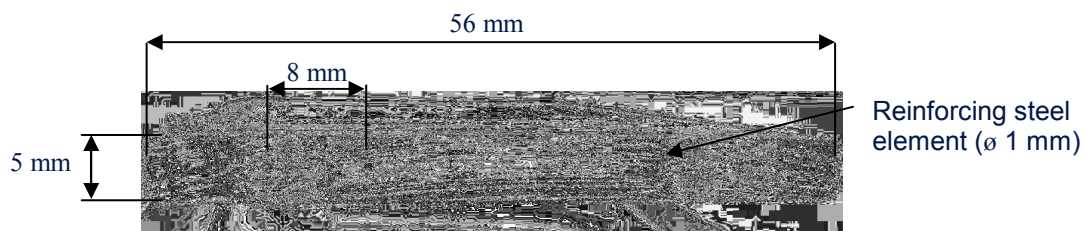

Fig. 7: Extruded EN AW-6060 T4 aluminium alloy with reinforcing elements

The nature of this composite material makes it difficult to weld with fusion welding processes like BHLW, since it would combine two materials with considerably differing properties (in terms of density, melting point, absorption coefficient etc.) in one fusion zone. Furthermore, the forming of brittle intermetallic phases is not desired. Promising results are expected to be possible with solid state joining processes which are not as susceptible to different material properties. Because of that, Friction Stir Welding (FSW) is evaluated for the joining of this composite material.

Friction Stir Welding is a solid state joining process, combining frictional and deformation heating to obtain defect free high quality joints. It is a modification of common rotary friction welding, but does not need the relative movement between the work pieces as joining is achieved by a non consumable rotating tool (see Fig. 8). This tool consists of two functional areas, the tool shoulder and the tool pin. The tool is forced into the join partners where the shoulder generates most of the frictional heat, and the welding is achieved by material transport around the tool pin. The material of the work pieces is not melted, and the temperature in the joint is kept below the liquidus line. The absence of a liquid phase during the joining process results in excellent weld quality without pores and low distortion. Drawbacks of this process are the high process forces which act upon the equipment and the joint partners.
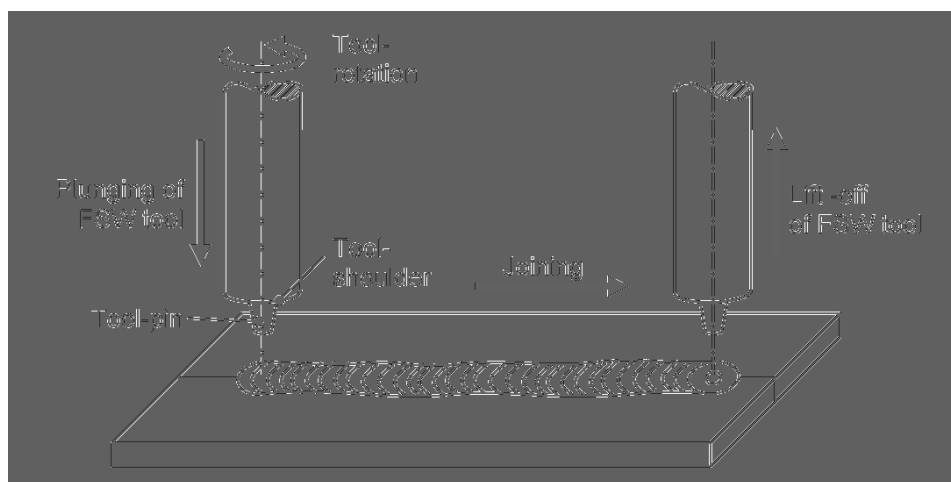

Fig. 8: Friction Stir Welding Process

The research on FSW of reinforced aluminium extrusion alloys seeks answers to the following questions:

- How do the process forces react?
- What happens to the reinforcing elements during the welding process?
- Which consequences does this have for the strength of the joint?

All experiments were conducted on a Heller MCH 250 high performance machine tool. The used tools had a shoulder diameter of 10 mm with a pin diameter of 4 and 5 mm. The length of the pin is 4.7 mm. All welds are done with a tilt angle of the tool of 2° and a programmed plunge depth of the tool shoulder of 0.2 mm.

Friction Stir Welding of non-reinforced Aluminium

As mentioned before, the focus of this study is to weld extruded aluminium profiles, reinforced with steel wires. In order to successfully join this composite material it is necessary to know how the base material reacts during friction stir welding. Therefore the weld properties of the base material are explored beforehand. The base material is an aluminium extrusion alloy, EN AW-6060 (AlMgSi0.5) tempered T4, with dimensions 56 mm x 5 mm. There are two reasons for preliminary weld experiments with the base material:

- Finding a parameter window for the non-reinforced aluminium as a basis for weld experiments for the reinforced alloy
- Documenting the process forces during welding in order to compare the forces with these occurring during welding of the composite material

The varied parameters for these tests were the rotation speed of the tool and the welding speed. They were changed from 500 rpm to 1500 rpm and 100 mm/min to 300 mm/min respectively.

To evaluate the process parameters, metallographic analysis was conducted for each weld. A cross section of a defect free and a flawed joint are shown in Fig. 9a and accordingly 9b. The weld joint in Fig. 9a was manufactured with a welding speed of 200 mm/min and a rotation speed of 1250 rpm. The other cross section in Fig. 9b shows a joint welded with a rotation speed of 1500 rpm and a welding speed of 400 mm/min. These parameters led to a flawed joint very likely caused by too little heat input [12] resulting from the high welding speed. Cavities in the lower area oft the FSW-nugget occur in all welds with too little heat input. According to these results, the process window for further tests with reinforced aluminium components was set to a range of 750 rpm to 1500 rpm and 100 mm/min to 200 mm/min.
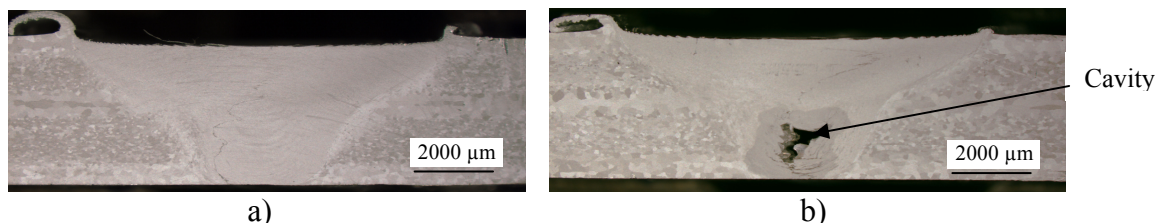
Fig. 9: Metallographic cross section of friction stir welded aluminium without reinforcing elements a) without cavity b) with cavity

During these preliminary tests, the downward force and the force in weld direction were recorded by the control system of the machine tool. Generally, forces tend to rise with colder welds. In the chosen parameter window, downward forces range from 2 kN to 5 kN, forces in weld direction lie between 0.3 kN to 1 kN.

Friction Stir Welding of reinforced Aluminium

With the specified process window, butt joints of reinforced aluminium sheets were welded. The orientation of the steel wires in the aluminium sheets is illustrated in Fig. 10. It also shows how the reinforcing elements are deformed during welding. Regarding the surface of the welded parts, the reinforcing elements in profile 1 seem to be bent upwards and downwards in profile 2. This fact is supposed to be caused by the thread of the FSW-pin which creates a vortex of plasticized material in the weld zone.
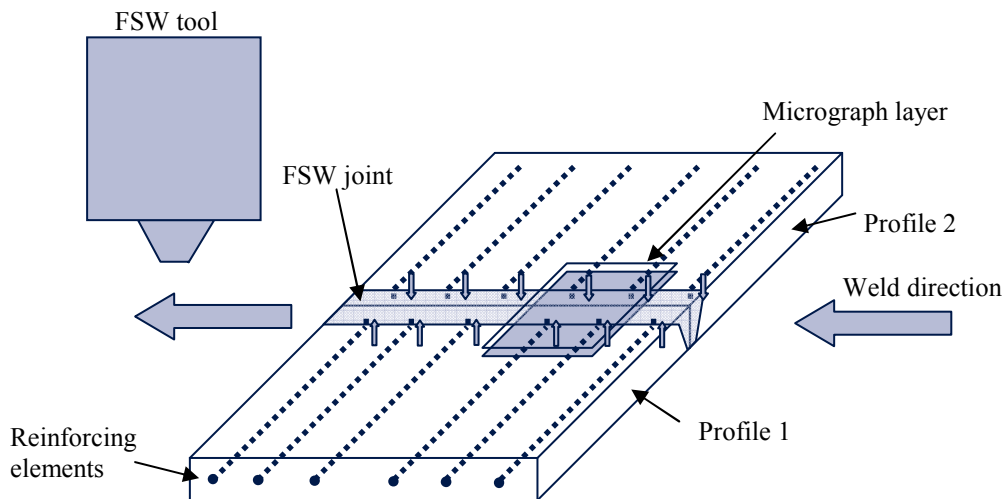

Fig. 10: Deformation of reinforcing elements during the welding process

This is also observable in the top view of an FSW weld seam. While welding through the location of the steel wires, aluminium is pushed upwards and creates clearly recognizable bumps the surface (see Fig.11).
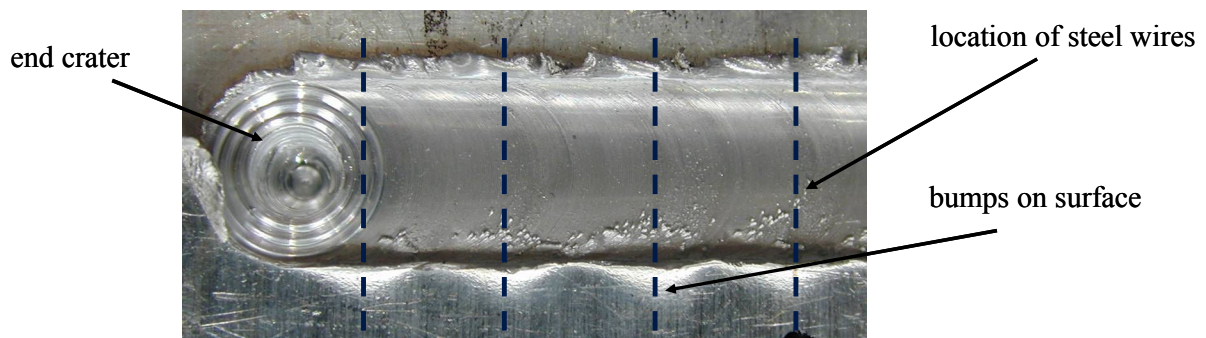
Fig. 11: Top view on FSW weld seam of reinforced aluminium alloy

Fig. 10 also shows the layer of the micrographs, displayed in Fig 12. They were made by the Institute of Material Science and Engineering 1 at the Universität Karlsruhe as a part of the TR10. Both micrographs were taken in a depth of about two millimetres from the surface and include two wires. Because of the deformation mentioned before, only one half of the wires can be seen. The micrographs hold further information on what happens to the steel wires during the welding process. Fig. 12a and Fig. 12b exemplarily show two welds with different process parameters. The joints were welded with a welding speed of 150 mm/min and a rotation speed of 750 rpm and 1250 rpm. The welding direction and rotation of the tool are indicated with arrows. The influence of the rotation speed on the reinforcing elements can clearly be seen in these micrographs. At lower rotation speeds, the steel wires are deformed towards the weld direction which leads to cavities in the direct vicinity of the steel wires. At higher rotation speed, the tips of the wires are smashed into

little fragments which are distributed over the weld zone in the wake of the tool. This directly influences the mechanical properties of the joints. Further studies on these effects, including the determination of the tensile strength at different welding parameters, were done by the Institute of Material Science and Engineering 1 and are presented in [13].
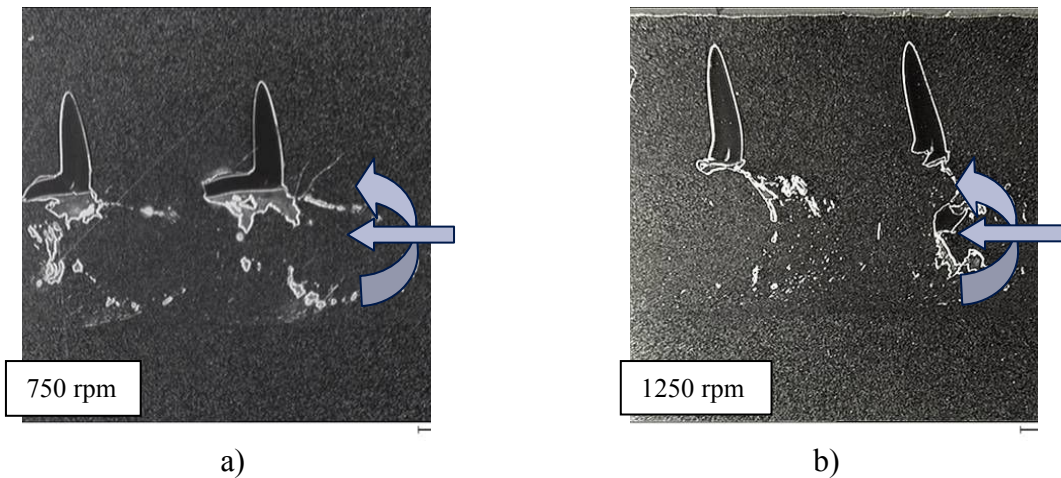

Fig. 12: Micrographs of friction stir welded reinforced extruded aluminium, a) rotation speed 750 rpm, welding speed 150 mm/min, b) rotation speed 1250 rpm, welding speed 150 mm/min

As mentioned before, next to the mechanical properties, the effect of the steel wires on the process forces was investigated. These forces act upon the FSW machine and on the joint partners. For aluminium parts with sufficient backing, process forces can often be neglected. For more complex aluminium structures, which are considered in the TR10, process forces are of fundamental importance. Generally, downward forces during FSW are considerably higher than forces along the joint line [14, 15]. Fig. 13 shows representative downward forces and forces in welding direction during the welding of non-reinforced and reinforced aluminium sheets. The overall magnitude of the forces during welding is the same for both types of material. Yet, there is a big discrepancy in the curve progressions between plain aluminium and the composite material. The downward force reacts abruptly at the location of the steel wires, whereas the force along the joint line increases and decreases more gradually. The value of the force along the joint line during welding of composite material is always higher than for plain aluminium, whereas the downward force oscillates around the value during welding of the base material.
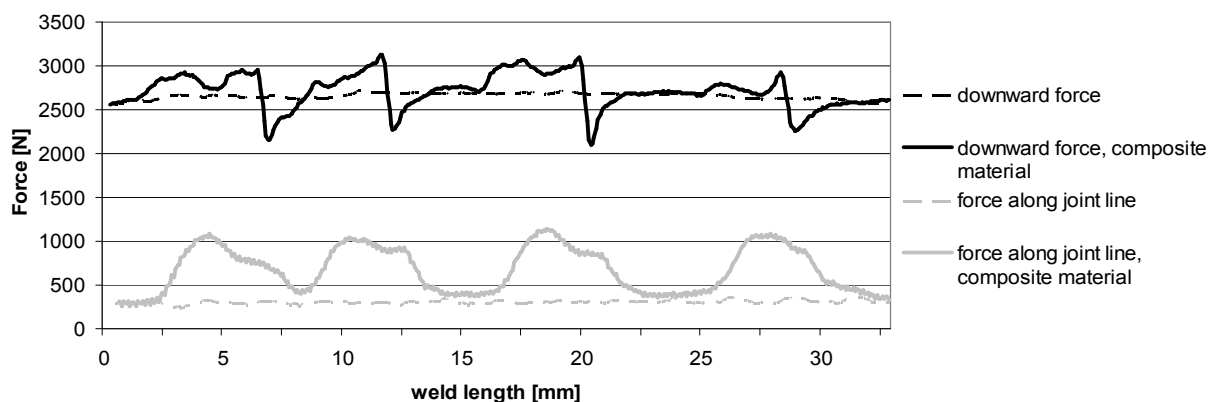

Fig. 13: Process forces during welding (rotation speed 1250 rpm, welding speed 200 mm/min)

The weld experiments show that there is a relationship between weld parameters and process forces. As mentioned before, both forces tend to rise with colder welds. For the forces in the direction of

the joint line, it can be noticed, that force peaks rise for colder welds, whereas such a correlation can not be recognized for the downward forces.

Conclusion

The research work up to now demonstrated the feasibility of Bifocal Hybrid Laser Welding of aluminium alloys. It was shown that certain requirements of industrial manufacturing, e.g. a reproducible and stable process, are met by this technique. This paper aimed at presenting current and future work, concentrating on its further proceedings. The prototypical optical head will be substituted by a more compact design allowing new fields of application together with the integration of new laser technologies. The implementation of a method for process monitoring will underpin the already existing advantages of BHLW of aluminium alloys.

For components that can not be joined with BHLW, like composite materials, Friction Stir Welding was presented to be a suitable alternative. The principle weldability of aluminium sheets, reinforced with steel wires could be shown. Furthermore, the relationship between process parameters and the process forces during FSW of reinforced aluminium was presented, which is a basis for adapting the process to join more complex aluminium structures. Future work will concentrate on extending the flexibility of the process, regarding the geometry of parts that are to be welded. Additionally, further experiments concerning weld quality and the resulting mechanical properties are planned. As a final step, these results will be used as a basis for experiments on the welding of aluminium with non-metallic reinforcing elements.

Acknowledgements

References

[1] A. Trautmann and M. F. Zaeh: *Prozesssicheres Fügen von Aluminium-Tragwerks-strukturen mit einem hybriden, bifokalen Lasersystem*. In: M. Kleiner, H. Baier, J. Fleischer, D. Löhe , K. Weinert, M. F. Zaeh, and M. Schikorra (Eds.): Integration von Umformen, Trennen und Fügen für die flexible Fertigung von leichten Tragwerkstrukturen, Fortschritt-Berichte VDI: Ergebnisbericht der Phase 1, Jan. 2003 – Dez. 2006, Duesseldorf, Germany, Reihe 2, pp. 153 – 181

[2] W. M. Thomas, International Patent 9,310,935. (1993)

[3] A. Trautmann and M. F. Zaeh: Laser *Bifocal Hybrid Welding of Aluminium*. In: M. Kleiner, J. Fleischer, M. F. Zaeh and M. Schikorra (Eds.): Advanced Materials Research: Flexible Manufacture of Lightweight Frame Structures, 2006, Germany, Vol. 10, pp. 65 -77

[4] S. Huber, A. Trautmann and M. F. Zaeh: *Bifocal Hybrid Laser Welding of Aluminium*. In: A. Geiger, A. Otto and M. Schmidt (Eds.): Proceedings of Laser Assisted Netshape Engineering, 2007, Erlangen, Germany, Volume 2

[5] M. Beckert and H. Herold: *Kompendium der Schweißtechnik – Band 3: Eignung metallischer Werkstoffe zum Schweißen* (DVS Verlag, Germany 2002).

[6] A. Trautmann, S. Roeren and M. F. Zaeh: *Welding of Extruded Aluminium Profiles by a Hybrid Bifocal Laser System*. In: A. Geiger and A. Otto: Proceedings of Laser Assisted Netshape Engineering, 2005, Erlangen, Germany, Volume 1

[7] B. Denkena; R. Kling, U. Stute, A. Moalem and T. Hesse: *Quality control in laser welding with fast inline spectral analysis of the process radiation*. In: F. Vollersten, C. Emmelmann, M Schmidt and A. Otto: Lasers in Manufacturing 2007, June 18.–22., 2007, Munich, Germany, pp. 477 - 481

[8] M. Dahmen, W. Fiedler, B. Regaard and S. Kaierle: *Continuous process control during laser beam welding of small section Aluminium sheet*. In: F. Vollersten, C. Emmelmann, M. Schmidt and A. Otto: Lasers in Manufacturing 2007, June 18.–22., 2007, Munich, Germany, pp. 471 - 475

[9] J. Müller-Borhanian, C. Deininger, F. H. Dausinger and H. Hügel: *Spatially resolved Online Monitoring during Laser Beam Welding of Steel and Aluminium*. In: International Congress on Applications of Lasers & Electro-Optics, October 4.–7., 2004, San Francisco, USA

[10] I. Radivojevic: *Spectrochemical Analysis of Solid Samples by Laser-induced Plasma Spectroscopy*. (Dissertation Technische Universität München, 2004, Munich, Germany)

[11] EN 10088-1: *Stainless steels – Part 1: List of stainless steels*. Beuth, 2005, Berlin, Germany

[12] Y. G. Kim, H. Fujii, T. Tsumura, T. Komazaki and K. Nakata: *Three defect types in friction stir welding of aluminium die casting alloy*. In: Materials Science and Engineering, Part A, 2006, Volume 415, pp.250-254

[13] P. Barreiro, V. Schulze and D. Löhe: *Influence of Process Parameters on Structure and Mechanical Properties of Joints produced by Electromagnetic Forming and Friction Stir Welding*. In Advanced Materials Research: Flexible Manufacture of Lightweight Frame Structures, 2008, Germany

[14] D. Eireiner: *Prozessmodelle zur statischen Auslegung von Anlagen für das Friction Stir Welding*. (*iwb* Forschungsberichte, 2006, Munich, Germany)

[15] R. Johnson.: *Forces in Friction Stir Welding of Aluminium Alloys*. In: TWI Ltd. (Ed.): Proceedings of 3rd International Friction Stir Welding Symposium, September 27.-28., 2001, Kobe, Japan

Optimization of the Die Topology
in Extrusion Processes

T. Kloppenborg[1,a], M. Schikorra[1,b], J. P. Rottberg[1,c], and A. E. Tekkaya[1,d]

[1]Institute of Forming Technology and Lightweight Construction, Technische Universität Dortmund,

Baroper Str. 301, Dortmund 44227, Germany

[a]Thomas.Kloppenborg@iul.uni-dortmund.de, [b]Marco.Schikorra@iul.uni-dortmund.de,
[c]Jan.Rottberg@iul.uni-dortmund, [d]Erman.Tekkaya@iul.uni-dortmund.de

Abstract. This paper presents the results of investigations on topology optimizations in extrusion dies. The change of material viscosity of finite elements in the numerical model is utilized to allow or to block the material flow through the finite elements in simplified two-dimensional extrusion models. Two different optimization procedures are presented. In the first part of the paper dead zones in a flat and in a porthole die were improved by enhance the streamlining of the extrusion die. In the second part an evolutionary optimization algorithm has been used to optimize the extrusion die topology in order to reduce the difference between the strand exit velocities in a multi extrusion process. Finally, both methods were sequentially combined.

Introduction

The commercial extrusion process is an important manufacturing method to produce profiles used in different applications, for example automotive and aerospace engineering. In recent decades especially the extrusion of materials with low density, such as aluminum or magnesium, became more interesting for the industry to reduce the weight of the components. Typical examples are car space-frames and similar structures where the main supporting elements are utilized for the stabilization of the entire structure. These components are often manufactured by extrusion; this is why extrusion is a successful application in lightweight structures.

Die manufacturing for complex profiles is mainly based on expert knowledge in design, manufacture, and adjustment, which has been gathered over many decades and is mostly kept confidential by the manufacturing companies. Hence, the manufacturing process requires time-and cost-consuming trial-and-error experiments to achieve an optimized die design. In 1988, Akeret noted that die design and die correction is more an art than a science-based technology. The lack of quantitative models and rules regarding the control of the metal flow were a serious obstacle for a computer-aided design [1].

In recent decades the extrusion process simulation has been increasingly used to analyze the conditions which are not measurable, for example distribution of temperature, pressure, or material flow in complex and/or porthole dies [2, 3]. Hence, as a result of the revised numerical codes [4] the extrusion process simulation is just before being introduced in extrusion companies.

Research and development centres like software developers and universities currently take a step further than the simple simulation of the process. They realized that the responses of the numerical calculations can be used for process optimization or, in fact, for process adjustment by optimization algorithms. Ongoing projects, for example, use parametric optimization for a defined control of the material flow by adaptation of the bearing geometry [5, 6]. Other works use a multi-objective optimization to improve the deviation of the effective strain as a measurement for the material quality, combined with exiting velocity optimization [7].

Contrary to previously published works on extrusion die optimization, this paper will focus on the simulation-based optimization of the die topology. A first approach is used to homogenize the

material flow in the die by improving the die geometry. Especially dead zones in the material flow, which occur in areas of acute angles or behind undercuts, have been reduced by a adjustment of the die streamlining. But the application in a multi-extrusion process leads to different exit velocities. Therefore, in a second approach the application of an evolutionary algorithm is presented, which was defined and developed for an automated free topology optimization of the extrusion die. The evolutionary algorithms are based on the idea of copying the Darwin-Evolution-Model. The evolutionary operations mutation, recombination and production have been used to generate equal strand exit velocities in a multi-extrusion process with a porthole die in a simplified two-dimensional model.

Model Setup

Mesh Generation. There are two methods for mesh generation, *Solid-Modeling* and *Direct-Generation-Method* in the used ANSYS software. Solid-Modeling creates a mesh on a solid geometry, implying the advantage that designs generated in CAD programs can be used to auto-mesh the model. For this type of meshing, a meshing tool is needed which provides the needed discretization for the analyzed problem. The Direct-Generation-Method generates nodes and elements and thus, the mesh itself. The method requires knowledge about the model geometry and programming knowledge. The Direct-Generation-Method has been used to create the extrusion model. To simplify the meshing process and to reduce calculation time only two-dimensional models were considered (Fig. 1). They consist of four node quad elements with linear shape functions. To simulate a multi-extrusion process with a porthole die, a barrier in the center of the material flow before the die orifice was considered in a second model shown on the right front side of Fig. 1.
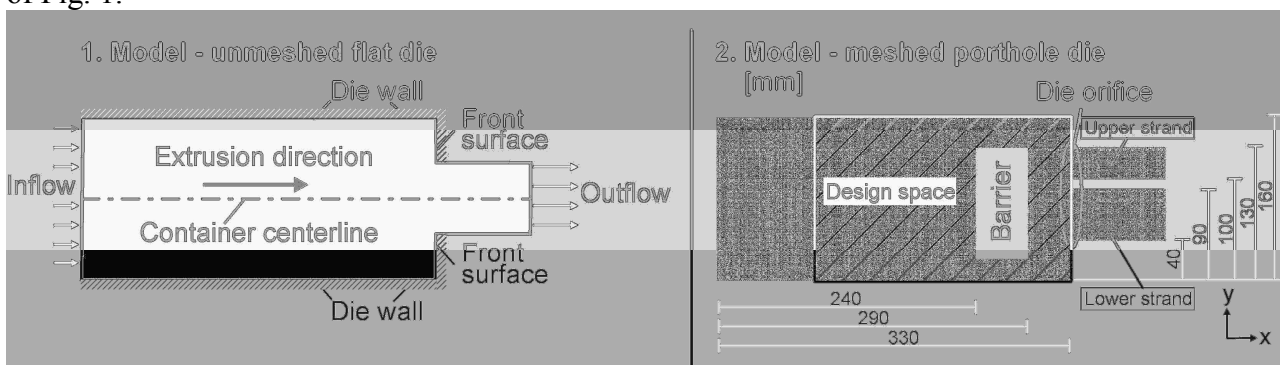

Figure 1: Geometry and FE-model used for the optimization processes

Material. The element type FLUID 141 was used for the extruded material, which is implemented in the ANSYS software. The extrusion has been adapted to the mechanical properties of 450°C preheated aluminum EN AW-6060 (Material-1) by adjusting the viscosity by means of achieving a die pressure of 200 MPa. Here, a viscosity of 10 kg/mms and a density of 2.7e-09 kg/mm³ were applied to simulate the extrusion of aluminum. During optimization another material (Material-2) was defined which represents die material with an extremely high density and viscosity to prevent material flow. Preheating conditions, heat exchange and the thermal evolution were not taken into account.

Boundary Conditions. The nodes on the left border of the models are assigned to the inflow velocity representing the stamp and the extrusion direction. The border nodes of the top side and bottom side of the strands as well as the nodes on the die wall are assigned with a velocity of zero normal to the extrusion direction. Thus, the nodes of the die front surface are assigned with a velocity of zero in the extrusion direction, representing the front surface. No pressure is assigned to the nodes on the outflow. In the second model the nodes around the barrier are assigned with a velocity of zero to avoid material flow through them, analogous to a porthole die.

Manual Improvement of Dead Zones

During the extrusion process the preheated material is pressed through a die to form the profile cross section. Depending on the complexity of the die geometry, areas of different flow velocity occur. The distribution is mainly physical-based by friction or sticking effects in the contact zone between extrusion material and die wall. Hence, there emerge areas where the material stops flowing, especially in acute angles or behind undercuts. These areas are called dead zones. In Fig. 2, the dead zones are shown for the initial design of the multi-extrusion process model.

Figure 2: Example of dead zones in the material flow for the initial die design

Manual Improvement Procedure. Due to the problems which are caused by the appearance of dead zones in extrusion dies an optimization of the material flow has been carried out. The optimization is mainly focused on the method of the topology optimization, friction effects were unaccounted. The objective of the optimization is to reduce the dead zones in the material flow. First, an initial numerical calculation with Material-1 in all elements is performed (Fig. 2). The material flow velocity in each element was identified to sort them according to value. Then the elements with less than 10% of the maximum flow velocity were selected and assigned to Material-2. The extremely high viscosity of this material leads to a blocking of the material flow through these elements in the next calculation step (Fig. 3). The restart for the numerical calculation can be done manually.
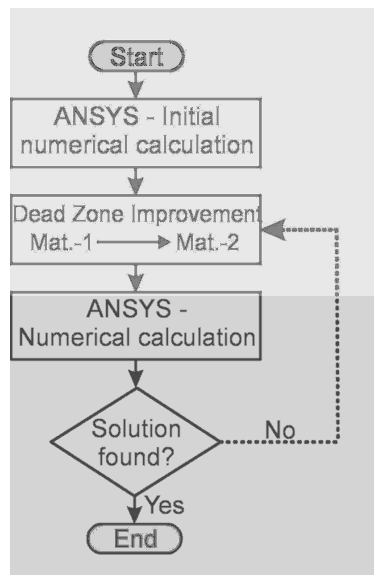
Figure 3: Process procedure to improve dead zones

Results for the Flat Die. In a first calculation run a simplified extrusion model with a flat die was analyzed and than sequentially improved. The initial step was performed to identify the dead zones in the numerical model. As shown in Fig. 4, the dead zones occur in the upper and lower corner of the front surface. In optimization step 1 it can be seen that the material in the initial step shears along the corners at an angle of approximately 40°. The elements which have been changed from Material-1 to Material-2 are not considered further due to the low flow velocity. The angle increased in further steps due to the change in material flow conditions. The geometry of the die gets more streamlined during the improvement of the dead zones, but an ideal improved model without dead

zones could not be achieved. Hence, the uneven line along the element edges, which were changed in material, implements local dead zones in the changed models.

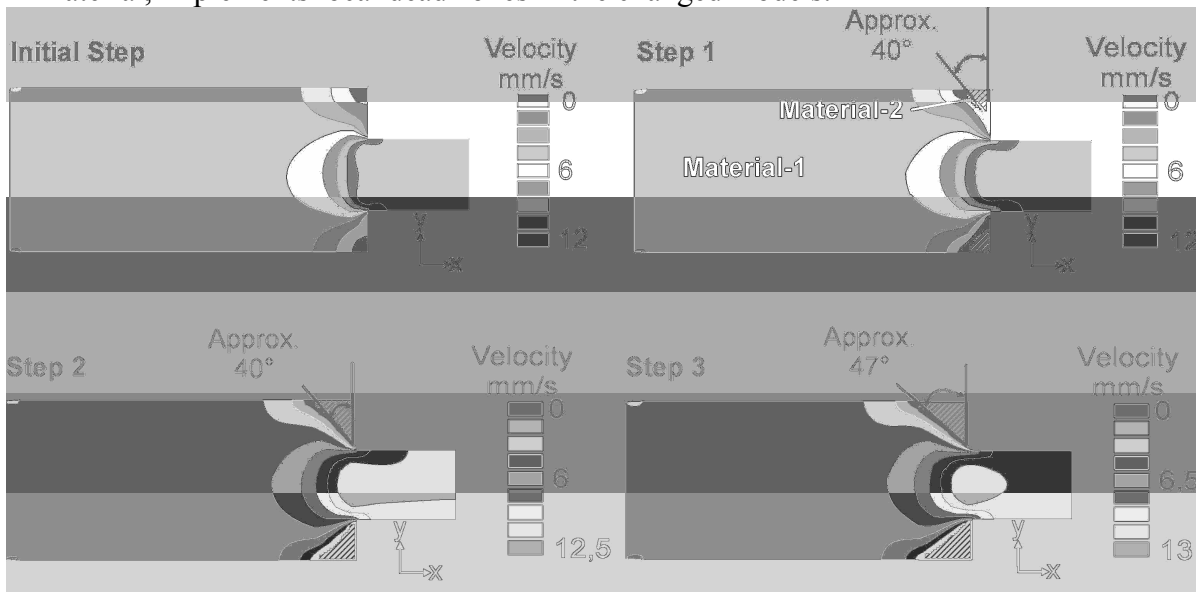Figure 4: Improvement steps in a flat die to avoid dead zones

The shear angles of the manual improvement steps of the simplified finite element model are approximately concordant with experimental results of Hinkfort [8], as it can be seen in Fig. 5.
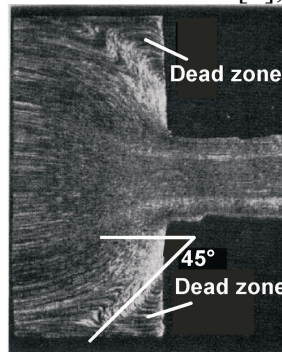
Figure 5: Position and angle of dead zones [8]

Results for the Porthole Die. To raise the extrusion model complexity, the dead zones of a porthole die were improved by four manual optimization steps. Within the loops between numerical calculation and improvement step the number of elements, which were blocked for flow reasons, increases (Fig 4). It is obvious that the barrier geometry changes during the optimization steps to an streamline-shaped geometry. In step 4, the design space limits the change of the barrier geometry, thus on the left hand side no more elements are changed in material. The dead zones in the corners of the front surface are optimized during step 1, 2, 3 and 4. In this area the die geometry is chamfered analogue to the results of the flat die. In step 4 it is shown that the material flow is divided into two different flows after passing the barrier. Furthermore, the barrier changes from the mostly symmetric shape in step 1 and step 2 to an asymmetric shape in step 3 and step 4.

Figure 6: Improvement steps in a porthole die to avoid dead zones

The difference between the profile exit velocities increases with each improvement step. This can lead to production problems. Therefore a genetic algorithm is introduced in the second approach described in the next section.
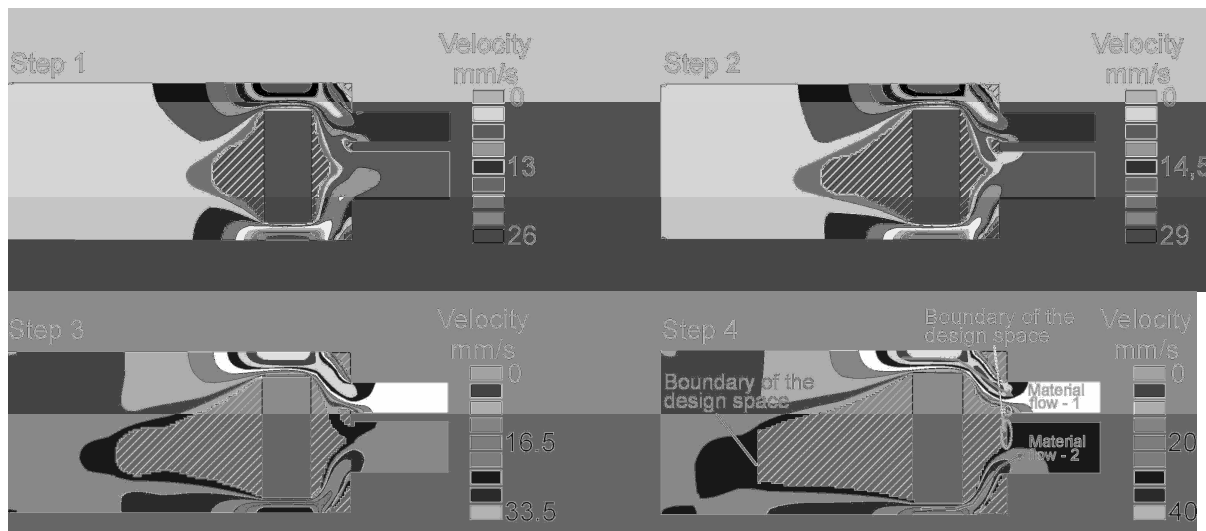
Optimization of the Material Flow by Reducing the Differences in Strand Exit Velocity

For handling reasons and for subsequent processing it can be necessary that the manufactured profiles of the multi-extrusion process have been extruded with the same length. The difference in profile length is the result of different strand exit speeds during the multi-extrusion process. The adjustment of the die orifice, the individual position to the container centerline, and the different profile cross sections have, for example, an influence on the material flow, which can induce a difference between the strand exit speeds. Thus, a temperature gradient in the die can have an effect on the flow stress and, thereby, on the material flow in the feeders. The problems occur not only in multi-extrusion processes, but also during the extrusion of complex hollow cross sections if the profile thickness is different along the profile center line [5, 9]; here, for example unwanted bending or torsion effects can occur.

In practice, these problems are eliminated by the use of expert knowledge in design and manufacturing and by manual adjustment of the die. In order to monitor the influence of the adjustments, time consuming and costly trial-and-error experiments are necessary. In contrast to this, a simulation-based optimization of the exit velocities in the orifice of the extrusion die is presented in the following. The objective of the optimization is to achieve equal exit velocities in the strands of the multi-extrusion process model. Before starting the automated optimization the design space, the design variables, the termination criterions, and the optimization algorithm were defined.

Design Space and Design Variables. The design space is defined by the finite elements between the die orifice and the inflow of the material as shown in Fig. 2. The elements which are assigned to Material-1 and which are at the boundary of the die wall or in contact with Material-2 are defined as design variables for the next optimization run. The type of design variable is discrete; it can only be changed from Material-1 to Material-2.

Fitness Function and Termination Criterion. The fitness of the individuals "i" is evaluated by the difference of the averaged exit velocities at the nodes in the upper strand ($v_{upper}(i)$) and the lower strand ($v_{lower}(i)$). The objective of the optimization problem is to minimize the result of the fitness function. For a fitness value less than 0.1 mm/s the termination criterion is reached.

$$fitness(i) = | v_{upper}(i) - v_{lower}(i) | \qquad\qquad (1)$$

Genetic Algorithm. Genetic algorithms are part of the evolutionary algorithms with the idea of implement a Darwin-Evolution-Model approach for process optimization. To achieve an equal exit velocity in both extrusion strands, the evolution operations mutation, recombination, and production have been used. For an individual of the start population, elements along the die wall of the multi-extrusion process model are stochastically selected. For each selected element the immediate neighbor elements are selected additionally by a random number between 1 and 4 to produce noses along the die wall with different depths (Fig. 7) to change the material flow. All selected elements are assigned to Material-2.
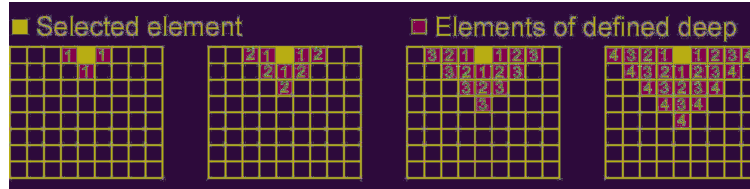

Figure 7: Definition to create noses in the material flow

After creating the initial generation with a population of 10 individuals, the velocities in the strands are evaluated. Within the optimization the fitness value for each individual has been calculated to sort them according fitness. Next, the individuals are utilized for the classical genetic algorithm, using the genetic operations to find the children of the parent generation. The operations are sequentially applied on the 10 individuals.

The algorithm runs as long as the population has not reached start population value (Fig. 8a). The classic genetic algorithm uses a random number between 0 and 1 to decide which operation should be conducted to find new individuals for the next generation. If the number is less than 0.6, a recombination of two parents is used. Thereby the geometry of the best two individuals is horizontally divided and then one half of both individuals is exchanged (Fig. 8c, recombination). If the random number is between 0.6 and 0.7, a mutation of the next individual is utilized. Thereby, a stochastic selection is used for a mutation of each nose of one individual by extending, reducing, or keeping the depth (Fig. 8c, mutation). The operation production is utilized when the number is larger than 0.7. The genetic operation production finds a new independent individual, as described for the start population. The probabilities to use recombination, mutation, or production have been taken from literature [10].
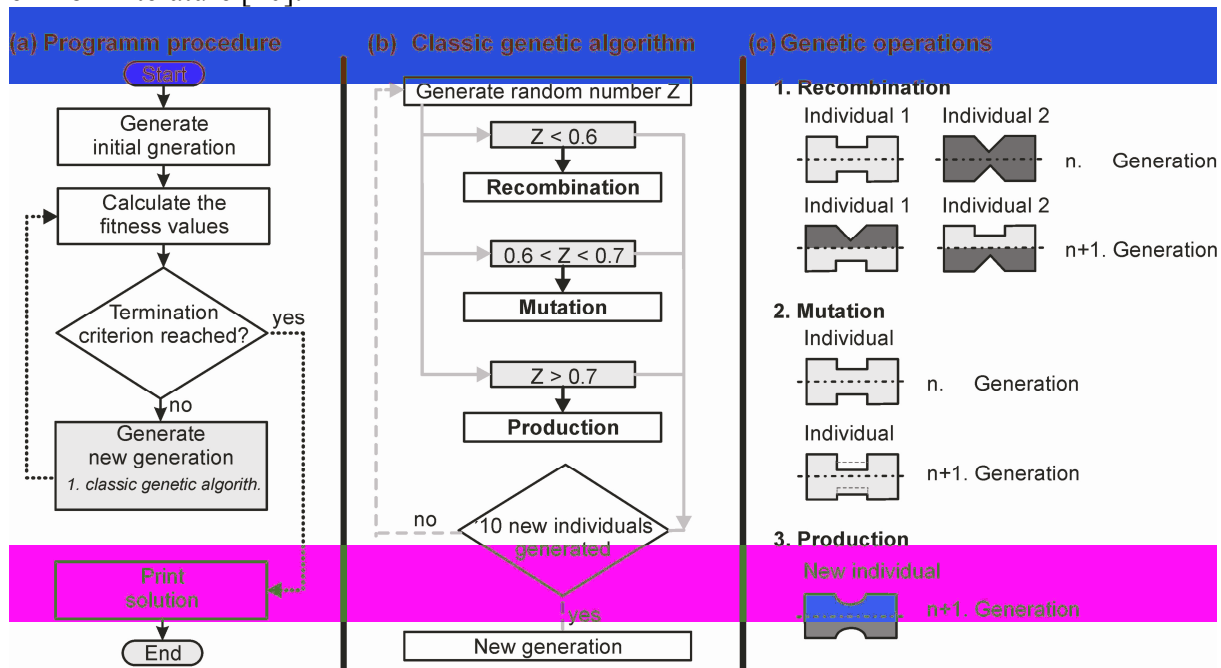

Figure 8:   (a) Optimization program procedure; (b) Used classic genetic algorithm; (c) Examples for genetic operations

Results. The evolutionary algorithm is not deterministic. Due to this, it is possible to find different results for the same starting conditions. To study this, seven optimizations were conducted. The number of generations in every optimization run is representative for the convergence of the algorithm. In average, 9 generations with 10 individuals each, were needed to optimize the strand exit velocities. The scatter in the needed generations is extremely high between 3 generations in the second run and 15 generations in the seventh run.

To compare the different extrusion die topologies, the optimized geometries of the first four optimization runs are presented in Fig. 9. It is obvious that the changes in geometry are very different to each other. As presented in Fig. 2, the upper strand velocity was higher than the lower strand velocity before optimization. In the optimized geometry of run 1, run 3, and run 4 the material flow in the upper feeder slows down due to the geometry change between barrier and container wall (A). The material flow is changed in the upper feeder, thus, an equal exit velocity in both strands occurs. In contrast to this, in run 2 the maximum velocity is 26 mm/s, which is much smaller than in the other results. Very small variations at the barrier and on the lower side of the container wall cause equal exit velocities. It can also be seen that in run 1, different from the other runs, material from the upper feeder now flows towards the lower strand.
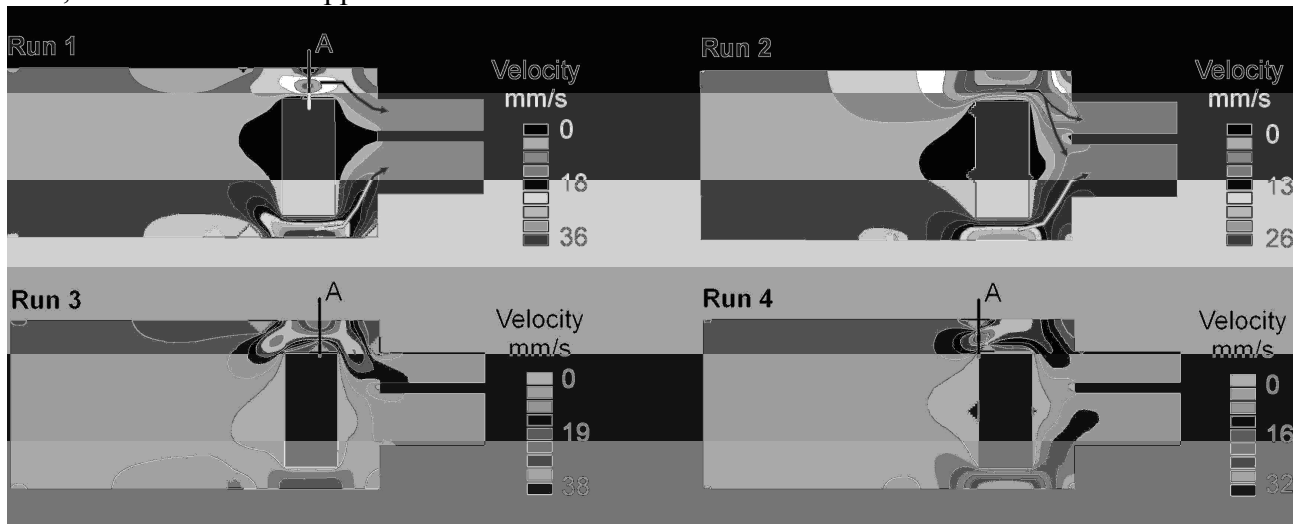
Figure 9:   Optimized extrusion die for different optimization runs

Consecutively Combination of the Approaches

In the previous parts the working principle of the topology optimization methods for optimizing extrusion dies were demonstrated. Finally, the algorithm intended to improve dead zones in the extrusion die and the algorithm intended to achieve equal strand exit velocities were combined. On the one hand, they can be used consecutively, for example by reducing the dead zones first and achieving the equal strand exit velocity afterwards. On the other hand, it may also be beneficial to use both optimization procedures alternately. This means that every new generation of individuals, which causes equal strand exit velocities, is improved by a minimization of the dead zones. In the following, the results are demonstrated exemplarily by optimizing the dead zones first and subsequently achieving equal strand exit velocities.

Two manual optimization steps were applied to reduce the dead zones before the automated genetic algorithm was utilized to achieve equal strand exit velocities. It can be seen that due to the reduced cross section of the feeders the maximum velocity increases up to 56 mm/s. The maximum velocity occurs in both runs in the lower feeder (Fig. 10).

Figure 10: Results using a sequentially combined optimization
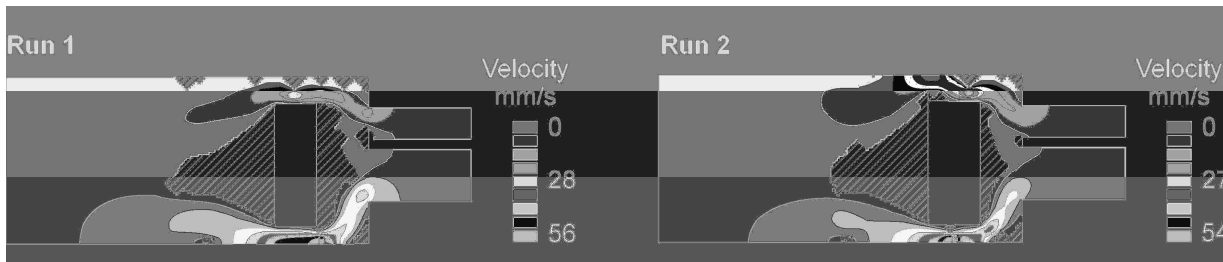
Conclusion

Methods for the optimization of dead zones and strand exit speeds by topology optimization of two extrusion dies are presented, analyzed and optimized using these methods individually or consecutively. The optimization method developed to avoid dead zones accounts for streamlined die geometries in the application of a flat and a porthole die on simplified two-dimensional extrusion models. The genetic algorithm to achieve equal strand exit velocities requires in average nine generations with 10 individuals for the topology optimization. Fore these simplified models every calculation has been done in a short time, but it has to be taken into account that for more complex geometries and three-dimensional models the calculation time can strongly. Therefore, aspects of parallelization of calculation will be utilized in the future.

Acknowledgement

References

[1] R. Akeret, W. Strehmel: *Control of Metal Flow in Extrusion Dies*, Proceedings of the 4th International Aluminum Extrusion Technology Seminar (1988), Chicago, USA, pp. 357-367

[2] M. Schikorra, M. Kleiner: *Simulation-Based Analysis of Composite Extrusion Processes*, In: Vol. 56/1 CIRP Annals (2007), General Assembly, Dresden, Germany, pp. 317-320

[3] M. Schikorra, L. Donati, L. Tomesani, M. Kleiner: *Role of Friction in Extrusion of 6060*, Journal of Materials Processing Technology, Volume 191, Issues 1-3, pp. 288-292

[4] N.N.: Results of the Extrusion Benchmark 2007, Proc. of the 2nd Extrusion Benchmark (2007), ISBN 978-88-548-1286-4, Bologna, Italy

[5] M. P. Reddy: A*nalysis and Design Optimization of Aluminum Extrusion Dies*, Proceedings of the 8th Aluminum Extrusion Technology Seminar (2004), Orlando, USA, Vol. 2, pp.171-178

[6] T. Kloppenborg, M. Schikorra, M. Schomäcker, A. E. Tekkaya: *Numerical Optimization of Bearing Length in Composite Extrusion Processes*, Proc. of the 2nd Extrusion Benchmark (2007), ISBN 978-88-548-1286-4, Bologna, Italy

[7] D. Y. Yang: C*omputer-Aided Optimization of Metal Forming Processes as Applied to 3-D Extrusion of Profiles*, Proceedings of the 8th ICTP (2005), Verona, Italy

[8] P. Hinkfoth: *Massivumformung*, 1. Edition, ISBN 978-3-86130-184-4, Verlagshaus Mainz – Aachen, Germany (2003)

[9] X. Zhang, J. Heathcock: *Modeling of Metal Flow for Bearing Design*, Proceedings of the 7th International Aluminium Extrusion Technology Seminar (2000), pp. 169-176

[10] W. Kinnebrock: *Optimierung mit genetischen und selektiven Algorithmen*, ISBN-10: 3486226975, ISBN-13: 978-3486226973, Oldenbourg Publisher (1994)

Dynamics and Temperature Simulation in Multi-Axis Milling

Eduard Ungemach[1, a], Tobias Surmann[1, b], Andreas Zabel[1, c]

[1] Department of Machining Technology, University of Dortmund, Germany

[a]ungemach@isf.de, [b]surmann@isf.de, [c]zabel@isf.de

Abstract.
Lightweight extrusion profiles with reinforcement elements are promising news in the domain of lightweight construction. The machining of them suffers from several problems: Aside from the question of choosing a suitable tool, feed rate, and milling strategy, an excessive rise in temperature could lead to stress and even a distortion due to the differing thermal expansion of the reinforcement material and the surrounding matrix material. A simulation of the milling process could, in addition to force and collision calculations, recognize this case before manufacturing.
For certain milling applications like seal surfaces, a certain roughness of the manufactured surface is necessary. In many other cases, a smooth surface of very high quality is desirable. Available simulation systems usually completely lack the simulation of dynamic effects, which have a great effect on the final surface quality, and therefore are not able to predict the resulting surface quality.
In this paper simulation methods are presented that are capable of simulating the dynamic behavior of the tool in the milling process and the resulting flank and ground surface structures.
Additionally, a fast temperature simulation for heterogeneous workpieces with reinforcement elements, which is based on the finite difference method and cellular automata, is introduced.

Introduction

Rising energy cost and the growing awareness of environment protection lead to a demand for weight reduction in fields like vehicle production and aerospace. At the same time, additional safety and comfort elements increase the weight. Lightweight construction elements are an important countermeasure while offering additional flexibility. This paper shows advantages in two different areas of simulation-based machining.

To provide properties that are comparable to conventionally built products, the use of reinforcement elements, like steel wires, is a matter of current research e.g. in the "Sonderforschungsbereich Transregio 10" which mainly deals with aluminum extrusion elements with reinforcements. After the production of the reinforced extrusion elements, it is usually necessary to machine them e. g. to add holes for rivets. Previous publications already describe the use of simulation software to ensure that occurring forces are below a certain limit [1, 2] and to guarantee that no collisions occur in the real production [3, 4, 5]. Reinforced extrusion elements are prone to distortion and stress from heat, which can be the result of too much energy added by the machining process. The reason for this sensitivity is that reinforced extrusion elements are built from different materials having differing thermal expansion coefficients. In [3] a milling simulation software with a temperature simulation that is suitable only for homogeneous materials is described. In this paper, methods are shown that are fast enough to be used in a realtime simulation and that are capable of simulating heterogeneous materials. The finite element analysis (FEA) method, which is a common method for the calculation of temperature distributions, offers a high accuracy, but is usually too slow to evaluate complete NC programs. The explicit finite difference method approximates a differential by a difference quotient and is therefore faster while introducing a discretization error.

The second area dealt with in this paper is the field of dynamics in milling. For certain applications a defined surface quality is necessary. A certain surface roughness for joint elements to generate a reliable form fit connection and for seal surfaces so that the adhesive sticks optimally. In other cases the surface should be as smooth as possible. Even in the ideal milling process, there is a relevant surface structure which is generated by the interrupted cut. Additionally, the resulting roughness is strongly influenced by dynamic effects like vibrations or chatter. Chatter can also be the reason for excessive wear of the tool. The conventional procedure to optimize the surface properties is a loop that consists of changing process parameters and remanufacturing until the results are satisfying. Stability charts are used only rarely because their compilation is very time consuming and they depend on both the used tool and the used machine.

In this paper a simulation system is introduced that is able to predict the dynamic trajectory of the milling tool and thus is able to reproduce the generated surface structure of the flank and ground. It simulates the self-excited chatter of the tool on the based on a damped harmonic oscillator. The input parameters are conventional NC files and several geometric and modal parameters describing the tool. For the calculation of the oscillator behavior, knowledge of the forces on the tool is necessary. The simulation is a time domain milling simulation working in discrete time steps. The utilized force model is based on the Kienzle equation. For each small time step, the generated chip form is calculated. Therewith, the forces on the tool can be deduced, which have influence on the tool deflection in the next iteration. With this simulation software it is possible to automatically create stability charts for variable radial immersions and cutting depths. The geometric structure of the flank and ground can be constructed and visualized.

Simulation of the Dynamic Milling Process

In the past several types of simulation of the milling process have been developed. Depending on their focus, different concepts have been used. Generally, the milling process is simulated by discretizing the movement of the tool and removing its occupied volume. An obvious choice for the simulation of the workpiece is the utilization of a voxel-based model [6]. In a voxel model, space is discretized into small, uniform cubes whereas each cube is either filled with material or empty. This model is easy to implement and ready-to-use libraries are available. The drawback of this modeling technique is that the amount of voxels depends on the resolution by $O(n^3)$. This leads to both high memory demands and runtime if a higher resolution is used.

In the average case, the dexel format [2] demands only $O(n^2)$ memory while offering floating point accuracy in one selected direction. In this model the workpiece consists of parallel line segments that are arranged on a regular grid. Each end of a line segment corresponds to a point where the material is entered or left. To support the modeling of undercuts, each of the line segments must be replaced by a list of line segments.

In [2] an improved model is also described: by aligning three dexel boards with the main Cartesian axes, an equally high accuracy in each of the three directions can be achieved. Especially steep flanges benefit from this improvement.

These three models suffer more or less from discretization errors. The quantity of the error can be reduced by increasing the resolution. The modeling of surface structures resulting from dynamic effects demands a very high accuracy, which usually cannot be fulfilled with either voxel- or dexel-based models.
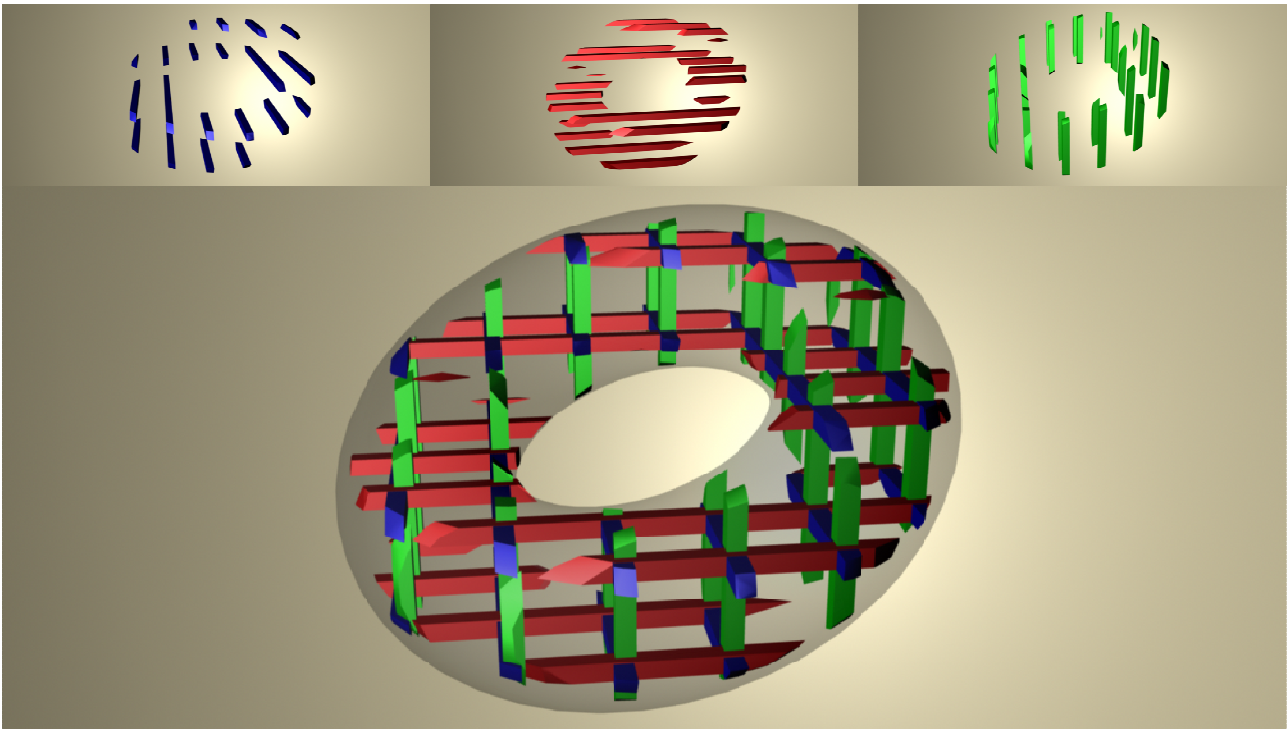
Figure 1: Torus modelled by a triple dexel model: X board (top left), Y board (top middle), Z board (top right) and their combination.

A higher accuracy can be achieved by using a Constructive Solid Geometry (CSG)-based [6] model which is a syntactical model. An object is described by a so-called CSG-tree. These Boolean trees consist of geometric primitives like spheres, cubes, etc., which form leafs of the tree. These primitives and each sub-tree can be connected by the Boolean set operators difference, union, and intersection (Fig. 2). Each (sub-)tree can be interpreted as a mathematical set and the operators form set operations. In simple implementations of milling simulations, the CSG-tree grows with every intermediate position of the tool. In this case the time necessary for each evaluation of the CSG-tree increases with the length of the previously milled path.

In this paper an enhanced CSG-based simulation of the dynamic milling process is presented. A more detailed description can be found in [7].
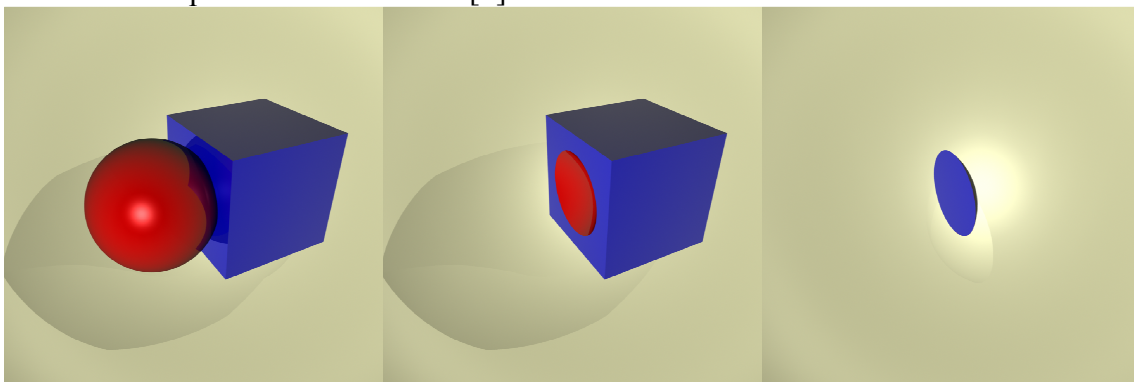
Figure 2: CSG Example: Primitives (here: sphere and cube) and the set operations: union (left), difference (cube-sphere) (middle), and intersection (right)

Oscillator Model As a simplification the tool can be interpreted as a mass point whose movement is determined by the model of a harmonic oscillator where the z-direction is assumed to be sufficiently stiff. Each of the two remaining directions of the tool movement is regarded independently (Fig. 3) and can be described by the equation

$$m\ddot{x}(t) + c\dot{x}(t) + kx(t) = F(x(t), x(t-T), t) . \tag{1}$$

x(t) designates the deflection, *k* is the spring rate, *c* is the damping constant, and *T* depicts the time between two tooth engagements. The force *F* on the tool depends on the current deflection *x(t)* and on the deflection at the time of the previous tooth engagement *x(t-T)*. This dependency shows the self-excited up-building character of the tool oscillations. The progression of forces on the tool can be approximated by a finite number of forces that are constant over a short span of time Δt. If *n* previous forces $F(t_i)$ each of the duration Δt are known, Eq. 1 can be solved in an approximate way by Eq. 2

$$x(t) = \sum_{i=0}^{n-1} \frac{F(t_i) \cdot \Delta t}{m \cdot \omega} e^{-\gamma(t-t_i)} \sin(\omega \cdot (t - t_i)) \qquad (2)$$

with ω denoting the angle velocity and γ being the damping constant.
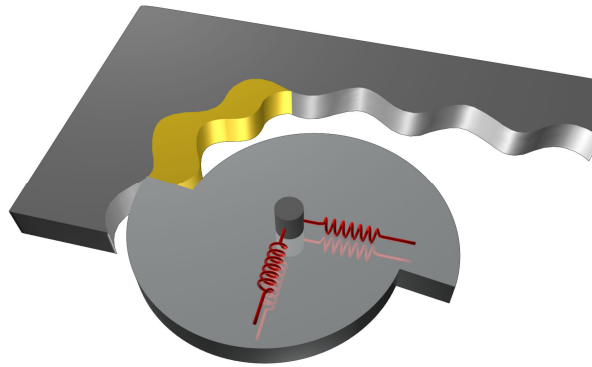
Figure 3: Regenerative effect leading to self-excited vibrations/ chatter

Force calculation For the calculation of forces on the tool, the cutting edge of the tool is split into many small cutting wedges (Fig. 4). For each wedge the forces in cutting direction, and normal and tangential to the cut are calculated based on the Kienzle equation. The overall force on the tool is the sum of forces across all wedges. The current chip thickness is an important input value for the Kienzle equation and can to be calculated by computing intersections between a straight line and the chip form. The generation of the chip form is covered in the next chapter.

Figure 4: Model of the tool composed from several cutting wedges

Modeling of the chip form Each input NC program can be reduced to a sequence of short straight line segments. In the following the tool position is identified by a pair *(s, p)* with *s* being the index of the current line segment and *p* the distance of the tool from the beginning of segment number. *s*. The chip form *C* can then be described by Eq. 3

$$C(s,p) = \left(W_0 - \bigcup_{i=0}^{s-1} V(i) \right) \cap \left(T(s,p) - T(s, p - f_z) \right) \tag{3}$$

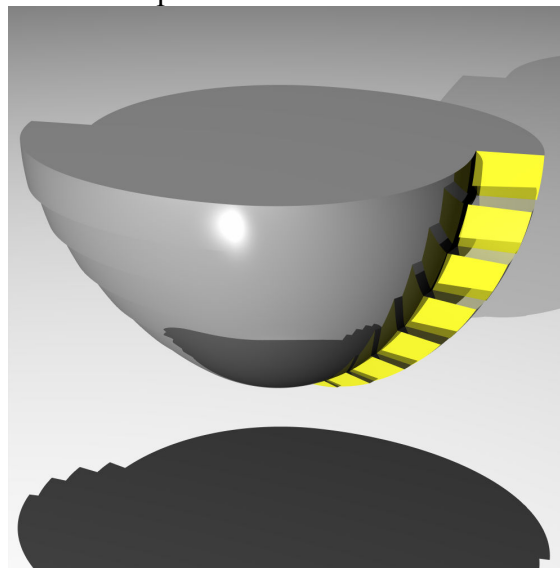where W_0 is the starting workpiece e.g. a cuboid, $V(i)$ is the sweep volume of the tool for segment i, and $T(s,p)$ and $T(s, p - f_z)$ are the occupied volumes of the tool at position *(s, p)* and at the position of the previous tooth engagement, respectively. Eq. 3 can be modeled by the previous mentioned CSG method directly element by element. If the generation of the sweep volume $V(i)$ is too complex, it can be approximated by discretizing the tool movement and uniting the volumes of the tool at their distinct positions. For fast evaluation in the calculation of the chip thickness, it is not necessary to consider all sweep volumes V_i as they may be far away from the current place of interest and thus have no influence on the generated chip form. One way to avoid a lot of calculations is to sort the line segments into a data structure like octrees. Therewith, it is possible to efficiently find the line segments with an index lower than *s* that reside in an area around *(s, p)*. These are the only segments that may influence the chip form. By this and additional optimizations, the size of the generated CSG-tree can often be reduced by about 80% without altering the chip form. The intersection of a straight line and a complete CSG-tree can be reduced to the intersection calculation between a straight line and the used primitives.
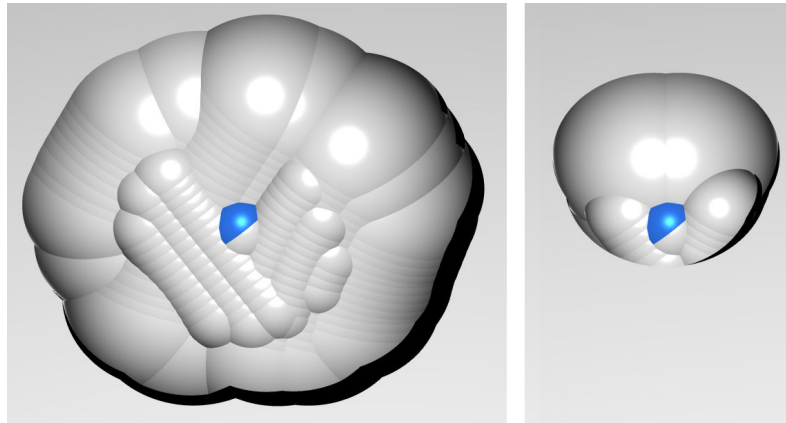

Figure 5: Workpiece model without (left) and with (right) minimization of the CSG tree. The generated chip form (blue) is identical

Modeling of tool vibrations For the simulation of the dynamic behavior, it is necessary to consider that the current chip thickness depends on the current tool deflection and on the tool deflection that has formed the current surface. This can be modeled by splitting the duration of each tool rotation into many steps. For the calculation of the chip thickness, the current deflection at a specific tool rotation angle and the tool deflection exactly one tooth engagement before are to be applied to the tool positions in the CSG-tree. By this procedure the self-excitation is modeled as the force on the tool influences the chip shape and the chip shape influences the force on the tool. Due to the fact the actual structure of the CSG-tree is not modified by this operation (only the values representing the two tool positions are altered), it can be accomplished very efficiently.

Merging the parts At this point all necessary parts for the simulation of the dynamic milling process have been described separately. The complete simulation works in the following order: First the chip form is calculated. Depending on the chip form the forces on the tool are determined and stored. With the knowledge of previous forces the deflection of the tool is computed. Based on this the deflections the next chip form can be calculated and so forfth. The surface can be modeled by superimposing the computed trajectory with the tool movement and subtracting the sweep volume of the tool from the stock material. For a correct modeling of the ground structure, it is important to consider that in case of oscillation the tool is not shifted but bent around a pivot. The resulting

CSG-tree can be visualized in photo quality by methods like ray-tracing and radiosity (Fig. 6). Complete stability charts can be generated by simulating different combinations of radial immersions and feedrates. By examining the trajectory of the tool, it is possible to draw conclusions whether chatter occurs or not.
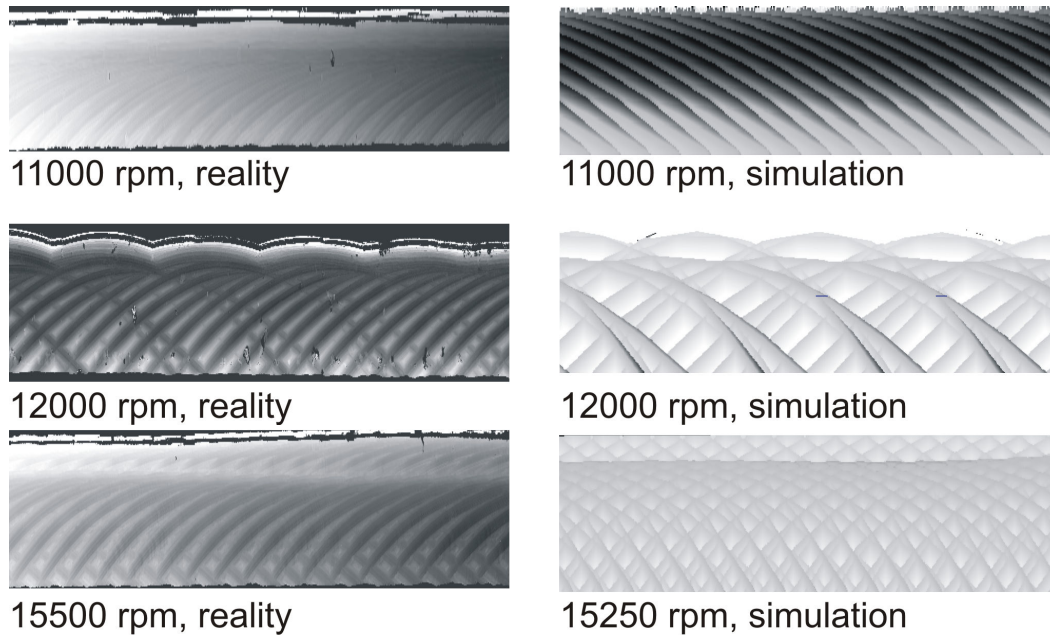

11000 rpm, reality   11000 rpm, simulation

12000 rpm, reality   12000 rpm, simulation

15500 rpm, reality   15250 rpm, simulation

Figure 6: Visualization of ground structures: left column reality, right column simulation

Temperature Simulation

In the course of the scientific project TR10, reinforced aluminum extrusion elements have been successfully produced by the subproject A2. Currently the reinforcements consist of steel wires- the usage of other materials is planned. For many applications the machining of the reinforced extrusion elements is necessary. Complex multi-axis machining could lead to a considerable heat-up of the workpiece. In case of reinforced materials, this is very problematic because the different thermal expansion coefficients can lead to the build-up of stress or even bending of the material easily. The utilization of a temperature simulation makes it possible to recognize problems before the real machining could damage a workpiece.

Numerical Solutions For practical temperature problems, it is usually not feasible to compute a analytical solution. A remedy to this problem is the utilization of numerical solution procedures. In the field of mechanical engineering, it is common to calculate the solution to static and to dynamic problems with the help of the finite element analysis, which is capable of providing a numerical solution in fields like temperature simulation, deforming, stress calculation, etc. One disadvantage with the FEA is its long runtime. The computing time for a temperature simulation of a few seconds of machining can take many hours to days and therefore is not suitable for the simulation of whole NC programs.

The simpler finite difference method is a faster alternative. In this method a differential equation is solved by replacing the differentials with difference quotients, which introduces an error. Therefore, this method is in comparison to the FEA-method less exact but much faster. For the temperature simulation of non-homogenous materials, it has to be considered that the spatial differentiation of the heat conduction coefficient is not constant.

In our software implementation two different ways of partitioning the workpiece were chosen. In the simpler solution the workpiece is divided into a regular grid. In the second solution the workpiece can be split adaptively into tetrahedron. Both implementations only consider heat conduction as both convection and thermal radiation are of little relevance for the temperature distribution inside the workpiece material.

Regular Grid In the simpler of the two implementations, space is split evenly in each of the three Cartesian directions. Each resulting voxel is treated as being homogenous i.e. each voxel has only one temperature value and conductivity coefficient. The accuracy is identical over the complete volume.

Adaptive Grid Areas of the workpiece that are far away from the NC paths or that have a low density of NC paths can be expected not to suffer from a high temperature build-up. These areas can easily be identified prior to the temperature simulation. It would be an optimal utilization of computing time if areas of higher interest were examined with a high resolution while the other areas could be discretized roughly. One possibility is to determine a tetrahedralization of the volume on a point set. It is planned to choose the density of vertices according to the importance of the area e.g. a high density should be chosen where many NC paths are near and a lower density in the remaining areas. As the temperature of each tetrahedron is represented by only one value, the generated tetrahedrons should be as compact as possible. Long, thin objects should be avoided. The Delaunay triangulation is a good way to fulfill these demands [8]. In 3D a Delaunay triangulation has the property that all tetrahedrons fulfill the so-called circumsphere constraint. This means that no other vertices reside inside the circumsphere of other tetrahedrons. Thus the minimum interior angle over all tetrahedrons gets maximized and the generated objects are usually compact.

As the tetrahedrons are distributed unevenly and as only one temperature value per tetrahedron is included in the calculation, it is necessary to find an interpolation scheme to deduce the current temperature on a random position. In our implementation this problem of scattered data interpolation is solved by the use of a radial basis function. Radial basis functions are functions whose value only depends on the distance of the parameter value to the origin or a chosen point e.g. $f(x)=f(|x|)$. The interpolation function is a linear combination of the basis functions, the general form is

$$f(\vec{p}) = \sum_{i=1}^{n} \alpha_i f_i(d(\vec{p}_i, \vec{p})) + p_m(\vec{p}) \tag{4}$$

where α_i are coefficients that are to be determined, $d(\vec{p}_i, \vec{p})$ is the distance between p_i and p, and p_m is a d-variate polynomial with dimension m.

The chosen basis functions are the Hardy's multiquadrics [9], functions of the form $f(d) = (d^2 + r^2)^\mu$ with $r>0$ and $\mu \neq 0$. The α_i can be determined by setting up a linear equation system with additional constraints whereas the polynomial p_m is zero.

Cellular Automaton The cellular automaton is a concept for abstract machines mainly used in mathematics and computer science, especially in computability theory [10]. It is used to model spatial discrete dynamic systems. Space is divided into discrete cells, usually formed as a lattice. Each cell is in one of a predefined finite number of states. Time is discretized into steps. The status of a cell at time $t+1$ depends only on its own status and on the state of the cells in a finite predefined neighborhood each at time t. Formally, a cellular automaton A is a tuple (d,S,V,f) where d (the number of dimensions of A) is a positive integer, S is a finite set of states, V is the finite neighborhood, and $f : S^V \rightarrow S$ is a local transition function. It has been proven that certain cellular automata are computationally universal. This means that their computational power is equivalent to that of a Turing machine and therefore that everything that can be calculated on a computer (and probably, according to the Church's theorem, everything that can be computed intuitively) can be calculated on a cellular automaton. With this background it is not surprising that the previously shown temperature simulations can be interpreted as a cellular automaton, but it is remarkable that the analogy is very direct and intuitive: The cells of the automaton correspond to the voxels of the regular grid and the finite neighborhood corresponds to the voxels surrounding the examined voxel. The temperature, though usually seen as a continuous value, is digitally stored with a fixed memory

consumption and so the number of different temperature values is finite. Therefore, it can be interpreted as finite set of states. The calculation of a new temperature for a voxel depends on its previous temperature and the temperature of the voxels surrounding in a predefined neighborhood. The way it is implemented, the calculation directly fits into the requirements for the local transition function of the cellular automaton.

Conclusion and outlook

This paper shows advantages in two fields of milling simulations. For the simulation of dynamic effects in milling, the resulting flank and ground structures are generated and compared to machined ones, which show a very similar structure for the tool used. With the knowledge of the transfer function it should be possible to simulate the behavior of a complete production system. At the moment, oscillations of the workpiece, which may have a significant influence, are not considered. Additionally, the influence of the exact tool form should be analyzed.

For the temperature simulation, the runtime of the adaptive model should be compared to the one of the regular grid model. As the interpolation scheme in the case of the adaptive grid is very time consuming, alternative methods could be searched for. The resulting temperature distribution should be compared to experimental data.

Acknowledgement

References

[1] M. Stautner: Simulation und Optimierung der mehrachsigen Fräsbearbeitung, Dissertation, Vulkan Verlag, Essen, 2006, ISBN 3-8027-8732-3, 978-3-8027-8732-4

[2] P. Damm: Rechnergestützte Optimierung des 5-Achsen Simultanfräsens von Freiformflächen, Dissertation, Vulkan Verlag, Essen, 2006, ISBN 3-8027-8734-x, 978-8027-8734-8

[3] E. Ungemach, S. Odendahl, M. Stautner and J. Mehnen in: In-Process Simulation of Multi-Axis Milling in the Production of Lightweight Structures

[4] A. Zabel, M. Stautner, P. Kersting: Improvement of Machine Tool Movements for Simultaneous Five-Axes Milling; in: Proc. of the 5th CIRP Int. Seminar on Intelligent Computation in Manufacturing Engineering Ischia, Italy, pp. 159-164, ISBN: 88-95028-01-5

[5] A. Zabel, M. Stautner: Einsatzfelder der mehrachsigen Frässimulation, wt Werkstattstechnik online, 95 (2005) 1-2, S. 56-61

[6] J. D. Foley, A. Van Dam, S. K. Feiner, J. F.Hughes, Computer Graphics, Principles and Practice. Addison-Wesley Professional, 1995

[7] T. Surmann: Geometrisch-physikalische Simulation der Prozessdynamik für das fünfachsige Fräsen von Freiformflächen, Dissertation, Vulkan Verlag, Essen, 2006 ISBN 3-8027-8733-1, 978-8027-8733-1

[8] B. Delaunay: Sur la sphère vide. In: Bulletin of Academy of Sciences of the USSR 7 (1934), No. 6, pp. 793-800

[9] R. L. Hardy: Multiquadric equations of topography and other irregular surfaces. Jour. Geophys. Res. v. 76 no. 8, 1971, pp. 1905–1915

[10] J. von Neumann: The Theory of Self-reproducing Automata, A. Burks, ed., Univ. of Illinois Press, Urbana, IL. 1976

Experimental and Computational Analysis of Machining Processes for Light-Weight Aluminium Structures

Weinert, K.[(1)]; Biermann, D.[(1)]; Kersting, M.[(1)]; Grünert, S.[(1)]

[1]Institute of Machining Technology (ISF), Technische Universität Dortmund

Baroper Str. 301, Dortmund 44227, Germany

kersting@isf.de, gruenert@isf.de

Abstract. Different possible reasons for defects have to be considered in machining light-weight aluminum structures. In the machining process, the cutting power affecting the workpiece leads to a thermo-mechanical load that can cause undesirable workpiece deformations and thus shape deviations. Moreover, the microstructure and the machined surface can be influenced, which is detrimental to the later application of the structures. Previously conducted experimental and simulative investigations, estimated the circular milling process to be the most suitable machining operation that provides the best compromise between mechanical and thermal loads compared to drilling operations [1,2].
In this paper the results of machining end-cross-sections of an aluminum profile are presented. The machining was obtained by a milling process, which is demanding, because of the low profile stiffness. For this process it is important to know the effects of machining in view of the shape deviations. By means of a Finite-Element-Analysis the deformations of the profile web can be calculated as well as validated by experiments. Based on these results, the appropriate process parameter values for end machining can be defined.

Introduction

The machining of light-weight aluminum profiles raises different problems due to the small wall thickness. The process forces subjecting the workpiece can cause discrepancies in tolerances or even damage. This can lead to a reduction of functional capability and, therefore, a failure. Moreover, the heat, generated within the dry machining process due to the friction and the chips, can cause local displacements.
With the help of advanced workpiece clamping devices, some situations of workpiece damage can be well avoided. However, in most cases the process design has to be optimized.

Experimental Setup

In order to produce light-weight metallic structures, especially the machining of the section ends requires certain attention. The machining of these profile end-cross-sections is necessary for different subsequent production steps, for example a welding process. In this case not only the exact profile length is important, but also the shape of the machined profile end-cross-section.
The main goals of these investigations are the analysis and the optimization of the process design concerning the applied cutting data. Therefore, the best solution for short major processing time and minimum workpiece deflections has to be determined. Particularly, the plastic yield of the workpiece can cause problems if subsequent processes are to perform. The investigated aluminum alloy was AW 6060, a very ductile workpiece material and therefore very susceptible to deformation due to the process forces.
In order to create structures consisting of profiles with different cross section shapes, a machining operation is necessary to create small welding seams for following welding processes (**Fig. 1**). As a first example for developing an appropriate part design a rectangular hollow profile was machined

by a milling process to create a concave end-cross-section. This contour can be used for a T-junction of rectangular and circular structures.
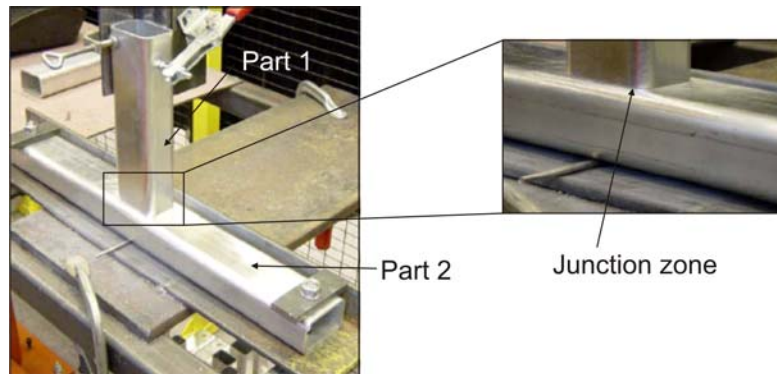

Figure 1: Example for a T-junction with a rectangular profile

At the first step, experimental investigations have been conducted. Therefore, a hollow aluminum profile has been fixed on a three axis machining center, as shown in **Fig. 2**.
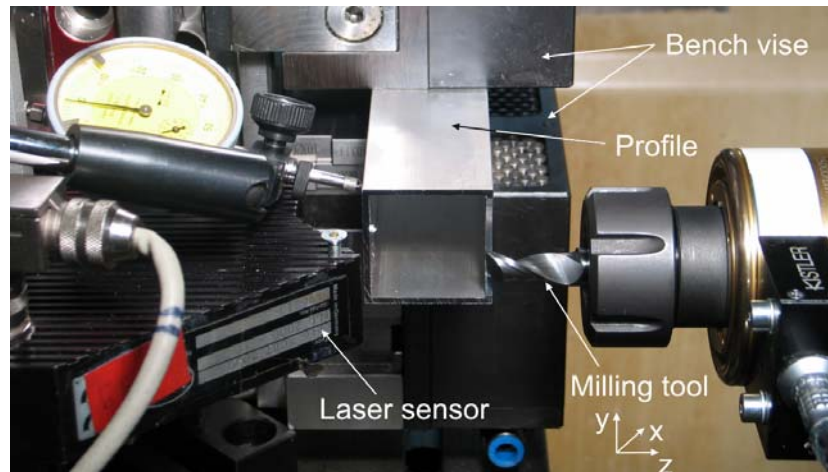

Figure 2: Experimental set up

The profile was fixed on both sides by a conventional bench vise. The hollow aluminum profile had a cross section of 40 x 40 x 2 mm and in one flange of the profile, a circle segment with diameter D = 40 mm was machined. The end-cross-sections were deburred for process preparation. The machining operation was performed in up-milling. The offset of the radius to the end-cross-section was 12.3 mm. The used tool was a single tooth milling cutter with diameter D = 12 mm and a rake angle of 30°. It was made of fine grain cemented carbide and the cutting edge design is specialized for the machining of aluminum. The machining parameters were varied between feed rate 0.2 mm and 0.8 mm and the cutting speed between 200 m/min and 800 m/min.

During the experiments', the deformation in Z-direction of the machined flange was monitored with the help of a laser tracker system. A schematic drawing of the experimental and measuring set up is shown in **Fig. 3**. Therefore, a small hole was drilled in the middle of the undersurface of the profile. The distance between hole and profile edge was 12 mm. A small laser beam aimed through that hole under the upper surface which was to be machined. The reflected beam was detected by a sensor at a fixed angle. When the machined flange moves or bends due to the process forces the reflection angle changes. This change was measured and the current distance between laser source and upper profile flange can be calculated. Due to the rake angle of the used milling cutter, a movement of the flange in Z-direction is always to be expected. Additionally, a small nozzle for

compressed air was positioned in front of the profile to ensure that no chips were in between the laser and the detector.
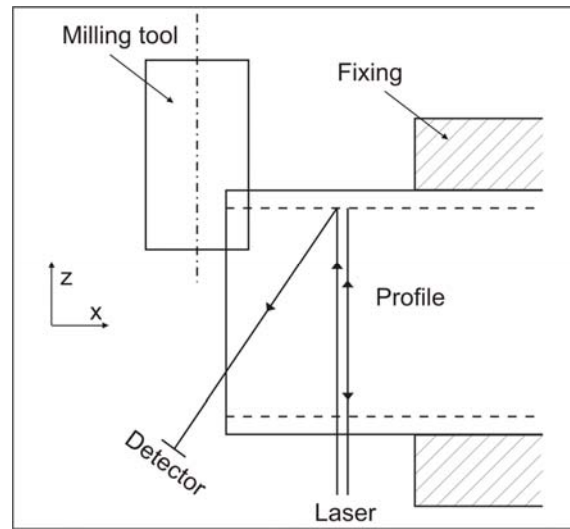

Figure 3: Measurement set up for the detection of the deformation in Z-direction

Furthermore, the mechanical load e.g. the feed force and the cutting torque of the tool is recorded during the process with the help of a dynamometer. In such a way the correlation between mechanical loads and deflected web can be determined. However the stress situation in the machined section can not analytically calculate. With the help of FEA the stress situation can be calculate but therefore the mechanical loads are necessary as input parameter. The feed force and drilling torque was applied on the workpiece (see paragraph FEA of machining end-cross-sections) and the measured deviations of the web during the process were used for validation of the simulation results. Moreover, the measured deviations show which process parameter values are more suitable for the end-cross-section machining of this aluminum alloy. The measured mechanical loads for a certain process parameter set are presented in **Fig. 4** and **Fig. 5**.
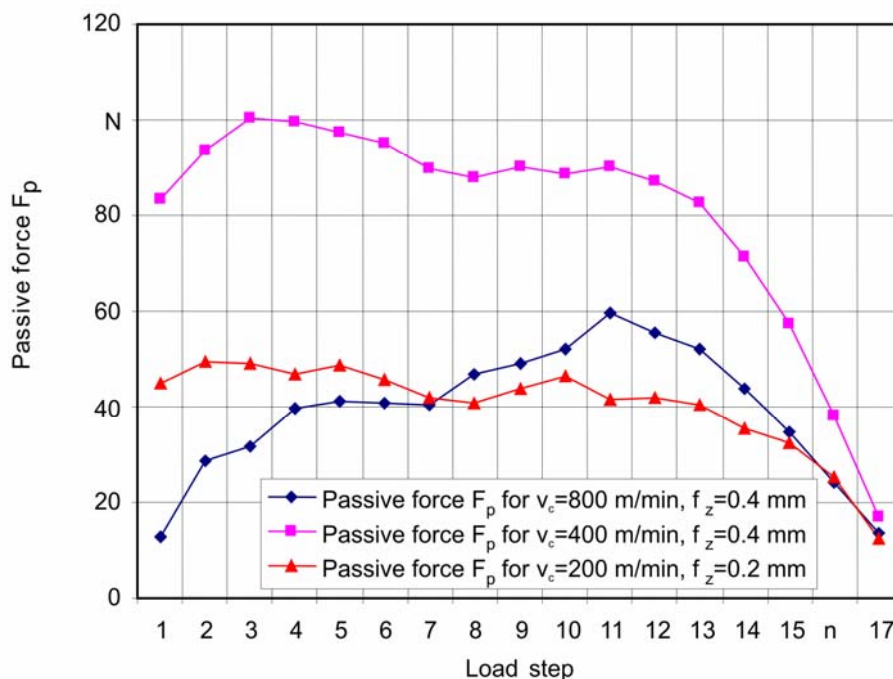

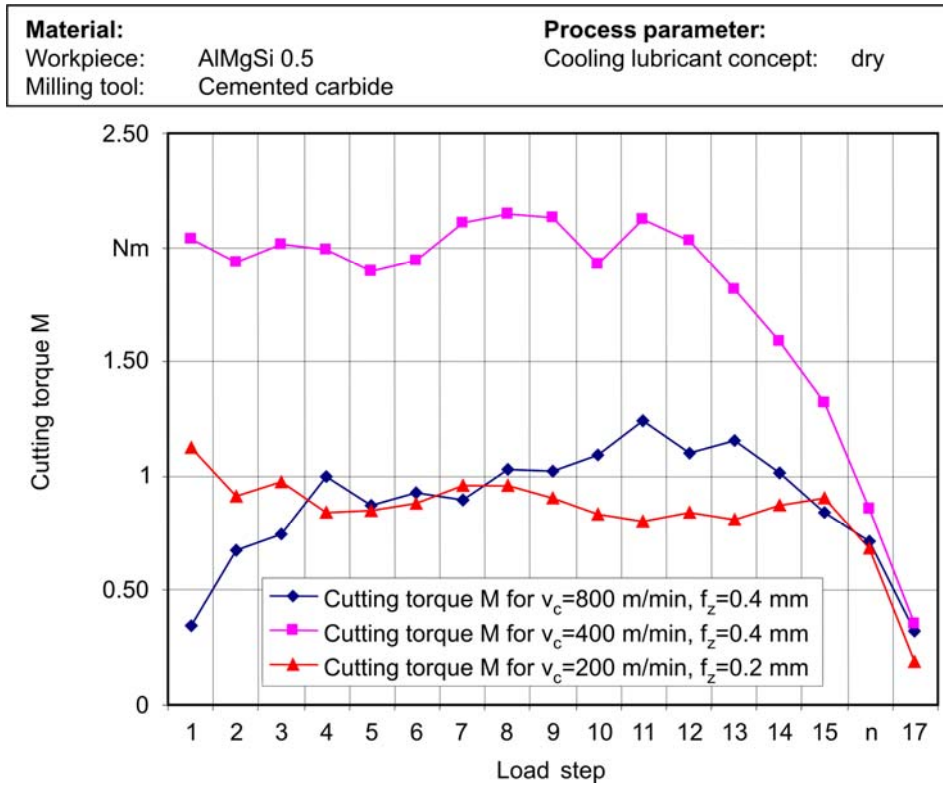Figure 4: Illustration of passive forces due to varying process parameters

Figure 5: Illustration of cutting torque due to varying process parameters

It is obvious that at a cutting speed of vc = 400 m/min and feed rate of f = 0.4 mm/rev the highest mechanical load was measured. At a higher cutting speed combined with the same feed rate this load is lower. This can be attributed to a decrease in thermal stiffness of the material caused by a higher cutting power in the process accordingly to the equation:

$$Q_w = A \cdot v_c \,. \qquad\qquad (1)$$

Q_w = Material Removal Rate; A = Cross Section of Undeformed Chip; v_c = Cutting Velocity

Due to the high process forces the profile was relocated during the machining operation. This movement caused a deviation to the preprocess coordinates. The clamping situations pre- and post-process were observed by a test gauge. The amounts of deviation are listed in **table 1**.

Table 1: Measured profile deviation pre- and post-process

	v_c = 200 m/min	v_c = 400 m/min	v_c = 800 m/min
f_z = 0.1 mm	0 mm	0.002 mm	0.005 mm
f_z = 0.2 mm	0 mm	0.005 mm	0.005 mm
f_z = 0.4 mm	0.02 mm	0.02 mm	0.05 mm

Finite-Element-Analysis of machining end-cross-sections

After the experiments, an analysis of the forces and the cutting torque was performed. Especially these data are important for the definition of loads within the FE-modeling. The simulation model for circular milling previously developed at the Department of Machining Technology (ISF) was applied for the simulation of machining process at section ends [3]. In comparison to the circular milling, the end-cross-section machining is a conventional milling operation without movement in Z-direction.

When analyzing the data 17 peaks were observed in the datasheet. For each revolution the major cutting edge of the tool gets into a new engagement and therefore, a peak is observed at the cutting torque and the feed force. These 17 peaks are the reason for discretization of the modeled material

to be machined within 17 substeps. Within the process material was removed gradually from the model to simulate the chip removal. After each tool revolution one-seventeenth of the material to be machined was detached therefore the model has to be prepared in order to remove the material in the appropriate order. The area which will be machined was modeled as a certain volume. As in former analyzes already proved, the approach of discretisizing is a reasonable way to describe the tool movement along the machined workpiece surface [3].

The simulation of the entire process is only performed without investigating the chip building. The chip building itself is of a high complexity and, therefore, a high amount of calculation time is required [4,5]. In order to develop a productive and economic method for prediction of in-process conditions or limitation of functions, only the machined area of the profile should be observed.

To represent the tool and its engagement condition in the workpiece material, an exact measurement of the shape of the used tool was conducted. This data was used to model an exact image of the tool in the FEA environment. During the modeling process different challenges occur due to the complex shape of the single tooth milling cutter. Thus, several idealizations were necessary. On the one hand, the modeling became easier and on the other hand, simpler structures consume less elements and therefore less calculation time.

The major simplification concerns the engagement situation of the tool during the operation. The used tool has a rank angle of 30°. Due to that angle, the line of contact representing the major cutting edge has the shape of a helix. This is difficult to model into the workpiece. Therefore, the major cutting edge was modelled as a straight inclined line (**Fig. 6**). Due to that supposition the meshing process became easier, too.

The tool material consisting of cemented carbide is very stiff in comparison to the ductile aluminum and thus is assumed as linear elastic material model. The workpiece material is represented as an elastic plastic material depending on the temperature. Therefore an isotropic plasticity was assumed. The Young´s modulus was measured of subproject A3 with $E = 63$ GPa and a yield point with $R_{p0.2} = 74$ MPa. For the FEA-model the 3-D 8-node structural solid element type SOLID185 implemented in the FE-code ANSYS was used. This element type is a trilinear element, but a linearized shape function is sufficient for structural analyzes with a reduced number of nodes compared with quadratic elements.
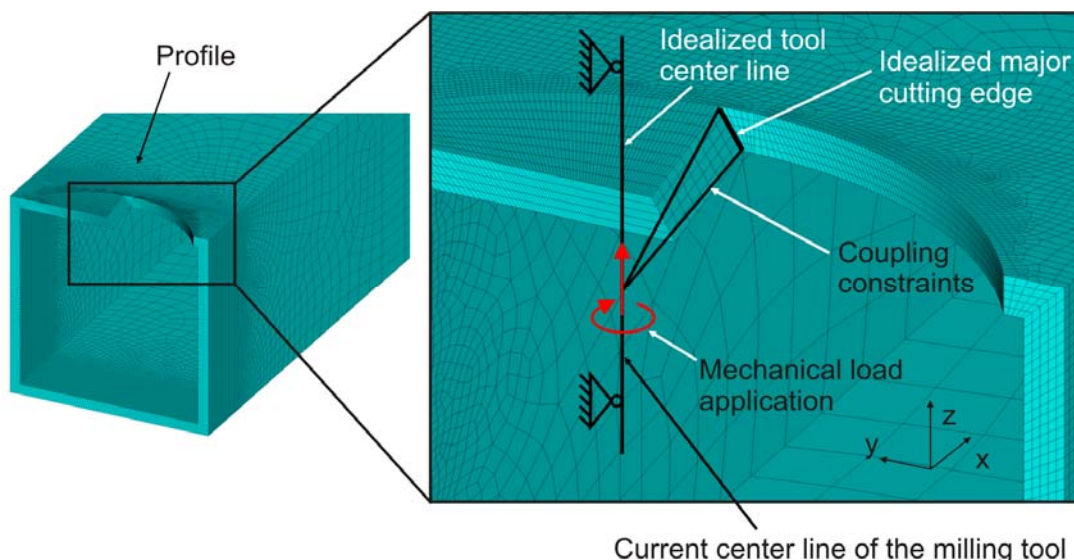

Figure 6: FE-model for end-cross-section machining

The load application was implemented by joint nodes on the supposed tool and the machined area. Therefore, on the virtual tool centre line, a master node was selected and coupled with nodes on the major cutting line in the machined area. On the master node the mechanical load at each load step

was applied and transferred to the coupled nodes. In the virtual process the tool center line as well as the master node changes along the cut edge due to the movement of the tool in the XY-plane.

The displacement in Z-direction can be compared between calculated and measured values. **Fig. 7** and **Fig. 8** show that the calculated deformations are lower than the measured ones. Also, it could be observed that the qualitative accordance is good and the difference between the two values is nearly constant. This leads to the conclusion that the approach provides a promising procedure to the experiments, but some improvements are still conceivable. The simulation was conducted for different cutting data (**Table 2**).

Table 2: Selected process parameter values for the FE-simulation

	Cutting speed v_c	Feed rate f_z
Parameter value combination 1	200 m/min	0.2 mm
Parameter value combination 2	400 m/min	0.4 mm
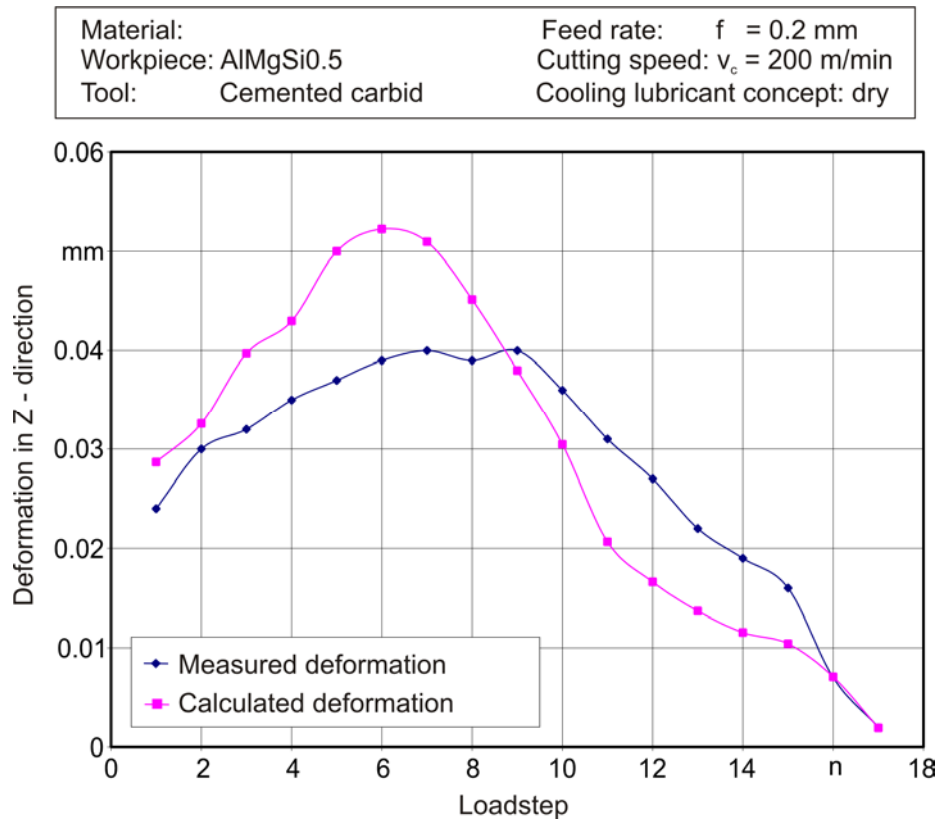
Figure 7: Comparison calculated and measured deformation for the first parameter value combination
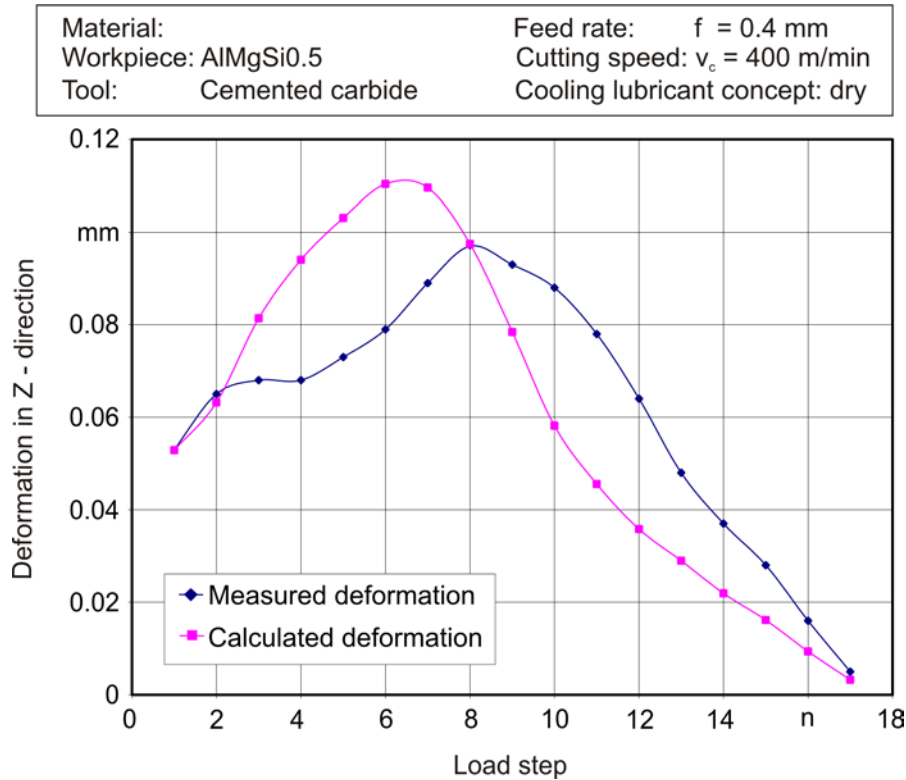
Figure 8: Comparison calculated and measured deformation for the second parameter value combination

The good accordance between measured and calculated displacements offers an interpretation of the stress values calculated by the FEA software. The stress values depend on the deformations therefore high deformations lead to higher stress values. The stress is shown as von Mises equivalent stresses (**Fig. 9**), this is a commonly used hypothesis for aluminum [6]. It is obvious that the stresses are limited on a small area around the contact zone. There is no additional influence on the entire profile. At the load steps 7 and 8 the stress values are the highest accordingly to the highest deformations. Furthermore the stress values are not that high that plastic deformations takes place.

Figure 9: Von Mises equivalent stresses for selected load steps and parameter values

Summary and Conclusion

The investigations of machining end-cross-sections of aluminum hollow profiles with a low stiffness show the complexity of this process. The measured deformations in axial direction of the tool center line show varying results. Contrary to the expectance the mechanical load at low cutting speed and 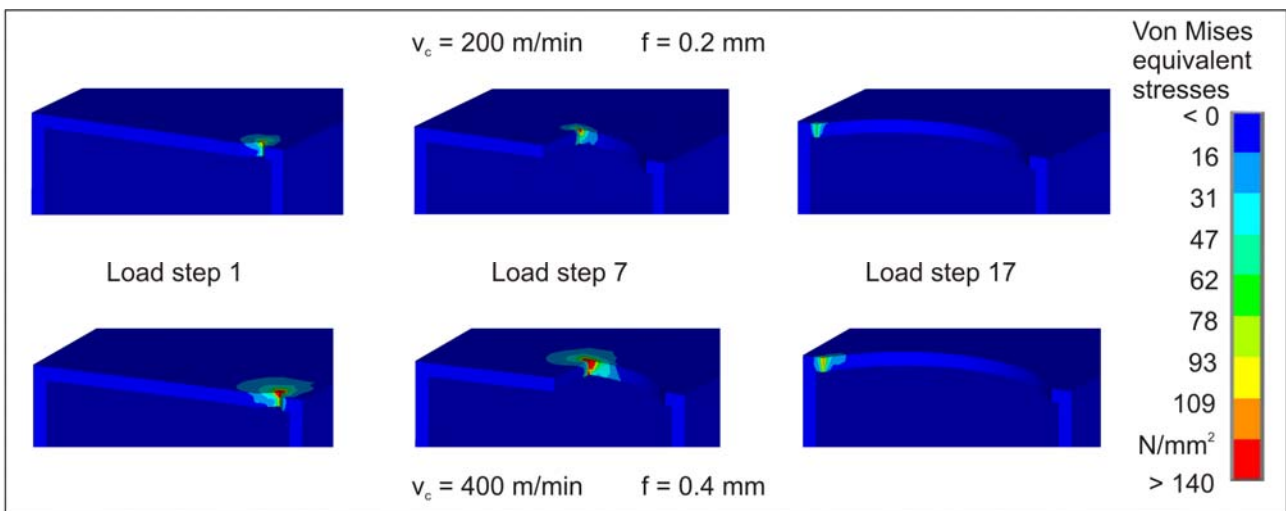feed rate is equal or higher than on higher parameter values. This phenomenon can be explained by decreasing stiffness of the material in consequence of generated heat at higher cutting speed.

Following on from the investigations of the machining process, the simulation is to be integrated into a virtual process chain for small-batch manufacturing of unreinforced and reinforced profiles with different, including multi-cell cross sections. Especially the reinforced extruded profiles contain residual stresses, because of the different thermal expansion of matrix and reinforcement elements during the cooling phase after extrude moulding. The residual stresses may have negative effects on the manufacturing accuracy when cutting the reinforcement during the machining process. Because of this, it is necessary to consider these internal stresses of the profile as an initial condition for the machining simulation. This is necessary for bore holes, especially when they are located close to each other, and for section ends, because of the shape accuracy influencing the following welding process.

Acknowledgement

References

[1]   Weinert, K.; Kersting, M.; Schulte, M.; Peters, C.: *Finite Element Analysis of Thermal Stresses During the Drilling Process of Thin-Walled Profiles.* Production Engineering – Research and Development, Annals of the German Academic Society for Production Engineering, XII (2005) 1, ISBN 3-9807670-6-x, pp. 101-104

[2]   Weinert, K.; Grünert, S.; Hammer, N.; Kersting, M.: *Analysis of Circular Milling Processes for Thin-Walled Space-Frame-Structures Applying FEA-Simulation.* Production Engineering - Research and Development, Annals of the German Academic Society for Production Engineering, XII (2005) 1, ISBN 3-9807670-6-x, pp. 99-102

[3]   Weinert, K.; Grünert, S.; Kersting, M.: *Analysis of Cutting Technologies for Lightweight Frame Components. In: Flexible Manufacture of Lightweight Frame Structures*, Kleiner, M. et al. (eds.), TTP Trans Tech Publications Ltd, Switzerland, Vol. 10 of Advanced Materials Research, ISBN 0-87849-403-0, pp. 121-132, 2006

[4]   Risse, K.: Einflüsse von Werkzeugdurchmesser und Schneidkantenverrundung beim Bohren mit Wendelbohrern in Stahl. Dissertation, RWTH Aachen, 2006

[5]   Söhner, J.: Beitrag zur Simulation zerspanungstechnologischer Vorgänge mit Hilfe der Finite-Element-Methode. Dissertation, TU Karlsruhe, 2003

[6]   Schnell, W.; Gross, D.; Hauger, W.: Technische Mechanik. Band 2 Elastostatik. Springer-Verlag Berlin, ISBN 3-540-64147-5, 1998

Approach for Modelling Process Effects during Friction Stir Welding of Composite Extruded Profiles

Michael F. Zaeh[1,a] and Alexander Schober[1,b]

[1]Institute for Machine Tools and Industrial Management (*iwb*)
Technische Universität München, Boltzmannstr. 15, D-85748 Garching, Germany

[a]michael.zaeh@iwb.tum.de, [b]alexander.schober@iwb.tum.de

Abstract. In the field of light weight frame structures the assurance of dimensional accuracy and the prediction of structural properties especially during and after welding processes are of great importance. The problem in this regard mostly arises from the used welding technique which is characterised by complex interactions of various parameters. A simulative approach is useful in order to predict the structural behaviour and to improve the geometrical quality of joined light weight components after welding. As such, it contributes to reduce process adjustments in the early stage of the product life cycle, and therefore helps to save time and costs. In this paper an approach for modelling the innovative joining process of composite extruded profiles by friction stir welding is presented.

Introduction

This paper discusses some results that were achieved in sub-project B4 within the Transregional Collaborative Research Centre 10. The scientific objective of this project is the simulation of the interactions between the considered thermal joining processes (friction stir welding and laser beam welding) and the component structure [1]. In particular the joining of composite extruded profiles will be investigated. In doing so, various new aspects have to be considered. For instance, the different material parameters – in particular the coefficient of thermal expansion – of the matrix and the reinforcing elements cause the generation of stresses during a heat treatment, particularly when a welding process is performed. In this regard it is of interest to study low heat joining technologies such as friction stir welding. The benefit of applying such an innovative process should be proved. Processes during which a great amount of heat is applied to the treated components will be examined as well, in order to test the limits of their applicability. The particular joining technique that will be studied in this regard is laser beam welding. The evaluation of the applicability of these joining techniques for various profile types will be clarified in cooperation with other sub-projects that investigate the process sensibility, particularly sub-project A11. It is intended to compare experimental results to those of appropriate simulations for mutual benefit, meaning, on the one hand, to gain information for optimising the process and, on the other hand, to validate the results obtained from the simulation. Depending on the geometrical properties and the used materials of the various profiles, methods will be derived to calculate the state of the regarded component during and after the examined welding process.

Presentation of the considered example

The joining process of two composite extruded profiles by means of friction stir welding provides an application example for the examination discussed within this paper. This example describes the experiments that were conducted by sub-project A11, which studies the joining techniques of friction stir welding and laser beam welding. In the course of that sub-project various experiments were and will be conducted at the authors' institute. As a starting point the setup of the above mentioned experiment provides the basis for modelling. In detail this experiment involves a butt joint of two extruded composite sheet metals – each made of an aluminium matrix reinforced with six steel wires that are distributed equidistantly – with the dimensions $35 \times 56 \times 5$ mm. These extruded composite profiles are shown in Fig. 1. A detailed description of the experimental setup is discussed in a following paragraph. A transient temperature field is calculated in a thermophysical simulation of the welding process until cooling of the structure to the ambient temperature. Within a thermomechanical simulation, the welding distortion and the residual stresses of the workpiece are finally calculated considering the influence of the reinforcing elements in the structure and the clamping conditions during friction stir welding.

Setup of the simulation

To conduct the above mentioned computations the finite element method is applied. Therefore the complex physical effects that occur during a welding operation become computable due to a discretisation in space and time – by using a finite element mesh and a partition in discrete time steps respectively. The increasing available computing power and the advancement of commercial software both contribute to increase the accuracy of the results of a simulation and to decrease the amount of time to compute them. From another point of view, it is possible to examine structures with more complex geometries or include more physical effects by coupling different computations.

To compute the structural results, commercial software is used. There are two main computation steps in this regard. Firstly the transient temperature field is computed. The definition of the intensity of the heat source as an input parameter is determined iteratively. To validate the results of the simulation various ways are possible. These include examinations of cross sections of the weld seam, temperature measurements during the welding process, evaluations of experience based data sets or a combination of the above. Secondly the effects of the thermomechanical and mechanical loads during the joining process within the component structure are calculated. The result herefrom is a global state of residual stresses, which combines the consequences of the various influences. In the simulation it is important to take into consideration both the modelling of the clamping situation and the stress formation that occurs on the interface between the different materials of matrix and reinforcing elements.

All simulations are conducted using commercial software. As a starting point all meshing tasks are handled with HyperMesh (Altair) while all further modelling tasks and computations are performed with SYSWELD (ESI Group). Further software tools will be used as well in the course of the project. Therefore, it will be possible to compare results even between two or more numerical simulations using different software tools. In addition numerous experiments will be conducted to validate the numerical results.

Approach for modelling

The basic setup of the described friction stir welding experiment − size of the sheets to be joined, clamping conditions etc. − will be adopted for the modelling. Furthermore, measurement results which were captured during the experiments are used to calibrate various influencing parameters in the simulation.

Fig. 1 shows the schematic clamping situation of the experiments. The two sheets that are to be joined are indicated in the figure. Additionally a third sheet – marked as supporting sheet in the figure – can be seen in the back. These three sheets are mounted onto the support surface by two clamps. The supporting sheet is used to allow an easier experimental performance. In this sheet the pin of the tool plunges in vertically at the beginning of the friction stir welding operation. After that the tool moves in a horizontal motion along the joining line of the two sheets. By the use of a supporting sheet a stable welding process can be achieved in the experiments. The supporting sheet can either be considered or omitted in the simulation. To clarify this aspect, both variations will be examined in the course of the project. For the investigations in this paper the latter case was selected.
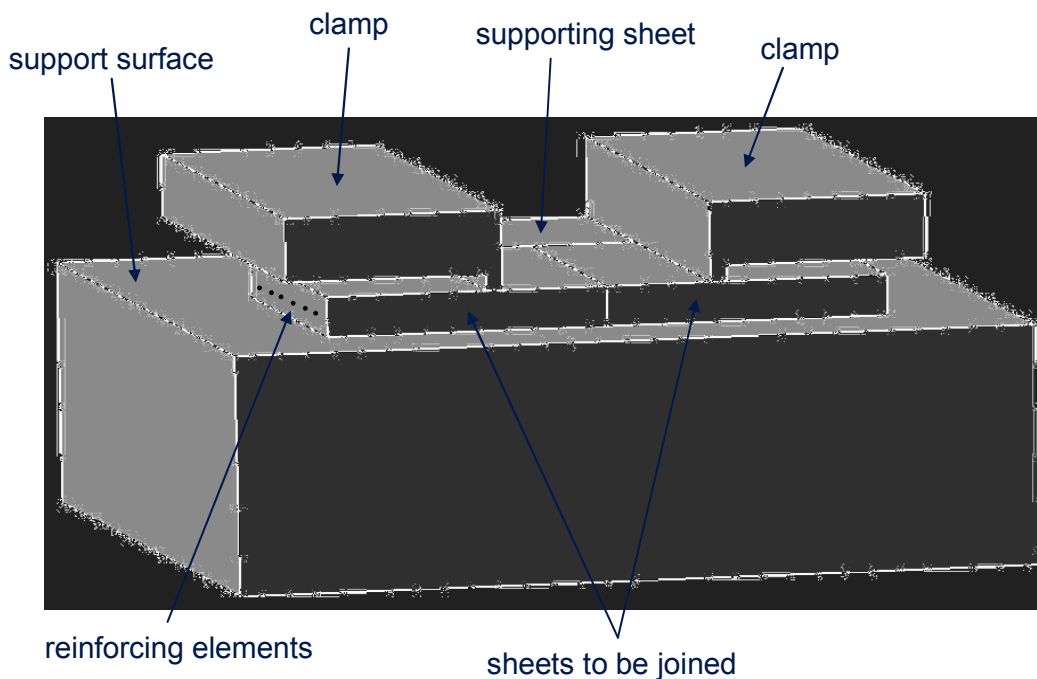

Fig. 1: Schematic clamping situation for the regarded friction stir welding experiments

The definition of the clamping situation plays an important roll in the simulation. The sheets are fixed tightly so that no movement during the welding process is allowed. Through this setup the heat transfer is specified. There are three different ways of heat transfer [2]. The majority of the heat that is input into the structure by the welding process will be transferred from the sheets to the support surface through heat conduction. The contact area between each clamp and the sheets is a thin rectangle that is smaller than the area between the sheets and the support surface. Nevertheless heat conduction will occur through these two areas as well. In addition to conduction, heat is also transferred from the sheets to the surroundings via convection and radiation, although its contribution to the overall heat transfer is lower – taking into account the temperature range that is

attained during the welding process up to a maximum of 500°C for aluminium alloys – than that of heat conduction. Nevertheless, once the workpiece is unclamped, heat transfer will occur only through convection and radiation.

All experimental process parameters that are of importance for the simulation are going to be adopted for the modelling in this case. These parameters are listed in Table 1 below.

parameter	value [unit]
feed of the tool	200 [mm/min] ≈ 3.33 [mm/s]
length of the weld seam	56 [mm]
sheet thickness	5 [mm]
reinforcing element diameter	1 [mm]
initial temperature	20 [°C]

Table 1: Selected process parameters of the friction stir welding experiments

Modelling of the friction stir welding

The first step in the modelling is the generation of an appropriate mesh of solid elements for the composite structure. Usually the mesh is subdivided into two sections − a fine mesh and a coarse mesh. The fine mesh is used to handle the high temperature gradients that appear in the elements where the heat source is applied. Once such a mesh for a single sheet is generated, the mesh of the second sheet is created by mirroring the whole mesh structure in respect to the weld line. If a weld gap shall be considered, solid elements need to be implemented between the two sheets. The handling of the material behaviour of these elements is described below. In addition to the solid elements, groups of two-dimensional elements are defined in order to model the heat exchange. Finally, to describe the welding trajectory, groups of one-dimensional elements are defined. Two nodes indicate where the trajectory starts and where it ends respectively. In the intended simulation the trajectory is a straight line.

Three different materials have to be specified for the simulation. The aluminium matrix consists of EN AW-6060 and the reinforcing steel elements are made of S 355 J2. If a weld gap should be considered, the elements defined between the two sheets need to be handled by setting Young's modulus to a value that corresponds to 0.7% of Young's modulus of aluminium [3]. To define the material properties, appropriate databases are used. These are included in the commercial software, which was referred to above, and are complemented by experimental data provided by sub-project A3.

Furthermore, the heat input needs to be defined. As in the first phase of sub-project B4, a conical heat source is one type of heat source that can be used [4]. Fig. 2 illustrates such a heat source and indicates the parameters that define it. These parameters are the maximum source intensity Q_0 [W/mm³] and four geometrical parameters that define the position relative to the workpiece and the shape of the cone.
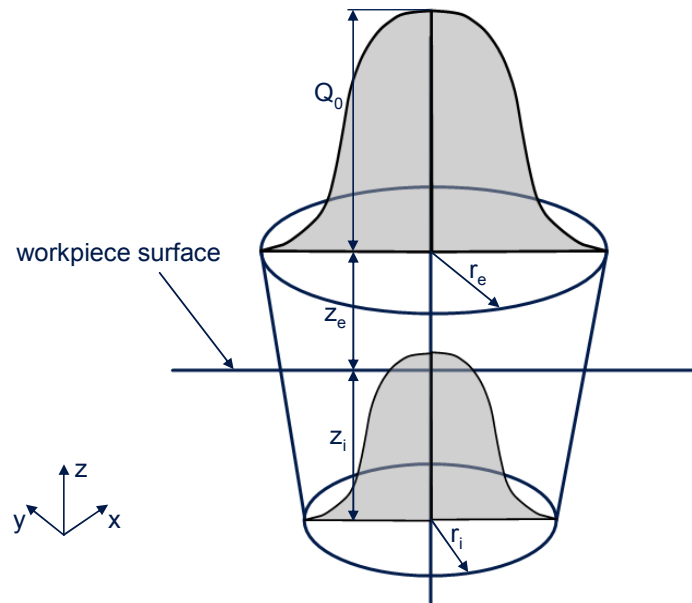
Fig. 2: Conical heat source with its defining parameters

The five defining parameters are determined using cross sections which are provided by sub-project A11 and temperature measurements that were generated by various friction stir welding experiments at the authors' institute [5]. In addition to the conical heat source other types of heat sources are going to be tested in order to replicate the real process as close as possible. The influence of a cross section for the parameter definition is discussed in the following. Such a cross section is shown in Fig. 3.

Fig. 3: Cross section of a weld seam from a friction stir welding experiment

The shape of the weld seam that can be observed in Fig. 3 is typical for friction stir welding. Both the tool shoulder diameter and the tool pin diameter are indicated in the figure. The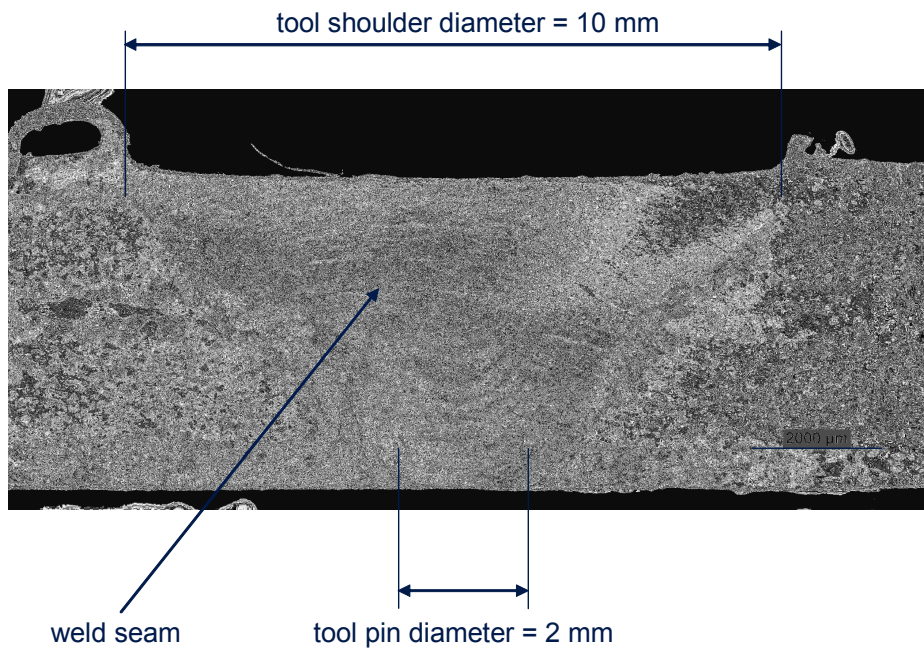se diameters are mainly responsible for the shape of the weld seam. For a good recreation of the real welding process the parameters of the used heat source have to be chosen in a way that the shape of the temperature field, which is calculated during the simulation, matches well with the shape of the weld seam in the cross section. More heat sources of varying types can be combined simultaneously to accomplish this intention.

Outlook

Both friction stir welding and laser beam welding are complex processes each with its own specific effects that need to be taken into consideration within a simulation. As an example for such a specific effect the rotation of the friction stir welding tool was examined. As the rotating tool moves along the workpiece it causes a material flow in the welding zone. This process phenomenon is very complex to model and, therefore, it is difficult to be included in a simulation. As usual, various simulations have to be conducted to quantify the different influences and to decide which effects are important and should be considered in the simulation and which are of minor or no importance and can therefore be neglected. In addition to that, some new aspects have to be taken into account in future investigations. The fact that the composite extruded profiles are made of different materials with different material properties leads to additional structural effects that have to be taken into consideration. Taking into account these influencing factors will yield accurate results of the examined welding processes.

Acknowledgement

References

[1] S. Roeren: *Komplexitätsvariable Einflussgrößen für die bauteilbezogene Struktursimulation thermischer Fertigungsprozesse.* Diss. Technische Universität München. Herbert Utz Verlag, München, 2007, ISBN 978-3-8316-0680-1, *iwb* Forschungsbericht Nr. 203.

[2] D. Radaj: *Heat Effects of Welding: Temperature Field, Residual Stress, Distortion.* Springer-Verlag Berlin Heidelberg 1992, ISBN 3-540-54820-3.

[3] L. Papadakis, S. Roeren: *Anwendungsnahe Modelle zur FEM-Berechnung des Verhaltens gefügter Bauteile beim Laserstrahlschweißen.* Tagungsband SYSWELD Forum 2005, S. 37-46, Weimar, 1st September 2005.

[4] *SYSWELD Reference Manual.* ESI Group, 2000.

[5] P. Gebhard, M. F. Zaeh: *Empirical Model for the Tool Shoulder Temperature during Friction Stir Welding.* Sixth International Symposium on Friction Stir Welding 2006, Saint-Sauveur, 10th-13th October 2006.

Knowledge-Based Modeling of Manufacturing Aspects in Structural Optimization Problems

M. Huber[1,a], Ö. Petersson[1,b], H. Baier[1,c]

[1]Institute for Lightweight Structures (LLB) – Technische Universität München

Boltzmannstraße 15, 85748 Garching, Germany

[a]huber@llb.mw.tum.de, [b]petersson@llb.mw.tum.de, [c]baier@llb.mw.tum.de

Abstract. In this paper we present a method for the multidisciplinary optimization of structures including qualitative expert knowledge. In addition to multi objective and discrete tasks, which are solved with a genetic algorithm, mainly expert knowledge and experience is available for certain influences in early design stages. Fuzzy Rule Based Systems (FRBS) provide a powerful tool to model such influences via qualitative human knowledge. Based on this idea, a method for building qualitative, knowledge based models has been developed at the institute and enhanced. As an example, structural components constructed from composite aluminum profiles with embedded continuous reinforcing elements have been optimized.

Introduction

The ultimate performance and cost of automotive and aerospace structures are determined disproportional highly in the early stages of product development [1]. Depending on the field of application, many disciplines may influence an optimal design not only via different load cases, but also by economic considerations. For example, while automotive structures are mainly driven by crash loads and low cost bulk production, aeronautical structures are determined by function, life cycle loads, and small batch manufacturing processes. An optimal design for these structures which meets the requirements of different disciplines can be found by using the methods of multidisciplinary structural optimization [2]. While well known methods such as stochastic optimization algorithms [3], robust design [4], and approximation models [5] are applied in later product development stages, their use in early stages is often limited, especially if disciplines which are part of the product development itself influence the optimal structural design, such as newly developed manufacturing processes.

For common manufacturing processes, broad information is available from test data such as shape distortion [6], producibility [7] and economic aspects. Newly developed manufacturing processes such as aluminum-steel composite extrusion [8] are less well known. Several techniques are used to consider manufacturing processes in structural optimization problems. Computationally expensive numerical models [9] and empirical models from simulation and test data [10] are available for some. All still need an extensive data set to build the approximation model or to validate the simulation code respectively.

To integrate manufacturing influences for which a few or no simulations and tests are available at least in a roughly estimated way Hajela [11], suggests the use of fuzzy logic [12] to include expert knowledge in the model. Natural language is utilized for parameterizations of so called Fuzzy Rule Based Systems (FRBS) and 'if … then' rules link the input and output parameters. The single input/single output models in [11] were extended to multiple inputs/single output by the authors [13].

In the following sections, knowledge based fuzzy models are described together with the applied knowledge acquisition technique and the influence of the knowledge base. A short description of the utilized genetic algorithm, GAME, is given. This algorithm is applied to optimize structural

components constructed from composite aluminum profiles with embedded continuous reinforcing elements. Finally the according results are discussed.

Knowledge Based Approximation Models

Different approximation techniques are well established for several engineering problems [5]. The most common are Response Surface Approximation (RSA), Kriging, and Neural Networks, which depend on large data sets to fit/train the model. Of these three methods, e.g. RSA offers a reasonable ability to consider both physical understanding and prior knowledge of the problem [14] in the building process of the approximation model. Examples can be found in [15]. This ability is useful to improve the quality of the approximation using a limited number of support points.
Fuzzy Rule Based Systems offer this ability by definition. They were originally developed by Zadeh [12] and many Fuzzy Logic based approximation techniques have been subsequently established such as Fuzzy Regression [16], Neuro-Fuzzy Systems, etc. [17]. The basic idea to use FRBS for expert knowledge representation in structural optimization was used by Hajela and Yoo in [11] to build a model for the layup time of a composite wing panel depending on one input parameter. For a detailed description of the 'if … then' rules refer to [13]. The rules are built by the knowledge engineer after the knowledge acquisition is performed.

Knowledge Acquisition. During the knowledge acquisition phase the input and output parameters of the model and their relations are identified and described by an expert or a group of experts. Afterwards this knowledge is transferred to a proper knowledge representation. An overview of different techniques can be found in [18]. It is important to distinguish between implicit and explicit knowledge. Implicit knowledge is general knowledge about a problem, whereas explicit knowledge contains rules and problem solving strategies. The approach for knowledge acquisition used in this paper is twofold: to gain implicit and explicit knowledge.

First Card or Concept Sorting techniques [19] are used to structure the expert´s knowledge. Previously defined objects, experiences, and rules are written on cards and the knowledge expert sorts them into groups. The expert describes what each group has in common so they can be hierarchically organized. This method is more efficient than the commonly used protocol analysis [19].

From the Card Sorting results, a structured interview [18] can be derived to develop the rule base of the FRBS by the knowledge engineer. Card sorting and the structured interviews can be easily supported by graphical user interfaces in, for example, EXCEL® or MATLAB®.

As an example, different *events* were found for the extrusion process of composite aluminum profiles with embedded continuous reinforcing elements. They are listed in Table 1. A more detailed description of this manufacturing technique is given for the example later.

Event	Effects on Structural Properties
residual stresses in profile after extrusion	$\sigma_{Allowed}$, suitability for subsequent manufacturing steps
debonding - loss of adhesion between fibres and base material	$\sigma_{Allowed}$, reject due to defects
deformation of profile cross section	cross section area, section modulus, tolerances
profile contour deviation due to gravity	overall geometry, tolerances
torsion of the profile	overall geometry, tolerances

Table 1: Events for the extrusion process of composite aluminum profiles with embedded continuous reinforcing elements

The following parameters for the event *residual stresses in profile after extrusion* are hierarchically ordered by their importance.

residual stresses in profile after extrusion		
Parameter	Hierarchy	Design Variable in Struct. Opt.
cooling conditions	very high	no
welding chamber geometry	high	yes, profile cross section
number of reinforcing elements	above average	yes, reinforcing ratio
contour of the profile	average	yes, topology of structure
base material	average	yes
reinforcement material	below average	yes
reinforcement coating	low	no
reinforcement configuration	very low	yes

Table 2: Parameters for one event

For calculating the local residual stresses, $\sigma_{residual}$, for a certain material combination and cross section a simulation model is under development but not yet available. From the knowledge gained by knowledge acquisition, a qualitative performance number PM_{res} can be approximated. From the parameters in Table 2, a structured interview is derived, which is used to establish the rule base of the Fuzzy Rule Based System. The first parameter has no equivalent design variable in a structural optimization problem and can be neglected, because optimal cooling settings will be used always. The second parameter, *welding chamber geometry*, depends on the profile cross section. The third parameter, *number of reinforcing elements*, is directly related to the reinforcement ratio. The *contour of the profile* is changed only in topology optimization of the overall structure. The *base and reinforcement material* can be described by discrete design variables. The last two parameters, *reinforcement coating*, and *reinforcement configuration*, have only small influences because they are often fixed due to process reliability. A detailed model for PM_{res} is described in the example.

Structural Optimization of Composite Vehicle Space Frame Profile

A composite aluminum profile with embedded continuous reinforcing elements from the generic motorcycle space frame, shown in Fig. 1, was optimized with regard to mass and deformation. In addition to the geometric cross section parameters in Fig. 1, the material combination, and the reinforcing ratios, f_1 (horizontal outer section), and f_2 (vertical outer section) were changed. This can lead to large thermal stresses because the stiffeners are not reinforced. A detailed description of the design variables is given in Table 3.
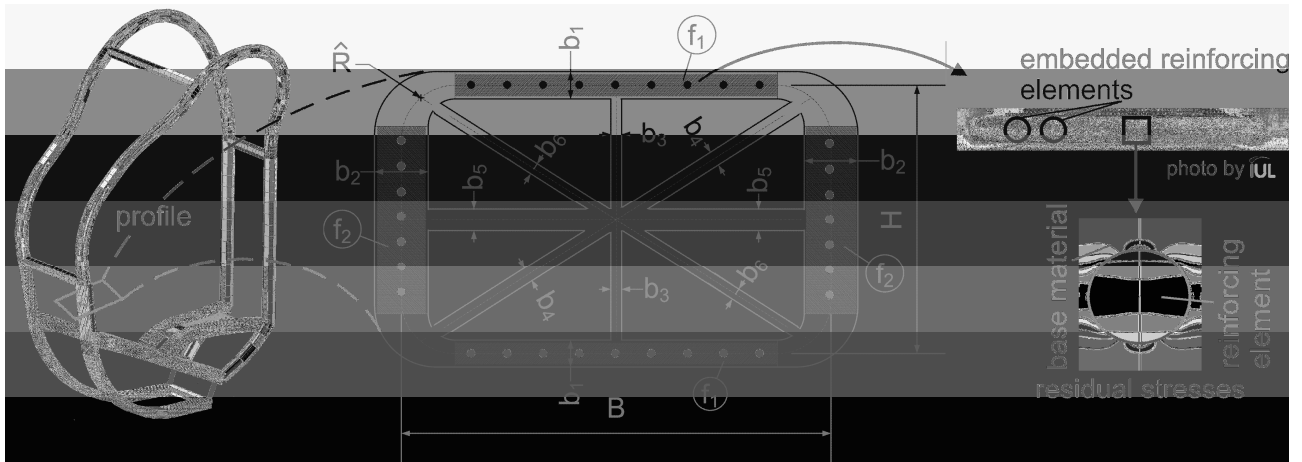
Fig. 1: Geometry parameters of the reinforced profile

Parameter	Description	Lower Bound.	Upper Bound.	Step Size	Type
R	radius ratio[1]	0	1		continuous
H	height	15 mm	100 mm		continuous
B	width	15 mm	100 mm		continuous
$b_{1...2}$	wall thickness outer section	2 mm	10 mm		continuous
$b_{3...6}$	wall thickness stiffener[2]	0 mm	3 mm		continuous
$f_{1...2}$	reinforcement ratios	0 %	30 %		continuous
M	material combination[3]	1	4	AlSt, AlCF, MgSt, MgCF	discrete

[1]this is only a ratio: $R = 0 \rightarrow \hat{R}_{min}$ and $R = 1 \rightarrow \hat{R}_{max}$ $\hat{R}_{min}$ and $\hat{R}_{max}$ predefined by H, B and finite element discretization
[2]if ≤ 1.5 mm the stiffener does not exist
[3]Al: Al6060 T4, Mg: AZ31HP, St: steel wire 1.4310, CF: Thornel 25

Table 3: Design variables of the profile optimization problem

Because of the newly developed curved profile extrusion [20] for reinforced hollow profiles, a heat treatment after the extrusion to minimize residual stresses is not possible since the intended curved shape would deform. The reinforcement induces additional high local residual stresses in the profile, which can lead to problems in subsequent production processes, such as drilling, milling, and joining. A second optimization is performed and a qualitative performance index for the residual stresses PM_{res} is introduced as third goal to be minimized.

The formulation for the first optimization problem is:

$$\min \bar{z}_1(\bar{x}) = \vec{f}(\bar{x}) = [Mass\,(\bar{x}), Deflection\,(\bar{x})]. \tag{1}$$
$$such\ that\ g_{1i} \leq 0; \quad i = 1...16. \tag{2}$$

The formulation for the second optimization problem is:

$$\min \bar{z}_2(\bar{x}) = \vec{f}(\bar{x}) = [Mass(\bar{x}), Deflection(\bar{x}), PM_{res}(\bar{x})]. \tag{3}$$

such that $g_{2i} \leq 0; \quad i = 1 \dots 16$.   (4)

The constraints $g_{1i} = g_{2i}$ are described later in detail.

Load Cases. The three static load cases computed are listed in Table 4 (support according to Fig. 2). Load cases 1 and 2 refer to a typical loading condition during normal use. The third load case considers the different coefficients of thermal expansion in sections with reinforcement ratio f_1, f_2, and the base material. For each load case a linear buckling analysis is performed to ensure the stability of the lightweight profile and the first eigenfrequency is calculated by modal analysis.

LC Nr.	Description	Load	Support
1	pothole - driver standing	$F_{LC1} =$ 2.94 kN $M_{LC1} =$ 220.50 Nm	tread tread
2	pothole - driver seated	$F_{LC2} =$ 0.74 kN $M_{LC2} =$ 1102.50 Nm	tread support 2
3	temperature difference	ΔT = 100.00 K	-

Table 4: Load cases

Constraints. The sixteen constraints consider the stresses both in line and perpendicular to the direction of the embedded continuous reinforcing elements for the three load cases ($\sigma_{i\parallel}, \sigma_{i\perp}, \sigma_{i,Allowed}$ depends on material combination M and reinforcement ratio f_i), the linear buckling (λ_i, a safety factor of 50 was chosen after comparison with nonlinear results), the overall deformation of support 2 in load case 1 (u_{LF1}, max.~7.5~mm), and the first eigenfrequency (ω_1, min. 40 Hz). Also, the differences of the wall thicknesses in the single parts of the cross section should be small ($b_x / b_y \leq 3$, five combinations considered).

Finite Element Model. The finite element model (ANSYS[®]) with the supports of the profile is displayed in Fig. 2. The tread for the driver on the left side of the profile is used for loading support. The wide range of design variables leads to finite element models with different numbers of elements. This effect is reduced by an automatic element size calculation based on the cross section geometry. A study performed for approximately 1800, 2000, 4000 and 8000 elements on one profile showed negligible effects on the maximum stresses and a minor increase in deformation as expected. During optimization the element number varied between 3792 and 5216 elements. The reinforcement was modeled via homogenized material constants, both in and perpendicular to the direction of the continuous reinforcing elements.
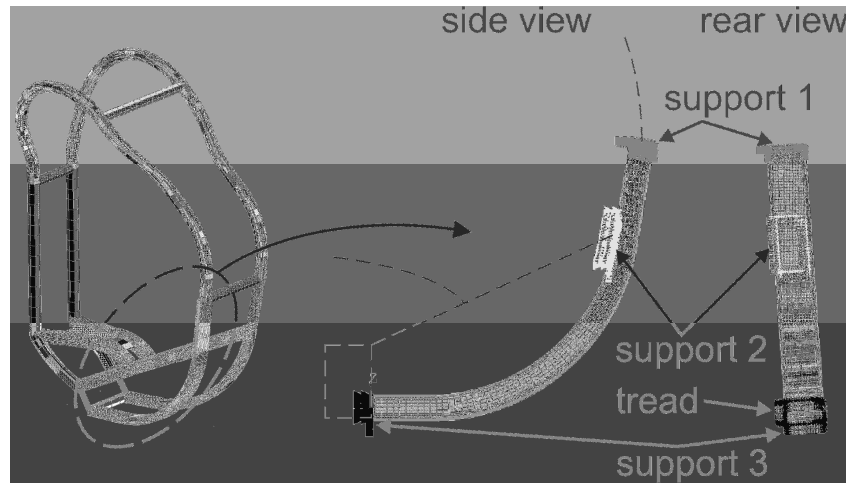
Fig. 2: Support of the profile in finite element model

Knowledge Based Model. Based on the knowledge acquisition described before, two submodels for a qualitative performance measure on residual stresses PM_{res} in the profile were developed. The first model considers the effect of the welding chamber geometry which is mainly defined by the cross section. The second model takes the reinforced parts of the profile into account - the more reinforcement elements the higher the local residual stresses. Although residual stress investigations are available for aluminum profiles [21] (and with some restrictions also for reinforced profiles), the influence of the base material was not modeled due to lack of data and knowledge for extruded magnesium profiles. The inputs of the models are listed in Table 5.

Model Nr.	Input 1	Input 2	Input 3
1	b_{max}/b_{min}	H/B	No. of chambers $2*No_{Stiffeners}$
2	f_1	f_2	-

Table 5: Input parameters for knowledge based models

In the first model, the welding chamber geometry is taken into account. b_{max}/b_{min} has a high influence on the local residual stresses and H/B has a medium influence. If the cross section has stiffeners and reinforcement, different material flows have to be joined in the die. This leads to chambers ($=2*No_{Stiffeners}$) in the die which have a very high influence due to the longitudinal seam weld lines from the material flows. The resulting interaction PM_1 is shown for different numbers of chambers in Fig. 3. For each input three membership functions ('small', 'medium', 'large') are utilized resulting in 27 rules. The output has eleven membership functions in order to model the increase of residual stresses for a high chamber count.
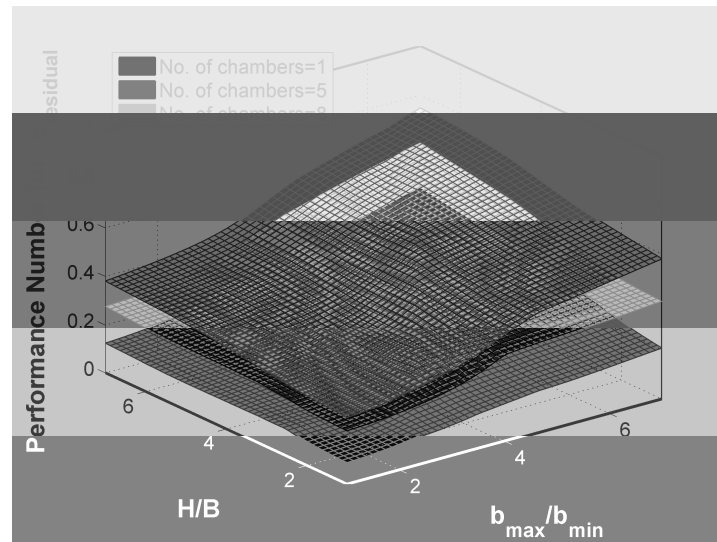
Fig. 3: Knowledge based model for performance measure PM_1 - influence of welding chamber geometry

In the second model the two different reinforcement ratios, f_1 and f_2, are equally important. The local residual stresses around one reinforcing element (steel wire, carbon fiber rope) are high. The stresses decrease rapidly with increasing distance from the reinforcement, but for high reinforcement ratios, these local residual stress fields can overlap. For the homogenized material parameters only qualitative estimations are possible. The overall performance measure PM_{res} is calculated according to the following formula:

$$PM_{res} = a_1 * PM_1 + a_2 * PM_2 \qquad a_1 = a_2 = 1. \tag{6}$$

The weighting factors a_i could be used to change the influence of the to sub models on PM_{res}. In this example they were set to 1 because both aspects, the geometry of the welding chamber due to the profile cross section and the influence of the reinforcing elements, are assumed to have the same significance. The models are programmed in the MATLAB® Fuzzy Logic Toolbox.

Optimization algorithm. The genetic algorithm GAME (Genetic Algorithm for Multicriteria Engineering) is used to solve the optimization problem. An overview can be found in [22], a detailed description in [23]. The performance of GAME is comparable to the well known NSGA-II [24] (iSIGHT-FD implementation). The settings for the optimization algorithm are listed in Table **6**. They were chosen according to the available computation time and the problem dimensionality. Convergence plots of the goals also showed that in the last five generations only minimal improvements were achieved, indicating that the solution had converged.

5760 and 5790 system evaluations were performed by GAME for the 2-goals and 3-goals optimizations respectively. The computation time on a 17-node cluster (8GB RAM, Intel® Xeon 5160 3GHz each) was 24.5 – 33 hours depending on the overall workload of the cluster.

Population Size	Generations	Number of Children	Elite Size	Size of NonDom.[1]	Mutation Probability	Standard Deviation[2]
100	30	200	5	300	80 %	15 %

[1]size of non dominated individuals storage
[2]1st gen., linearly decreased with increasing no. of generations

Table 6: Optimization settings for the genetic algorithm GAME

Results. In Fig. 4, the Pareto-optimal solutions of the 2-goals and 3-goals optimization runs are shown in the 'mass-deflection' plane. For a wide range of the Pareto-front, the designs have a similar mass and deflection performance. The 2-goals optimization generates better results only for very light designs. The designs $2G_1$, $2G_2$ and $3G_{1-4}$ represent different possible solutions. Their corresponding cross sections are displayed on the right side of Fig. 4.

Fig. 4: Result of the 2-goals and 3-goals optimization in 'mass-deflection' plane

In Table 7, the design variables and the goals of the highlighted solutions are listed. All profiles are made of Magnesium with carbon fiber reinforcement (material and actual manufacturing cost were not considered!) and the width B is at its upper boundary. Design $2G_1$ and $3G_1$ have small masses and large deflections. This is caused by a very small height, H, which is approximately half the height of the other designs. In the 2-goals optimization, a two-stiffener design for all Pareto-optimal solutions evolved during the optimization run. To reach similar mechanical performance without stiffeners, the design $3G_1$ has a higher reinforcement ratio f_2 in the vertical walls of the cross section. This indicates that, with regard to the local residual stresses, a simple hollow profile with a higher reinforcement ratio has better results than a multi-chambered cross section.

Designs $2G_2$ and $3G_2$ have a very small deflection of less then 2.4 mm. Taking the local residual stress performance measure into account, a higher overall reinforcement ratio and considerably different maximum and minimum wall thickness are preferable to a complex multi stiffener layout. Design $3G_3$ has only slightly worse mechanical properties but a much smaller PM_{res}. The lowest local residual stresses are predicted for design $3G_4$ which has no reinforcement at all. This good suitability for subsequent manufacturing processes comes with a ~5% higher deflection.

Parameter	Unit	2G1	2G2	3G1	3G2	3G3	3G4
R	[1]	0.697	0.109	0.269	0.048	0.000	0.000
H	[mm]	23.400	48.200	22.100	45.700	45.200	44.400
B	[mm]	90.000	99.200	91.100	100.000	100.000	98.300
b_1	[mm]	4.700	6.200	6.600	8.100	7.300	8.600
b_2	[mm]	6.000	5.200	6.800	5.900	7.800	5.200
b_3	[mm]	3.000	2.600	-	-	-	-
b_4	[mm]	-	-	-	-	-	-
b_5	[mm]	-	-	-	-	-	-
b_6	[mm]	2.500	2.800	-	-	-	-
f_1	[%]	1.8	3.1	1.7	22.8	15.3	0.0
f_2	[%]	6.0	5.4	16.3	12.1	7.6	0.0
Mat. M	-	Mg/CF	Mg/CF	Mg/CF	Mg/CF	Mg/CF	Mg/CF
Mass	[kg]	2.618	4.007	2.781	4.021	4.025	4.011
Deflection	[mm]	3.040	2.335	3.042	2.358	2.386	2.474
PM_{res}	[1]	-	-	0.492	0.560	0.484	0.349

Table 7: Design variables and goals of six selected designs of the solution

In Fig. 5, the Pareto-optimal solutions of the 3-goals optimization are given for the other two projections of the three goals. Whereas the left diagram provides basically the same information as Fig. 4, the right diagram 'Performance Measure over Mass' clearly indicates the jump from profiles with low local residual stresses to profiles with high local residual stresses for designs with a mass less then 3 kg.
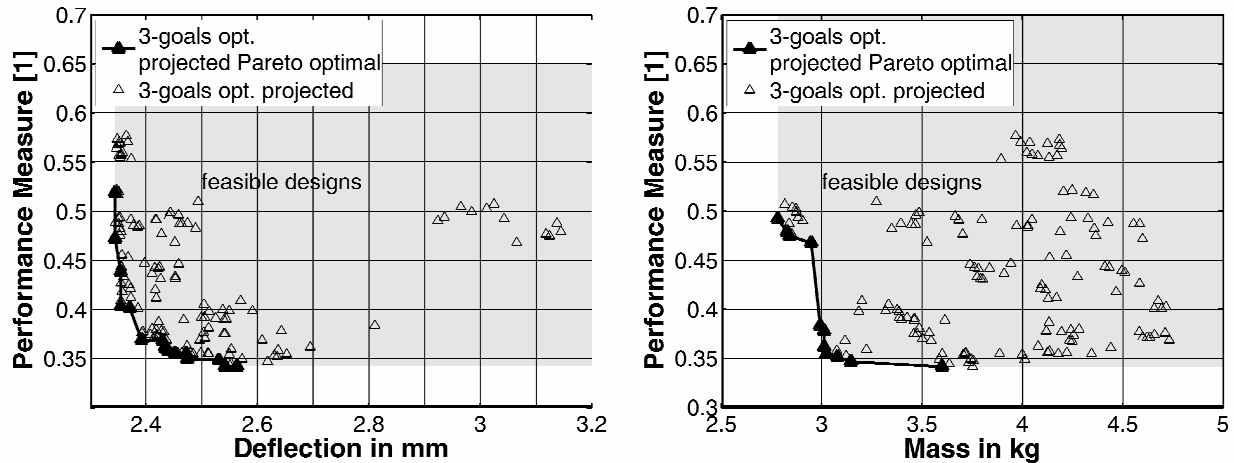
Fig. 5: Results for the 3-goals optimization projected to different planes

The different optimal designs also have different limiting constraints ($g_i \leq 0$), which are shown in Fig. 6. The curves are related to the minimum and maximum mass profile respectively. For the 2-goals optimization, the minimum mass design is restricted by the deformation in the first load case, u_{LF1}, and the stresses perpendicular to the embedded continuous reinforcing elements in load cases 1 and 2 ($\sigma_{1\perp}, \sigma_{2\perp}$). The maximum mass design is limited by u_{LF1} and the two buckling constraints for λ_2 and λ_3. The latter indicates an unfavorable thermal deformation behavior for such profiles.

For the 3-goals optimization, the minimum mass design is restricted by u_{LF1}, $\sigma_{2\perp}$ and λ_2 whereas the maximum mass design is restricted by the first eigenfrequency ω_1 and u_{LF1}.
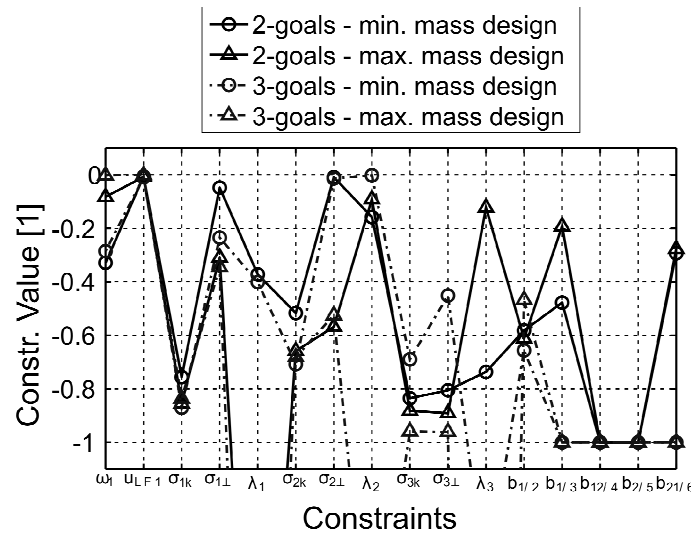
Fig. 6: Constraints for the min./max. mass designs of the 2-goals and 3-goals optimization

Summary

In this paper, the authors investigate a method to implement qualitative knowledge into multiobjective optimization problems. With the help of knowledge acquisition techniques, fuzzy models are built for influences for which little or no simulation or test data is available. The method is demonstrated on the optimization of an extruded hollow profile in a vehicle space frame. The manufacturing of reinforced, curved aluminum and magnesium profiles leads to local residual stresses, which are unfavorable for subsequent manufacturing processes, and can't be eliminated by a heat treatment. A qualitative performance measure for the residual stresses is approximated with the help of expert knowledge.

The described optimization runs showed the benefits of the approach. A 2-goals optimization for just the mechanical performance resulted in complex profile cross sections. The optimal designs of a 3-goals optimization, also taking into account the qualitative residual stress performance, have similar mechanical performance but considerably better predictions for the local residual stresses. Reinforcement is preferred to the use of stiffeners.

The knowledge based approximation models can provide only a rough estimation and further investigations are necessary to take these uncertainties into account during the optimization process. This affects not only the approximation model itself, but also the optimization algorithm. The proposed method is a promising complement to other soft computing techniques utilized in early product development stage optimization.

Acknowledgment

References

[1] J. Hirsh, P. Hajela, J.C. Spering, G.A. Coen, E. Mytych: *MADEsmart: An Environment for Improved Development of Aircraft Components in Preliminary Design*, Engineering with Computers, Vol. 17 No. 2, pp 162-185, 2001

[2] O. de Weck, J. Agte, J. Sobieszczanski-Sobieski, P. Arendsen, A. Morris, M. Spieck: *State-of-the-Art and Future Trends in Multidisciplinary Design Optimization*, 48th AIAA/ASME/ASCE/AHS/ASC Structures, Structural Dynamics, and Materials Conference, Waikiki Honolulu, Hawaii, 2007

[3] J.T. Alander: *Empirical comparison of stochastic algorithms,* Proceedings of the Second Nordic Workshop on Genetic Algorithms and their Applications, Vaasa, Finland, 1996

[4] A. Giassi, F. Bennis, J.J. Maisonneuve: *Multidisciplinary design optimisation and robust design approaches applied to concurrent design*, Structural and Multidisciplinary Optimization, Vol. 28 No. 5, pp 356-371, 2004

[5] R. Jin, W. Chen, T.W. Simpson: *Comparative studies of metamodelling techniques under multiple modelling criteria*, Structural and Multidisciplinary Optimization, Vol. 23 No. 1, pp 1-13, 2001

[6] F. Paulsen, T. Welo: *A design method for prediction of dimensions of rectangular hollow sections formed in stretch bending*, Journal of Materials Processing Technology, Vol. 128 No. 1-3, pp 48-66, 2002

[7] B.L. Subramaniam, K.T. Ulrich: *Producibility Analysis Using Metrics Based on Physical Process Models*, Research in Engineering Design, Vol. 10 No. 4, pp 210-225, 1998

[8] M. Kleiner, A. Klaus, M. Schomäcker: *Composite Extrusion – Determination of the Influencing Factors on the Positioning of the Reinforcing Elements*, Advanced Materials Research: Flexible Manufacture of Lightweight Frame Structures, Vol. 10, pp 13-22, 2006

[9] M. Schikorra, M. Kleiner: *Seam Weld Positioning for Composite Extrusion*, Advanced Materials Research: Flexible Manufacture of Light Weight Frame Structures, Vol. 10, pp 100-110, 2006

[10] S.H. Hsiang, J.L. Kuo: *Applying ANN to predict the forming load and mechanical property of magnesium alloy under hot extrusion*, The International Journal of Advanced Manufacturing Technology, Vol. 26 No. 9-10, pp 970-977, 2005

[11] P. Hajela: *Soft computing in multidisciplinary aerospace design - new directions for research*, Progress in Aerospace Sciences, Vol. 38, pp 1-21, 2002

[12] L.A. Zadeh: *Fuzzy Sets*, Information and Control, Vol. 3 No. 8, pp 338-353, 1965

[13] M. Huber, H. Baier: *Qualitative Knowledge and Manufacturing Considerations in Multidisciplinary Structural Optimization of Hybrid Material Structures*, Advanced Materials Research, Vol. 10, pp 143-152, 2006

[14] B. Schaible, Y.C. Lee: *Fuzzy Logic Based Regression Models for Electronic Manufacturing Application*s, Advances in Electronic Packaging 1997 - Proceedings of the Pacific Rim/ASME International Intersociety Electronic & Photonic Packaging Conference (INTERPack '97), Kohala Coast, Hawaii, pp 147-155, 1997

[15] R. Gleichmar: *Approximationen und paralleles Rechnen bei der multidisziplinären Strukturoptimierung*, PhD Thesis - Technische Universität München, URN: urn:nbn:de:bvb:91-diss20050628-1119013588, 2004

[16] S.M. Taheri: *Trends in Fuzzy Statistics*, Austrian Journal of Statistics, Vol. 32 No 3, pp 239-257, 2003

[17] L. Rutkowski: *Flexible Neuro-Fuzzy Systems*, IEEE Transactions on Neural Networks, Vol. 14 No. 3, 2003

[18] R.R. Hoffman, R.N. Shadbolt, M.A. Burton, G. Klein: *Eliciting knowledge from Experts: A methodological analysis*, Organizational behavior and human decision processes, Vol. 62 No. 2, pp 129-158, 1995

[19] P.W. Wagner, L.M. Zubey: *Knowledge acquisition for marketing expert systems based upon marketing problem domain characteristics*, Marketing Intelligence & Planning, Vol. 23 No. 4, pp 403-416, 2005

[20] A. Klaus, D. Becker, M. Kleiner: *Three-Dimensional Curved Profile Extrusion – First Results on the Influence of Gravity*, Advanced Materials Research: Flexible Manufacture of Lightweight Frame Structures, Vol. 10, pp 5-12, 2006

[21] D. Becker, M. Schomäcker, A. Klaus, M. Kleiner: *Alternative Manufacture of Curved Profiles for Automotive and Railway Lightweight Constructions*, Proceedings of the 1st International Conference 'Aluminium in Transport', Moscow, Russia, 2005

[22] H. Langer, T. Pühlhofer, H. Baier: *A Multiobjective Evolutionary Algorithm with Integrated Response Surface Functionalities for Configuration Optimization with Discrete Variables*, Proceedings 10th AIAA/ISSMO Multidisciplinary Analysis and Optimization Conference, Albany, New York, USA, 2004

[23] H. Langer: *Extended Evolutionary Algorithms for Multiobjective and Discrete Design Optimization of Structures*, PhD Thesis - Technische Universität München}, URN: urn:nbn:de:bvb:91-diss20061108-1512163206, 2005

[24] K. Deb, A. Pratab, S. Agarwal, T. Meyarivan: *A fast and elitist multiobjective genetic algorithm: NSGA-II*, IEEE Transactions on Evolutionary Computation, Vol. 6 No. 2, pp 182-197, 2002

An Approach to Accuracy Improvements in the Flexible Machining of Curved Profiles

G. Lanza[1, a], J. Fleischer[1, b] and D. Ruch[1, c]

[1] wbk Institute of Production Science, Universität Karlsruhe (TH)

Kaiserstraße 12, 76128 Karlsruhe, Germany

[a] lanza@wbk.uka.de, [b]fleischer@wbk.uka.de, [c]ruch@wbk.uka.de

Abstract. This article describes a clamping concept for the flexible machining of spatially curved profiles developed at the wbk Institute of Production Science of the Universität Karlsruhe (TH). Simple geometrical considerations form the basis of the prototypically implemented clamping system design. The approach presented in this article allows for accuracy improvements regarding the positioning of the profile in the clamping system on the basis of markings applied onto the surface of the profile. Besides, the preliminary test rig set up and first results on the detection of the markings by means of digital image processing are presented.

Introduction

Automated small-batch production calls for a high degree of flexibility and adaptability in terms of both equipment and processes. This demand is one of the most urgent requirements and at the same time one of the most difficult to comply with for equipment and processes that are directly related to the products to be manufactured [1]. As far as the Collaborative Research Center (SFB) Transregio 10, which focuses on the small-to-medium batch production of space frame structures, is concerned, the call for a high degree of flexibility poses a major challenge to the handling and machining processes and to in-line quality measurements. Spatially curved profiles require machining along the entire profile length at different positions throughout the whole machining process. Control of the profile geometry has to be performed by a quality assurance system integrated into the machining process.

The highly flexible clamping devices partly used in the aviation industry for small-batch production can variably adapt to a three-dimensional profile contour. The profiles are secured at several flexibly adaptable clamping points along the entire profile length [2]. It must be pointed out, though, that highly flexible fixtures like these are very complex in terms of construction and design, requiring enormous investment. Adapted clamping fixtures, which clamp the profile at several fixed positions, are an alternative to the complex clamping system described before. Here, the clamping elements consist of modular standard clamping elements, which can be swapped manually in order to adapt the fixture to the product [3, 4, 5, 6]. Machine concepts for the machining of straight profiles with constant cross-sections allow for the use of geometrically simple clamping system constructions, due to the fact, that the orientation of the profiles surface does not change in reference to the clamping system. If required, the flexibility of these systems can be improved with clamping jaws adapted to the profiles geometry, which also are used for complex cross-sections or thin-walled profiles [7]. The highly flexible clamping systems as well as the adapted clamping fixtures necessitate the feed range of the machines kinematic mechanism to be at least as large as the component itself. For the automated handling of components predominantly additional devices, e.g. industrial robots or special-purpose machines are used. The processes of loading and unloading, however, are manual in small-batch production. In small-batch production, the profile geometry is currently mostly controlled on the basis of individual testing using either coordinate measurement systems or product-specific gauges. Any in-line quality assurance guaranteeing 100% of control would require enormous time and effort. Taking the above considerations into account, the

processes for quality assurance regarding profile handling and clamping currently used in the industrial environment are only conditionally suited for automated small-batch production.

For the purpose of eliminating the disadvantages of conventional machine concepts, a novel concept minimizing the above-mentioned downsides of conventional machine technology has been elaborated out of the close collaboration between the two subprojects "Flexible and intelligent gripping systems" and "Combined kinematic handling and machining mechanism" [8]. Figure 1 shows the model of the elaborated machine concept. The profile in question is gripped by an industrial robot, subsequently guided through a flexible clamping system and positioned there. Once the profile has been clamped, it is machined by the kinematic machining mechanism. The profile is repositioned by the industrial robot to allow it to be machined along its entire length. The machining process itself and its features are explained in the following paper of this issue (Accuracy Improvement of a Machine Kinematics for the Product Flexible Machining of Curved Extrusion Profiles).
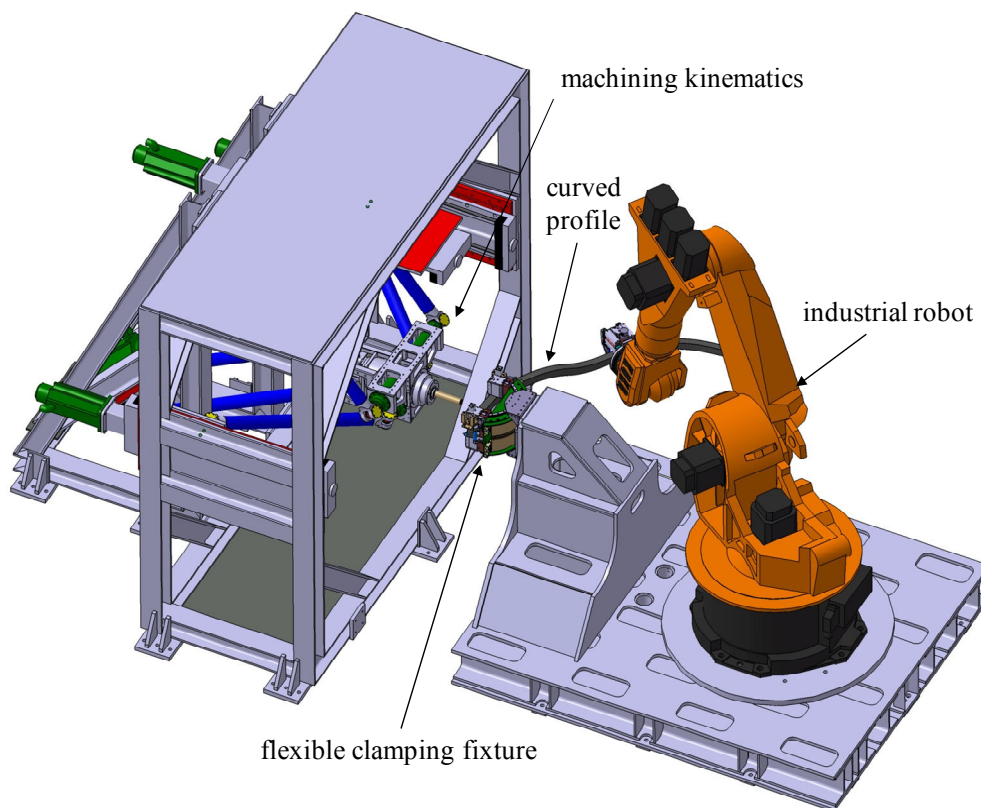
Figure 1: Model of an overall machine concept for the flexible machining of
spatially curved profiles

Design of the machining and clamping concept

In order to decouple the clamping process from a profile's three-dimensional geometrical shape, the clamping concept that has been developed distinguishes between the two functions "clamp profile" and "determine position of profile". If the physical profile contour is reduced to the profile's center line, it will always be possible to position this center line to meet two fixed points P1 and P2 (Figure 2, left). This purely geometrical approach can be used to determine four degrees of freedom of the curve, i.e. two rotational and two translational ones. The two degrees of freedom that are yet to be determined would consist in a movement of the profile along the x axis and its rotation about it in the local coordinate system, the x axis being the connecting line between points P1 and P2. If applying this approach to a physical clamping system, it would be possible for almost each profile geometry to meet two support points at the same time. As a physical profile cannot be reduced to its own center line, the number of imaginary support points needs to be raised to four.

Technology-wise, this approach may take the form of two lines each perpendicular to one another and molded as stop angles (Figure 2, right). Depending on each profile's cross-section, the contact patch between the profile's surface and the stop angle may take the shape of either points or lines. If the profile's cross-section has got a circular shape, there will be one punctiform contact patch between the profile and each of the four stop angles (Figure 2). This serves to determine both, the position of the profile and the above-mentioned profile center line in four degrees of freedom.
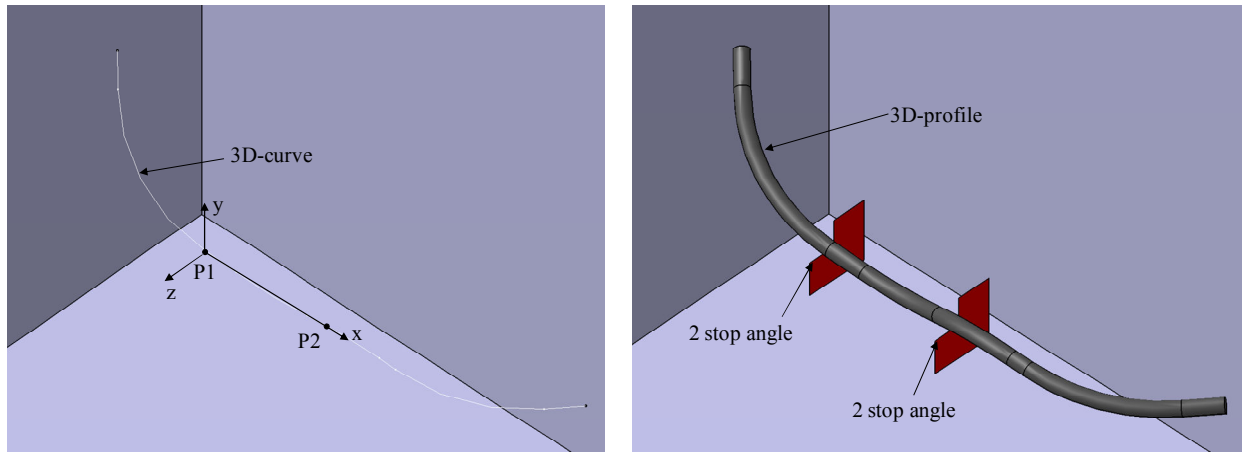
Figure 2: Spatial positioning of a three-dimensional curve

The two degrees of freedom being yet undetermined are narrowed down on the basis of the developing overdetermination of the system by means of a second gripper which is attached to an industrial robot. The function "clamp profile" was implemented by means of two clamping units that are adaptable to any workpiece surface geometry and attached next to the stop angles. This principle is described in detail in [9] and [10]. Machining of the profile takes place between the two clamping units. In case the profile requires machining outside this area, the industrial robot pushes it to the desired location with the gripper, where it is clamped again and machined. The pushing movement requires the stop angles of the prototype to be shaped as stop rollers. This way, the profile surface cannot be damaged during the pushing process. The prototypical design of this machine concept can be seen from Figure 3. The position of the stop rollers has been highlighted with white in the enlarged view of the clamping system shown in Figure 3. This picture does not include the kinematic machining mechanism arranged opposite the clamping system. The gripper has been gimbal-mounted to the chassis with a rotary and a swivel axis in order to ensure that boreholes will always be drilled perpendicular to the profile, for example. Each of these axes has been endowed with an angle measurement system, but neither has got its own drive. Both axes are indirectly driven by the industrial robot which is linked to the clamping system via the gripped profile. The results of the angle measurements are transferred to the robot control for angle readjustment. During machining both axis are mechanical fixed. This enables a direct force flow from the cutting tool over the profile to the machine base [9].
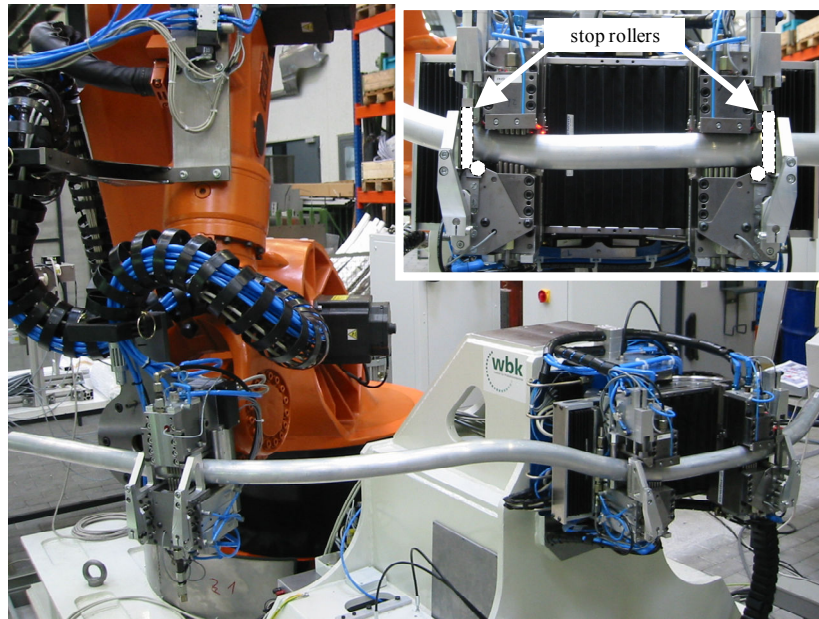
Figure 3: Prototype of the clamping system with clamped profile

An approach to profile positioning

The two degrees of freedom that cannot be determined on the basis of the mechanical stops have to be identified by means of a metrological approach. The measurement results can either be transferred to the industrial robot for fine positioning of the profile, or to the NC control of the kinematic machining mechanism for a correcting motion of the tool. Therefore, the section is measured from a reference point on the profile surface. The first test results have already been described in [11]. Markings applied onto the profile surface produced the best results in previous tests [12]. If several markings can be geometrically related to each other, these markings can be considered a form of "component-specific gauge" positioned on an imaginary line on the profile surface.

If the gaps between the markings can be made sufficiently accurate to allow for the exact positioning of the profile, the gauge can be considered precise in relation to a reference mark. The gauge can then be used as the measurement standard.

The following paragraph describes a way to identify the position of the profile by the example of a linear profile with a circular cross-section under these circumstances. The industrial robot positions the profile at the initial target position where the reference mark has been made. If there is no absolute position allocation for the markings, they need to be approached by the industrial robot one by one and analogically recorded in an incremental measurement system. The gaps then need to be totaled. Another possibility would be to give the marking an absolute reference by adding additional information. The simplest variant would be a number combination or a different form of coding. It might also be possible to integrate the absolute reference into the shape of the marking, for instance through circles with different diameters. The center of the circle would refer to the position, whereas the surface area would relate to the absolute reference. Other possible shapes are looked at in the following work steps.

In case it is impossible to achieve sufficient accuracy for the markings on the profile, there are two options. The markings can either be put on with repetitive accuracy or with variable accuracy, i.e. "subject to errors". Either way, it would be impossible to simply read out the markings at a random point on the profile. This being the case, the gauge on the profile could not be used as the measurement standard. It would be possible, though, to use a measurement system like a image processing system, for example, to measure the gap between two adjoining markings M_i and M_{i+1}.

The measurement would have to be carried out on the basis of a reference mark as well. If a gap

between two markings is too large to be measured with sufficient accuracy by one measurement system only, the distance between the markings

$$A_{M_i \to M_{i+1}} = a + \Delta a \qquad\qquad (1)$$

needs to be determined via a second measurement system positioned at the known distance a to the first measurement system (Figure 4). Δa is the deviation between the target and the actual position of the marking M_{i+1}. The resulting actual distance $A_{M_i \to M_{i+1}}$ between two adjoining markings needs to be buffered in a calibration file and allow for allocation to the respective marking at any point in time along the process chain. To permit calibration of the gauge along the entire profile length, the profile needs to be moved forward to the next marking by the industrial robot, a process that requires repetition until all markings have been recorded and stored in the calibration file.

For this approach to be applied to curved profiles, the profile geometry between the adjoining markings needs to be known also, because the above-described procedure is limited to the identification of the projected gap between two markings (Figure 4). Given that the geometry between two markings is known, the developed length of the imaginary surface line can be calculated. Figure 4 shows the schematic illustration of the metrological design with two flat profiles, one linear and one with a constant radius.
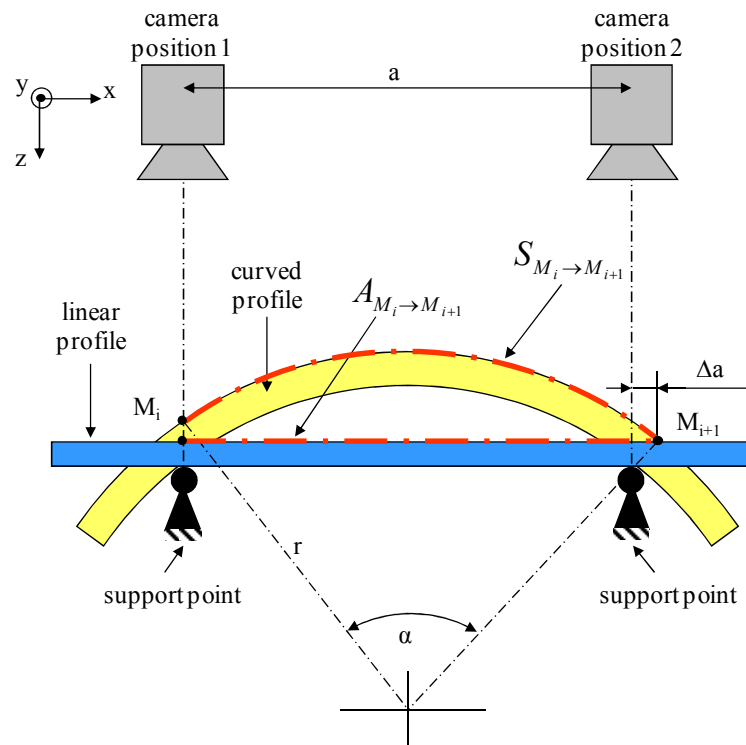
Figure 4: Schematic illustration of the calibration of two adjoining markings

In both cases, the fault Δa is measured on the basis of image processing, and then used to determine the actual gap between the two adjoining markings M_i and M_{i+1}. The developed length of the curved profile exceeds the gap between the markings on the linear profile as $S_{M_i \to M_{i+1}}$. The length $S_{M_i \to M_{i+1}}$ can be calculated with

$$S_{M_i \to M_{i+1}} = \frac{\pi r}{180°} \left[\arcsin\left(\frac{a}{2r}\right) + \arcsin\left(\frac{\left(\frac{a}{2} + \Delta a\right)}{r}\right) \right] \tag{2}$$

for a segment of a circle with the known outside radius r and the measured fault Δa. In order to move the profile to other positions, it needs to be continuously forwarded from one marking to the next, and the measurement process needs to be repeated as many times as necessary until the desired position has been reached. The markings should be applied onto the profile with a gap as big as possible between them. This prevents unnecessarily slowing down the process and minimizes the measurement faults resulting from totaling as much as possible.

If the profile geometry between two markings is not known, it needs to be metrologically identified, too. If the described procedure is applied to curved profiles with a non-constant radius or to spatially curved profiles, the mathematical description of the profile contour requires a splin interpolation. An optical sensor measuring two dimensions and operating on the basis of the triangulation method is used to identify the profile contour between the support points. The profile sensor is positioned opposite the profile and moved across it by means of a linear axis. A schematic illustration of the design can be seen from Figure 5. The distance $\Delta z(x_i)$ between the sensor and the profile is measured at different points x_i. If the profile is spatially curved, the transverse direction $\Delta y(x_i)$ of the profile sensor is additionally measured at each measuring point x_i. The resulting measurement results can be used to calculate the length of an imaginary surface line between two adjoining markings, approximated via a cubic spline, by means of a line integral. The calculated length matches the gap between the two markings as stored in the calibration file.
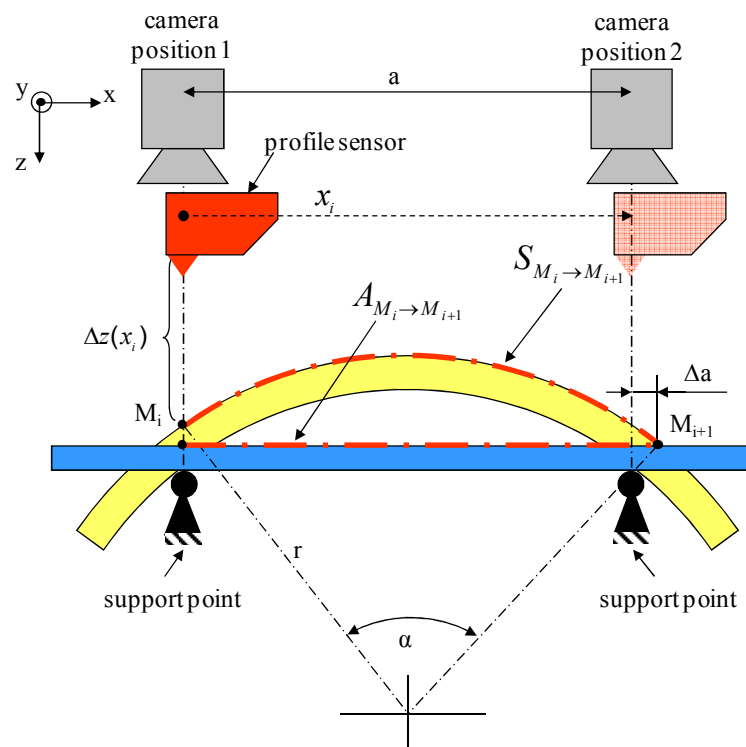
Figure 5: Design of the measurement devices for profile positioning and contour measurement

For this design to be implemented and for the described measurements to be performed in-line, the described measurement system needs to be integrated into the kinematic machining mechanism opposite the clamping system in the long run. It will then be used to achieve the correct positional

arrangement of the measuring devices in relation to the profile. To allow for the profile to be measured according to the above-described approach and for the gauge to be read, it needs to be ensured that the gripping system is correctly aligned during the measurements, i.e. that the rotatory and the swivel axes of the clamping system are each set to 0° by the industrial robot. Any angle other than 0° would cause the mechanical guide rollers to tip in relation to the measurement system and thus, leads to faulty camera and profile sensor measurements. Figure 6 shows the relevant principle of the control process of the industrial robot and the clamping system for a gauge that is "subject to error".
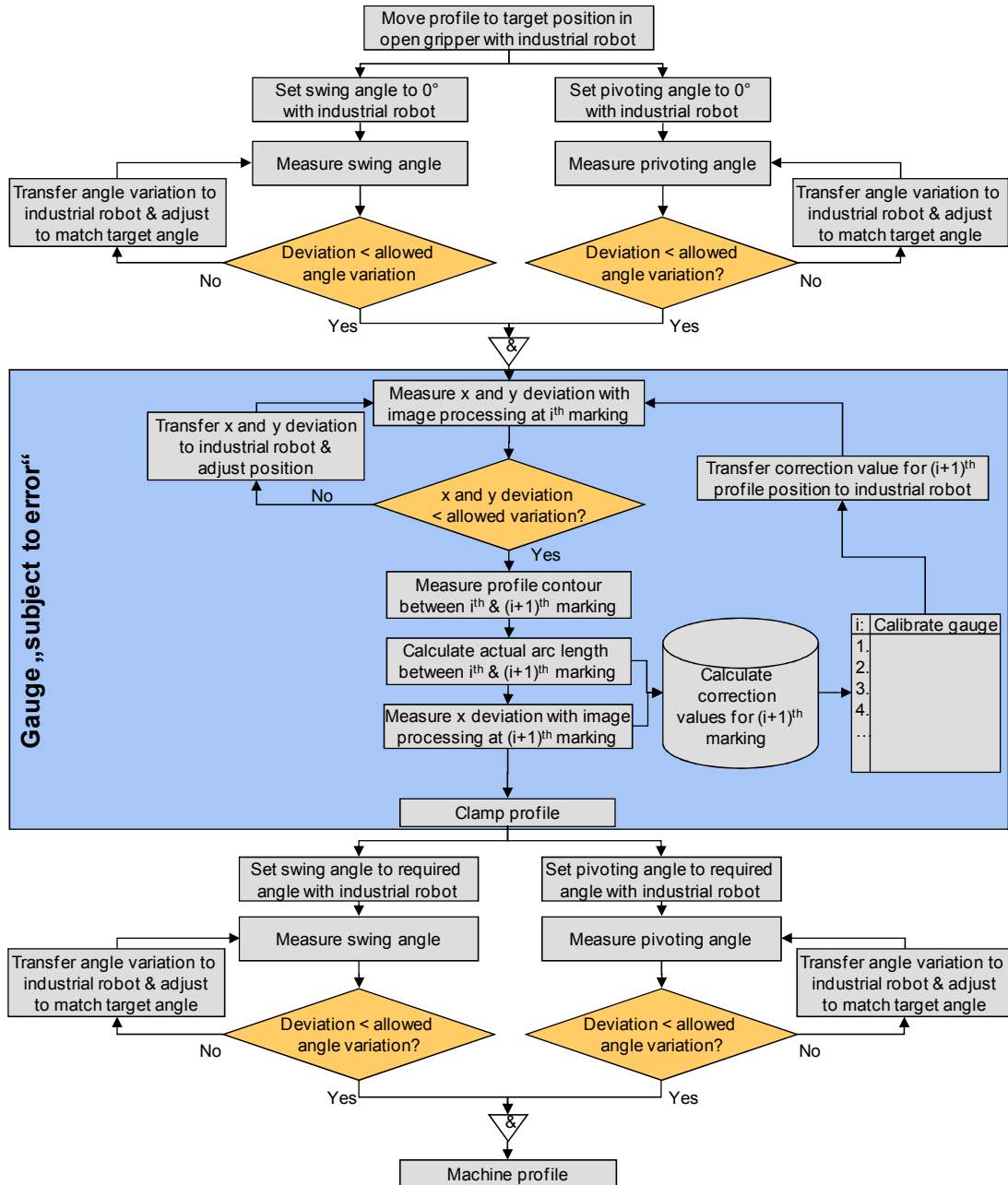
Figure 6: Control process during profile positioning

Marking application and detection

Numerous tests showed that the best and easiest way to position and align the profile is by using markings on the surface of the profile. The tested markings were applied onto the profiles using a marking laser. This method offers the advantage of being able to apply the markings with high accuracy and speed. These are the prerequisites to be met if the markings are to be applied simultaneously with the extrusion process, i.e. in-line, to avoid an additional process step having to

be integrated into the process chain. In order to prevent the marking process from interspersing the surface of the profiles with notches, the labeling process is adjusted to allow for a low application of energy into the material only to just slightly roughen the surface. The resulting markings are not easily visible, though, since depending on the incidence of light contrast might be low. This poses a challenge to an automated reading of the markings by means of a camera system. For this reason, tests with different lighting equipment were carried out. The highly reflecting aluminium surface may have a negative impact on image evaluation. The reflections may be reduced by using diffuse or polarizing light, for example [13]. If the profile surface is illuminated with polarizing light, the light reflected from the profile surface will also be polarized. This very light can be blocked by means of an analyzer installed in front of the camera objective. The analyzer is only light-transmissive if the light does not vibrate at the same polarization level as the reflected light. Faults on the profile surface or the surface sections roughened by the laser beam scatter the light diffusely, thus allowing a large part of this light to pass through the analyzer. As a consequence, the image produced by the camera shows the faint markings of the profile as bright against the unlabeled profile surface creating a high-contrast image, thus facilitating digital image processing (Figure 7**,** below).
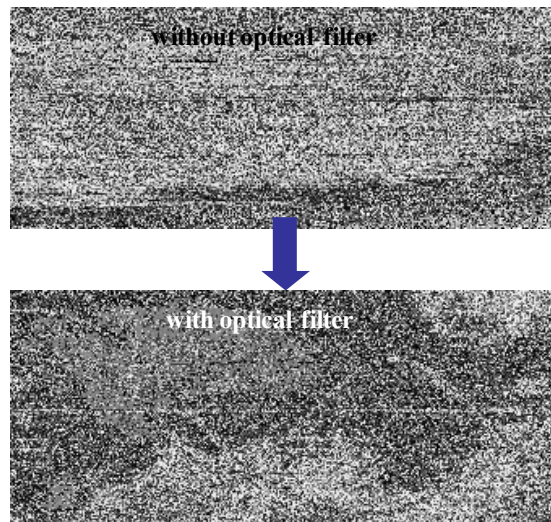
Figure 7: With and without optical filter

In order to measure the position deviation of a profile along its longitudinal axis and its rotation about it via image processing, a program was set up which is able to calculate the coordinates of the intersecting point of a marked cross and to transfer them to a primary control like the robot control, for example, via a serial interface (Figure 8, left). The absolute allocation of this intersecting point is ensured by a number combination positioned alongside the cross which is identified via character recognition. Figure 8, right, shows the binarized image of the marking.
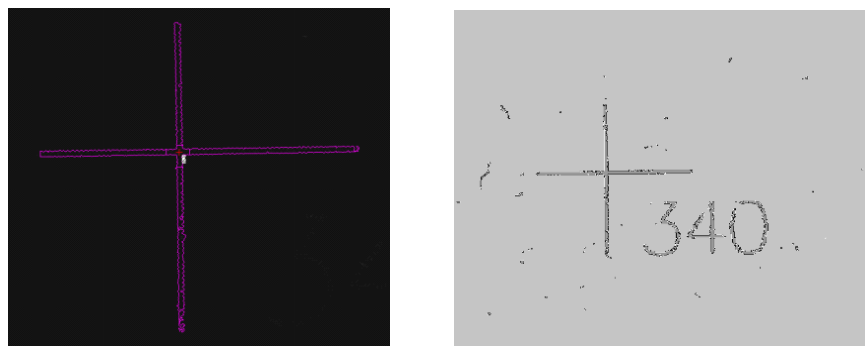
Figure 8: Illustration of cross and number

Set-up of the preliminary test rig and first results

Prior to integrating the measuring devices schematically illustrated in Figure 4 and Figure 5 (camera 1 & 2, profile sensor and linear axis with measurement system) into the gripping system or the kinematic machining mechanism respectively, they were incorporated into the preliminary test rig in a first step (Figure 9). The test rig serves to test the approach to profile positioning by means of component-specific markings and to profile measurements under ideal conditions and to identify the achievable accuracies. The theoretical resolution of the camera resulting from this test setup totals approx. 17,5 µm for a display detail of approx. 28 x 25 mm.
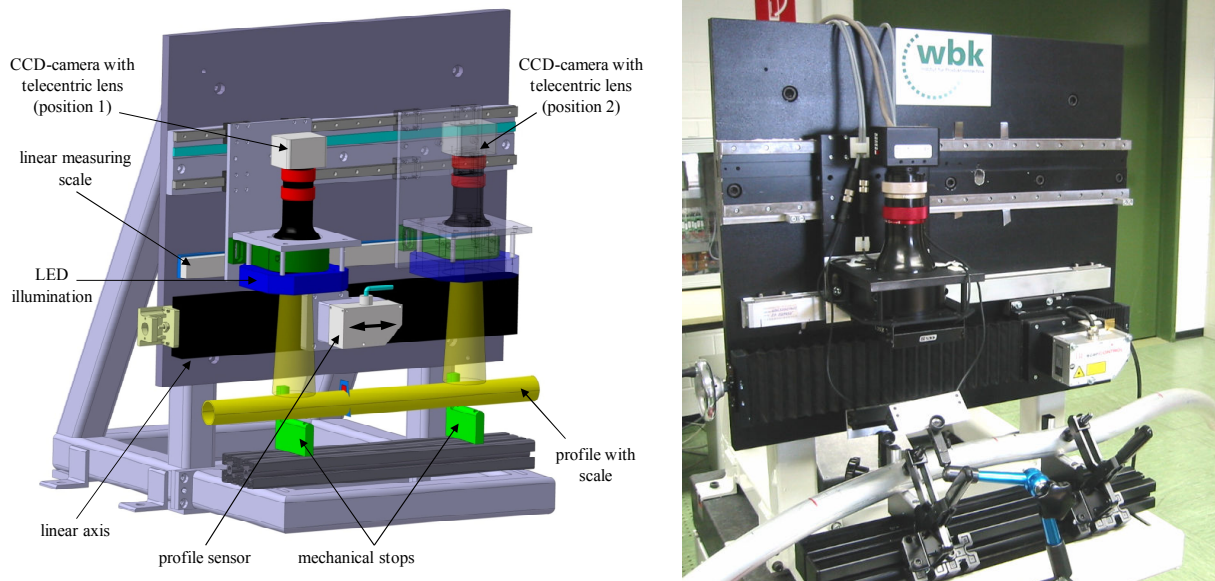
Figure 9: Preliminary test rig for profile measurements

In order to evaluate the system accuracy – camera with objective and lighting – one marking was measured several times without moving the profile between measurements. The x and y positions were determined in 400 measurements. Figure 10 shows the measured deviations. It became clear that the x position can be determined with a standard deviation of $\sigma_x = 1{,}8\,\mu m$, whereas this value amounts to $\sigma_y = 3{,}0$ µm for y. The slightly lower accuracy in y direction partly originates from the fact that the profile surface was strongly curved (r = 20 mm). The conversion of the y deviation into the profile twist results in a standard deviation of $\sigma = 31{,}2''$ for a profile with a radius of 20 mm. These results suggest that the use of an image processing system for the detection of markings is not only flexible but also allows for a high degree of accuracy.

y- and x-values number: each with 400
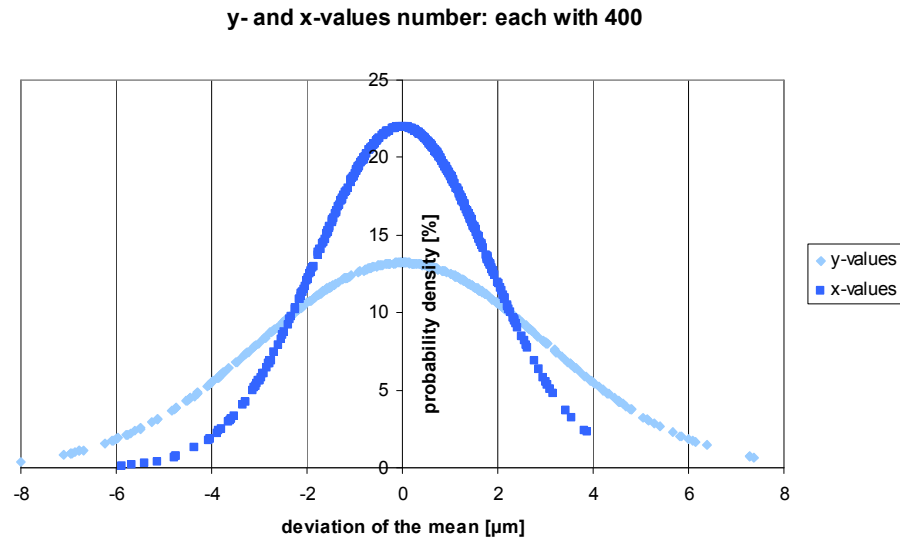
Figure 10: Probability density above the x and y deviations during marking detection

Summary and outlook

This article presents an approach that allows for the flexible clamping and machining of spatially curved profiles by means of a novel machine concept elaborated at the wbk Institute of Production Science. It then moves on to explain, on the basis of the previous results, the use of mechanical stops to determine the position and alignment of almost any profile contour inside the prototypically implemented clamping system. An approach based on profile-specific markings was presented allowing for metrological identification of the non-identifiable degrees of freedom via mechanical stops. The respective accuracy achievable when applying the above-mentioned gauge within the process chain was identified. Depending on the accuracy of the gauge, different metrological and control methods need to be chosen for the determination of position and alignment. In addition, the first results from gauge detection on the basis of digital image processing were presented.

Subsequent research will look into the ideal design of the markings on the profile surface and the achievable positioning accuracies with physical clamping systems on the basis of the above-described approach. Besides, the approach to profile positioning with gaugess subject to errors will be extended in that the entire three-dimensional profile contour is to be identified in-line on the basis of the measurement results gained from the profile sensor.

Acknowledgment

References

[1]   A. Trummer, H. Wiebach: Vorrichtungen der Produktionstechnik. Vieweg-Verlag (1994)

[2]   Homepage Fooke GmbH, http://www.fooke.de

[3]   Fleischer, J.; Denkena, B.; Winfough, B.; Mori, M.: Workpiece and Tool Handling in Metal Cutting Machines. in: Annals of the CIRP, Vol. 55/2 (2006), pp. 817-839

[4]   AMF Produkt Katalog, www.amf.de, (08.2007)

[5]   Horst Witte Gerätebau: Hauptkatalog Alufix, Sicherheit mit System, (2007)

[6]   Hesse, S.; Krahn, H.; Eh, H.: Betriebsmittel Vorrichtung, Kommentierte Ausführungsbeispiele, Hanser Fachbuchverlag, (2002)

[7]   Homepage ARLA Maschinentechnik GmbH, http://www.arla.de

[8]   Fleischer, J.; Schmidt-Ewig, J.P.: Innovative Machine Kinematics for Combined Handling and Machining of Three-Dimensional Curved Lightweight Extrusion Structures. in: Annals of the CIRP, Vol. 54 (2005), pp. 317-320

[9]   Fleischer, J.; Lanza, G.; Ruch, D.: Flexible and intelligent gripping technology for machining and handling of spatially curved extruded aluminum profiles. in: Advanced Materials Research, Vol. 10 (2006), pp.153-162

[10] Fleischer, J.; Ruch, D.: Flexibles Spannen räumlich gekrümmter Profile - Form- und konturflexibles Spannen räumlich gekrümmter Aluminium-Strangpressprofile. in: wt-Werkstattstechnik online, Jahrgang 95, Ausgabe 09 (2005), pp. 712-716

[11] Fleischer, J.; Lanza, G.; Ruch, D.: Using Part-Specific Scales for Positioning of Spatially Curved Profiles in a Highly Flexible Clamping System. in: Production Engineering Vol. XIII/2 (2006), pp. 39-42

[12] Lanza, G.; Fleischer, J.; Ruch, D.: Flexible und intelligente Greiftechnik. in: Fortschritt-Berichte VDI Reihe 2 Nr. 661, VDI-Verlag Düsseldorf (2007), ISBN 9783183661022, pp. 371 - 396

[13] C. Demant, B. Streicher-Abel, P. Waszkewitz: Industrielle Bildverarbeitung – Wie optische Qualitätskontrolle wirklich funktioniert, 2. Auflage, Springer-Verlag (2002)

Accuracy Improvement of a Machine Kinematics for the Product Flexible Machining of Curved Extrusion Profiles

J. Fleischer[1, a], J. P. Schmidt-Ewig[1, b]

[1] wbk Institute of Production Science, Universität Karlsruhe (TH)

Kaiserstraße 12, 76128 Karlsruhe, Germany

[a]Fleischer@wbk.uka.de, [b]SchmidtEwig@wbk.uka.de

Abstract

Within traffic engineering, the importance of lightweight space frame structures continuously grows. The space frame design offers many advantages for light weight construction but also brings challenges for the production technology. For example, the important requests concerning product flexibility and reconfiguration can only be achieved with a high technical effort, if current machine technology is used. For this reason, the collaborative research center SFB/TR10 investigates the scientific fundamentals of a process chain for the product flexible and automated production of space frame structures.

An important component in space frame structures are curved extrusion profiles. Within the investigated process chain, the extrusions must be machined mechanically in order to apply holes and to prepare the extrusion ends for the following welding operation.The machining is currently done by clamping the profile into a fixture and processing it within a machining center. This procedure has two disadvantages due to the complex geometry and the partially high length of the extrusion profiles: On the one hand, a complex fixture is needed for clamping the work piece [1]. On the other hand, a machining center with a large workspace and five machine axes is required [2]. Due to this, the product flexible machining with current technology is only possible with high technical and economical effort. For this reason, a new machine concept for the product flexible machining of three dimensionally curved extrusion profiles was developed at the University of Karlsruhe. In this paper, the function of the machine is explained and a prototype is presented. In addition, investigation results of the machining accuracy are shown and possibilities for improving the precision are discussed.

Machine Concept for Product Flexible Machining

Based on a systematic approach for integrating handling and machining capabilities [2], the machine concept shown in figure 1 was designed. It is build up out of three major components: An industrial robot, a parallel kinematic machine tool and a flexible clamping device which is located in between.
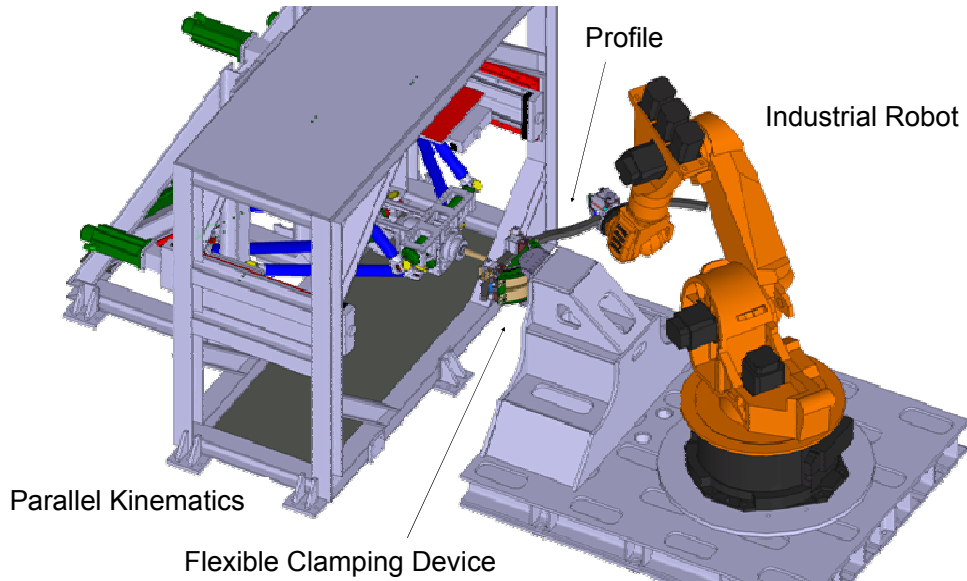
Figure 1: Machine Concept (wbk)

The industrial robot is used for the handling tasks which result from the process chain. In addition it also supports the machining process by moving the extrusion profile within the clamping device in order to position the workpiece area which is to be machined next to the tool center point. The machining angle can also be adjusted by turning the rear end of the profile around the clamping device. For this, the clamping unit is pivoted and possesses two rotational degrees of freedom that allow a rotation around the tool center point. After having adjusted the desired angle, the rotation axes can be blocked for reaching a high stiffness [1]. The translational movements between tool and workpiece needed for machining are executed by the parallel kinematic machine tool which was optimized for this task [3].

The machine concept several advantages. The number of required degrees of freedom of the machining kinematics can be reduced by adjusting the machining angle with the industrial robot. In addition the entire workpiece can be machined without needing a clamping fixture which was adapted to the longitudinal geometry of the extrusion. The required work space of the machining kinematics can also be reduced significantly which enables a high potential for reducing costs. Figure 2 shows the prototype of the machine concept.
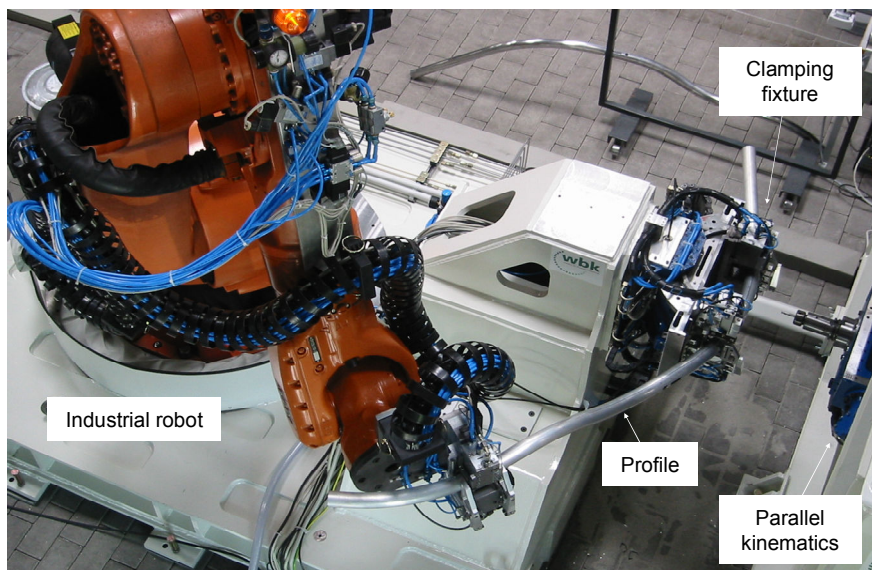
Figure 2: Prototype (wbk)

The three main components (robot, parallel kinematics and clamping device) are controlled by the robot control (KRC2 control) and a free programmable real-time interface (dSPACE system). Figure 3 shows the architecture of the entire control system. The procedure of the machining process is defined in the robot control. With the help of this control, all movements needed for handling and positioning the workpiece are executed. After having positioned the extrusion within the clamping device, the robot control sends a digital signal to the dSPACE system. This part of the control executes the clamping action and enables the machining movements of the parallel kinematics which were defined in an NC-program previously. The dSPACE system and the frequency converters together form a cascaded position control. The superposed position control, the required coordinate transformation and the error compensation are executed in the dSPACE system while the velocity and current control is located in the frequency converters.

When the machining action is done, a digital signal is sent to the robot control in order to move the workpiece to the next machining position.
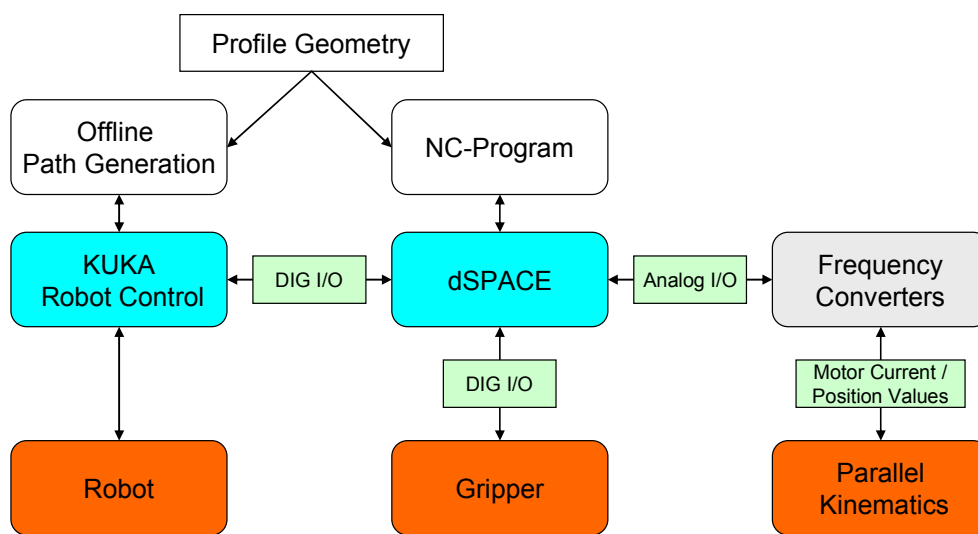
Figure 3: Control System

In order to move the extrusion profile precisely within the clamping device, a complex robot path must be generated which can not be done with conventional programming procedures. For this reason, the robot path is calculated with the help of a CAD-based kinematic model which precisely simulates the gliding movements of the extrusion on the positioning rolls of the clamping device [4]. Thus, the angular movements of the robot axes can be determined which result from a longitudinal and angular movement of the extrusion in the clamping device. The recorded data are transferred to the robot control. This method is similar to the procedure which is used within the collaborative research center for creating the tool path for the flying cutting [5].

Examination of the Positioning Accuracy

The offline path generation described above enables an easy creation of machining programs also for complex workpiece geometries. This is a prerequisite for a quick reconfiguration of the production system for new work pieces as it is necessary in a product flexible production. Due to a limited accuracy of the robot and deviations between the geometry of the kinematic model used for programming and the real machine, a limited positioning accuracy is expected. The precision of the parallel kinematics could be improved by an error compensation as described in [3], so that this part of the system does not cause major errors. Yet, the precise positioning of the workpiece within the clamping device is still a challenge. These deviations can already be limited by fixing the extrusion using positioning rolls. This way the extrusion position is always clearly defined orthogonal to the

longitudinal workpiece axis. The remaining deviations are errors in the longitudinal position and the machining angle.

The precession which is aspired within the collaborative research area SFB/TR10 is a deviation of ± 0.1 mm on one meter workpiece length. The desired angular precision is ± 0.01°. In order to quantify the actual deviations, positioning experiments were performed. Figure 4 shows the experimental set up.
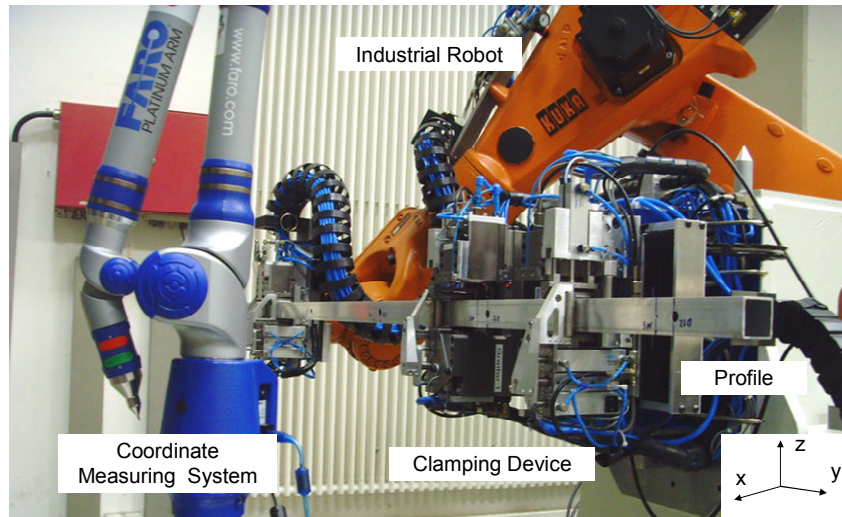

Figure 4: Experimental Set Up

The experiments initially focus on the positioning of a straight profile. Due to the fact that the error influences are the same for straight and curved extrusions, it can be assumed that the deviations for curved workpieces have the same dimensions. At first, the straight extrusion is shifted through the clamping device in five 200 mm steps and then moved back to the initial position. Next, the workpiece is rotated in 15° steps around a total angle of 90° around the turning axis of the clamping device (x-axis in figure 4). Finally the profile is turned ± 15° around the tilting axis (z-axis in figure 4). In each step the deviations of the two angles (turning and tilting angle) as well as the deviation of the longitudinal workpiece position are determined with the help of a coordinate measuring system. The angular deviations can precisely be determined by measuring the orientation of the workpiece surfaces. The longitudinal error is measured with help of an index hole. The following figure shows the results of three exemplary measurements.
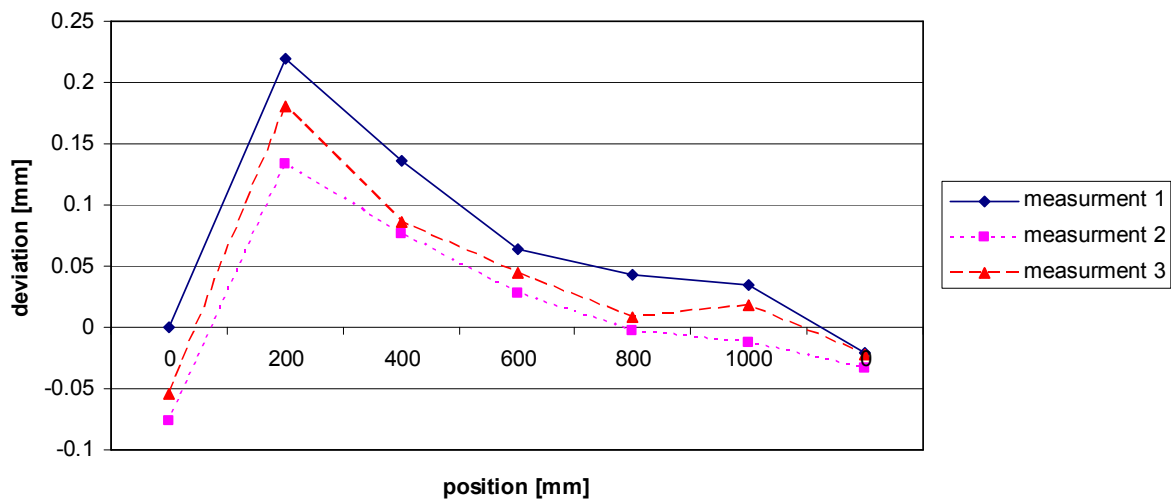
Figure 5: Longitudinal Deviations
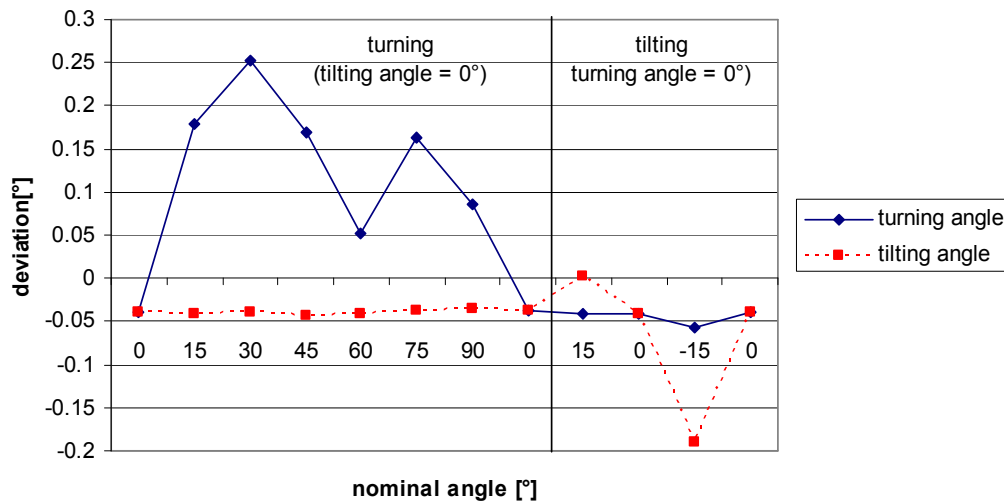
Figure 6: Angular Deviations

Figure 5 shows the longitudinal deviations of the profile. The maximum error is 0.25 mm and occurred after a displacement of 200 mm. When the experiment is repeated, the error pattern shows a similar progress. Yet, an error distribution within a range smaller than 0.1 mm can be recognized. This distribution can be referred to the repeatability of the industrial robot which is in the range of ± 0.1 mm, according to the manufacturer.

In Figure 6 the angular error is shown for different work piece orientations. The left side of the diagram refers to a rotation around the turning axis (x-axis), in the right side the profile is tilted ± 15° around the z-axis. The maximum deviation of the turning angle is 0.25° and occurs for a desired angle of 30°. The maximum error of the tilting angle is 0.19°. The repeatability of the rotation has turned out to be very good. This is also shown by the similar values for the different zero-positions (value 1, 8, 10 and 12 in figure 6). The errors follow a non-linear pattern for both rotations. In addition, it can be seen that the turning and tilting angle have only a small interdependency. According to this observation, the two angles can be corrected independently. In conclusion, the absolute deviations must still be improved in order to reach the aspired accuracy.

Approach for Accuracy Improvement

The major influences for the observed positioning errors can be summarized as follows:

- geometrical deviations between the kinematic model and the real machine
- deviating workpiece geometry
- clamping errors
- insufficient accuracy of the industrial robot

The geometrical deviations between the machine prototype and the kinematic model used for programming were eliminated as far as possible by measuring the position and orientation of the clamping device and the robot using a coordinate measuring system. The programming model was adapted to the deviations afterwards. A compensation of the influence of the workpiece geometry is more problematic. In order to position the workpiece precisely in the clamping device, the entire kinematic chain consisting of robot and extrusion profile must perform a high accuracy. In order to reach this aim, an improved accuracy of the robot in not sufficient. In addition, the geometry of every single workpiece must be determined and the robot path must be adapted adequately. Due to the fact that this procedure has a high technical and temporal effort, a different approach was chosen in order to enhance the machining accuracy.

The deviations of the workpiece position and orientation are detected by sensors directly located in the clamping device and can afterwards be compensated by a correction movement of the robot.

In order to detect the angular deviations of the extrusion, two rotary encoders were integrated into the clamping device. For a detection of the longitudinal errors, different approaches were investigated at the Universität Karlsruhe (TH) [6]. A procedure which is based on an image processing system seems to be very promising. This procedure is described more detailed in the paper "An approach to accuracy improvements in the flexible machining of curved profiles" of this issue.

After having detected the deviations, they can be reduced by correcting the position of the robot. For this, it is necessary to calculate the corrected robot coordinates in dependency on the sensor data and the actual position of the extrusion profile. Due to the complex geometry of the extrusion profiles this calculation seems to be very complex in the first instance. The following geometrical considerations show how the corrected coordinates are calculated for deviations of the turning angle, the tilting angle and the longitudinal position. It is shown, that the corrected position can be determined independently from the extrusion geometry.
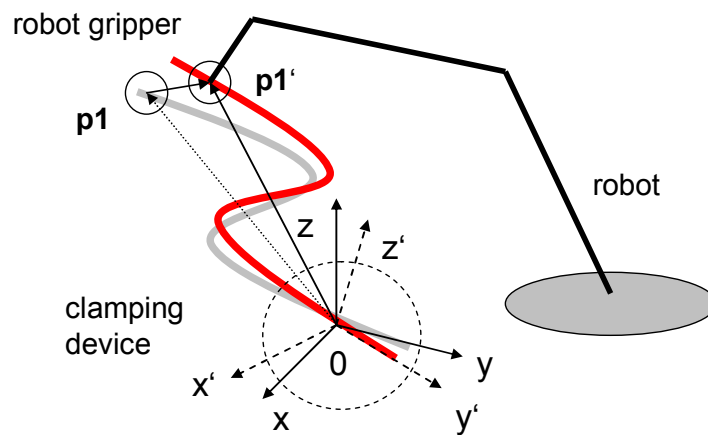
Figure 7: Rotation of the Extrusion

Figure 7 shows the arrangement of the rotational axes and the industrial robot. The point of origin (0) marks the center point of rotation of the clamping device. The vector **p1** describes the distance between the point of origin and the center point of the robot gripper. The coordinates of **p1** in relation to the center point of rotation can be accessed from the robot control. For this, the real center point of the clamping device and the robot gripper were measured and set as base and tool coordinate system in the robot control. Thus, the base coordinate system of the robot has the same position and orientation as shown in figure 7. The rotational axes of the clamping device allow the workpiece to turn around the x- and z-axis, whereas a turning around the x-axis changes the orientation of the z-axis. A rotation of the extrusion (**p1** → **p1'**) can therefore be described with a rotation of the x-axis and a following rotation of the z-axis. The rotation around the x-axis can be calculated with help of the rotary matrix **Rx**, whereas α represents the corresponding turning angle [7].

$$Rx = \begin{bmatrix} 1 & 0 & 0 \\ 0 & \cos(\alpha) & \sin(\alpha) \\ 0 & -\sin(\alpha) & \cos(\alpha) \end{bmatrix} \qquad (1)$$

The rotation around the z-axis (tilting angle β) can be described with **Rz**:

$$Rz = \begin{bmatrix} \cos(\beta) & \sin(\beta) & 0 \\ -\sin(\beta) & \cos(\beta) & 0 \\ 0 & 0 & 1 \end{bmatrix} \qquad (2)$$

The total rotary matrix **RM** can be calculated by multiplying **Rx** and **Rz**:

$$RM = Rz \cdot Rx \qquad (3)$$

If an angular deviation of the x-axis (dα) is measured, it can be compensated by a rotation around the x-axis of the base coordinate system. In practice, the robot can perform such an action with a circular movement. However, the end point of the path must be known for this. The point can be calculated independently from the workpiece geometry, as shown in figure 8.
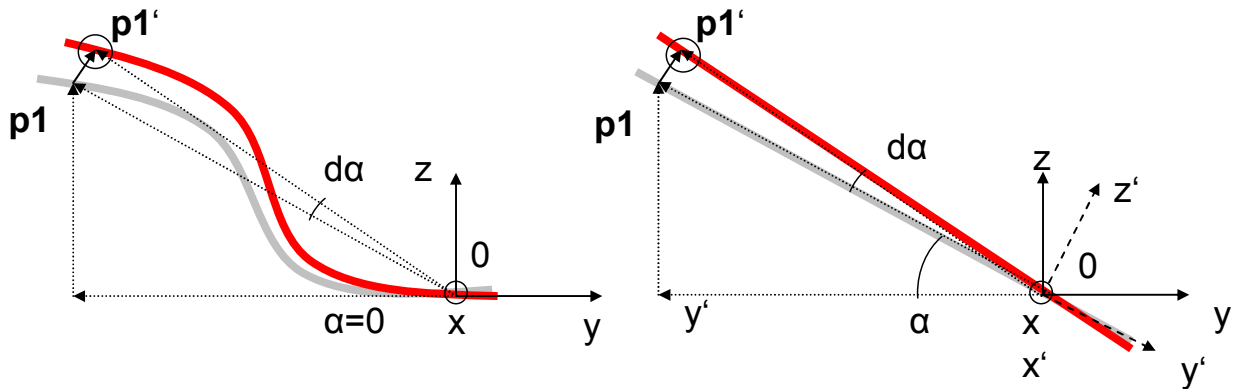
Figure 8: Angular Compensation

The end point of the path **p1**' can be determined with help of the actual position of the robot gripper **p1** and the angular deviation (dα). It can be calculated with the rotary matrix **Rx** as follows:

$$p1' = Rx^T \cdot p1 \qquad (4)$$

The robot paths which are needed for compensating the deviation dα shown in figure 8 are the same for both extrusion geometries. If a deviation dβ of the tilting angle (z-axis) needs to be compensated, it must be considered that the tilting axis is changed with a rotation of the x-axis (z → z'). Even though the robot gripper has the same position for both extrusions in the figure above, the orientations of tilting axes are different because the right extrusion was rotated about the angle α. For compensating the deviation dβ, a second end point (**p1''**) must be calculated. This can be done with help of the turning angle α, by transforming the actual position **p1** (which is only known in the base coordinate system) into the rotated coordinate system (x',y',z'), performing a rotation around the z-axis about dβ and, in a last step, transforming the new point back into the original system. The equitation for calculating the coordinates of p1'' in the base coordinate frame (x, y, z) is the following:

$$p1'' = Rx^T \cdot Rz^T \cdot Rx \cdot p1 \qquad (5)$$

Longitudinal deviations must theoretically be compensated by a movement which follows the extrusion contour. For a straight extrusion, a linear path is sufficient. Yet, for a curved extrusion the robot gripper must theoretically also follow a curved path for avoiding tensions in the kinematic system. If the curve radius of the workpiece contour is large compared with the longitudinal displacement, the compensation path can be very well approximated with a linear motion. This is clarified in figure 9:
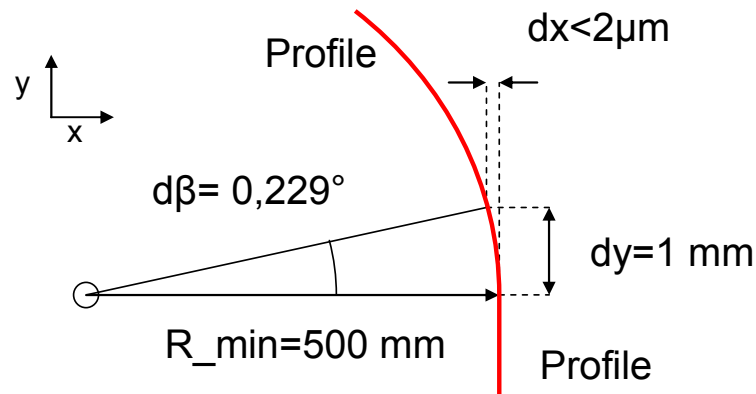
Figure 9: Approximation of the Longitudinal Compensation Path

In figure 9 the curve radius of the workpiece is assumed to be 500 mm, which corresponds to the minimal workpiece radius of the extrusion profiles regarded in the collaborative research center. The deviation which is to be compensated is assumed to be 1 mm. This is a realistic value corresponding to the previously performed measurements. If the compensation path is approximated with a linear motion, the deviation along the x-axis is smaller than 2 μm. According to this, small longitudinal deviations can be compensated with the procedure shown in figure 10.
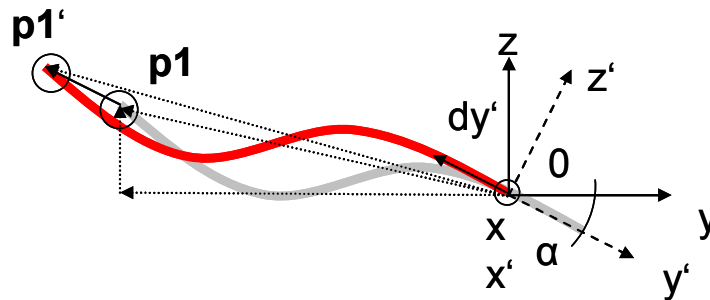
Figure 10: Longitudinal Compensation

A measured deviation can be send to the robot control as a scalar value (a). The required position **p1'** can be calculated with the orientation of the clamping device (α and β), the corresponding rotary matrix **RM** and the actual position **p1** as follows:

$$p1' = p1 + RM^T \cdot dy = p1 + dy' \tag{6}$$

The vector **dy** can be calculated with the deviation a and the unit vector **ey**:

$$dy = a \cdot ey \tag{7}$$

If the workpiece has a small curve radius, the compensation of a longitudinal deviation can lead to small angular errors. According to this, it is reasonable to compensate the longitudinal deviations first and correct the orientation afterwards. In a next step, the rotational axes of the clamping device can be blocked in order to ensure a correct orientation while machining the workpiece. Based on the calculations shown above, a sub program was integrated into the robot control which can be accessed by the main program after each positioning step and performs an automatic correction of the workpiece orientation. With this procedure, new positioning measurements of the workpiece were performed.

Positioning Accuracy with Compensation

The positioning accuracy with compensation was measured by new experiments. In order to guarantee the function of the compensation procedure for all eight space segments of the base coordinate system, the positioning experiment described above was extended. The turning angle is changed stepwise from 15° to -195°. In every step, a tilting angle of -15°, 0° and 15° is adjusted. After each positioning step, the sub program for error compensation is performed. Figure 11 shows the deviations before and after the compensation procedure.
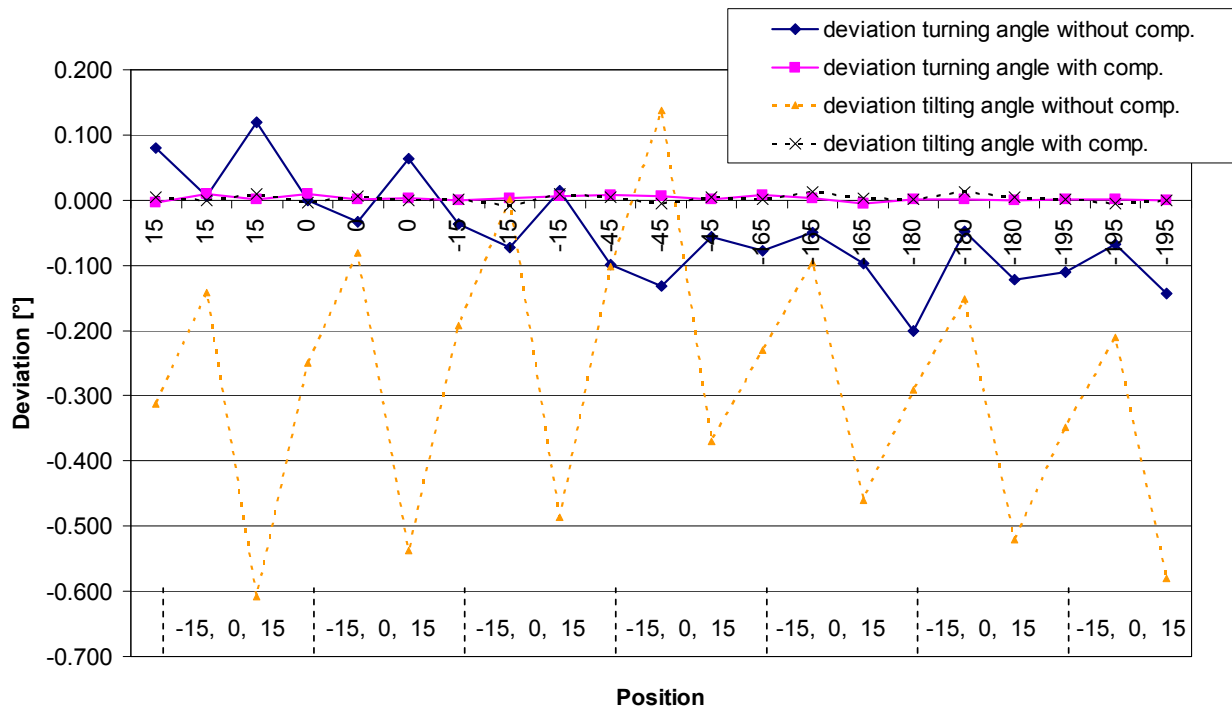
Figure 11: Deviations before and after Compensation

With the compensation procedure, a deviation <0.012° could be achieved in every position. This accuracy is sufficient for a precise machining. The duration of the procedure depends on the size of the error. The complete compensation takes between two and four seconds so that no appreciable non-productive time is added. The compensation time can be reduced further, if the robot speed is increased. Yet, a higher speed of the compensation movement can lead to larger deviations after compensation. If a lower target value is aspired (e.g. 0.04°) a compensation time smaller than two seconds can probably be reached. This will be investigated in further experiments.

For an automated compensation of the longitudinal deviations, the corresponding measuring system must be integrated into the clamping device first. This will be the aim of future work. Experiments in which the longitudinal error was measured manually have shown that a longitudinal accuracy of ± 0.025 mm is possible if the nominal value is approached gradually. Thus, the aspired accuracy should be achievable with the implemented measuring system.

Summary

A new machine prototype enables the product flexible machining of three dimensionally curved extrusion profiles with small technical effort. In order to achieve a high machining quality, a precise positioning of the workpiece is necessary. It could be shown in experiments that the positioning accuracy shows a high repeatability. The absolute error must yet be reduced in order to reach the aspired accuracy. For this reason, a compensation approach was developed. After having send sensor data to the robot control, a corrected position is calculated and the error is compensated automatically. By this, the angular precision could be enhanced significantly. The following work will concentrate on implementing an automated longitudinal compensation. In a next step experiments on positioning and machining curved extrusions will be performed.

References

[1] Fleischer, J.; Ruch, D.: Flexibles Spannen räumlich gekrümmter Profile - Form- und konturflexibles Spannen räumlich gekrümmter Aluminium-Strangpressprofile. in: wt-online, 09 (2005), pp. 712-716

[2] Fleischer, J.; Schmidt-Ewig, J.P.: Innovative Machine Kinematics for Combined Handling and Machining of Three-Dimensional Curved Lightweight Extrusion Structures. in: Annals of the CIRP, 54 (2005), pp. 317-320

[3] Fleischer, J.; Schmidt-Ewig, J. P.: Combination of a Parallel and a Serial Kinematics fort he Integrated Handling and Machining of Lightweight Extrusion Structures; In: 5th Chemnitz Parallel Kinematics Seminar, 05 (2006), pp. 289-306

[4] Fleischer, J.; Munzinger, C.; Schmidt-Ewig, J. P.: Kombinierte Handhabungs- und Bearbeitungskinematik. in: VDI Fortschritt-Berichte, 661 (2006), pp. 397-423

[5] Fleischer, J.; Stengel, G.: Bahngenerierung für eine robotergeführte Abtrenneinheit für räumlich gekrümmte Strangpressprofile. In: wt-online, 94 (2004), pp. 457-461

[6] Fleischer, J.; Munzinger, M.; Lamza, G.; Ruch, D. Schmidt-Ewig, J. P.; Stengel, G.; Schneider, M.: Maschinentechnik zur flexiblen Herstellung räumlich gekrümmter Strangpressprofile. In: ZWF – Zeitschrift für wirtschaftlichen Fabrikbetrieb, 7-8 (2006), pp. 426-430

[7] Shabana, A.A.: Computational Dynamics, John Wiley & Sons, Inc., New York (2001)

Mechanical Modelling of Wire Reinforced Metal Matrix Extrusion Profiles

M. Wedekind[1, a], H. Baier[1, b]

[1]Institute for Lightweight Structures (LLB) – Technische Universität München
Boltzmannstraße 15, 85747 Garching, Germany
[a]wedekind@llb.mw.tum.de, [b]baier@llb.mw.tum.de

Abstract. Compound extruded unidirectionally reinforced profiles are heterogeneously reinforced metal matrix composites. Profiles made from this material show a different mechanical behaviour than classical composite components. Homogenized material properties are required for an efficient design process. Within this paper an approach is shown to provide homogenized data for stiffness and strength for compound-extruded components. The usability of the Tsai-Hill failure criterion is investigated, and shown for cases with negligible residual stresses. Load cases including thermal stresses cannot be investigated by the Tsai-Hill failure criterion. Within the failure investigation a procedure is shown to include residual and thermal stresses.

Introduction

Extrusion profiles are used widely for frame structures, e.g. space frames in the automotive industry. Metal matrix composites (MMCs) have been researched and used for some decades. Most MMCs have the advantage of a high mechanical performance coming with the disadvantage of randomly orientated reinforcements or very high production costs. The production and utilization of heterogeneously reinforced metal matrix composites profiles (HRMMC-profiles) is investigated within the DFG collaborative research centre, TR-10. This new material provides the opportunity to bridge the gap between low cost and high performance with. Wire reinforced extrusion profiles are metal matrix composite profiles with a number of steel or other types of wire reinforcements. These are investigated in this paper according to their behaviour under mechanical loading. An investigation of material properties of compound extruded composites with different configurations is shown in [1]. Compared to classical metal

Figure 1: Cross section of a HRMMC profile

matrix composites, the cross section of a single reinforcement is quite large. As a comparison, the diameter of a steel wire reinforcement is about 1 *mm* while the diameter of carbon fibres is about 5-10 *μm* [2] which allows a smooth distribution of the fibres. The reinforcements of the profiles investigated are located in the centre plane of the wall. The reinforcement volume fraction is quite low, similar volume fractions can be found in SiC fibre reinforced copper used for high temperature applications [3]. A scheme of a cross section of a HRMMC-profile is shown in Figure 1. Due to this specific setup, HRMMCs show a particular mechanical behaviour which is investigated in the following to provide information for design with profiles made from this material.
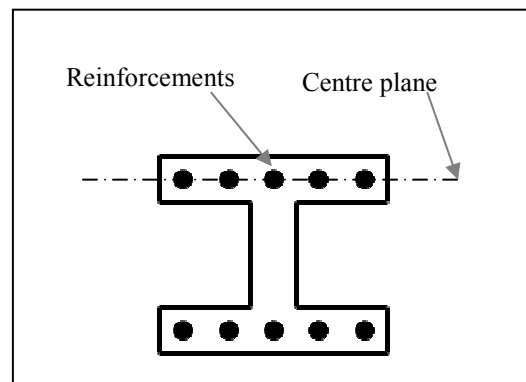
Analysis of existing metal matrix composites

Metal matrix composites can be subclassified in particle reinforced composites, discontinuously fibre reinforced composites and continuously fibre reinforced composites. The properties of the different material types vary over a large range.

Particle reinforced composites include small particles with a size of about 5-20 μm. This alters the mechanical properties and has an influence on the crack propagation under fatigue conditions [4].

Discontinuously fibre reinforced composites include fibres with a finite length. The load is introduced into the fibre by shear forces; therefore a critical length must be exceeded to utilize the strength of the fibre [5]. The load is carried partially by the reinforcements. Due to a short fibre length, the load is transferred between the fibres by the matrix. This causes a complex stress field within the matrix. Similar effects can be found at the boundaries and around the fibre damages within continuously reinforced composites.

The compound extruded profiles investigated are continuously reinforced components. These have an aluminium base material and steel wire reinforcements. In contrast to most continuously reinforced metal matrix composites, the reinforcements have a very large diameter. This results in a heterogeneous distribution of the stiffness at a macroscopic level.

Steel wire reinforced metal matrix composites have been investigated according to their mechanical properties [6] and crack propagation [7]. The influence of brittle intermetallic layers, generated by high temperature effects has been investigated [8], [9]. This material was used for the manufacturing of high pressure vessels with a service temperature up to 350°C [10].

During the compound extrusion process the reinforcements are embedded within the base material. The contact time between matrix material and the steel wires at a high temperature during the extrusion process is very short. Hence, there is no distinctive development of an intermetallic boundary layer [11].

Homogenization of profile properties

To enable an efficient design of structures made out of HRMMC-profiles and avoid large numerical models, the description of the material properties stiffness and strength should be provided with as little effort as possible. This description should enable the designer to realise a basic layout without being dependent on component tests within the early state of design.

An approach for a simplified calculation of a frame structure is shown. In the following the stiffness properties of the profiles are modelled by the role of mixture. The failure of the structure is determined by a failure criterion – either Tsai-Hill or a numerical criterion calculated by a FEM analysis.

For the undisturbed regions of the profiles a homogenization can be done easily. Due to the heterogeneous reinforcement boundary effects of the investigated profiles are very large. Boundary effects

Figure 2: Framework of demonstrator

can be found in areas with a high gradient of the stiffness, e.g. at load introductions and nodes of a framework. In this area the behaviour of the component are dominated by the design of nodes or load introduction, which results in a 3D-stress state. A typical setup of a space frame
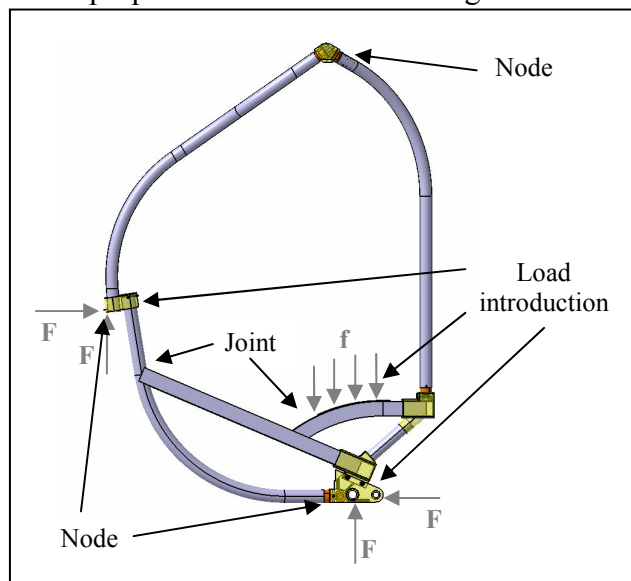
the setup of the demonstrator is shown in Figure 2. The configuration is taken from a demonstrator scenario of the TR-10 project, which represents the space frame of a C1 motorcycle.

Joints and nodes require either a more detailed modelling of the profiles or a further investigation e.g. FEM analysis using substructuring. For a detailed FEM analysis, the loads on the nodes are taken from a global model with homogenised properties. Within the following an analysis of the behaviour of undisturbed profiles is shown. Further investigation will be done on the profile homogenization in complex regions of nodes, joints and loading points.

Because the design loads cause only a linear elastic deformation, the homogenization of the elastic region is important. The homogenization of material properties for classical continuous fibre reinforced composites is well known. There are different methods to estimate the stiffness parallel and perpendicular to the fibres. An overview is shown in [5].

The predominant loads of the profiles are stresses in extrusion direction, bending forces and shear loads due to torsional moments. For elastic strain the stiffness of the profile in fibre direction can be described by the well known rule of mixture (ROM), see Equation (1). E is Young's modulus and φ is the fibre volume fraction.

Due to a homogeneous strain field in this case, there is no influence of the stiffness's heterogeneous distribution on the material properties.

$$E_{compound} = E_{fibre} \cdot \varphi + E_{matrix} \cdot (1 - \varphi)$$

(1)

To calculate the bending stiffness, the distribution of the strain within the profile has to be taken into account. In this case the effect of the reinforcement wires is dominated by their locations. These are displayed by the configuration's moment of inertia of all reinforcements I_{fibres}.

$$I_{compound} = \frac{E_{fibre} \cdot I_{fibres} + E_{matrix} \cdot I_{matrix}}{E_{compound}}$$

(2)

With this information the basic stiffness properties for flexural loads and loads in fibre direction are provided. The stiffness properties in perpendicular direction are dependent on the reinforcement position, and therefore no analytical investigation was performed.

Failure mechanism and failure criteria

For a failure analysis, 'failure' must be defined. Metal matrix composites with plastic matrix show different failure modes. For loading in the reinforced direction, the first failure mode occurs when the matrix's yield limit is exceeded. The second failure mode is a plastic deformation of the matrix exceeding a certain value, which leads to plastic deformation of the component [13]. In [13] this behaviour is utilized to take use of the very high ultimate stresses of this material. The application of the different failure definitions is dependent on the purpose. A further failure mode is known for steel wire reinforced metal matrix composites with a brittle intermetallic layer. Cracking of this layer causes notches and leads to a premature failure of the reinforcements [9]. This layer occurs due to diffusion at high temperatures. The maximal diffusion length during the extrusion process investigated is about 250 *nm*. Therefore only a very thin boundary layer is created [11] , which is assumed to be not critical because of the non-brittle fibres. For loading in direction perpendicular to the fibres additional failure modes can occur, e.g. debonding of the reinforcements. Since the bonding

between base material and reinforcement is very strong, a perfect bonding is assumed in the following investigation. This is shown in [11].

For most design cases exceeding the yield limit of the matrix, failure can be assumed. Beyond this point a plastic deformation of the component remains and residual stresses are generated. Furthermore, due to work hardening the material properties may be dependent on the load history.

Within a compound extruded component, large areas of undisturbed material exist. Hence it can be assumed that the reinforcing has no strengthening effect on the matrix properties. To achieve a strengthening effect these areas must be very small (in the order of 10 μm) [15].

Failure of uniaxial loaded HRMMCs

Axial loads refer to loads in fibre direction in the following. Loads perpendicular to the fibre direction will be called perpendicular loads. The associated strength will be called perpendicular strength. For axial loading, strain in matrix and reinforcements are equal. For equal Poisson's ratios of matrix and reinforcement following relations, given in (3), are valid. Since the Poisson's ratios of steel and aluminium are similar, the error is small. 'σ_{fibre}' and 'σ_{matrix}' describe the stresses in axial direction in the reinforcements and the matrix. '$\sigma_{compound\|}$' describes the averaged stress of the component in axial direction.

$$\frac{\sigma_{fibre}}{\sigma_{compound\|}} = \frac{E_{fibre}}{E_{compound\|}} \qquad\qquad \frac{\sigma_{matrix}}{\sigma_{compound\|}} = \frac{E_{matrix}}{E_{compound\|}} \qquad\qquad (3)$$

With this information the yield stress of the compound can be calculated. In Equation (4) the linear correlation between the reinforcement fraction and the maximal linear elastic stress of the component is shown.

$$\sigma_{\max\_compond\|} = \sigma_{\max\_matrix} \cdot \left[1 - \left(1 - \frac{E_{fibre}}{E_{matrix}} \right) \cdot \varphi \right] \qquad\qquad (4)$$

2D-stress fields resulting from loads perpendicular to the reinforcement direction are more complex. These are dominated by effects of the heterogeneous stiffness.
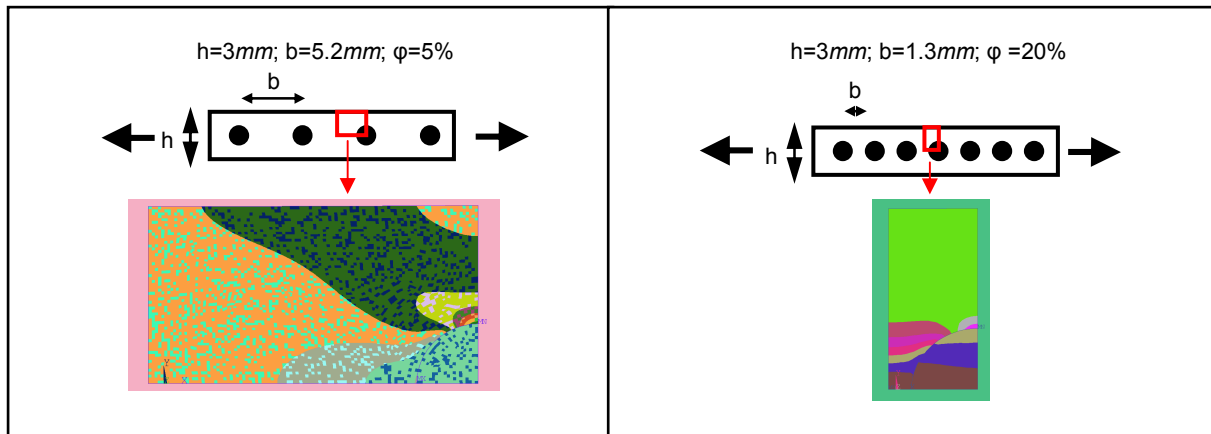
Figure 3: Stress field perpendicularly loaded profile

In **Figure 3** the schematic stress fields of perpendicularly loaded profile cut outs are shown. These stress fields are dependent on the height h of the profile and the distance b between the reinforcements. All reinforcements are located in the centre layer. This leads to stiffening and stress concentration within this layer, dependent on the distance between the reinforcement elements. The relation between the reinforcement fraction and the perpendicular strength is plotted in Figure 4. The assumed material properties are shown in **Table 1**. '$\sigma_{compound\perp}$' is the maximal average perpendicular stress on the component without plastic deformation within the matrix.
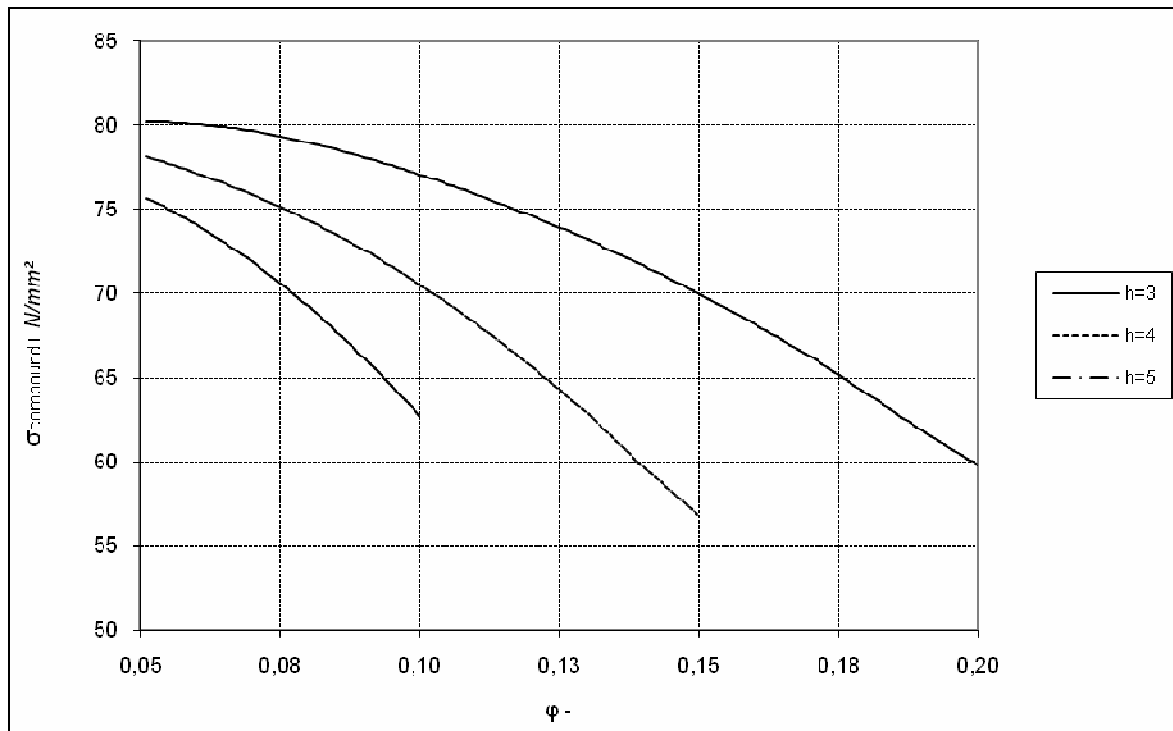
Figure 4: Perpendicular strength as function of reinforcement fraction (φ)

Failure of steel wire reinforced profiles under multi axial loading

To analyse the multi axial failure for steel wire reinforced aluminium, a FEM analysis is performed. A cut out of the component is modelled and investigated. The failure loads for this model are calculated with the same assumptions as discussed. Exceeding the yield stress of the matrix is assumed as failure. To eliminate boundary effects within the model, a specimen with three reinforcements is modelled. Only the data for the inner area is used for evaluation. Because of the shear stress state only one symmetry can be assumed.

The model has linear material properties for fibre and matrix. The connection between fibre and matrix is assumed as perfect bonding realised by merging the nodes. The material properties are shown in Table 1. The diameter of the reinforcements is 1 mm.

With this model the stress fields for the basic load cases (axial load, perpendicular load and shear load) are calculated. The data of the resulting stress fields is stored for further processing.

Fig. 5: FE-Model for stress analysis

Since the boundary of linear behaviour is of interest, the various load cases can be calculated by linear superposition of the basic load cases. For each load case a load vector is defined, which consists of a relation between σ∥ (axial direction), σ⊥ (perpendicular direction) and τ⊥∥ (shear). The field of equivalent stresses is calculated for this load combination with the von Mises hypothesis. The load vector is scaled to a size that the yield stress of the matrix is met. This is calculated for a defined set of load vectors and the result is shown as a 'yield surface'. The gained data is compared with the Tsai-Hill failure criterion to evaluate its usability. The objective of using such a failure criterion is the simplicity of its application. For an analysis with a Tsai-Hill failure criterion only a small amount of data is required. The Tsai-Hill failure criterion is an 'anisotropic von Mises' criterion. It was developed by Hill for the material description of anisotropic, rolled sheet metal. Afterwards Tsai adapted it for use with unidirectional laminates [16]. Tsai-Hill is a wide spread failure criterion for the analysis of unidirectional laminates.

Material properties for FEM-model		
Young's modulus matrix	70000	MPa
Young's modulus fibre	210000	MPa
Poison ratio matrix	0.33	-
Poison ratio fibre	0.29	-
α-matrix	0	1/K
α-Faser	0	1/K
Yield stress matrix	100	MPa

Table 1: Material properties

The information needed for Tsai-Hill, the failure loads for $\sigma_{\|max}$, $\sigma_{\perp max}$ and $\tau_{\perp\|max}$, are taken from the yield stresses calculated by the FEM analysis. At these points the deviation between the FEM analysis and the Tsai-Hill criterion is zero, as defined. The definition of the Tsai-Hill failure criterion is shown in Equation (5).

$$\left(\left(\frac{\sigma_\|}{\sigma_{\|max}} \right)^2 + \left(\frac{\sigma_\perp}{\sigma_{\perp max}} \right)^2 - \frac{\sigma_\| \cdot \sigma_\perp}{\sigma_{\|max}^2} + \left(\frac{\tau_{\perp\|}}{\tau_{\perp\|max}} \right)^2 \right)^{0.5} \leq 1 \tag{5}$$

With a comparison of Tsai-Hill and the FEM-failure analysis, the usability of the global failure criterion is investigated. The result of the comparison is shown graphically as a deformed sphere. The vector from the origin to a point at the surface describes the load combination. Its length is defined as the strength of the FEM failure analysis divided by the yield stress calculated with Tsai-Hill. A perfect sphere with the radius 1 represents exact correlation between both criteria. The colouring shows the deviation between the FEM failure and the yield stress calculated by Tsai-Hill. In Figure 6 the procedure is explained.
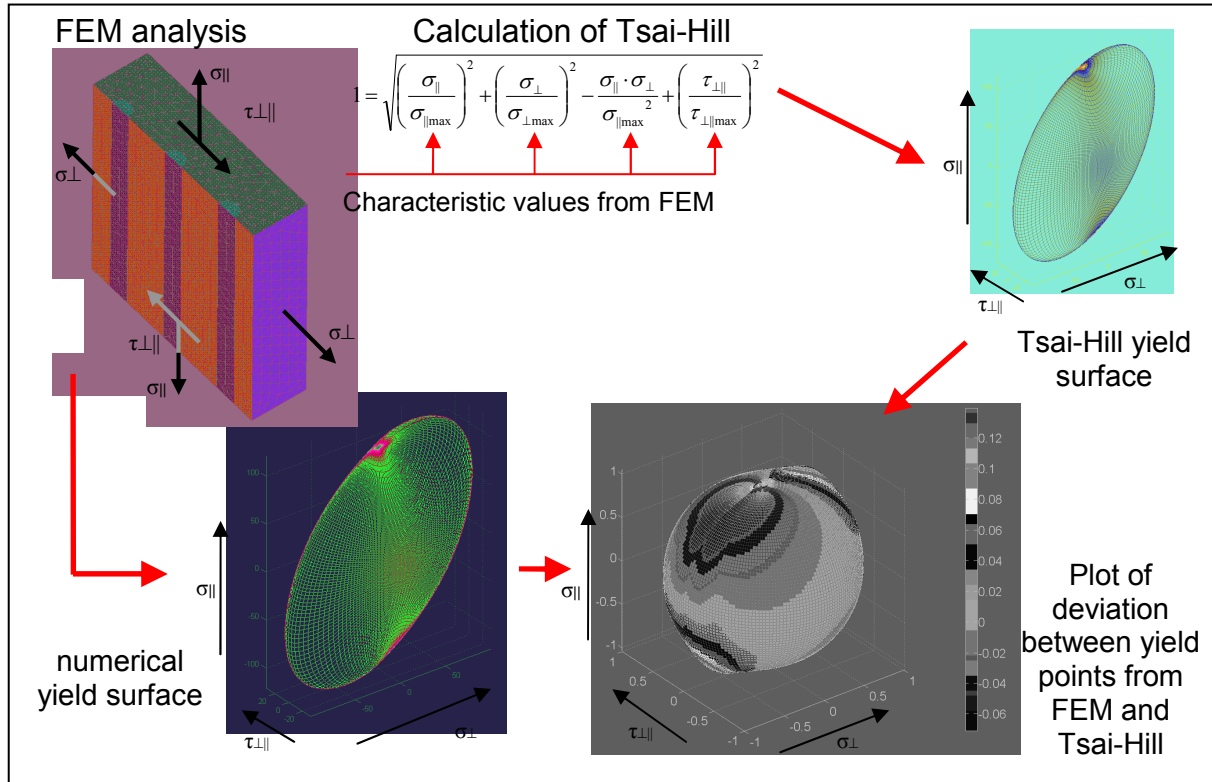
Figure 6: Procedure for comparison Tsai-Hill failure criterion with numerical failure analysis

Results

In the following a comparison of the analysis of different configurations of steel wire reinforced aluminium is shown. For the setup there are three design variables: the diameter of the reinforcement elements, the thickness of the material and the reinforcement fraction. Within this investigation only reinforcements with a diameter of 1 *mm* are taken into account. To enable the comparison of configurations with different reinforcement volume fractions a thickness of 3 *mm* is chosen. Since the reinforcements are only located in the inner area of the composite, the maximal possible reinforcement volume fraction is limited by the height of the component. With a thickness of 3 *mm* a reinforcement fraction up to 20% is possible without contact between the reinforcements – disregarding constraints of production.

The following figures show the yield surface calculated by FEM on the left. On the right the plots of the deviation between the FEM and the analytical solution is pictured out by the colouring. Their ratio is shown by the distance from the origin. In Figure 7 the configuration with a low reinforcement volume fraction of 5% is shown. The maximal deviation between the FEM solution and the Tsai-Hill failure criterion is approximately 8%. For the load cases with only axial or perpendicular or shear loading the deviation is, according to the definition, exactly zero. The highest deviation is found in the area with approximately equal loading in axial and normal directions with small shear load.

In **Figure 8** the results of a high reinforcement volume fraction of 20% is shown. The deviation between FEM and Tsai-Hill is increased for the larger volume fraction. The maximal deviation occurs in the case of approximately equal loads on both axes without shear loading. The highest deviation is approximately 12%.
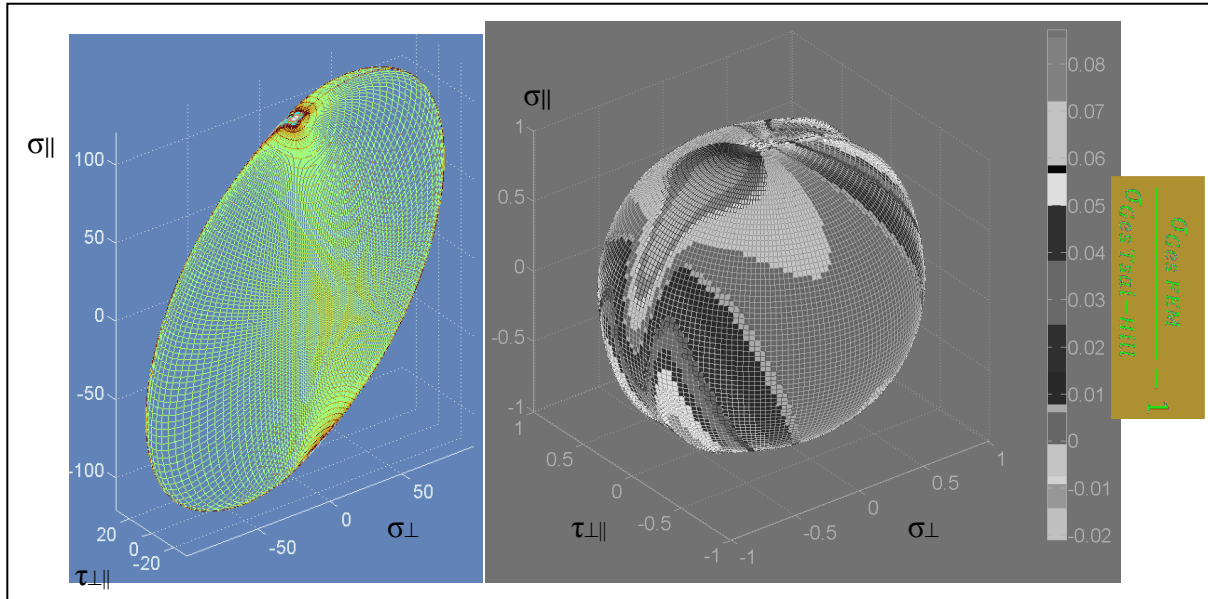
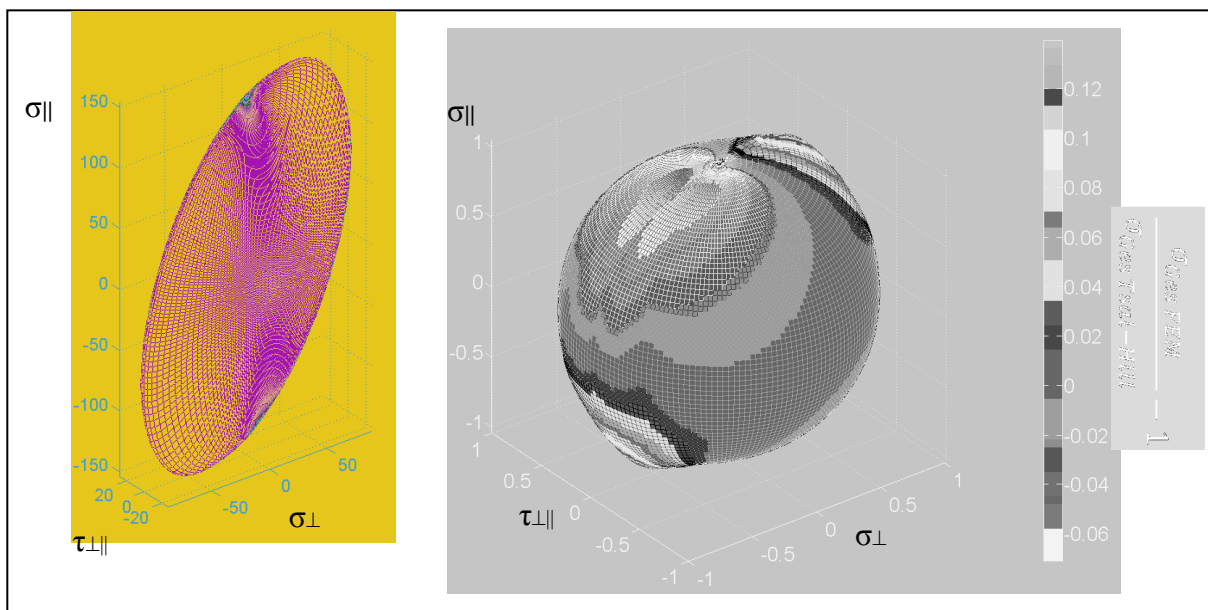Figure 7: Failure surface (left) and deviation from Tsai-Hill with reinforcement fraction 5% (right)

Figure 8: Failure surface (left) and deviation from Tsai-Hill with reinforcement fraction 20% (right)

Discussion of failure criterion

In case of pure axial loading, the whole cross section of the matrix reaches the yield limit simultaneously. This leads to a plastic deformation of the entire matrix material as well as the component. After decreasing the load residuals stresses are left.

In case of a perpendicular loading the complex stress field is dominated by effects of the stiff steel wire in the weak matrix. By definition, failure of the profile occurs with the first plastic deformation of the matrix material. In case of perpendicular loading only a small area of the matrix is affected. The influence of this plastic deformation on the component's global deformation is small. The stress fields are altered and the material properties are changed due to strain hardening. This has a significant impact on the fatigue properties and is assumed as a failure.

The application of this failure mode is useful for the layout of a framework for limit loads. In this case no plastic deformations are allowed. For a layout of an overload which exceeds the yield limit this approach is not valid.

Thermal effects on mechanical behaviour

For a typical framework the coefficient of thermal expansion (CTE) in axial direction is especially important. A CTE mismatch within a structure leads to thermal stresses and deformations.

The compound consists of two materials with a different coefficient of thermal expansion. This leads to residual stresses when exposed to a temperature load. The profile is produced at a temperature of approximately 550°C [14]. Thermal residual stresses result from the cool down process.. These depend on the recrystallisation temperature of the matrix material. The exact effect of the production on the residual stress fields will be investigated in further research. Residual stresses have been investigated by the subproject A3 of TR-10 [15]. In the following the general effect of a temperature offset on the component is investigated.

For a continuous fibre reinforced composite the coefficient of thermal expansion in fibre direction can be calculated by the internal balance of the forces. This leads to Equation (6) [5]. The coefficient of thermal expansion is represented by α.

$$\alpha_{compound\parallel} = \frac{E_{fibre} \cdot \alpha_{fibre} \cdot \varphi + E_{matrix} \cdot \alpha_{matrix} \cdot (1-\varphi)}{E_{fibre} \cdot \varphi + E_{matrix} \cdot (1-\varphi)} \tag{6}$$
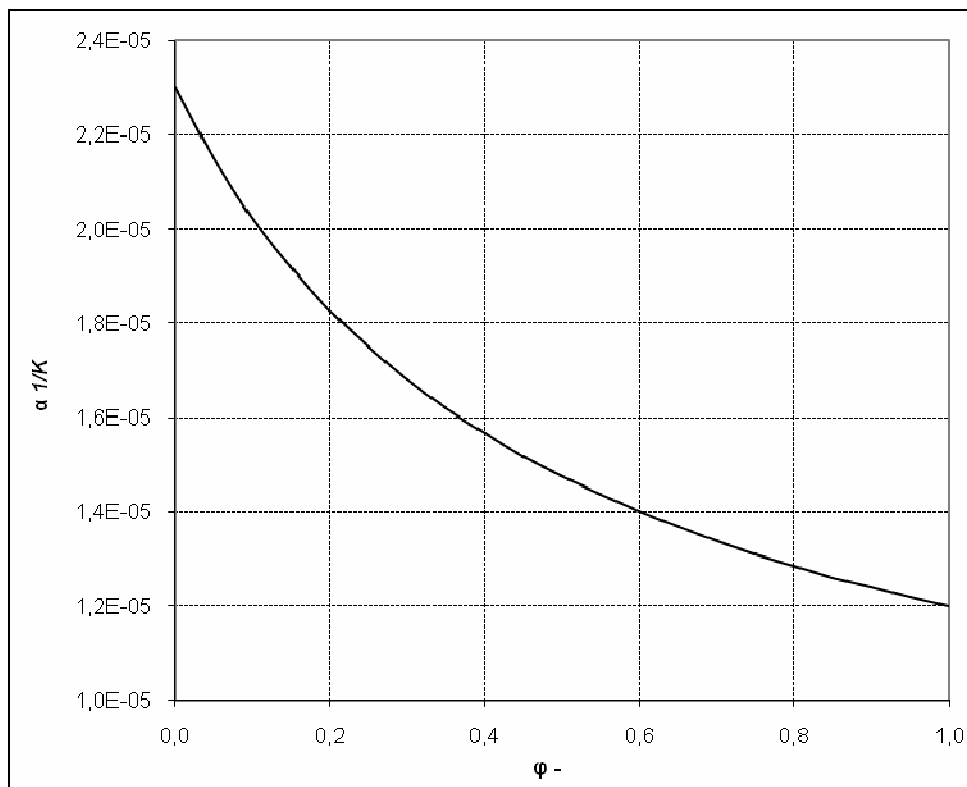
Figure 9: Coefficient of thermal expansion (α) as function of

reinforcement volume fraction (φ)

The CTE of the material can be adapted within a certain range. For the materials used currently the CTE can be chosen in between the properties of aluminium and steel. The

relation between CTE and reinforcement volume fraction is shown in Figure 9. Usage of other reinforcement materials (e.g. carbon fibres) will expand this range.

Thermal and residual stresses

The mismatch of CTE in the hybrid component causes thermal stresses. The thermal stress fields are multi-axial and depend on the geometry distribution of the fibres. Within the heterogeneous compound, the location of the reinforcement has a dominating influence.

These thermal stresses cause a change of the mechanical behaviour of the component. For the following investigation a temperature drop from a stress free state is assumed. A CTE of the matrix much higher than the CTE of the reinforcements results in a tensile stress within the matrix and a compressive stress within the fibres. The yield loads of the component are transferred to the compressive region. During the production process the profile passes a large temperature drop. The influence of this temperature drop and relaxation effects of matrix material will be investigated in further research.

With the FEM failure analysis an integration of thermal and residual stresses was performed, similar as described above. For the calculation the stress field is combined from variable part (external loads) and an invariant part (thermal and residual stresses). To calculate the yield limit an iteration process was implemented, which approaches the yield boundary from both sides and creates an interval containing the yield limit. This interval is reduced to a small size, and therefore convergence of the iteration process can be assumed.
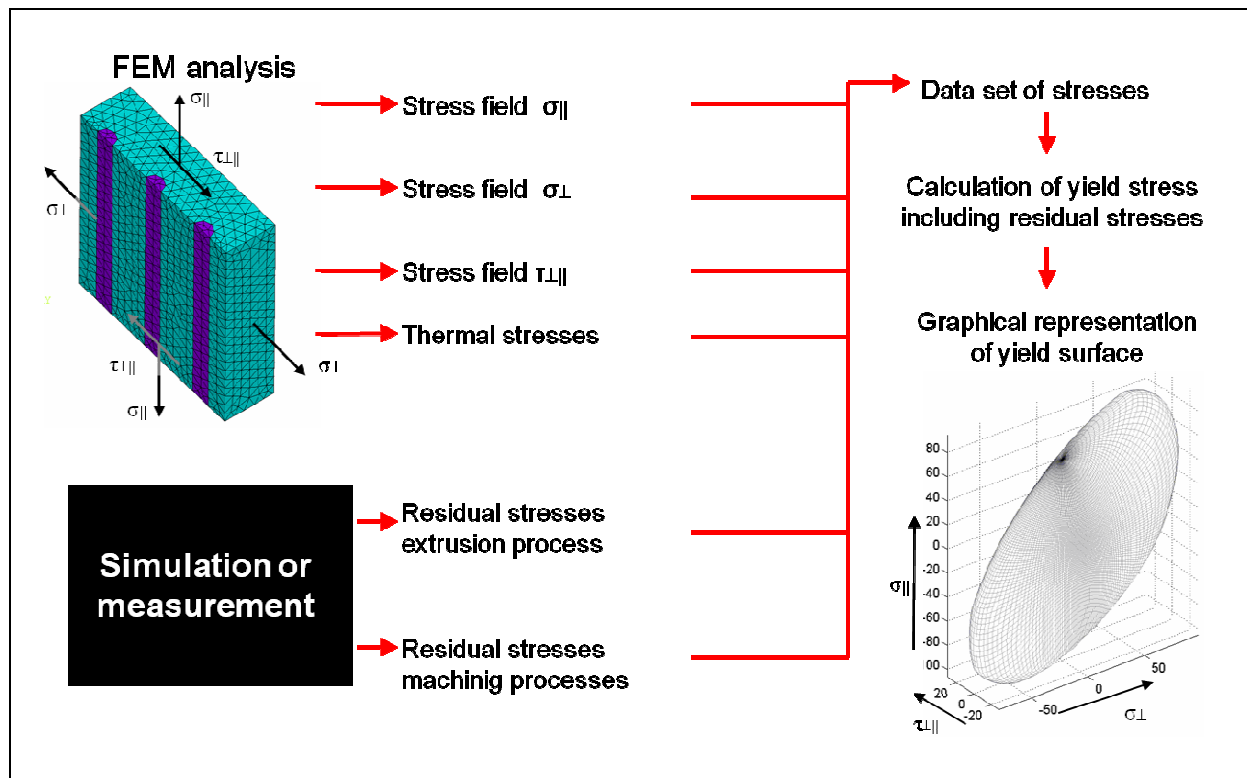
Figure 10: Scheme calculating yield load with residual stresses

In **Figure 10** the scheme of the calculation of the yield surface, including thermal and residual stresses, is shown for the configuration with a reinforcement volume fraction of 5% and thickness of wall of 3*mm*.
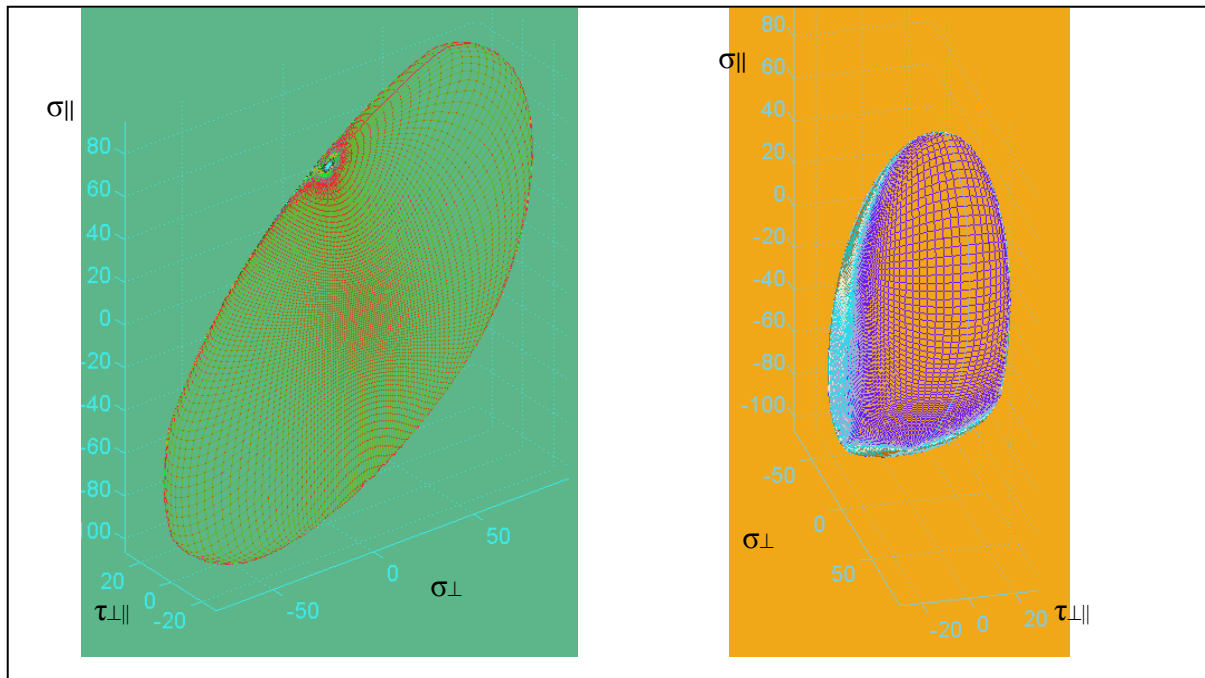
Figure 11: Yield surface with thermal offset ΔT=-50°C from stress free state

In **Figure 11** the yield surface for an aluminium matrix profile with a temperature offset of -50°C from a stress free state is shown. The yield stresses are moved to the compressive area. The tensile yield strength in axial direction is reduced from 110 *MPa*, without thermal loads, to about 60 *MPa*. Another interesting effect is the cut off in the compressive area. Due to the complex stress fields around the reinforcements not only an offset of the yield surface occurs, but also a change of the shape. The yield surface is no ellipsoid any more. Within the compressive region a flattened area is found, shown on the left in **Figure 11**. For an analysis of a component with thermal or residual stresses, evaluating a component with a failure criterion like Tsai-Hill is not possible.

Summary

The homogenized material properties of extrusion profiles have been investigated with the objective to provide an easy to use failure criterion for design of such components. A comparison of the Tsai-Hill failure criterion with a numerical calculation was performed. For simple cases without residual stresses, the deviation between Tsai-Hill and the numerical analysis is small. The influence of a stress field, resulting from a temperature, on the yield behaviour on a component was analysed. Under thermal loads an analysis with a global failure criterion is not possible. In further investigations the influence of the manufacturing process and plastic deformations will be integrated. The failure criterions will be compared and verified with results from biaxial testing. This paper is based on investigations of the collaborative research centre SFB/TR 10 which is kindly supported by the German Research Foundation (DFG).

Acknowledgment

References

[1] K. A. Weidenmann, E. Kerscher, V. Schulze, D. Löhe: Mechanical properties of compound-extruded aluminium-matrix profiles under quasi-static loading conditions. Advanced Materials Research Vol. 10, pp. 23-34 ,2006

[2] H. Schuermann: Konstruieren mit Faser-Kunststoff-Verbunden. Springer, Heidelberg, 2005

[3] C. R. Popescu: Processing and Characterisation of SiC-Fibre Reinforced Cu-Matrix Composites, http://nbn-resolving.de/urn/resolver.pl?urn:nbn:de:bvb:91-diss2004031818668

[4] M.T. Milan and P. Bowen: Fatigue Crack Growth Resistance of SiCp Reinforced Al Alloys: Effects of Particle Size, Particle Volume Fraction, and Matrix Strength. Journal of Materials Engineering and Performance, Volume 13 No. 5, pp. 612-618, 2004

[5] A. Zeidler: Abschätzung der Versagensgrenzen von Faserverbundwerkstoffen mit duktiler Matrix. Fortschr.-Ber. VDI Reihe 18 Nr. 236. Düsseldorf: VDI Verlag 1998

[6] M. Kh. Shorshorov, L. N. Moguchii, L. M. Ustinov, V. I. Zhamnova and M. P. Shebatinov: Investigation of the failure in tension of an aluminum alloy reinforced with steel wire. Strength of Materials, Volume 7, No. 8, pp. 961-965, 1975

[7] M. Kh. Shorshorov, V. G. Kudryashov, L. M. Ustinov, V. I. Zhamnova and E. N. Rudnitskii: Resistance to crack propagation in an aluminum-alloy-steel-wire composite. Strength of Materials, Volume 10, No. 4, pp. 378-381, 1978

[8] M. K Rybal'chenko and L. M. Ustinov: Effect of the fiber-matrix interface on the plasticity and strength of fibrous composites. Strength of Mat., Volume 4, No. 9, 1972

[9] M. Kh. Shorshorov, L. M. Ustinov, A. M. Zirlin, V. I. Olefirenko and L. V. Vinogradov: Brittle interface layers and the tensile strength of metal matrix-fibre composites. Journal of Materials Science, Volume 14, No 8, pp. 1850-1861, 1979

[10] E. R. Khismatulin, R. S. Yusupov, S. I. Kopylov and A. P. Alyab'ev: High-pressure vessels of aluminum-steel-wire composite material. Chemical and Petroleum Engineering, Volume 23, No 5, pp. 213-215 1987

[11] K. A. Weidenmann, Eberhard Kerscher, Volker Schulze, Detlef Löhe: Werkstoffsysteme für verstärkte Leichtbauprofile. VDI Fortschrittsberichte, Nr. 661, pp. 69 -105, 2007

[12] K. A. Weidenmann, E. Kerscher, V. Schulze, D. Löhe: Mechanical Properties of Compound-Extruded Aluminium-Matrix Profiles under Quasi-Static Loading Conditions. Advanced Materials and Research, Volume 10, pp. 23-33, 2006

[13] A. J. Svobodnik,: Numerical Treatment of the Elastic-Plastic Macromechanical Behaviour of Longfiber-Reinforced Metal Matrix Composites. Fortschr.-Ber. VDI-Reihe 18, Nr. 90, 1990

[14] A. Klaus, D. Becker, M. Kleiner: Three Dimensional Curved Profile Extrusion- First Results on the Influence on Gravity. Advanced Material Research, Volume 10, pp. 5-10, 2006

[15] K. A. Weidenmann: Werkstoffsysteme für verbundstranggepresste Aluminiummatrix-verbunde. Schriftenreihe Werkstoffwissenschaft und Werkstofftechnik, Vol. 33, 2006

[16] A. Kelly, G. J. Davies: The Principles of the Fibre Reinforcements of Metals. Metal. Rev. Vol. 10, 1965

[17] A. K. Kaw: Mechanics of Composite Materials. CRC Press LLC, 1997

A Modelling Approach for the Manufacturing Process Chain of Composite Lightweight Structures

Michael F. Zaeh[1,a], Mirko Langhorst[1,b]

[1]Institute for Machine Tools and Industrial Management (*iwb*)
Technische Universität München, Boltzmannstr. 15, D-85748 Garching, Germany

[a]michael.zaeh@iwb.tum.de, [b]mirko.langhorst@iwb.tum.de

Abstract. In order to support production tasks in the automotive industry, to reduce costs due to a trial and error procedure during process design and plant construction and to secure the accuracy of frame component assemblies, modern simulation methods are applied. In production chains a row of different manufacturing techniques are established. To accompany the number of manufacturing steps with the aid of calculation methods, an interacting of each simulation with the preliminary one is necessary. Such process chains help to determine the structural properties and geometrical accuracy of components and assemblies during manufacturing of composite lightweight structures and ensure their final quality. The basic difficulty of handling aluminium composites with steel reinforcements is the high residual stress level in the reinforcing elements and the adjoining matrix. This stress state can have a significant effect on the desired machining results and the related process itself. Contemplating this reveals the importance of defining a process chain by simulation.

Introduction

For the purpose of supporting the manufacturing of light-weight frame structures in the automotive industry, the following techniques are considered within the Collaborative Research Centre SFB Transregio 10: composite extrusion, laser beam welding and friction stir welding. To cope with the task of this research centre the TR-10 is partitioned into three domains. The partial projects within the A-domain work out the scientific and technological basics of the mentioned process steps. They provide novel and modified technologies respectively for the manufacturing and processing of extrusion-moulded work pieces. The B-domain includes the projects, which simulate the manufacturing processes. Core of the B-projects is the coupling of simulation with reality. The projects of the C-domain integrate the single process steps into a real and virtual process chain. Such a holistic treatment is necessary to study the influences of preliminary processes on the structural effects of components and assemblies along their manufacturing chain. Therefore, one aspect of the project is to merge single simulation models for calculating the structural properties during the manufacturing and transfer these on a modelled entire structure. In the first instance, the chaining should enable to analyse manufacturing problems and optimise the sequence of process steps. Thus, exact information of structural effects on the profile parts, introduced by the manufacturing process, is indispensable for realising an integrated simulation system. In order to achieve these objectives, an extensive knowledge of the projects, investigating the process effects in the A-domain, is also obligatory. Within the scope of the project C7 "An Integrated Simulation of Part-Structure-Interaction for Manufacturing Process Chains", this paper introduces a general approach for the integration of simulation models and an application example as a first step for the implementation.

Objectives and definition of the project

The flexible setup of lightweight structures requires adaptability in chaining the single manufacturing processes. The objective of the project C7 is to prepare single simulations of manufacturing steps and integrate them into an entire model to estimate the loads, remaining within the machined

structure. The editing and preparation pursues the concept of grading the complexity of the simulation model to lower levels with a view to reduce the modelling and computation effort. It is intended to develop an integrated model of the structural interference arising during manufacturing, which allows the variation of the input parameters. To increase the quality of computation results, physical changes have to be required as initial values for the simulation of following processes. For example, Tikhomirov [1] considered welding distortions within a virtual production chain; forming results can be taken into account in a simulation chain [2] and interlinking methods realise the integration of the preliminary forming simulation into the simulation of laser beam welding [3], [4]. Kerausch [5] developed a model to integrate preliminary process steps into a forming simulation of heat treated tailored blanks. By using SYSWELD and ABAQUS an interface was implemented, which realised the transfer of structural properties subsequent to a sheet metal pretreatment by laser processes into a deep drawing simulation. Bessert [6] elaborated applications to transfer IT-based data in his research activities. He used so-called mapping-functions to provide structural properties and geometrical characteristics of thin assemblies to subsequent simulation steps. Thus, the manufacturing history of the assembly is integratively considered in the following operations. A representative application of mapping-functions for transferring the characteristics of a forming model onto a crash specific FEM-mesh is described by Zöller [7]. In addition to the structural properties he transferred also complex material interrelations. The mapping of 3D-elements in simulations of material machining with multistage manufacturing processes was investigated by Ranatunga [8]. He introduced techniques and methods to determine the changes in the assembly's geometry during one manufacturing step and with this the associated process parameter, e. g. the strain rate and hence the stress field. Within this research project methods and models should be elaborated to simulate an entire process-chain for different manufacturing techniques, for example the composite extrusion of aluminium profiles reinforced with steel wire elements.

To achieve the described objectives, a three-phase concept should be pursued as shown in Fig. 1. This enables to achieve the complex requirements on the result accuracy and the required flexibility of the modelled process chain. The concept includes a cascade of three intertwined methods to meet the requirements for an efficient simulation of the manufacturing process chain.
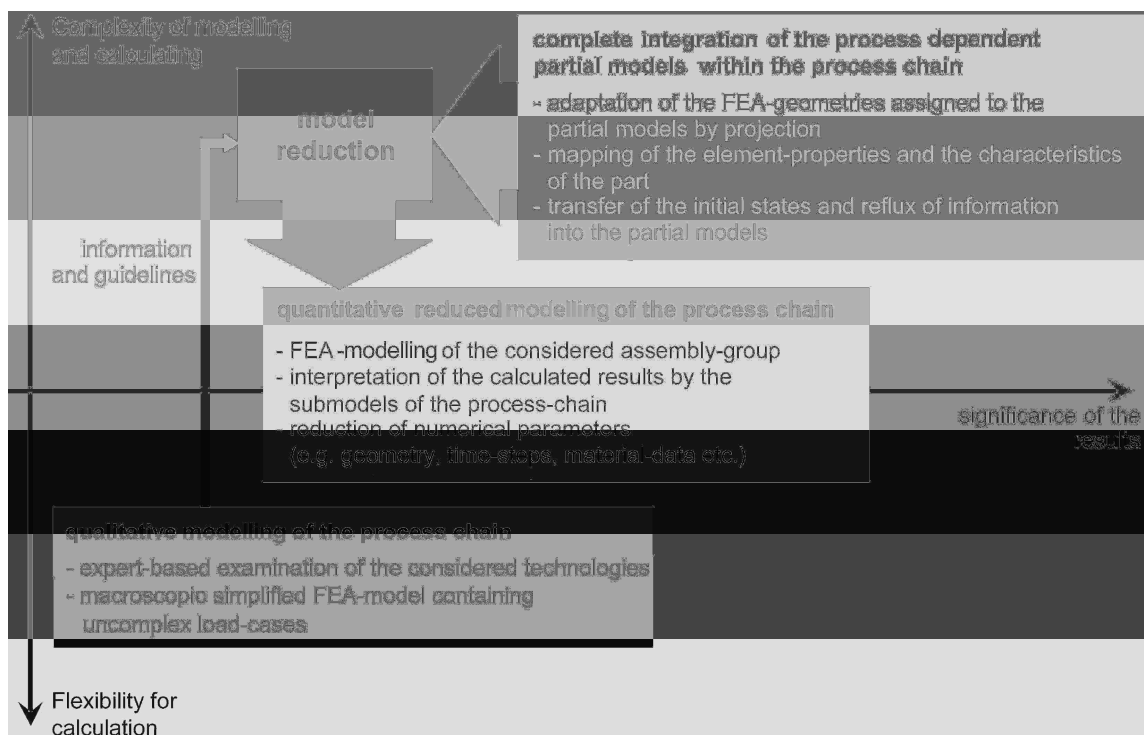

Fig. 1: A three-step-portfolio for an adaptive reduction of the modelling effort within an integrative simulation of the manufacturing chain

Core of the investigations within C7 is to use and to enhance the techniques in Fig. 1 to successively reduce the modelling and computation effort in order to get results that vary in the level of detail. The qualitative modelling of the process chain implies the knowledge integration of the individual processes of the manufacturing chain into an abstract entire model. Thus, a first estimation of the effects on the entire structure is possible. The collaboration with the A-projects should enable to identify tendencies of manufacturing effects on the entire structure. This approach provides a basis to detect the structural loads during the manufacturing phase and to estimate the effects on the assembly. The complete integration of the process dependent partial models in the process chain gives the feasibility to derive the state of the assembly at the beginning of the process specific simulation of the respective B-projects. For example, computed residual stresses should be considered as the initial state in a subsequent welding or drilling simulation. Within this research project the following part-specific values should be provided for the integration task:

- residual stresses as a result of the manufacturing processes
- transient deformation behaviour
- plasticizing
- transient temperature field

The integration of these values and the refeeding of the results should be realised by the master model, which integrates all the aspects of the partial models from the specific process simulations to transfer them as information data. On the basis of the FEM-programme ANSYS all the results of the B-projects can be transferred by capable interfaces. The transfer data is written in *.ASCII-format (text format), which is easy to interpret. Also the times between the manufacturing processes (e. g. cooling phases), which are modelled by the B-projects, can be integrated by means of the chaining model unless their structural influence is negligible for subsequent processes. Thus, the relevant structural influences of the specific processes can be considered along the entire process chain. The transfer of the unequally meshed geometry models from the B-projects can be realised by several mapping-systems, which facilitate the integration of unequal element types (e. g. shells, volumes), sizes and formulations (e. g. linear, quadratic, cubic) between different FEM-systems. Compared to the complete integration of the process dependent partial models as described above, the objective of the reduced modelling of the process chain is to reduce the computation and modelling effort. This approach of minimising effort allows varying the sequence of the manufacturing process models, which in turn supports the process chain optimisation. Otherwise, when using the described complete integration of results and geometries from the B-projects, the computation of variations would be too complex. Therefore, possibilities should be found that reduce the model complexity of the process chain without loosing the significance of the simulation results. Potentials for reduction are the idealising of the process-structure-effects, the coarsening of time lags within the FEM-computation, the coarsening of the FE-mesh or the homogenisation of anisotropic and temperature depending material data. With a view to a minimum effort of modelling the process chain, the reduction of the model is an important task within this project. Particularly, the number of independent parameters should be kept as small as possible when data is transferred or created respectively. This will assure a medium-term economic use of the method. However, the quality of the simulation results should not be decreased significantly for the considered use case. To ensure this, the simulation results will be validated by experiments.

Approach

To reach the discussed objectives, various steps are considered in the following. As already mentioned, a profound technology comprehension of the projects within the A-domain is fundamental to be able to include the results of the process simulations. Therefore, the processes, which are involved in the process chain will be analysed at their corresponding project location.

The influencing factors on the machined work pieces from the different manufacturing processes (e.g. stress state, temperature, distortion, local microstructure, changes in hardness) should be identified and related to each other. The disturbances may tend to global or local structural effects. Thereby, the transition between global and local influences can be smooth. For example, a drilling causes a local impact. Whereas, the residual stress from the composite extrusion is a characteristic global influencing value. The residual stresses are mainly caused by the different thermal expansion coefficients of the matrix material and the reinforcements. This leads to different elongations when the profile cools down and, thus, into a residual state of stress. These stresses interact with those that result from the complex interaction of the welding chamber geometry, the process parameters and the material flow. The calculation of this complex stress situation in the composite by analytical methods is difficult to perform. Because of this reason, it will be determined by measurement techniques. To detect residual stresses in structural parts several techniques are implemented in practise. These include the following non-destructive test procedures: radio graphical techniques [9], neutron diffraction [10], hole-drilling strain-gauge methods [11], ultrasonic tensile testing via transversal waves [12] or the Barkhausen noises [13]. In the near future it is planned to determine the residual stresses in the reinforcing elements and in the transition zone between the reinforcement and the composite using the neutron diffraction.

By means of the obtained findings and in extended consultation with the partners of the technology projects, the limits of the process feasibilities should be exposed. Within these bounds a structure for demonstration purposes (called demonstrator) is defined, which gives the possibility to integrate exemplary manufacturing steps in a process chain. The relevant demonstrator is shown in Fig. 2, where a quadratic hollow profile is joined with a pipe. Both aluminium profiles (EN-AW 6060) are reinforced with steel elements. To fit the profiles together, a circular recess, which is commensurate to the pipe, can be machined into the quadratic profile by the application of circular milling (see Fig. 2).
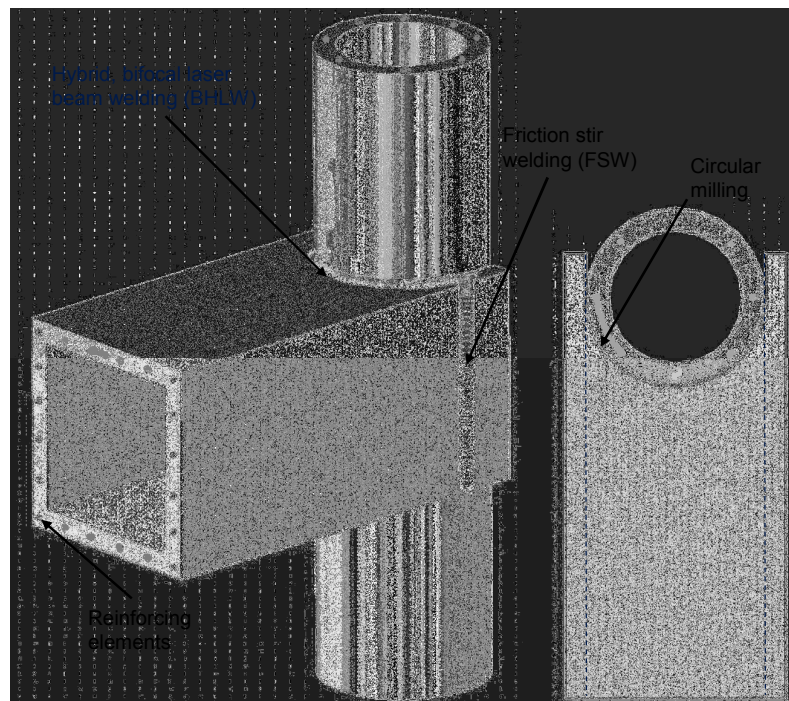
Fig. 2: Example for a demonstrator: T-joint of a round and square hollow profile with embedded reinforcing elements

The friction stir welding (FSW) [14] and the hybrid, bifocal laser beam welding (BHLW) [15] are intended to realise the joining. The semicircular weld line proves to be a huge challenge. Further difficulties for the BHLW are the different absorptive capacities of the laser light as well as the unequal melting points of aluminium and steel. Thus, the analysis of the processes and the consulta-

tion with the partners of the technology projects at first is a really important factor for technical feasibility.

The different joining techniques cause various requirements for the respective clamping. For example, in spite of the high processing loads coming up with FSW the exact position of the parts relative to each other and to the tool must be provided. The implementation of an appropriate clamping device for the joining using FSW or BHLW is also a task within this project. Subsequently, several welding tests will be performed. Measuring the geometry of the demonstrator before and after joining should give information about the welding distortions. Furthermore, the residual state of stress in the assembly will be analysed using a method mentioned above.

Another important point of this project is to gain the knowledge concerning the simulation projects within the B-domain. The basis for integration is to have detailed information about the activities, which have already been carried out or are planned within the partial projects B1 to B4. B1 is engaged in the simulation based optimization of composite extrusion and B2 in the simulation of five axis milling. The B3-project analyses the machining with cutting tools using the FEM and B4 simulates the BHLW to optimize the properties of the process and the product. The interaction between the B-domain and C7 is shown in Fig. 3.
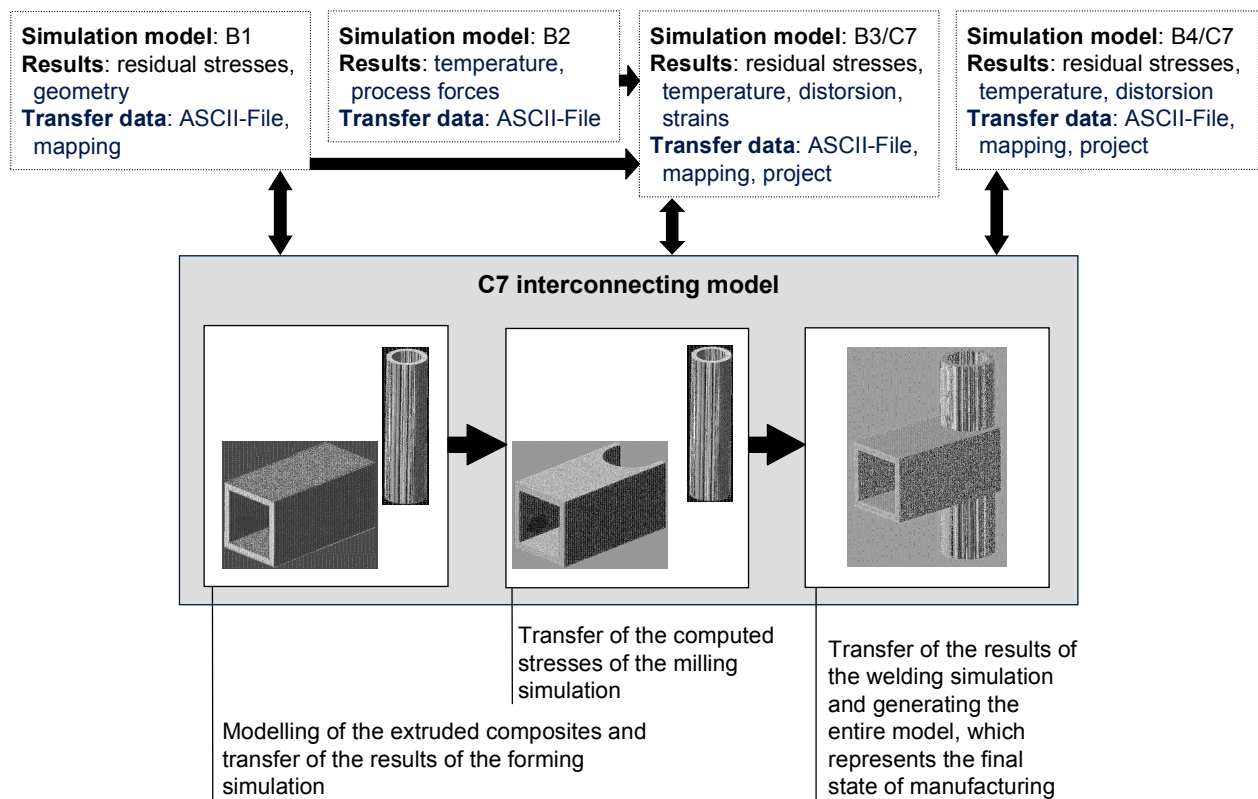
Fig. 3: Exemplary process chain for realising an integrated process simulation

A special collaboration exists between the projects B2 and B3. Therein B3 is supported by B2 with data generated by algorithms, which are not primarily based on the finite element method (FEM). The mainly used computation systems are the inverse kinematics [14], the finite difference method [15] or the discrete dexel model [16]. Therefore, the system provides a function to map the results and model characteristics on an FEM structure. The changes in geometry and properties may be transferred by using special project and mapping functions. These functions provide the process-specific shape of the FE-model, e.g. a fine mesh in the heat affected zone in a welding or machining simulation. Project functions are used to transfer element characteristics between geometries of an identical position and dimension. For example, a temperature field can be transferred on a coarsened or refined mesh structure by inter- and extrapolating the characteristics. Advanced possibilities are

provided by mapping functions. These functions include the transfer of geometry changes (e.g. deformation as a result of a heat impact) between two process steps.

Subsequently, with the consolidated knowledge of the technology and simulation projects, it should be possible to build up the FE-models of the considered processes. For the demonstrator shown in Fig. 2 the following processes have to be considered: composite extrusion, circular milling, friction stir welding and hybrid bifocal laser beam welding. Fig. 3 shows how to phase the simulation of a manufacturing process chain.

The computed distortion and residual stress state of the demonstration example have to be compared with real measurements. The next step is to analyse and optimise the manufacturing sequence. For that it is advantageous to reduce the modelling effort at the beginning. With regard to Fig. 1 the reduction can be performed by an analysis of the sensitivity of exemplary parameters (design of mesh and geometry, material data, time steps: transient vs. quasi static). After reducing the modelling effort, the order of all involved process steps along the manufacturing chain (except of the simulation of the composite extrusion as the first step) could be varied in order to support the optimisation of the manufacturing chain. As a start for the variation of the manufacturing steps, the related restrictions are secondary. To maximise the solution space, the objective is to find as many combinations of manufacturing chains as possible. Based on the numerous variants of simulations, the optimisation of the manufacturing chain can be supported with a minimum effort.

The importance of defining a process chain by simulation becomes apparent by the analysis of the results. The integration of physical values, resulting from previous steps (e. g. temperature, residual stresses), leads to a different structural behaviour as in comparison to a mere geometry-model as input data for the succeeding simulation. This is demonstrated by a first step example in the paragraph below.

An example of use as a first step of the approach

As already mentioned above, the first manufacturing step of the integrated process chain within these investigations is usually the extrusion of composite profiles. In this process, wires or wire ropes (e. g. made of steel) are inserted as reinforcements into an aluminium alloy during the profile extrusion. For this, the extrusion process is executed at temperatures up to 450 °C by heating up the chamber. Due to the different coefficients of thermal expansion of the aluminium matrix and the steel wires, the cooling to ambient temperature leads to a state of initial stress of the reinforcements and the matrix material. The proof of residual stresses in the cooled profile was already furnished in [17].

To model the extrusion process, simplifying assumptions are made. For example, one assumption is to consider merely stresses in the profile; potential damages are not considered. Furthermore, for the simulation, the entire composite extrusion is reduced to a process of transient cooling. In particular, a rectangular aluminium matrix (70 mm x 5 mm x 56 mm) with six embedded reinforcing elements (diameter = 1 mm) is cooled from 450 °C to almost ambient temperature. In the simulation the energy is transferred to ambient air over the profile surface. To cool down to ambient temperature, the section needs approximately ten minutes (Fig. 4). After cooling, a pressure stress state dominates the reinforcements and tensile stresses affect the aluminium matrix. As mentioned before, this is caused by the different thermal expansions of the matrix material and the reinforcements, which results in a lower shrinking of the steel wires with regard to the surrounding aluminium. The materials, which have to be specified for the simulation, are EN AW-6060 for the aluminium matrix and S 355 J2 for the steel reinforcements. A set of material properties is already stored in the database of the commercial software HyperMesh (Altair) and SYSWELD (ESI Group) while HyperMesh is used for the meshing tasks and SYSWELD for the computation. Concerning the materials mentioned above the database is complemented by experimental data provided by the subproject A3. For modelling the profile as a statically determinate system, all six degrees of freedom

(three rotatory and three translatory) of a single node in the corner of the profile, marked as the restraint in Fig. 5, are blocked. Thus, the system is over-constrained and kinematically stable.
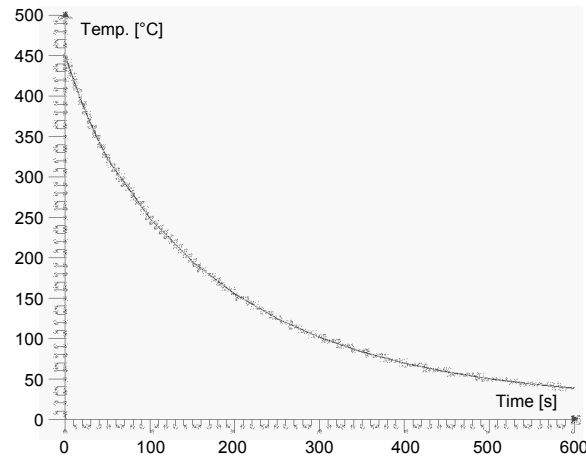

Fig. 4: Temperature development in the profile while cooling subsequent to the composite extrusion

The objective of the investigations within this project is to realise the chaining of simulations. Therefore, the simulation of the composite extrusion is concatenated with the simulation of a subsequent process step – the friction stir welding (FSW). The modelling of the FSW process is a subject matter of the project B4. In this example, the simulation includes a composite, which is friction stir welded transverse to the direction of the reinforcements. With regard to the discussed objective of reducing the modelling amount (see Fig. 1), a method to model the FSW process is to simplify the impact by defining a heat input. Thus, the deformations and the development of residual stresses can be calculated based on the heat source parameters. The specific heat input of the process is calibrated within the project B4, thus, the required parameters for modelling the heat source are supplied.
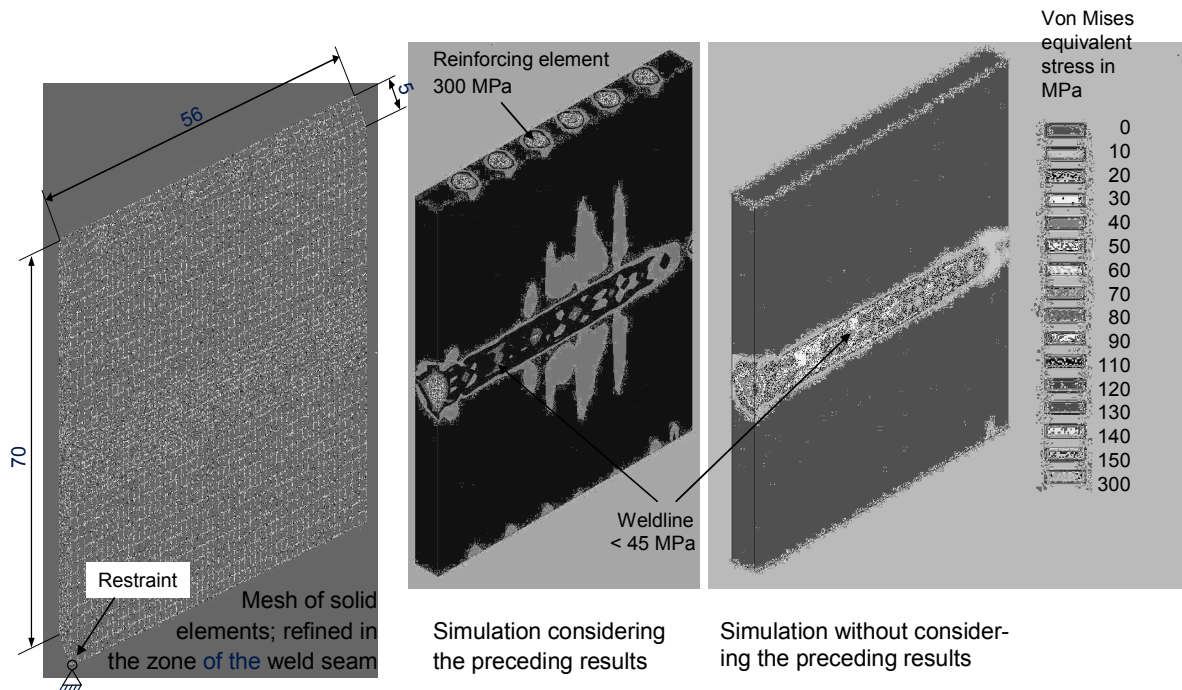
Fig. 5: Stresses in comparison with and without considering the preceding simulation results

Fig. 5 illustrates the stress situation in the composite profile as one output value. On the left side of Fig. 5, the preliminary extrusion process was considered as the initial state of the FSW simula-

tion. The right side displays the residual stress state after the simulation of FSW without considering the structural effects of the preceding process. As mentioned above, the unequal coefficients of thermal expansion of the matrix and the reinforcements cause the resulting stress situation. The high stress level in the reinforcing elements demonstrates that the consideration of the preceding process is necessary to describe the stress state in composite structures. Thus, the chaining of the simulations (Fig. 5, left side) results in a maximum stress level that exceeds the highest stresses in the simulation without considering the preliminary process by up to five times.

In addition to residual stresses another significant output value for welding simulations is the distortion. Information about shape distortions are fundamental to cope with deviations caused during manufacturing. Subsequent to the FSW simulation and after unclamping the profile, the residual displacements are compared in Fig. 6. The comparison shows that considering the preceding process step results in a 14% lower distortion. Thus, it appears that a chaining of single process simulations is necessary to predict the structural effects more accurately along the manufacturing process chain of composite structures.
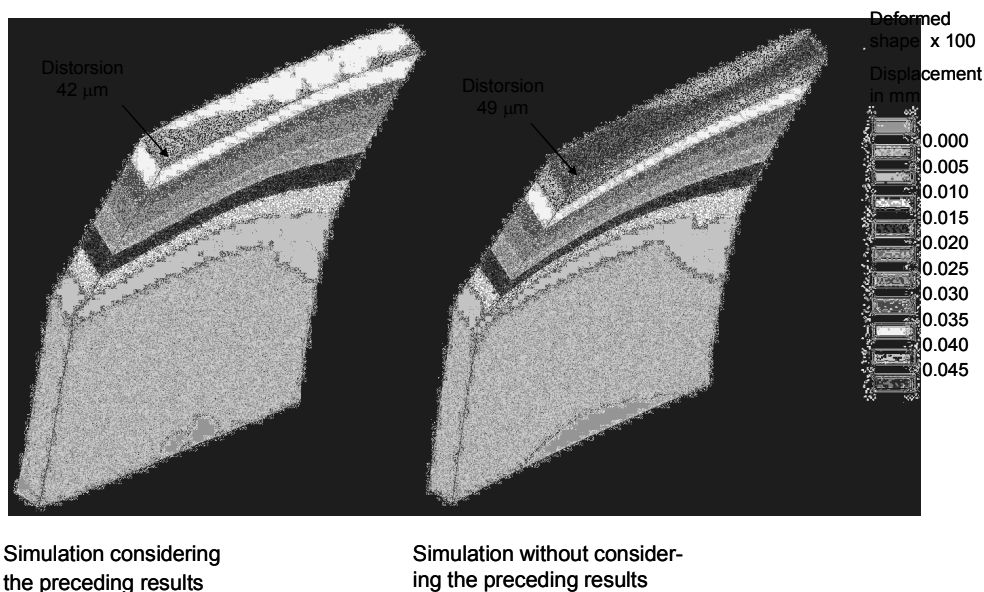
Fig. 6: Comparison of the distortion with and without considering the preceding simulation results (overstated shape: x 100)

Outlook

This contribution presents an approach of chaining two specific sub process simulations, which has been successfully realised for a basic geometry within one simulation environment. In the future, it is planned to expand the simulated process chain including the FE-programmes ANSYS (ANSYS, Inc.), HyperForm (Altair), HyperMesh (Altair) and SYSWELD (ESI Group), which are used by the projects of the B-domain. In particular, the manufacturing processes, contemplated in the context of the specific projects as part of the Transregio 10, will be integrated in an entire model. The objective is to create interfaces enabling the transfer of data between the different FE-programmes in order to calculate welding distortions considering all preliminary manufacturing processes, e.g. forming, circular milling and drilling.

References

[1] Tikhomirov, D.: Computing Welding Distortion: Comparison of Different Industrial Applicable Methods. Advanced Materials Research 6–8 (2005), pp. 195–202

[2] Kose, K.; Rietman, B.: Combining forming results via weld models to powerful numerical assemblies. 7th Esaform Conference. Trondheim, Norway, 28th–30th April, 2004

[3] Zäh, M. F.; Auer, F.; Roeren, S.; Hoffmann, H.; Häussinger, S.: Simulationsgestützte Optimierung der Prozesskette Umformen – Laserstrahlschweißen. Final report, FOSTA P 567. Düsseldorf: Verlag und Vertriebsgesellschaft mbH 2004

[4] Zäh, M. F.; Roeren, S.: One Modified FE-model to simulate the Process Chain of Forming and Welding. Steel Research International 76 (2005) 2/3, pp. 235–239

[5] Kerausch, M.: Finite Element Analysis for Deep Drawing of Tailored Heat Treated Blanks. Advanced Materials Research 6–8 (2005), pp. 343–350

[6] Bessert, N.: Die virtuelle Prozesskette als Baustein der digitalen Fertigung. INPRO Workshop: Optimierung von Bauteilen unter Berücksichtigung der Fertigungseinflüsse. Berlin, 17th–18th June, 2004

[7] Zöller, A.: Berücksichtigung von Blechumformergebnissen in der Crashberechnung. 3rd LS-DYNA Anwenderforum. Bamberg, 14th–15th October, 2004

[8] Ranatunga, V.: A volume-based method for parameter estimation in multi-stage material processing. Journal of Material Processing Technology 147 (2004), pp. 292–301

[9] Spieß, L.; Schwarzer, R.; Behnken, H.; Teichert, G.: Moderne Röntgenbeugung – Röntgendiffraktometrie für Materialwissenschaftler, Physiker und Chemiker. Wiesbaden: Teubner Verlag 2005

[10] Albertini, G.; Ceretti, M.; Coppola, R.; Lodini, A.; Perrin, M.; Rustichelli, F.: Neutron Measurements of Residual Strain in some Technological Materials and Components. In: Hutchings, M.; Krawitz, D. (Eds.): Measurement of Residual and Applied Stress Using Neutron Diffraction. Dordrecht, Boston and London: Kluwer Academic Publishers 1992, pp. 525–534

[11] Rendler, N. J.; Vigness, I.: Hole-drilling Strain-gage Method of Measuring Residual Stresses. Experimental Mechanics 6 (1966) 12, pp. 577–586

[12] Schneider, E.: Ultrasonic techniques, Structural and Residual Stress Analysis by Nondestructive Methods. Amsterdam: Elsevier Science B.V. 1997, pp. 522–563

[13] Altpeter, I.: Hochauflösende Zerstörungsfreie Ermittlung lokaler Gefüge- und Eigenspannungszustände mit Hilfe der Barkhausen-Mikroskopie. Werkstoffprüfung 1995, DVM-Berlin 1995, pp. 341–349

[14] Mishra, R., S.; Mahoney, M., W.: Friction Stir Welding and Processing. American Society for Metals (ASM) International 1 Edition, 30th March, 2007

[15] Trautmann, A.; Zäh, M. F.: Laser Bifocal Hybrid Welding of Aluminum. Advanced Materials Research 10 (2006), pp. 65–77

[16] Sorby, K.: Inverse kinematics of five-axis machines near singular configurations. International Journal of Machine Tools and Manufacture 47 (2007) 2, pp. 299–306

[17] Grzesik, W.; Bartoszuk, M.; Nieslony, P.: Finite difference analysis of the thermal behaviour of coated tools in orthogonal cutting of steels. International Journal of Machine Tools and Manufacture 44 (2004) 14, pp. 1451–1462

[18] Stifter, S.: Simulation of NC machining based on the dexel model: A critical analysis. The International Journal of Advanced Manufacturing Technology 10 (1995) 3, pp. 149–157

[19] Weidenmann, K. A.; Fleck, C.; Schulze, V.; Löhe, D.: Analysis of the microstructure and the residual stress state of aluminum extrusion reinforced with ropes. Materialwissenschaft und Werkstofftechnik 36 (2005) 1, pp. 307–312

Prototype Manufacturing of Extruded Aluminum Aircraft Stringer Profiles with Continuous Reinforcement

T. Kloppenborg[1, a], T. Hammers[2, b], M. Schikorra[1, c], E. Kerscher[2, d],
A. E. Tekkaya[1, e], D. Löhe[2, f]

[1]Institute of Forming Technology and Lightweight Construction, Technical University of Dortmund, Baroper Str. 301, 44227 Dortmund, Germany

[2]Institute of Materials Science and Engineering 1, University of Karlsruhe,

Kaiserstr. 12, 76131 Karlsruhe, Germany

[a]Thomas.Kloppenborg@iul.uni-dortmund.de, [b]Thilo.Hammers@iwk1.uni-karlsruhe.de,
[c]Marco.Schikorra@iul.uni-dortmund.de, [d]Eberhard.Kerscher@iwk1.uni-karlsruhe.de,
[e]Erman.Tekkaya@iul.uni-dortmund.de, [f]Detlef.Loehe@iwk1.uni-karlsruhe.de

Abstract. For an increase in safety against crack initiation and growth in metallic structures of airplanes different concepts were developed in the past. In the focus of this work are profiles made of continuously reinforced extruded aluminum. The production and the used die set of these profiles is presented as well as problems occurring in terms of geometrical inaccuracies of the embedded high strength wires. In addition, this paper attends to the problem of lateral seam weld formation. The interface between the AA-2099 as well as AA-6056 aluminum alloy and the high strength wires Nivaflex and Nanoflex were characterized by metallurgic investigations and push-out tests. As a result it can be stated that a sufficient geometrical accuracy could be achieved and a high interface strength can be accomplished even if a slight gap is still present in the interface layer between matrix and reinforcing element.

Introduction

Demands for reduced costs for aircraft structures, reduced fuel consumption and less emission of green house gases led to the development of a large variety of innovative concepts for lightweight components. One development in the area of metallic structures is the extrusion of continuously reinforced aluminum profiles, usable, for example, as aircraft stringer profiles [1]. The fundamentals of this process have been analyzed and are described by Schomäcker, Schikorra and Weidenmann according to [2,3,4] for the embedding of high strength wires in a base material of AA-6060. It was shown that the reinforcement can significantly increase the strength as well as stiffness, depending on the amount of wires embedded in the profile.

However, the typical aluminum profiles used in aircraft fuselages, for example, in this case stringers in aircrafts are made of high strength alloys of the 2xxx or 7xxx series. In this case, a significant increase of profile strength would require an extremely high strength and/or a large volume fraction of the reinforcing elements. Nevertheless even low volume fractions of reinforcement can be useful in fulfilling certain other functions. One example is the use of reinforcing elements as crack stopping elements, which can increase the residual strength of a structure for instance after a previous object damage of the aircraft body. This function is treated within the project "Improvement of material and part properties of aircraft stringers by composite extrusion" of the Collaborative Research Center SFB/TR 10, funded by the German Research Foundation (DFG). The works are carried out at the Institute of Forming Technology and Lightweight Construction (IUL) of the Technical University Dortmund and the Institute of Materials

Science and Engineering 1 (IWK1) of the University Karlsruhe and are supported with materials, process knowledge, and testing facilities by Alcan, Alcoa, Aleris, Alu Menziken, EADS Innovation Works, Sandvik Materials Technology, and VAC Vacuumschmelze.

When focusing on continuous wire reinforcement, a detailed knowledge about the reinforcement position in the extrusion product is necessary for the application area as well as for the subsequent manufacturing processes like drilling, milling or welding. The position mostly depends on the material flow in the die, however, deflections in the positioning can occur. According to [2], two different kinds of deflections can take place (Fig. 1): The reinforcements are located in the longitudinal weld seam (horizontal deflection), or the reinforcements are placed in the longitudinal weld seam but do not lie on the profile centre line (vertical deflection). The horizontal deflection of the reinforcing element is mostly determined by the supply position and the process parameters, whereas the vertical deflection depends for example on the symmetry of the die and the temperature gradient in the material flow [2].
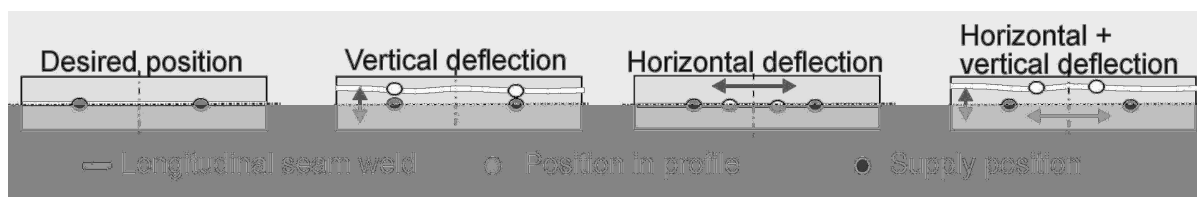
Figure 1: Definition of the horizontal and vertical deflections [2]

Extrusion Setup

For the extrusion process of aircraft stringer profiles with endless wires made of high strength material a modular tool concept was used. It consists of a sealing plate which divides the base material flow into different feedings, a supply plate with the reinforcing elements being supplied sideways by the use of feeding cartridges, and a die plate which defines the final cross section of the exiting profile (Fig. 2). Initially, before starting the extrusion process, the reinforcement had been supplied manually through feeding holes. At the moment of rejoining the base material strands in the welding chamber, the reinforcing elements are continuously pulled and embedded by the material flow.

Because the maximum press load was limited to 10 MN and the needed extrusion load increases with increasing press ratio the profile geometry has been adapted in the way that two stringer profiles are included in one large profile. Fig. 2 shows the two stringer profiles in the half-finished product. The final shape of the stringer profiles is produced by milling.

Figure 2: Modular die concept of the tool design and extruded Z-profile cross section

The experiments were carried out using a direct extrusion press, the aircraft aluminum alloys AA-2099 and AA-6056 as base material and the high strength wires Nivaflex and Nanoflex as reinforcement elements. For the extrusion process the AA-2099 billets were preheated to 480°C and the billets made of AA-6056 were preheated to 500°C. The die was heated to approximately 420°C

and the container to 450°C. A ram speed of 1mm/s was used. Before extrusion the reinforcement was cleaned manually with acetone.

Former investigations of stringer profile extrusions have shown that the reinforcement has not been fully embedded in the base material, which led to a gap between reinforcement and surrounding base material. To reduce the gap the bearing surfaces were angled 0.5° normal to the extrusion direction to increase the pressure in the welding chamber, similar to the die modification which is used to improve the welding conditions of the longitudinal seam welds in the industry.

Extrusion Results

Four billets of AA-6056 and four billets of AA-2099 were extruded to test the homogeneity of the process parameters temperature, punch speed and reinforcement position. In Fig. 3, the die temperature is diagrammed over the extruded profile length for the AA-6056 alloy. The temperature was measured continuously by thermocouples within the die tool package. It can be seen that the temperature increases especially in the first half of every press process and then remains rather stable between 470°C and 490°C. This temperature characteristic is a result of the equilibrium between the billets preheat, heat generated by dissipation when forming the material, and the heat loss at the backup plate. The whole process is not isothermal at all and a change of temperature might lead to a change of the reinforcement element position.
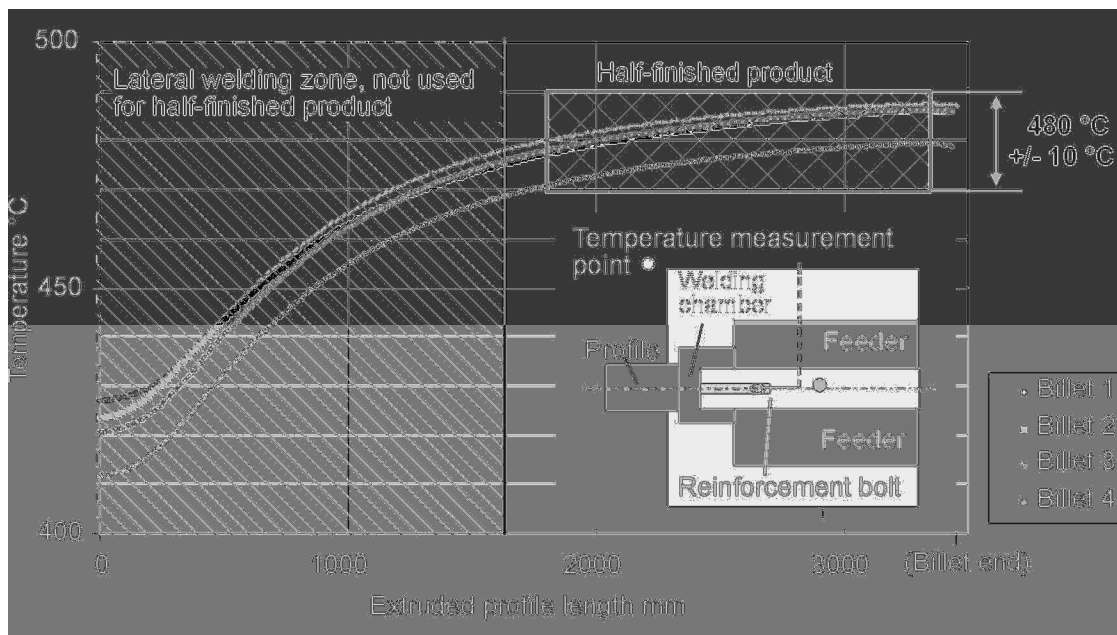
Figure 3: Distribution of the die temperature over the extruded profile length for AA-6056

To analyze the reinforcement position, the profiles were divided into six parts for extracting specimens of a length of approximately 50 mm (Fig.4). The positioning of the wires in the aluminum base material of the specimens was analyzed with the help of a light optical measurement system.
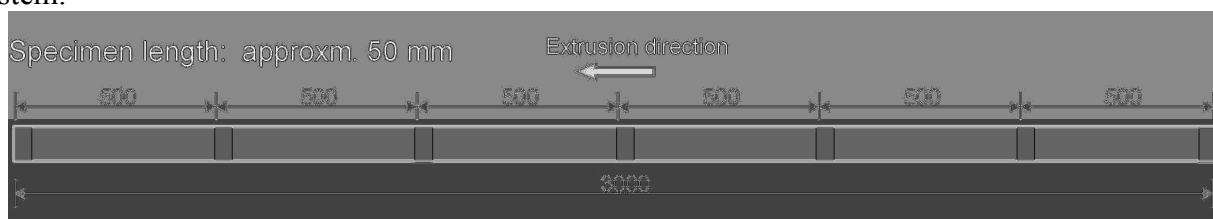
Figure 4: Specimen extraction to analyze the reinforcement position

In Fig. 5 the mean horizontal deflections are plotted over the profile length for the four billets. The diagram is divided into areas with and without the lateral welding zone. The profile part containing the lateral welding zone is not used for the half-finished product of the aircraft stringer profiles. There is a small mean positive deflection of wire 1 and a small mean negative deflection of wire 2, so that both wires are deflected towards the profile middle. The horizontal positioning error of the wires is not greater than 0.1 mm and is expected to have no further influence on the testing.
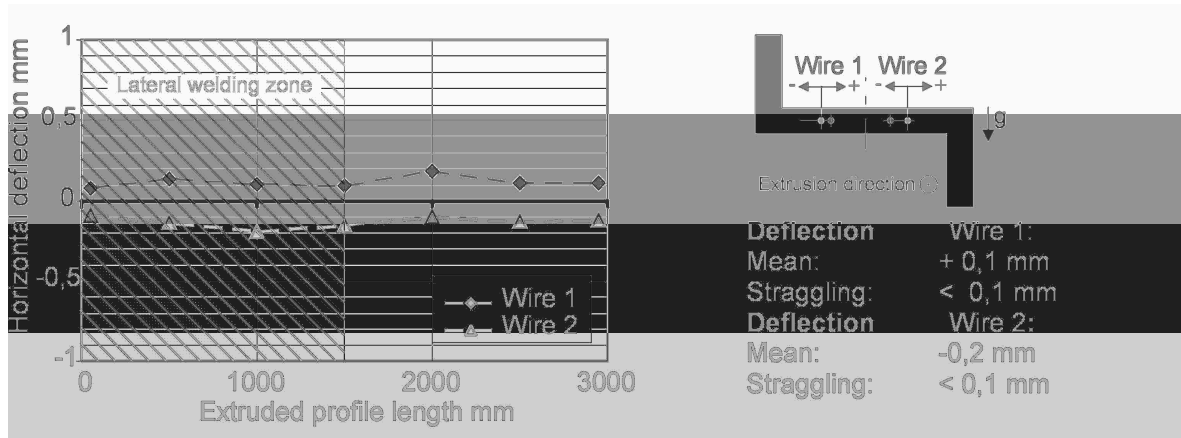
Figure 5: Distribution of the horizontal deflections over the extruded profile length

The vertical deflections of the reinforcement are essential for the further treatment. Large unknown vertical deflections can result in a cutting of the reinforcement elements during the milling process, which is necessary to mill the aircraft stringer profiles from the extruded Z-profile. The vertical deflections are shown in Fig. 6. Again there is a positive deflection of wire 1 and a negative deflection of wire 2 with a variation of less than 0.1 mm. Considering the mean vertical deflections, a high geometrical accuracy can be obtained during the composite extrusion process and the milling of the 2 mm thick aircraft stringer profiles can be done without the danger of reinforcement cutting.
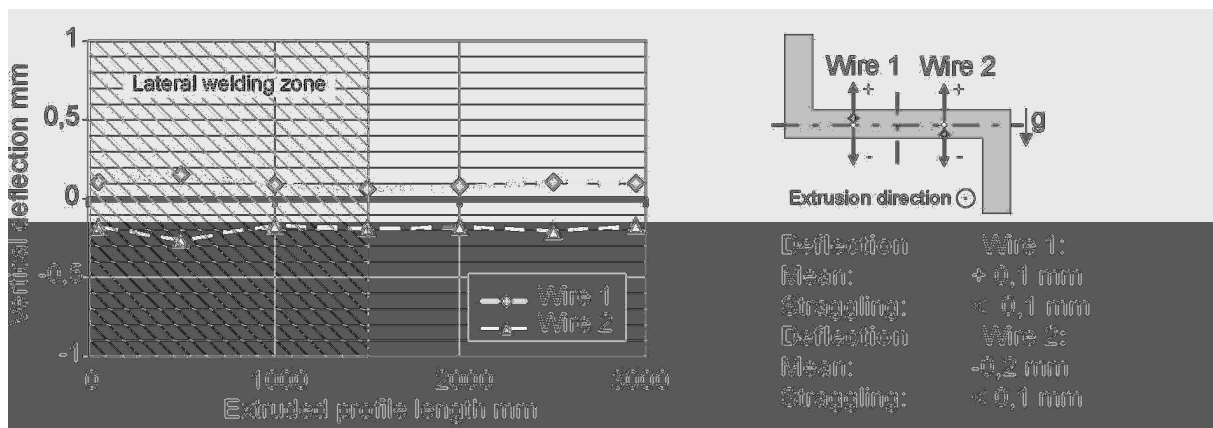
Figure 6: Distribution of the vertical deflections over the extruded profile length

Detection of the Lateral Weld Seam

Because of the limited maximum press load of the laboratory extrusion press of 10 MN an extrusion of AA-2099 or AA-6056 billets longer than 200 mm was not possible. Hence it was necessary to stop the extrusion at the end of each billet and to load the next billet for semi-continuous extrusion. Between two billets there is always a billet oxide surface layer leading to a loss of metallic continuity and, consequently, to a lateral weld seam in the extruded profile. To identify the length and characteristic of the lateral weld seam, the faces between two billets were coated with boron nitride before pressing. Since boron nitride is easily detectable after metallographic grinding the

position of the lateral weld seam could be identified as follows: At the beginning of the lateral weld seam (Fig. 7 a) the new billet material replaces more and more the older one (Fig. 7 b + c) until the older material disappears completely. The replacing starts in the middle of the profile where the speed of the flow of material is highest during the extrusion process.
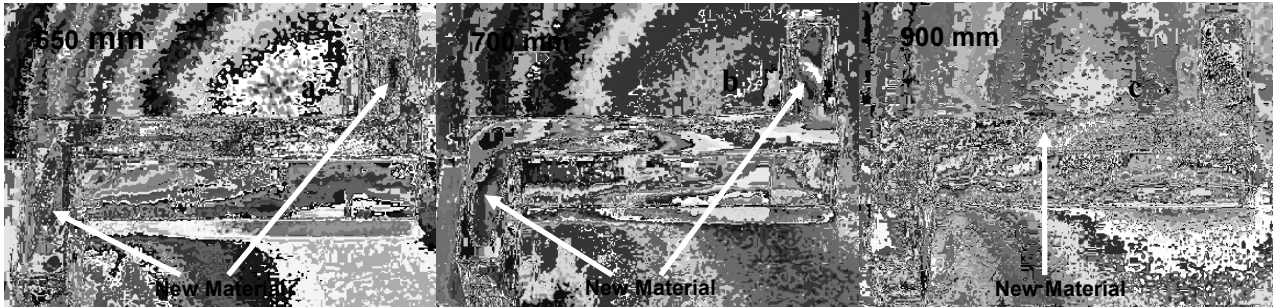

Fig. 7a-c: Distribution of the lateral weld seam at 650 mm, 700 mm, and 900 mm
measured from the beginning of the extruded profile

This investigation shows that approximately 1500 mm of the profile, which is 3100 mm long, are affected by the lateral weld seam. In order to avoid that a different strength in the lateral weld seam negatively influences the properties of the profiles, this zone has been marked and removed before further investigations were conducted. This left 1600 mm, which did not contain any lateral weld seam and which were then used for the production of the prototype aircraft stringers.

Metallographic Investigations on the Extruded Composite Profile

To see if the composite is capable of being used as aircraft stringer, it is necessary to analyze quantitatively its interface between reinforcement and base material. In particular, it needs to be tested whether the optimization of the angle of the bearing channels in the die have increased the local pressure and lead to a reduction of the gap between reinforcement and base material that was found in the initial tests. This was realized by metallographic sections. First, a piece of the profile was separated and cold embedded. Afterwards it was ground and polished and finally examined with a light optical microscope.

In certain areas around the wire a slight gap could be still identified between the AA-6056 base material and the Nanoflex wire with a width of approximately 2 µm (Fig. 8 a gap "1"). Furthermore, the wire seams locally plastic deformed due to plastic deformation during the embedding process (Fig. 8 a deformation "2"). In Fig. 8 b, the AA-2099 is shown with a Nivaflex-wire. Again, a gap is visible at the interface (1) and the wire is also non-circular (2). This indicates that a still higher pressure is needed to close the gaps.
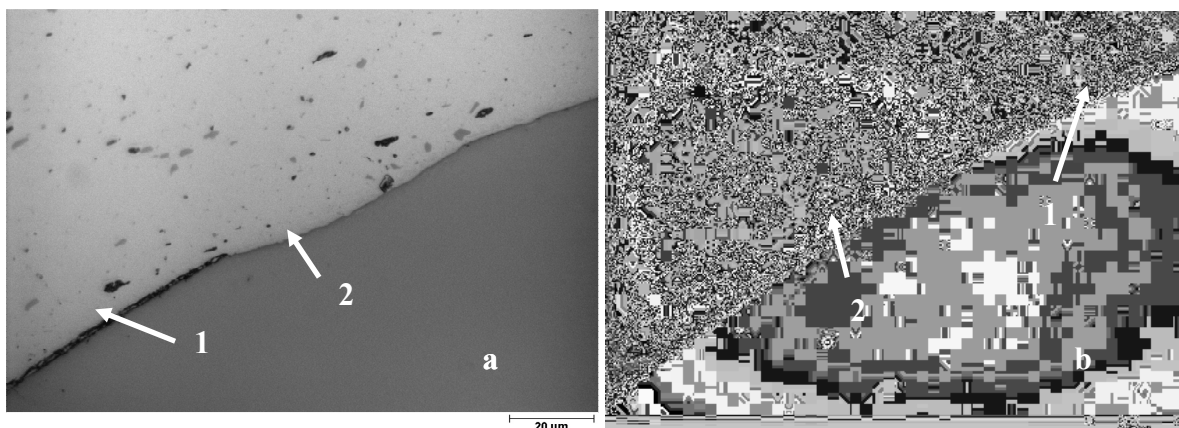
Fig. 8 a: Metallographic section AA-6056 + Nanoflex, 1000x
b: Metallographic section AA-2099 + Nivaflex, 1000x

After etching the microstructure of AA-6056 showed small grain sizes just around the reinforcing elements and at the border of the profile as well as in the longitudinal seam welds. These areas are those where the highest plastic deformation occurred during the extrusion process.

In addition to this, the microstructure of AA-2099 showed the same formation, but between the regions with fine grains the microstructure partly showed grains larger than in AA-6056.

Compared to the extrusions done before the optimization of the bearing channel angles, the interface quality has improved, but there is still a slight gap left. Future investigations are expected to show whether the gap emerges because of rough separating of the profile and in which way this gap has an influence on the mechanical properties of the profile. In particular, the effect on the debonding shear strength in the interface will be analyzed.

Reinforcement Push-out Tests

To characterize the mechanical properties of the interface between matrix and reinforcing element, push-out tests [5] were performed. In this test the debonding shear strength is determined by pushing the reinforcing element out of the base material.

The test is carried out on a Zwick Z 2.5 testing machine with a maximum load of 2.5 kN. A disc with a thickness of 1 mm, which is cut out of the reinforced profile section, is fixed on the machine and optically adjusted so that the reinforcement is centered. With a micro indenter a force is applied to push the reinforcement out of the base material. The maximum force necessary to reach a debonding of the interface between reinforcement and base material related to the surface of the interface is called the debonding shear strength. The push-out tests were carried out with specimens from a former pressing with AA2099 as matrix material and both wires before the optimization of the die.

The debonding shear strength was in the same range as in former investigations, which were carried out with other alloys and reinforcement materials. While in [3,6,7] values between 61 and 138 MPa depending on the reinforcing element and additional pretreatments of the wire occurred, the interface between base material and Nanoflex wire showed a debonding shear strength of 105 MPa and between base material and Nivaflex wire 123 MPa without special pretreatments of the wires.

Fig. 9 a shows a scanning electron microscope (SEM) picture of a pushed out Nanoflex-wire from the rear of the push-out specimen. Two conclusions can be drawn from this: First, the base material surrounding the reinforcement element is deformed plastically and, second, there is still base material sticking at the surface of the wires, as can be seen in Fig. 9 b, which shows signs of a dimple fracture. Both observations prove that even with a small gap remaining between wire and base material an excellent base material-wire bonding can be achieved. Future push-out tests on the current profiles are expected to show whether the debonding shear strength increases due to the optimization of the die.
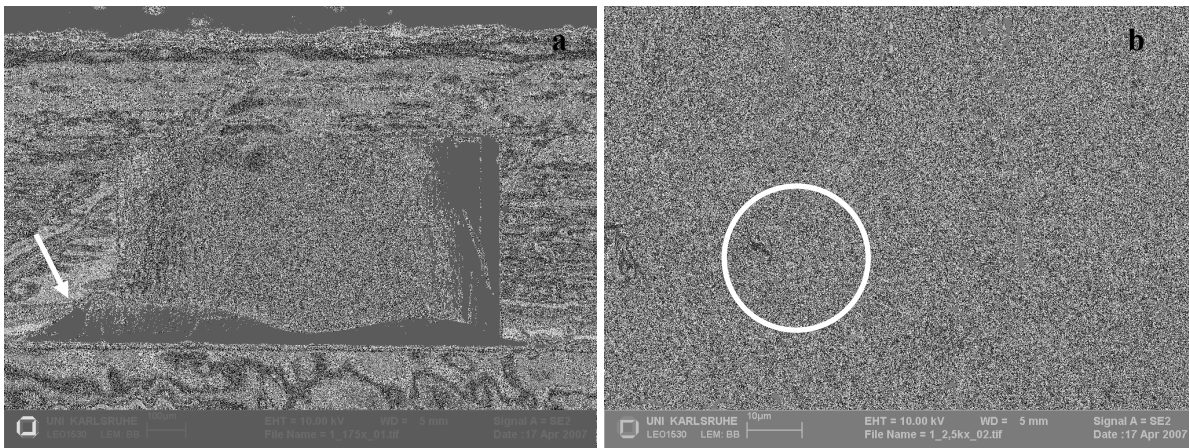
Fig. 9 a: Wire (Nanoflex) pushed out, matrix material is deformed plastically;
b: Magnification of the wire surface with aluminum alloy remaining on it

Summary

This work deals with the extrusion of continuously reinforced profiles for stringer profiles made of high strength AA-2099 and AA-6056 aluminum alloys and high strength wires.
Based on the extruded reinforced profiles the achieved geometrical accuracy of the reinforcement position was analyzed as well as the lateral seam welds. The gap between reinforcement and base material and the resulting debonding shear strength have been discussed. The results can be stated as follows:

1. When embedding the reinforcement, geometrical inaccuracies in horizontal and vertical direction of less than 0.2 mm occurred in the analyzed profile. This value is in close accordance with former investigations when extruding a relatively weak AA-6060 aluminum alloy. So high process stability can be expected even when changing the alloy.

2. Due to low pressure in the composite development zone a slight gap between reinforcement and base material was found in some areas. An increase in the bearing channel angle reduced this gap, although it was not completely closed.

3. SEM investigations on push-out specimens have shown base material sticking to the pushed-out reinforcement. Furthermore, plastic deformations of the base material were visible so that a debonding shear strength is higher than the strength of the base material can be assumed, even if a very small gap between base material and reinforcement remains.

The crack stopping properties of the aircraft stringers will be investigated in future testing.

References

[1] M. Schikorra, M. Schomäcker, T. Kloppenborg, E. Tekkaya, K. Weidenmann, E. Kerscher, D. Löhe: Improved Properties of Aircraft Stringer Profiles by Composite Extrusion, Proceedings of the Applied Production Technology APT'07 conference, Bremen, Germany,285-292, ISBN 978-3-933762-21-4, 2007

[2] M. Schomäcker: Composite Extrusion of Aluminum Profiles with endless metallic Reinforcements, Dr.-Ing. Dissertation, Institute of Forming Technology and Lightweight Construction, University Dortmund, Shaker publisher, ISBN 978-3-8322-6039-2, 2006

[3] K. A. Weidenmann: Werkstoffsysteme für verbundstranggepresste Aluminiummatrix-verbunde Dr.-Ing. Dissertation, Institute of Material Sciences 1, University Karlsruhe, Shaker publisher, ISBN 978-3832257606, 2006

[4] M. Schikorra: Modeling and Simulation of Composite Extrusion Processes, Dr.-Ing. Dissertation, Institute of Forming Technology and Lightweight Construction, University Dortmund, Shaker publisher, ISBN 978-3832255060, 2006

[5] D. B. Marshall, Journal of the American Ceramics Society, Volume 67, 259-260, 1984

[6] K. A. Weidenmann, E. Kerscher, V. Schulze, D. Löhe: Characterization of the interfacial properties of compound-extruded lightweight profiles using the push-out-technique, Materials Science and Engineering A 424, 205-211, 2006

[7] K. A. Weidenmann, E. Kerscher, V. Schulze, D. Löhe: Grenzflächen in Verbund-strangpressprofilen auf Aluminiumbasis mit verschiedenen Verstärkungselementen, Praktische Metallographie, Volume 37, 131-136, 2005

Keywords Index

Authors Index